UNIVERSITÄT DUISBURG ESSEN

Universitätsklinikum Essen

Exploring immune cell migration and its prognostic and diagnostic potential by time-lapse video and light sheet fluorescence microscopy

Inaugural-Dissertation

zur Erlangung des Doktorgrades

doctor rerum naturalium

(Dr. rer. nat.)

der Fakultät für Biologie

an der Universität Duisburg-Essen

vorgelegt von **Lea Bornemann, M.Sc.**

Datum der Abgabe: November 2019

Remember, in the burning heart

There can never be surrender

» Surrender «

Beast in Black

DOI: 10.17185/duepublico/71556
URN: urn:nbn:de:hbz:464-20210604-092313-1

Angaben zur Prüfung

Die der vorliegenden Arbeit zugrunde liegenden Experimente wurden am Institut für Experimentelle Immunologie und Bildgebung der Universität Duisburg-Essen durchgeführt.

1. Gutachter:
Prof. Dr. rer. nat. Matthias Gunzer
Institut für experimentelle Immunologie und Bildgebung
Essen, Deutschland

2. Gutachterin:
Prof. Dr. rer. nat. Wiebke Hansen
Institut für medizinische Mikrobiologie
Essen, Deutschland

Vorsitzende des Prüfungsausschusses:
Prof. Dr. rer. nat. Perihan Nalbant
Institut für Molekulare Zellbiologie
Essen, Deutschland

Tag der mündlichen Prüfung:
26.03.2020

List of publications and awards

The following scientific articles were published during this thesis. Parts of these publications were additionally used in this work and cited accordingly.

Scientific articles

Bornemann, L.*, Merz, S.F.*, Korste, S.*, Michel, L., Stock, P., Squire, A., Soun, C., Engel, D.R., Detzer, J., Lörchner, H., Hermann, D.M., Kamler, M., Klode, J., Hendgen-Cotta, U.B., Rassaf, T., Gunzer, M. & Totzeck, M.
Contemporaneous 3D characterization of acute and chronic myocardial I/R injury and response.
Nature Communications **10**, 2312 (2019).
* these authors contributed equally

Cited as [1].

Schuster, M.*, Moeller, M.*, **Bornemann, L.**, Bessen, C., Sobczak, C., Schmitz, S., Witjes, L., Kruithoff, K., Kohn, C., Just, O., Kündgen, A., Pundt, N., Pelzer, B., Ampe, C., Van Troys, M., Nusch, A., Haas, R., Germing, U., Martens, L., Jöckel, K.-H. & Gunzer, M.
Surveillance of Myelodysplastic Syndrome via Migration Analyses of Blood Neutrophils: A Potential Prognostic Tool.
The Journal of Immunology, ji1801071 (2018).
* these authors contributed equally

Cited as [2].

Grüneboom, A., Hawwari, I., Weidner, D., Culemann, S., Müller, S., Henneberg, S., Brenzel, A., Merz, S., **Bornemann, L.**, Zec, K., Wuelling, M., Kling, L., Hasenberg, M., Voortmann, S., Lang, S., Baum, W., Ohs, A., Kraff, O., Quick, H.H., Jäger, M., Landgraeber, S., Dudda, M., Danuser, R., Stein, J.V., Rohde, M., Gelse, K., Garbe, A.I., Adamczyk, A., Westendorf, A.M., Hoffmann, D., Christiansen, S., Engel, D.R., Vortkamp, A., Krönke, G., Herrmann, M., Kamradt, T., Schett, G., Hasenberg, A. & Gunzer, M.
A network of trans-cortical capillaries as mainstay for blood circulation in long bones.
Nature Metabolism (2019).

Cited as [3].

Schleier, L., Wiendl, M., Heidbreder, K., Binder, M.T., Atreya, R., Rath, T., Becker, E., Schulz-Kuhnt, A., Stahl, A., Schulze, L.L., Ullrich, K., Merz, S.F., **Bornemann, L.**, Gunzer, M., Watson, A.J.M., Neufert, C., Atreya, I., Neurath, M.F. & Zundler, S.
Non-classical monocyte homing to the gut via alpha4beta7 integrin mediates macrophage-dependent intestinal wound healing.
Gut (2019).

Cited as [4].

Manuscripts in preparation / submission

Bornemann, L., Schuster, M., Schmitz, S., Sobczak, C., Bessen C., Merz, S.F., Pundt, N., Jöckel, K.-H., Haverkamp, T., Dührsen, U., Gunzer, M., Göthert, J.R.
Defective migration and dysmorphology of neutrophil granulocytes in a case of atypical chronic myeloid leukemia.

Merz, S.F., Jansen, P., Ulankiewicz, R, **Bornemann, L.**, Schimming, T., Griewank, K., Cibir, Z., Stoffels, I., Aspelmeier, T., Brandau, S., Schadendorf, D., Hadaschik, E., Ebel, G., Gunzer, M., Klode, J.
Identification and quantification of hidden melanoma metastases in human sentinel lymph nodes using light sheet fluorescence microscopy.

Richter, E., **Bornemann, L.**, Korencak, M., Juszczak, P., Alter, G., Schuster, M., Esser, S., Gunzer, M., Streeck, H.
Reduction of CD8 T cell activity by Integrase Inhibitors may impact HIV eradication attempts.

Oral and poster presentations

Poster presentations at the
17th Day of Research of the Medical Faculty of the University of Duisburg-Essen,
Essen, Germany, 07/12/2018
20th EMBL PhD Symposium of the EMBL Heidelberg, Heidelberg, Germany, 22-24/11/2018
5th European Congress of Immunology (ECI) 2018, Amsterdam, Netherlands, 02-05/09/2018
"Identification of high-risk myelodysplastic syndrome via migration analyses of blood neutrophils: A Diagnostic Approach."

Oral and poster presentation at the
13th ENII EFIS EJI Summer School on Advanced Immunology, Porto Cervo,
Italy, 02-12/05/2018
"Eosinophil migration as a prognostic marker for immune checkpoint blocker therapy in metastatic melanoma patients."

Poster presentations at the
16th Day of Research of the Medical Faculty of the University of Duisburg-Essen, 17/11/2017
47th Annual Meeting of the German Society for Immunology (DGfI), Erlangen, Germany, 11-15/08/2017
"Introduction of 2D human leucocyte migration assays suited for the application in the diagnostic setup."

Awards and Grants

Poster award at the
17th Day of Research of the Medical Faculty of the University of Duisburg-Essen,

07/12/2018
"Identification of high-risk myelodysplastic syndrome via migration analyses of blood neutrophils: A Diagnostic Approach."

Travel grant from EFIS EJI, 04/2018

Travel grant from the DGFI, 03/2018

Poster award at the
16th Day of Research of the Medical Faculty of the University of Duisburg-Essen, 17/11/2017
"Introduction of 2D human leucocyte migration assays suited for the application in the diagnostic setup."

Travel grant from BioLegend, 06/2017

Abstract

The ability to migrate is inherent to most cells, regardless of their origin. Indeed, life, as we know it, only exists because cells can change their location in a highly organised way. Cell migration plays a pivotal role during fundamental processes in multi-cellular organisms, like implantation of the fertilised egg, morphogenesis, wound healing, and immune surveillance. For immune cells, migration is essential throughout their whole lifetime to patrol the tissues, follow cytokine gradients to a site of inflammation as well as find and ultimately battle a pathogen or degenerate host cell. Additionally, defective or abnormal migration can be both, cause and effect across a large collective of diseases, such as cancer, rheumatoid arthritis or vascular diseases. This work focusses on the visualisation and quantification of immune cell migration in man and mouse as a novel parameter for clinical and biological applications.

In humans, specific immune cells were isolated from the peripheral blood and analysed in specifically tailored and standardised *in vitro* assays to study their migratory behaviour. This yielded novel insights into immune cell migration behaviour in healthy individuals, such as an independence of eosinophil and $CD8^+$ T cell migration from age of the donor. Furthermore, immune cell migration in various disease settings was screened, revealing the power these assays have in clinical routine and surveillance. In this regard, neutrophil granulocytes from myelodysplastic syndrome (MDS) patients exhibited profound migratory defects in the more severe cases, while milder cases displayed relatively normal migration. Strikingly, these migration patterns correlated not only with disease severity and scoring, but they also correlated with therapy success. In a patient suffering from atypical chronic myeloid leukaemia (aCML), neutrophil migration remained impaired throughout the observation period. Yet, there is evidence that these neutrophils were still able to sense and react to on-going infections, as displayed by a peak in neutrophil migration shortly before infection. Additionally, patients suffering from metastatic malignant melanoma before and during immune checkpoint blocker therapy (ICBT) revealed a close relationship between eosinophil baseline migration and therapy success. Before therapy, neutrophil and eosinophil migration was indistinguishable from healthy patients, while $CD8^+$ T cells were strikingly unresponsive. During ICBT, eosinophil migration proved to diminish in a progressive disease, while neutrophil migration increased during a partial remission. $CD8^+$ T cells, however, remained unresponsive.

In mice, the effect of induced ischemia on the influx of neutrophil granulocytes and on the heart vasculature was investigated using light sheet fluorescence microscopy. This end-

point measurement of neutrophil migration revealed that the cells localised to the damaged tissue 24 hours after ischemia yet did not penetrate further into the healing tissue after 5 days.

These findings spotlight immune cell migration as not only a highly important, but quantifiable parameter that can assist routine diagnostics and prognostics of human patients with a broad range of diseases. Additionally, these assessments might lead to future therapeutic approaches in blocking or boosting immune cell migration and therefore their responses to battle opportunistic infections, reduce tissue damage or enhance cancer rejection.

Keywords: immunology, cell migration, time-lapse video microscopy, light sheet fluorescence microscopy, clearing, *in vitro* assays, ischemia / reperfusion, MDS, aCML, metastatic melanoma, immune checkpoint blocker therapy

Zusammenfassung

Die meisten Zellen können sich eigenständig fortbewegen, unabhängig von ihrer Herkunft. In der Tat ist das Leben, wie wir es kennen, nur möglich, da Zellen ihre Position zielgerichtet verändern können. Zellmigration spielt daher eine zentrale Rolle während vieler fundamental wichtiger Prozesse in multizellulären Organismen, wie zum Beispiel während der Implantation der befruchteten Eizelle, der Morphogenese, der Wundheilung oder der Überwachung durch das Immunsystem. Gerade für letzteres ist Migration essenziell, damit die Zellen die Gewebe patrouillieren, entlang Zytokingradienten an einen Infektionsherd gelangen sowie Pathogene und entartete Körperzellen finden und diese eliminieren können. Des Weiteren kann fehlerhafte oder abnormale Migration sowohl der Grund für als auch die Auswirkung von einer Bandbreite an Krankheiten, wie zum Beispiel Krebs, rheumatoider Arthritis oder Gefäßerkrankungen, sein.

Diese Arbeit befasst sich mit der Visualisierung und Quantifizierung von Immunzellmigration des Menschen und der Maus, um diesen Parameter für weitere klinische und biologische Anwendungen zugänglich zu machen.

Im Menschen wurden spezifische Immunzelltypen aus dem Blut aufgereinigt und ihr Migrationsverhalten in speziellen und standardisierten *in vitro* Untersuchungen charakterisiert. Dadurch konnten neue Erkenntnisse über das Migrationsverhalten von Immunzellen aus gesunden Probanden gewonnen werden, wie zum Beispiel, dass die Motilität von Eosinophilen und $CD8^+$ T- Zellen unabhängig vom Alter des Probanden ist. Des Weiteren wurde Immunzellmigration in verschiedenen Erkrankungen untersucht, was das Potential dieses Parameters und der etablierten Untersuchungen für die klinische Routine und Überwachung von Patienten aufzeigte. Hierbei weisen neutrophile Granulozyten von Patienten mit einer schweren Form von myelodysplastischem Syndrom (MDS) einen deutlichen Defekt ihrer Migration auf, während leichtere Fälle eine relativ normale Migration zeigten. Auffallend ist, dass diese Migrationsmuster nicht nur mit der Schwere und dem Scoring der Krankheit korrelierten, sondern auch mit dem Therapieerfolg. Bei einem Patienten, der an atypischer chronischer myeloischer Leukämie (aCML) litt, blieb die Migration der Neutrophilen während des gesamten Beobachtungszeitraums beeinträchtigt. Es gab jedoch Hinweise darauf, dass diese Neutrophilen noch in der Lage waren, auf bevorstehende Infektionen zu reagieren, wie eine Spitze der neutrophilen Migrationsfähigkeit kurz vor einer Infektion zeigte. Darüber hinaus zeigten Patienten mit metastasierendem malignem Melanom vor und während der Immun-Checkpoint-Inhibitor Therapie (ICBT) einen engen Zusammenhang zwischen eosinophiler Basismigration und Therapieerfolg. Vor der Therapie war die

Neutrophilen- und Eosinophilenmigration ununterscheidbar von gesunden Probanden, während $CD8^+$ T-Zellen auffallend gering ansprachen. Während der ICBT zeigte sich, dass die Eosinophilenmigration bei einer fortschreitenden Erkrankung abnahm, während die Neutrophilenmigration während einer partiellen Remission zunahm. $CD8^+$ T-Zellen blieben jedoch ohne Reaktion.

Darüber hinaus wurde die Wirkung einer induzierten Ischämie auf den lokalisierten Einstrom neutrophiler Granulozyten und die Herzgefäße mit Hilfe der Lichtblatt Fluoreszenzmikroskopie in Mäusen untersucht. Diese Endpunktmessung der Neutrophilenmigration ergab, dass die Zellen 24 Stunden nach der Ischämie im geschädigten Gewebe lokalisiert waren, aber nach 5 Tagen nicht weiter in das nun heilende Gewebe eindrangen.

Diese Ergebnisse weisen Immunzellenmigration nicht nur als einen sehr wichtigen, sondern auch quantifizierbaren Parameter aus, der die Routinediagnostik und -prognose von menschlichen Patienten mit einem breiten Spektrum von Krankheiten unterstützen kann. Darüber hinaus könnten diese Analysen zu zukünftigen therapeutischen Ansätzen führen, um die Migration von Immunzellen zu blockieren oder zu fördern und damit ihre Reaktionen auf opportunistische Infektionen zu erhöhen, Gewebeschäden zu reduzieren oder die Krebsabwehr zu verbessern.

Schlagwörter: Immunologie, Zellmigration, Zeitraffervideomikroskopie, Lichtblattfluoreszenzmikroskpie, optische Klärung, *in vitro* Analyse, Ischämie / Reperfusion, MDS, aCML, metastatisches Melanom, Immun-Checkpoint-Inhibitor Therapie

Table of Contents

1. Introduction

1.1. Cell migration – driver of life

Motility, the collective term describing the ability of cells to change their location, is inherent to many nucleated cells. While certain eukaryotic cells mostly move using a specialised organelle called flagellum[5], it gets more complicated in multicellular organisms, where cells do not only migrate alone in liquid medium, but also in larger cohorts inside the organ tissue[6].

Migration is an essential feature of cells during various stages of development and host defence in an organism, yet also a general hallmark of cancer[7, 8]. Most cells, e.g. stromal, epithelial or neuronal cells, cease to migrate once their organ has fully formed during development and they have terminally differentiated[6]. This does not mean, however, that they cannot regain this ability during processes like tissue regeneration[6]. The cells of the immune system, on the other hand, are responsible for host defence against exogenous pathogens and host-derived degenerate cells and completely reliant on their ability to migrate throughout their entire life[9]. Guided by extracellular stimuli, they emerge from the bone marrow - the seat of haematopoiesis -, enter the circulation, and may actively leave it, e.g. at a site of infection or injury[10]. Once crossed through the endothelium, they must actively migrate through the tissue to find invading pathogens and perform effector functions, but also to interact with other immune cells to direct, enhance or suppress an immune reaction.

A prerequisite for migration is the polarisation of the cell into a front and a back, which can either happen randomly and thus be short-lived or be influenced by external chemical or physical factors[11, 12]. After that, cell migration has been historically described in five successive steps[11] (**Figure 1**). Firstly, lamellipodia or filopodia, which consist of the cytoskeletal protein actin and its associated proteins, form at the cell's leading edge – this is called membrane extension or elongation. In this regard, lamellipodia are fast-moving and short-lived membrane extensions, which promote cell migration by attaching and pulling the cell body, while filopodia move slower, but are long-lived and direct cell migration[13]. With these protrusions, the cell can attach to the substrate at a point in front of it. Once these attachments are fully formed, myosin-based motors generate the contractile force to move the cell body into the direction of the protrusions. Subsequently, the adhesive attachments on the cell's rear are released and the cell translocates to the new position. Finally, all proteins needed for this process are re-used to start a new cycle of migration.

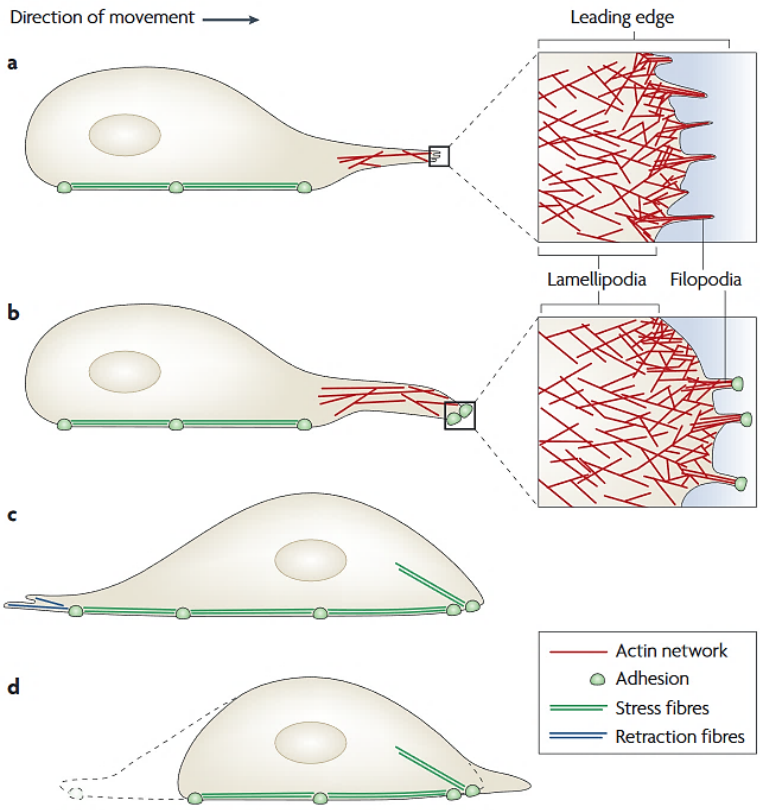

Figure 1: Schematic overview of cell migration.

Four of the five processes of cell migration. (**a**) During membrane elongation, lamellipodia or filopodia are formed at the cell's leading edge, which consist of the cytoskeletal protein actin and its associated proteins. (**b**) These protrusions allow the cell to adhere to the substrate. (**c**) Once these attachments are fully formed, contractile force is generated to move the cell body into the direction of the protrusions. This process is mediated by adhesion-associated stress fibres. (**d**) Subsequently, the adhesive attachments on the cell's rear are released and the cell translocates to the new position. In the end, all proteins needed for this process are re-used to start a new cycle of migration (not shown). This figure is adapted from [14].

Most processes in the organism are tightly regulated and the cells, thus, attracted to move into a certain direction. This is called directed migration and may be caused by e.g. extracellular, soluble (chemotaxis)[15] as well as immobilised molecules (haptotaxis)[16], density of the extracellular matrix (topotaxis)[17] or electric fields (galvanotaxis)[18]. Gradients of these cues are necessary to successfully guide a cell to a specific place. Additionally, cells may possess intrinsic directionality, which allows them to maintain a more direct path to their target[12]. But not all migrating cells move in a directed fashion. Random migration is characterised by the absence of a directional trajectory in the cell's movement, as well as multiple protrusions that allow the cells to change their path, which mostly occurs randomly[12]. This type of migration is also influenced by external cues if they appear uniformly. Furthermore, immune cells have been shown to randomly migrate *in vivo*[19, 20] and *in vitro*[2, 21], leading to the conclusion that this mechanism is important during immune surveillance.

Both types of cell migration are therefore highly important for the immune system in the dynamic processes during homeostasis and host defence.

1.2. The immune system – protector of the organism

The immune system encompasses a complex network of tissues, organs, single cells and molecules that collectively protect the host organism against diseases, not only caused by exogenous microbes, but also by degenerated host cells. Here, it is of utmost importance that the compartments of the immune system work tightly together to find and detect the pathogen, recruit other specialised cells and ultimately eliminate the threat in a timely manner. To ensure this, immune cells either actively patrol organs as highly specialised cells or can be transported via the blood vessel or lymphatic system that distributes them throughout the body. While immunity is generally divided into two compartments – the adaptive and the innate immune system –, they are hardly separated from each other. In fact, both parts share closely linked and interdependent mechanisms that enable a sufficient host defence.

1.2.1. Innate immunity

The innate immune system is a highly evolutionarily conserved mechanism that protects both vertebrates and invertebrates from infections[22]. It provides protection on several layers of defence, ranging from anatomic barriers, such as the skin, over chemical and enzymatic systems, e.g. complement, to specialised innate immune cells that coordinate the defence, once the first two barriers have been breached[23]. It is classically viewed as an unspecific, yet fast response to invading pathogens that does not form an immunological memory and reacts similarly in case of a second infection with the same pathogen[23].

The cells of the innate immune system, such as macrophages and granulocytes, recognise common structural components of the pathogen, so called pathogen-associated molecular patterns (PAMP) through pattern recognition receptors (PRR)[24], which can be localised on the outer plasma membrane, the membrane of the endosome or phagosome, or in the cytoplasm[25]. These germline-encoded PRRs detect a variety of molecules specific to bacteria, viruses and parasites[25]. In response to PRR stimulation, the production and release of cytokines is a major effector function of all immune cells. Cytokines are small proteins that may act on the cells themselves (autocrine), on adjacent cells (paracrine) or even on distant cells (endocrine) if they are stable enough[26]. Interleukins (IL) are a group of cytokines with a plethora of functions: they promote inflammation (IL-1, IL-6), reduce inflammation (IL-4, IL-

10, IL-12), induce cell growth and differentiation (IL-2, IL-5) and chemotaxis (IL-8, also termed CXCL8)[27]. Another versatile group are the tumour necrosis factors (TNF), consisting of TNF-α and TNF-β, which are both pro-inflammatory and promote migration[27]. Interferons (IFN) can be both pro- and anti-inflammatory and are vital during anti-viral immune responses[28]. Colony stimulating factors (CSF), such as granulocyte colony-stimulating factor (G-CSF) or granulocyte-macrophage colony-stimulating factor (GM-CSF), induce the production, differentiation and release of granulocytes[29] and monocytes[30]. A special group of cytokines are those that induce migration in the target cells, so called chemokines. They cause changes in cell adhesion and cytoskeletal rearrangements that allow the immune cells to move more freely[31]. They may guide cells of the innate and adaptive immune response and are important regulators of cell recruitment. Among those are C-X-C motif ligand (CXCL) 8, which induces migration in mainly neutrophil granulocytes[32], or C-C motif ligand (CCL) 5 that recruits eosinophil granulocytes[33] and T lymphocytes[34].

But innate immune cells do not only release cytokines. Most of them are professionals in engulfing and ultimately destroying a pathogen, a process called phagocytosis[35]. Macrophages are the major phagocyte population in the homeostatic tissue, where they patrol and phagocytose foreign pathogens and, in case of infection, recruit other immune cells to aid them[36]. Granulocytes, which will be discussed in greater detail under **1.2.1.1**, are highly important for the immediate responses to infection. Especially neutrophil granulocytes exhibit the greatest phagocytic activity and are the first to arrive at a site of infection as back-up[37]. Dendritic cells are part of the innate immunity, but their main task is to connect innate and adaptive responses by phagocytosis and antigen-presentation to adaptive immune cells[38]. They are found in peripheral and lymphoid tissues, such as the skin or the lymph node, where they patrol for tissue imbalances or activate T and B lymphocytes[38].

1.2.1.1. Granulocytes

Granulocytes are a family of myeloid, innate immune cells that were named for the large amount of small, membrane surrounded vesicles called granules in their cytoplasm. Granulocytes encompass neutrophil, eosinophil and basophil granulocytes, which were named based on their histological staining[39]. Another striking feature is their multilobed nucleus, whose functions are not yet fully understood[40, 41]. Granulocytes arise and mature in the bone marrow (BM), before they are released into the circulation[42]. Without exogenous stimulation, neutrophils circulate for a few days, before they undergo spontaneous apoptosis and are cleared from the blood system by phagocytes in the liver or spleen[43-45]. Eosinophil granulocytes, short eosinophils, however, leave the blood stream and migrate to the tissues,

where they accumulate, help in tissue homeostasis and eventually die[46]. As especially neutrophils are the first to arrive at a site of infection, granulocytes are specialists in migrating from the blood stream into the tissue in a process called extravasation[47] (**1.3**). Chemokines, such as CXCL8 for neutrophils[48] or eotaxins for eosinophils and basophils[49, 50], stimulate them to roll, firmly adhere and transmigrate through the endothelium and the tissue to a site of infection or an accumulation of damaged cells. On site, they may directly release toxic molecules to battle invading pathogens and perform effector functions like phagocytosis and cytokine release[51]. However, granulocytes are also known for the damage they inflict on healthy tissue and it is therefore of importance that their functions are tightly regulated, lest they do more damage than they do good[52].

1.2.1.1.1. Neutrophils

Neutrophils are, with about 70% of all leucocytes, the most abundant cell type in the healthy, human peripheral blood and are considered the first line of cellular defence of the immune system[53]. Due to their short lifespan (few hours up to days[47]), they need to be continuously produced and released from the BM, which is why a large portion of the BM is dedicated to the production of granulocytes, especially neutrophils[54].

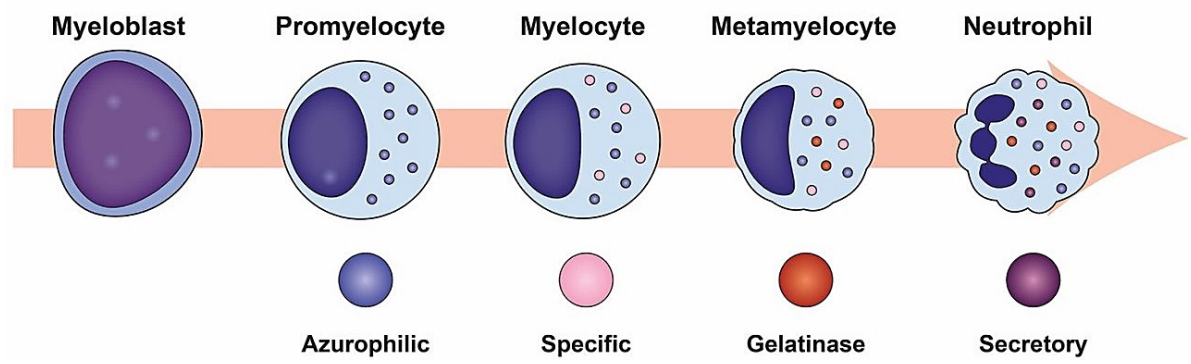

Figure 2: Neutrophil maturation process.

Neutrophils arise from the bone marrow, from haematopoietic stem cells, that commit to the granulocyte lineage by differentiation into multipotent progenitors and granulocyte-monocyte progenitors. Upon G-CSF stimulation, they further differentiate into myeloblasts, the first stage of neutrophil maturation. Promyelocytes follow the myeloblasts and generate primary, azurophilic granules. Then, they further mature into myelocytes that contain secondary, specific granules. Metamyelocytes finally generate the last granule type, tertiary, gelatinase granules. On the way to mature neutrophils, the nuclear shape changes from round to banded (banded neutrophil, not shown here) into its characteristic lobulated shape. Fully matured neutrophils also possess secretory vesicles that contain plasma proteins and membrane receptors. This figure is adapted from [55].

Haematopoietic stem cells (HSC) are the birth point for every blood cell[56]. On their way to neutrophils, HSCs differentiate into multipotent progenitors (MPP) that ultimately transform into lymphoid-primed multipotent progenitors (LMPP) and granulocyte-monocyte

progenitors (GMP), which commit to the neutrophil fate upon G-CSF stimulation[29] by differentiating into myeloblasts[54]. These myeloblasts mature into neutrophils via various stages that are well characterised based on the formation of neutrophil-specific granules as well as nuclear shape[55] (**Figure 2**).

Mature, human neutrophils strongly express surface receptors like cluster of differentiation (CD) 15[57], a glycan determinant expressed by human myelomonocytic cells, and CD16[42, 58], the Fcγ receptor III. To sense gradients of N-Formylmethionine-leucyl-phenylalanine (fMLP), a specific bacterial peptide, or of the C-X-C motif chemokines, such as CXCL1 and CXCL8, they express high levels of the fMLP receptor (fMLPR)[59] and the C-X-C chemokine receptors (CXCR) 1 and 2[60]. Furthermore, human neutrophils express CD11b, a subunit of the heterodimeric integrin, macrophage-1 antigen (MAC-1), which is expressed by almost all innate immune cells and is important during inflammatory processes, like extravasation and phagocytosis[61]. Additionally, neutrophils express the granulocyte specific CD66b, however its exact functions remain unclear[62]. Both are upregulated upon neutrophil activation[63]. L-selectin (CD62L) is expressed on almost all human leucocytes and plays an important role during leucocyte rolling and adhesion to the endothelium during extravasation[10]. CD62L is cleaved and shed rapidly after neutrophil activation[64], thus, functioning as an additional activation marker. In mice, mature neutrophils express the specific marker lymphocyte antigen 6 complex locus G6D (Ly-6G)[42], whose role in neutrophil biology and trafficking is not yet fully understood[65, 66].

Once a neutrophil leaves the BM, it is fully equipped with PRRs and antimicrobial granules to find and kill invading microbes. But neutrophils do not only release their numerous granules and vesicles to get rid of a pathogen, they may also engulf and digest microbes via phagocytosis[67]. Additionally, neutrophils are capable of a special kind of effector function that mostly results in their death; they can release so called neutrophil extracellular traps (NETs)[68]. In this process, DNA of different origins, nuclear or mitochondrial[69], is explosively released in spiderweb-like form from the neutrophil into the extracellular space[68]. This DNA is decorated with histones and antimicrobial enzymes normally contained in the neutrophil's granules and traps as well as kills microbes[68].

However, neutrophils gain rising awareness not only in terms of microbial defence, but as producers of cytokines and thereby the regulation of inflammation as well as their complex participation in diseases such as cancer[70]. Many cancers contain neutrophils, then termed tumour-associated neutrophils (TANs), and both tissue and blood neutrophilia are most commonly associated with a poorer prognostic outcome[71, 72]. However, neutrophils have also been reported to kill specific cancer cells[73], inhibit early carcinogenesis[74] and thus

be important for the rejection of different cancer types. How and why neutrophils react so diversely to cancers is still not completely understood and neutrophils subtypes, such as pro- and anti-tumour neutrophils, are hotly discussed[67].

1.2.1.1.2. Eosinophils

In contrast to neutrophils, eosinophils are rare cells making up under 1-3% of peripheral blood leucocytes[75]. However rare, this makes them no less important than other cell types. Eosinophils are well known for their role in host defence against infections with parasites, such as helminths[76]. On the other hand, they are most infamous for their involvement in allergy, their contribution to the development of asthma and gastrointestinal disorders[77].

Eosinophil development and maturation is very similar to that of neutrophils. HSCs differentiate into MPPs, but then develop along the erythro-myeloid lineage[54]. Finally, in the presence of IL-5[77], eosinophil-basophil progenitors[54] go through the same maturation process as neutrophils, from myeloblasts to mature eosinophils. Human eosinophils then express key receptors like C-C chemokine receptor type (CCR) 3[78] and sialic acid-binding Ig-like lectin 8 (Siglec 8)[79]. CCR3 binds ligands such as CCL5 (RANTES), CCL7 (MCP-3), CCL11 (eotaxin), CCL24 (eotaxin 2) and CCL26 (eotaxin 3) and is therefore responsible for eosinophil migration into and inside of the tissue. Furthermore, they were shown to express increasing levels of CD44 and CD69 upon activation following IL-5 stimulation and in diseases like asthma[80, 81]. CD44 is the receptor for hyaluronic acid, which is widely expressed on leucocytes and best understood in its role in T cell migration and activation[82]. CD69 is also termed the early activation antigen for very early expression in activated T cells, where it acts as a costimulatory molecule during further activation and maturation[83].

Recent reports describe an emerging role of eosinophils in human cancer and experimental mouse models for cancer. They are present in both solid and haematologic tumours, as some tumours and tumour-associated cells can recruit eosinophils from the circulation by release of, e.g. CCL24, CCL11, vascular endothelial growth factor or histamine[84]. On site, eosinophils seem to mostly exert anti-tumorigenic functions. Several human cancers are associated with a good prognosis, e.g. gastric, colorectal or breast cancer, while others, such as Hodgkin's lymphoma, are associated with a bad prognosis if eosinophils are present in the tumour[85]. In black skin cancer, melanoma, eosinophils have been reported to facilitate tumour rejection by recruitment of $CD8^+$ T cells from the blood via production of chemokines and their contribution to vessel normalisation[86]. Thus far, it is reasonable to appreciate them as important bystander cells that are equipped to kill cancer cells[87], but are more likely to modulate the tumour microenvironment by recruitment of other immune cells.

1.2.2. Adaptive immunity

What is known as the adaptive branch of the immune system is, phylogenetically, much younger than its innate brother[88]. It is, as the name suggests, much more adaptive in its response to threats and characterised by slower, but more durable response kinetics and the formation of an immunological memory[89]. This great variability originates from a substantial difference between innate and adaptive immune cells. Where innate immune cells sense pathogens via PRRs, adaptive immune cells are additionally equipped with custom tailored and unique receptors that allow them to detect a specific antigen on a specific pathogen[89]. The refinement of these receptors is also the reason for the much longer response time of adaptive immune cells towards an inflammation. However, once fully formed, the receptors are highly specialised and the cells very proficient in detecting and eradicating foreign pathogens or rogue host cells[89]. The cellular effectors of the adaptive immune system are T and B lymphocytes[89]. Both originate from the BM, but while B cells complete their initial development there[89], T cell progenitors migrate to the thymus, where they undergo maturation and selection[90]. After this, both T and B cells are mostly encountered in the secondary lymphoid organs, such as lymph nodes and the spleen, where they patrol for their specific antigen in the lymph and blood. While B cells are mainly responsible for producing and secreting antibodies[91], the humoral branch of the adaptive immunity, T cells, which will be discussed in the next section, execute versatile functions, such as killing, helping, and modulating the immune response.

1.2.2.1. T lymphocytes

The characteristic feature of T cells is their expression of a clonally distinct T cell receptor (TCR) that defines their specificity and affinity to a certain antigen[92]. During development in the thymus, this TCR is rearranged and tested for antigen binding and self-tolerance[93] before naïve T cells are released into the periphery. With age, however, the thymic T cell output and the abundance of naïve T cells[94] in the blood decline in humans, which is partially equalled by a peripheral production of naïve T cells in humans[95, 96]. This, along with immunosenescence and decreasing functionality, contributes to higher susceptibility to infection and immune dysregulation with higher age[97].

T cells can be generally subdivided into antigen-inexperienced, naïve cells, memory cells and regulatory cells[97]. Naïve T cells respond to new antigens that are encountered by the organism, while memory T cells have already recognised an antigen, have undergone affinity maturation and subsequent selection and maintain the long-term memory[97]. Regulatory T

cells are responsible for preventing overshooting immune responses, resolving inflammation and enforcing self-tolerance[97].

Furthermore, based on the expression of their co-receptors for the TCR and their function, T cells can be divided into $CD4^+$ and $CD8^+$ cells[97]. $CD4^+$ T cells, also called T helper cells, recognise major histocompatibility complex (MHC) class II loaded with short peptides[98]. MHC II is expressed mostly by antigen-presenting cells, such as especially dendritic cells, but also B cells or macrophages[99]. Thus, they essentially support the immune response by helping and activating other T lymphocytes, as well as modulating inflammation via the release of cytokines and chemokines, which in turn recruit and activate cells of the innate immunity, such as neutrophils, eosinophils or macrophages[100].

$CD8^+$ T cells, the cytotoxic T cells, bind peptides loaded onto MHC class I, which is expressed by all nucleated cells of the body[101]. They kill host cells that have been infected by intracellular pathogens, such as viruses, or show signs of degeneration, such as malignant transformation[101]. Once they recognise their antigen, they produce pro-inflammatory cytokines, such as TNF-α or IFN-γ, and kill their target either by expression of cell death-inducing ligands, such as the Fas ligand, or release of their cytotoxic granules[102]. These granules contain perforins and granzymes that jointly induce apoptosis or lysis of the target cell[102]. In case of infection, specific, naïve $CD8^+$ T cells are primed in secondary lymphoid organs, such as the lymph nodes, where they interact with antigen-presenting cells that present fragments of an invading pathogen the TCR may recognise[97]. This recognition, alongside co-receptor and cytokine stimulation, results in a drastic proliferative burst, the expansion phase, and maturation of the antigen-stimulated T cells[103]. These activated $CD8^+$ cells then actively migrate from the secondary lymphoid organs into the periphery, where they are recruited to the site of infection by other immune cells, such as $CD4^+$ T cells[104] or eosinophils[86]. On site, they perform their effector functions, such as target cell killing, but are also able to protect the organ from extensive damage[105]. After their work is done, most effector $CD8^+$ T cells become apoptotic and die, while some survive and make up the immunologic memory for future infections[106]. These central memory T cells are long-lived and will persist in the body for extended periods of time[107]. In case of re-infection, central memory cells are activated and can respond to the infection faster and more rigorously[107].

1.3. On the move – migration in the immune system

For all the above-mentioned processes, migration is essential for the involved immune cells to reach a site of infection, communicate with each other or find and eliminate invading pathogens. Migration encompasses more than just cytoskeletal rearrangements, it also

means breaking the BM retention, crossing the normally impermeable blood vessel system and basal membrane, and orient and move inside the complex tissues of an organism. HSCs are kept in the BM by interaction of their receptor CXCR4 with stromal cell-derived factor 1 (SDF-1, CXCL12), which is produced by BM stromal cells. All descendants of HSCs must break the CXCR4-CXCL12 axis to leave the BM and enter the circulation[67]. For example, neutrophil release from the BM is induced by G-CSF[108], which interferes with the CXCR4-CXCL12 interaction[109] and results in upregulation of CXCR2 ligands on endothelial cells outside the BM[110]. This cuts the tethers of neutrophils in the BM and leads them directly to the blood vessels, where they actively migrate through sinusoidal endothelium to rapidly enter the blood stream[110, 111].

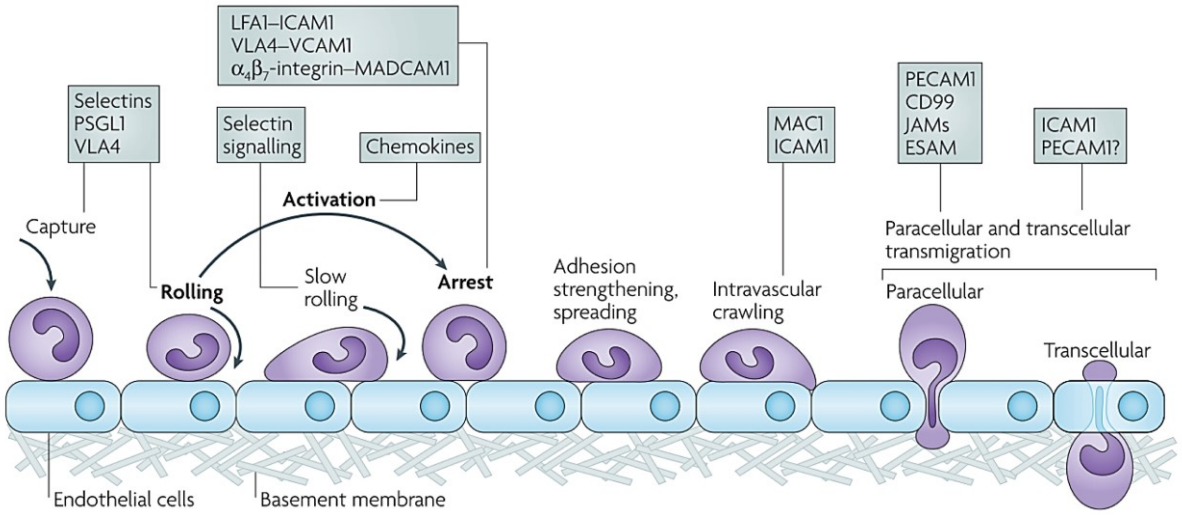

Figure 3: The leucocyte adhesion cascade.

The adhesion and transmigration of leucocytes through the endothelium is a multistep process of interconnected interactions between the migrating leucocyte and the endothelial cells. First, immune cells are captured and roll along the endothelium via weaker interactions between glycoproteins called selectins and their glycosylated ligands. These interactions are strengthened by intracellular signalling and activation of the rolling leucocyte by chemokines which decorate the endothelium. Cell-adhesion proteins, such as integrins, facilitate a tighter binding and ultimately the arrest of the leucocyte on the endothelial cells. Immune cells are then able to crawl along the endothelium, which requires the interaction of ICAM-1 and MAC-1. Finally, the cells transmigrate through the endothelial cells, either paracellularly or transcellularly, and exit the vascular basement membrane at sites of lower density. This figure is adapted from [10].

Through the blood circulation, immune cells are distributed throughout the body. In case of infection, the cells are equipped to leave the circulation and enter the tissue in a tightly regulated process known as the leucocyte adhesion cascade[10] (**Figure 3**). This process relies on a fine-tuned interaction between selectins as well as integrins and their ligands. Capture and rolling on inflamed endothelium depend on selectins, such as L-selectin (CD62L) on immune cells and P-selectin or E-selectin expressed by endothelial cells, as well

as integrins like lymphocyte function-associated antigen 1 (LFA-1) or very late antigen 4 (VLA-4) on immune cells[10]. Selectins are glycoproteins which interact with glycosylated ligands, such as P-selectin glycoprotein ligand 1 (PSGL-1) on immune cells[112] and endothelial cells or glycosylated CD44 on immune cells[113]. This also leads to secondary capture of circulating leucocytes by already captured or rolling leucocytes via interaction of L-selectin with PSGL-1[114].

Integrins, on the other hand, are heterodimeric receptors, which bind ligands such as vascular cell-adhesion molecule 1 (VCAM-1) or intercellular adhesion molecule 1 (ICAM-1)[10]. Both, selectins and integrins, work in concert to facilitate rolling, slow rolling and ultimately arrest. This last step requires the presence of chemokines and other chemoattractants, in addition to the interaction of selectins and integrins[115]. These chemokines decorate the endothelial cells, activate the rolling immune cells and lead to an increased affinity of integrin interactions, thus facilitating arrest and adhesion strengthening under blood flow conditions[116]. However, transmigration, the eventual crossing of the endothelial barrier, does not necessarily occur at the place of rolling or arrest. In fact, neutrophils have been shown to probe or scan their surroundings, once arrested on the endothelium[117]. They crawl perpendicular to the blood flow, reliably finding the next cell-cell junction between two endothelial cells through which they may transmigrate[47, 117]. This active crawling is facilitated by the interaction of ICAM-1 on the endothelium and MAC-1 on the neutrophil[118].

Finally, leaving the blood vessel system means crossing the vascular endothelium and its basement membrane. Transmigration is dependent on cell-adhesion molecules, like ICAM-1 or VCAM-1, as well as proteins present in the endothelial cell-cell junctions, which essentially guide immune cells through the tight, normally sealed spaces between two endothelial cells[10]. In addition to this paracellular route, neutrophils have also been reported to use transcellular gateways to migrate directly through endothelial cells, instead of around them[119]. However, this only seems to occur in the minority of transmigration events[47]. To cross the vascular basement membrane, immune cells have been shown to preferentially exit at sites of lower basement membrane density[120]. These are poorer in extracellular matrix proteins and show overlaps with the gaps between pericytes, which line the endothelium, thus representing the easiest path for immune cell exit into the tissue[121]. After leaving the vessel, the cells must incorporate a plethora of new signals, as well as discard the old ones that have brought them over the endothelial barrier. In fact, strongly infection-related chemotactic molecules, such as fMLP, can essentially override the endothelial signals[122] and therefore lead the immune cell, in this case a neutrophil, to its final target.

These are only two examples, but they already highlight the importance of cell migration in basic immune system functions, such as cell release from the BM and cell recruitment to a site of infection. Furthermore, T lymphocytes, on their quest to find their antigen in the periphery, actively migrate and scan secondary lymphoid organs for antigen-presenting cells with whom they can interact[123]. Therefore, it is essential for immune cells to be able to migrate and integrate the signals around them to successfully reach their destination so that they may execute their effector functions properly.

1.3.1. Immune cell migration in acute and chronic diseases

Changes in the migration patterns of immune cells are among the most commonly observed phenomena in human diseases and mouse models. In fact, this seems natural as immune cells are the first to react to an ongoing disease setting, often before any symptoms have manifested. These changes have also been exploited on the quest for new therapeutic targets[124]. As some diseases, such as ischemia / reperfusion injury, multiple sclerosis or Crohn's disease, are linked to an overshooting reaction of the immune system against itself, the infiltration of immune cells has been targeted to open new treatment options[124]. Blocking the entry of neutrophils, via selectin, integrin or chemokine receptor blockage, into ischemic areas in mouse models has elicited considerable protection against further damage, yet this did not wholly apply for the translation into human therapies[125]. However, blocking the migration of pro-inflammatory T cells and macrophages during Crohn's disease[126] or multiple sclerosis[127] yielded more promising results. Notwithstanding, these therapies have a serious downside. Blocking the infiltration into organs on a systemic level leads to defective migration into every other organ as well, therefore evoking serious complications such as increased susceptibility to infections[124] and even recurrence of life-threatening, so far dormant viruses, such as human polyomaviruses[128].

Besides its therapeutic potential, immune cell migration is, theoretically, an excellent early warning system for detrimental patient progression or relapse. Multiple studies have already been conducted to evaluate the clinical relevance of immune cell migration. For example, neutrophils were shown to migrate less in severe sepsis cases[129] and in asthma patients[130], while their migration was increased in inflammatory bowel diseases[131]. Also, T cell migration was accelerated in e.g. multiple sclerosis[132] and inflammatory bowel disease[133]. Thus far, the assessment of immune cell migration has not been implemented into routine clinical applications, mostly due to lack of equipment, of rigorous standardisation and of indications for further treatments.

1.4. Analysing cell migration

An assay to assess cell migration must be carefully tailored to the scientific question at hand. It is therefore important to consider the advantages and disadvantages of each method, as well as include the availability of biological material needed for a specific analysis, e.g. mouse models or human samples. There are two main angles from which to determine cell migration: endpoint and live cell measurements. While the former is very versatile and can be investigated with different kinds of methods, the latter revolves all around imaging techniques of living cells.

1.4.1. Endpoint measurements

Endpoint measurements seek to describe the outcome of migration events[134]. Mostly, this is done by investigating the presence of e.g. immune cells after a specific treatment at the site of interest, e.g. an organ. As this is a very basic principle, the downstream applications are highly adaptable.

Flow cytometry is a broadly used tool to study the composition of single cell suspensions, which can be generated from solid organs. By staining with fluorescently labelled antibodies, subsets of cells can be identified and described[135]. The depth of this analysis depends entirely on the number of investigated epitopes. However, creating a single cell suspension from an organ is not trivial, especially as the cells must stay intact and unperturbed for the coming analysis. Additionally, flow cytometry can give no information on the original localisation of the cells as well as their neighbourhood within the organ.

Imaging techniques can retain the architecture of the organ, while simultaneously providing insight into its anatomy and cellular composition. Most widely employed are histological or immunohistological approaches[136], which involve the embedding and cutting of the tissue of interest into thin slices. These are then further processed to highlight specific structures within tissue, e.g. nuclei, proteins, organelles, cell surface receptors and others, while giving an overview of the tissue architecture[136]. While histology allows the analysis of cellular localisation and abundance, it is a 2-D approach, that can be taken to the third dimension by sequential slicing of the tissue into many single sections. All of these must be imaged and analysed afterwards, which is time-consuming, costly and prone to error. Recent developments in optical clearing and 3-D imaging have revolutionised the analyses of whole organs[137] or even entire organisms[138], by enabling the visualisation of both the overall architecture as well as single cells. In this regard, the combination of tissue clearing and light sheet fluorescence microscopy (LSFM) are now well established[139].

Endpoint analysis of cell migration is however not restricted to organisms and organs, but is readily applicable for primary, isolated cells or cell culture. Here, the most famous representative are workflows based on the original published by Stephen Boyden in 1962[140], also called Boyden or trans-well assay. The core of this assay is a two-chamber system that consists of a, mostly, multi-well cell culture plate and an insert for each well[140]. The chambers are separated by a membrane or small pores that the cells must pass in order to migrate from the upper chamber, where they are seeded, to the lower chamber, where a stimulus has been applied. Numerous approaches exist to modify this system to mimic migration through e.g. extracellular matrix proteins[141] or monolayers of epithelial cells[142]. Subsequently, the cells that reach the lower well are quantified after different timepoints, thus providing the number of migrating cells as well as a proxy for their speed[143, 144].

1.4.2. Live cell imaging

In contrast to the methods mentioned above, the analysis of live cell migration requires direct imaging[134]. With the advent of multi-photon microscopy, cell migration analysis in living animals has yielded unprecedented insights into the steady-state and disease-altered migration of various immune cell subtypes[145]. This intravital imaging, however, requires, first and foremost, the availability of the organ to the microscope, while it is still inside the living animal and functioning properly. Various protocols have sought to overcome this obstacle for easier organs, such as the skin[146], but also for the ones that are harder to reach, like bone[110], lung[147] or brain[148]. Intravital microscopy has also been employed on humans, e.g. muscle cells[149] or during intraoperative investigations of tumours[150]. In addition to multi-photon microscopy, LSFM has also been used to study the migration of cells in inherently transparent organisms, such as zebra fish larvae[151] or drosophila[152].

However, before there was intravital microscopy, scientists relied on *in vitro* assessment of live cell migration, which can be performed with either primarily isolated cells or immortalised cell lines, using time-lapse video microscopy[134]. With this technique, the desired location is imaged for a fixed amount of time with images being taken in a chosen interval. Coupled to motorised tables, this setup is capable of imaging different locations with the limiting factor being the interval time between the images. For the assessment of their migration, the cells do not necessarily have to be fluorescently labelled and these assays can move from 2-D[153], where cells only adhere on the plastic of the cell culture dish, to 3-D[154], where they are plated in a gel to mimic the extracellular matrix. Furthermore, similarly to the Boyden chamber approach, systems exist to create gradients of attracting or repelling agents to study live directed cell migration, e.g. µ-Slide chemotaxis chambers by ibidi. As

with all *in vitro* approaches, video microscopy does not fully represent the processes that occur in an organ or the entire organism[134]. However, these methods are well suited for fast screening approaches or basic research.

1.5. Investigated diseases

This thesis includes the analysis of immune cell migration in the frame of two sterile inflammatory conditions, myocardial infarction and cancer. These diseases either directly affect the investigated immune cells, e.g. leukaemia, or involve them through recruitment and on-site effector functions, e.g. melanoma and myocardial infarction. As these diseases are quite different from each other, the following chapter seeks to cover the basis of each of them.

1.5.1. Leukaemia

1.5.1.1. Myelodysplastic syndromes

Myelodysplastic syndrome (MDS) is the collective term for a variety of BM disorders that culminate in its inability to produce fully matured blood cells during haematopoiesis[155]. This results in the lack of peripheral blood cells, cytopenia, depending on which kind of blood cell is affected. Additionally, due to clonal instability that caused MDS in the first place, the risk of transformation to acute myeloid leukaemia (AML) is high[155, 156]. MDS is more common in elderly people between 60 – 80 years and men are more often affected than women[155, 156]. Due to cytopenia, patients suffer from excessive bleeding, if thrombocytes are affected, and increased risk for infections, if immune cells are affected[155].

MDS is diagnosed based on a collective assessment of peripheral blood and invasive BM aspirates and biopsies[155, 156]. Here, peripheral cytopenia and the number of immature cells in BM, called blasts, as well as cytogenetics to determine mutational load are assessed to formulate a diagnosis, calculate the risk for AML transformation and select a therapy. The revised international prognostic scoring system (IPSS-R)[157] was devised to help with the prognostic scoring of MDS patients. The IPSS-R utilises the clinical variables, such as cytogenetics, number of BM blasts, peripheral blood parameters, as well as age and gender, to generate a score for each category, ranging from 0 to 4[157]. Based on these scores, the risk category for the individual is defined, from very low (score ≤ 1.5) to very high (score > 6)[157]. This risk category directly describes the patient's overall survival and risk for AML transformation[157].

As MDS is such a heterogenous disease, its treatment is equally as diverse, but limited[156]. Transfusions are often used to supplement the patients with the needed peripheral blood

cells that the BM fails to produce[156]. Additionally, agents that stimulate blood cell maturation, such as erythropoietin and GM-CSF[158], or immunomodulatory agents, like lenalidomide[159], show good responses especially in lower risk MDS. Hypomethylating agents, like 5-azacytidine, are approved for most of the MDS subtypes and result in prolonged time to AML transformation and haematologic improvement[160]. As a last resort, the patients may receive haematopoietic stem cell transplantation or intensive chemotherapy, if no donor is available[156]. MDS still lacks more adequate treatment options and thus research into this direction is imperative. Furthermore, additional, more readily accessible scoring factors would facilitate clinical work and reduce the burden that repetitive BM biopsies and aspirates impose on the patients.

1.5.1.2. Atypical chronic myeloid leukaemia

Atypical chronic myeloid leukaemia (aCML) is a rare subtype of myelodysplastic / myeloproliferative neoplasms that has a poor prognosis and no established standard of care[161, 162]. Predominantly, aCML occurs in male, elderly patients between 60 – 76[163]. In contrast to MDS, its characteristics are an elevated white blood cell (WBC) count, mainly due to increased granulocyte numbers, splenomegaly and severe dysgranulopoiesis[163, 164]. aCML patients suffer from recurring, badly controlled infections, but normally present with general symptoms, such as night sweats, malaise or fatigue[161]. The lack of distinct genetic defects to diagnose aCML, which would results in potential therapeutic targets, complicates clinical work further[163]. However, some aCML cases seem associated with mutations of spliceosome proteins, epigenetic modifiers or signalling molecules, like colony-stimulating factor 3 receptor (CSF3R)[165]. Especially the mutation status of CSF3R in aCML is controversially discussed, as certain CSF3R mutations are used to characterise chronic neutrophilic leukaemia (CNL)[166]. The patient investigated in this thesis had a CSF3R T618I mutation, which is a membrane proximal mutation that causes ligand-independent activation of the down-stream signalling janus kinase (JAK) / signal transducers and activators of transcription (STAT) pathway, predominantly JAK1/2[167]. This, in turn, leads to unchecked proliferation of neutrophils. In this regard, Ruxolitinib, a JAK1/2 inhibitor, has been tested as a therapeutic option as it was able to potently control the leukaemic burden in a few studies of CNL[168, 169]. Because of these promising reports, Ruxolitinib is currently in clinical trials for CNL and aCML patients with CSF3R mutations (NCT02092324).

However, despite supportive care, haematopoietic stem cell transplantation and standard cytoreductive therapies, aCML remains without adequate treatment options[170] and stud-

ies elucidating underlying genetic and cellular mechanisms in aCML progression would facilitate clinical work and improve the patients' therapy options.

1.5.2. Melanoma

Based on the GLOBOCAN cancer estimates of 2018, melanoma is the 8th most common cancer across all ages and genders and accounts for 1.7% of cancer-related deaths annually in Europe[171]. Even though non-melanoma skin cancers are much more common (14.8% in Europe), they have a lower mortality rate (0.6% in Europe), which makes melanoma the most dangerous form of skin cancer[171-173]. The major risk factor for melanoma is increased ultraviolet (UV) radiation by high sun exposure or indoor tanning, but also the presence of moles, fair skin type and a personal history with melanoma[174].

1.5.2.1. Development of melanoma

Melanocytes are distributed along the basal membrane of the epidermis, but also elsewhere, e.g. in the eye or the inner ear. They originate from the neural crest and produce melanin, a dark pigment that gives the skin its colour and absorbs UV light, thereby protecting the deeper skin layers from UV-induced deoxyribonucleic acid (DNA) damage[175]. They normally divide very slowly[176], but structurally normal melanocytes may accumulate in clusters (benign naevi or moles), caused by local proliferation of melanocytes[177] (**Figure 4**).

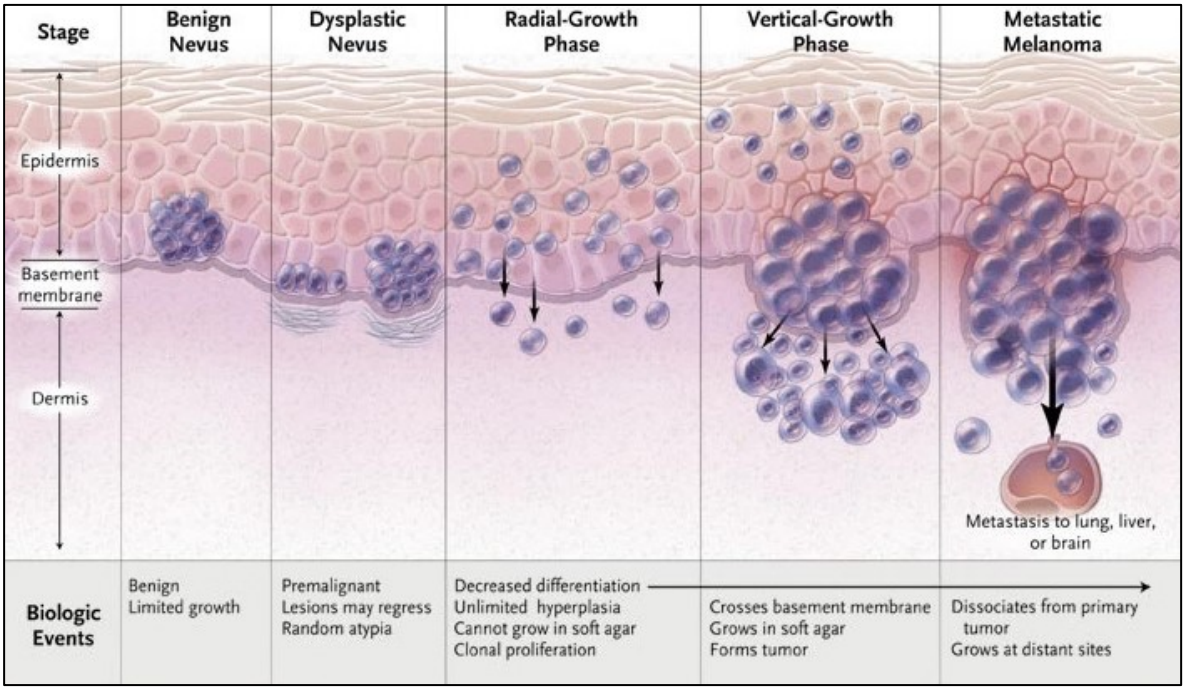

Figure 4: Schematic of melanoma progression.

Malignant melanoma starts off as a benign naevus, basically a skin lesion caused by proliferation of structurally normal melanocytes. Benign naevi exhibited limited growth, may be flat or slightly

raised, are of uniform or regular colouration and occur along the basal membrane. Due to genomic mutations, the nevus enters the dysplastic stage, where the cells start to proliferate, sometimes even at new locations. In the radial-growth phase, the cells grow into the epidermis and single cells may penetrate the dermis. The next stage, the vertical-growth phase, is characterised by dermal invasion and the ability to form tumours in immune-compromised mice. Metastatic melanoma is the very last stage of this disease model, where the cells may leave the primary tumour and form metastases in distant organs, like lung, liver or brain. Each step is accompanied by a complex set of genetic mutations that allows the cells to enter the next stage. This figure is adapted from [177].

This proliferation is most commonly induced by mutations that activate the mitogen-activated protein kinase (MAPK) pathway[178, 179], a central signalling hub that communicates signals from the extracellular space via signalling receptors to the nucleus to induce target transcription. Importantly, the MAPK pathway is responsible for cell proliferation induced by growth factors[180]. Hence, a large variety of cancers exhibit mutations that abnormally activate the MAPK pathway, such as BRAF or N-RAS mutations, and therefore lead to uncontrolled cell proliferation[177]. The next stages towards metastatic melanoma are characterised by the formation of naevi with structural anomalies, decreased differentiation and exit from the cell cycle, as well as clonal expansion[177]. The cells start disseminating and invading beyond the basal membrane into the dermis and ultimately the lymphatic or blood vessel system[181].

1.5.2.2. Classifications

Melanoma is traditionally diagnosed by histopathology of biopsies from irregular skin lesions and the draining lymph node[174]. This diagnosis is based on three criteria: the thickness of the primary tumour; whether or not metastases have reached the draining lymph node and finally the metastasis status to distant sites, such as distant skin areas, the lung or the brain[174, 182]. According to this, the patients are then grouped into stages, ranging from Stage 0 (intact basal membrane, no lymph node involvement or metastases) to Stage 4 (distant metastases)[182]. Furthermore, the presence or absence of key genetic alterations, such as BRAF mutations, are tested to determine whether the patient might benefit from targeted therapy against this special mutation, e.g. BRAF inhibitors[174].

1.5.2.3. Treatments

Most melanomas are detected early during routine check-up by an experienced physician[174]. These are easily cured by wide local excision with safety margins depending on the tumour thickness[174]. However, once melanoma metastasises, it is increasingly hard to treat. Depending on the mutation status of the primary tumour, BRAF inhibitors, mostly in com-

bination with MEK inhibitors, are employed which show high response rates in tumours positive for BRAF V600E[183, 184].

Beyond this, recent developments in the understanding of T cell biology and exploitation of this knowledge have driven systemic cancer therapy to new heights. Tumour cells, tumour-associated immune cells and cytotoxic, $CD8^+$ T cells share a complex relationship[185] (**Figure 5**).

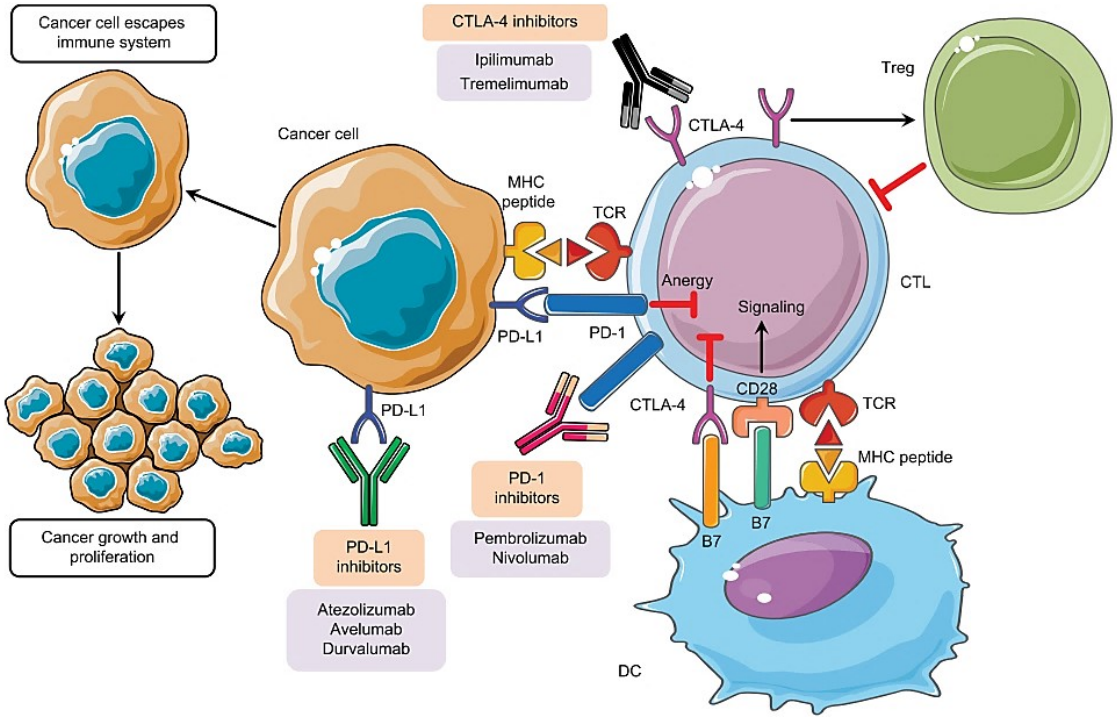

Figure 5: Tumour immune evasion and immune checkpoint inhibitors.

Tumour cells, their associated immune cells and $CD8^+$ T cells, which are responsible for killing rogue host cells, share a complex relationship. Cancer cells may escape immune surveillance by expressing immune modulatory molecules, such as PD-L1 that, if binding to its receptor PD-1 on T cells, triggers anergy and exhaustion. On the other hand, $CD8^+$ T cells may express inhibitory molecules like CTLA-4 due to overexposure to their antigen, which competes with the co-stimulatory CD28 for the binding of the B7 complex on dendritic cells or macrophages. Furthermore, regulatory T cells (T_{reg}) also act via CTLA-4 and inhibit $CD8^+$ T cell function. This causes the cancer cells to grow and proliferate uncontrollably. However, these immune checkpoints, which are crucial to resolve and confine an ongoing inflammation, may be blocked by suitable blocking antibodies. This unleashes the power of $CD8^+$ T cells on the tumour and leads to tumour shrinkage and clearance. This figure is adapted from [185].

Tumour cells may express restrictive molecules, such as the programmed cell death protein 1 ligand 1 (PD-L1) that, if binding to programmed cell death protein 1 (PD-1) on $CD8^+$ T cells, directly inhibits the $CD8^+$ T cell in its function[186]. Triggering of these immune checkpoints is therefore viewed as an immune-evasive strategy. Furthermore, $CD8^+$ T cells can be restricted by their expression of cytotoxic T-lymphocyte-associated protein 4 (CTLA-4)[187], which binds to the B7 complex on dendritic cells or macrophages and inactivates $CD8^+$ T

cells[188]. The antibody-mediated blocking of these targets, CTLA-4, PD-1 and PD-L1, unleashes the power of the adaptive immune system and enables $CD8^+$ T cells to kill their target cells with high efficiency. This has revolutionised the field of systemic anti-cancer therapy[174].

However, this power comes at a cost. Under non-cancer conditions, these immune checkpoints are important in enforcing self-tolerance[189]. If this control is removed, the cells do not only react to cancer cells, but to all entities that trigger their TCR. These so called immune-related adverse events (irAE) mostly occur at sites of environmental exposure, such as the gastrointestinal tract, the lungs and the skin, but also liver, heart and endocrine organs[190]. Overall response rates, especially for combination therapies of CTLA-4 and PD-1 blocking antibodies, are quite high (56% – 59%)[174]. However, it is still unclear whether and why a patient will respond to immune therapy or not. Hence, reliable biomarkers to either pre-test the susceptibility of a patient to ICBT, predict the therapy outcome or the occurrence of irAE early during ICBT are sorely needed.

1.5.3. Myocardial infarction

Coronary heart disease is still the leading cause of death worldwide, with myocardial infarction (MI) as its most common form. Even though the incidence of MI is declining in industrialised countries[191], it is increasing in developing countries, where 80% of worldwide deaths occur from cardiovascular disease [192]. MI is defined as local dysfunction and ultimately death of the myocardium due to a shortage of blood supply, ischemia, by the coronary arteries. This is caused by dropping oxygen concentration and therefore the termination of the energy-providing oxidative phosphorylation in cardiomyocytes[193]. However, under 15 minutes of ischemia causes reversible damage and the afflicted tissue may be completely salvaged[194]. MI is caused by occlusion of the coronary arteries, most commonly by a fatty coronary plaque or thrombus[195]. Risk factors are, among others, old age, male gender, smoking or alcohol drinking, as well as high blood pressure and cholesterol[196].

MI is normally treated by unblocking the affected vessel and allowing reperfusion of the undersupplied tissue, reducing the risk of other thrombi due to cardiac arrhythmia and preventing further MIs[197]. The occluded coronary artery is most commonly unblocked via percutaneous coronary intervention, which uses catheters to insert a stent into the narrowed vessel and re-open it or, in rare cases, via fibrinolysis (thrombus) using e.g. tissue plasminogen activator[197]. However, the restoration of perfusion (reperfusion) after MI may inflict damage on the myocardium and the vasculature, the so-called ischemia / reperfusion injury (I/R injury)[198, 199]. The release of molecules normally retained inside the cells, damage-

associated molecular patterns (DAMP), activate the endothelium, which in turn leads to recruitment of immune cells, such as neutrophils, following reperfusion[200]. Additionally, reactive oxygen species (ROS), which are produced by undersupplied cardiac cells[194], but also endothelial cells[201] and invading neutrophil granulocytes[202], are a main cause for further damage following I/R, as they lead to extensive tissue damage and further cell death[203].

During the early stages of reperfusion, the inflammatory phase, neutrophils massively infiltrate into the damaged tissue and inflict further tissue damage by releasing ROS and matrix metalloproteases[200]. Pro-inflammatory monocytes arrive shortly afterwards, which differentiate into pro-inflammatory macrophages and dendritic cells on site[204]. However, during later stages of I/R, monocytes enter the tissue that exert more reparative roles and support healing of the infarcted tissue[204]. Yet, also neutrophils play a role in healing, as apoptotic neutrophils are phagocytosed by macrophages, which induces anti-inflammatory, pro-healing responses[205].

In spite of this, large parts of the influence of immune cells on cardiac damage and healing remain elusive. The depletion and manipulation of neutrophils during MI yields inconclusive results[206-209] and the exact pathways that underlie their diverse functions are only poorly understood. In this regard, understanding the precise kinetics and interplay of neutrophils with the injured myocardium and epithelium is of utmost importance.

2. Aim

Motility is an intrinsic and central ability of immune cells. During steady-state, immune cells patrol the organism in search of invading pathogens or rogue cells. This migration pattern is highly dynamic and can adapt to changes occurring in the whole body. During an infection, for instance, tissue-resident immune and non-immune cells sense the pathogen and signal for backup to immune cells in the blood. This changes their motility pattern and allows them to roll and adhere to the blood vessels closest to the target site, transmigrate and move through the tissue in a directed fashion.

During this process, both the affected organ and the blood immune cells are subject to changes. These two entities can be investigated to study immune cell migration either while it occurs (live) or after it has occurred (endpoint). On the organ level, changes in endothelial permeability and expression patterns, immune cell distribution and microenvironment take place that are mostly investigated by endpoint measurements. However, when looking at single cells, observing the changes while they occur yields more information.

This thesis explores and compares two possibilities to assess immune cell migration in mouse and man and seeks answers to the following questions: What impact do diseases, like leukaemia or solid tumours, have on the live immune cell migration and the activation status of peripheral blood immune cells? Can these changes be quantified, and live immune cell migration assays be standardised? Is immune cell migration a biomarker to be used in patient diagnosis and disease progression? How can we investigate endpoint immune cell migration into an organ in three dimensions? How can we quantify the distribution pattern in a relatable manner?

Finding answers to these questions will improve diagnostics and may predict treatment success in humans as well as open new treatment options by further understanding the role of immune cells in mouse models.

3. Methods

3.1. Human studies

Blood samples from healthy control patients were either provided by the Institute for Medical Informatics, Biometry and Epidemiology (IMIBE) as part of the Heinz-Nixdorf Recall MultiGeneration (HNRM) study or by the blood donation centre, both at the University Hospital Essen (Essen, Germany). Blood samples from patients suffering from metastatic malignant melanoma (Stage 3 and 4) undergoing immune checkpoint blocker therapy were obtained from the skin cancer Biobank (SCABIO) at the University Hospital Essen (Essen, Germany). Samples from MDS patients were obtained from the Düsseldorf MDS registry of the Düsseldorf University Hospital (Düsseldorf, Germany). Blood samples from the aCML patient were obtained in cooperation with Dr. Joachim Göthert of the University Hospital Essen (Essen, Germany).

3.1.1. Ethics committee approval

This study was approved by the relevant institutional ethics committees at the University of Duisburg-Essen. Written informed consent was obtained from all participants. Identification numbers of ethical approvals/registers: 15-6686-BO (HNMR samples, Essen, Germany), 16-6982-BO (aCML samples, Essen, Germany), 3768 (MDS samples, Düsseldorf, Germany), 17-7497-BO (ICBT samples, Essen Germany).

3.1.2. Blood Transport

All blood samples were obtained in ethylenediaminetetraacetic acid (EDTA)-supplemented tubes and transported for 30 minutes (min) up to 1 hour (h) in a VACUETTE® transport container (Catalogue number (Cat. No.): 800110, Greiner Bio-One, Kremsmünster, Austria) according to the UN 3373 regulation.

3.2. Animal studies

All animal experiments were conducted in cooperation with the Department of Cardiology and Vascular Medicine, University Hospital Essen, Essen, Germany. They were approved by the responsible governmental agency, the Ministry for Environment, Agriculture, Conservation and Consumer Protection of the state of North Rhine-Westphalia (MULNV) and complied with all relevant ethical regulations for animal testing and research.

3.2.1. Ischemia/Reperfusion (I/R) heart injury

Male C57BL/6JRJ and Catchup mice (12 ± 3 weeks of age) were subjected to a published myocardial I/R in vivo protocol[1, 210]. In short, mice were anesthetised by intraperitoneal (i.p.) injection of ketamine (100 mg/kg, Cat. No.: 9089.01.00, bela-pharm, Vechta, Germany) and xylazine (Rompun, 10 mg/kg, Cat. No.: 6324464.00.00, Ceva Tiergesundheit, Düsseldorf, Germany). They were orally intubated and ventilated throughout the operation procedure and anaesthesia was maintained during the operation by supplementing 2% isoflurane (Forene, Cat. No.: 2594.00.00, abbvie, Wiesbaden, Germany). The chest was opened through a left lateral thoracotomy and the left coronary artery was ligated. After 45 min of ischemia, reperfusion was allowed for indicated time points. Mice were treated with 0.1 mg/kg buprenorphine (Temgesic, Cat. No.: 997.00.00, Indivior, Richmond, Virginia, USA) subcutaneously every 8 h after operation for a total of 72 h. Mice received 1000 international units heparin (Cat. No.: 27586.00.00, LEO Pharma, Neu-Isenberg, Germany) i.p. 10 min before the end of the experimental protocol and were killed by cervical dislocation.

3.2.2. Stainings for Light sheet fluorescence microscopy (LSFM)

For light sheet experiments mice were treated as published[1]. In short, mice received intravenous (i.v.) tail vein injections 10 min before sacrifice with 5 µg of each antibody in phosphate buffered saline (PBS) in a total volume of 150 µl per animal: anti-mouse CD31 (clone: Mec13.3, purified: Cat. No.: 553369, BD Biosciences, Franklin Lakes, New Jersey, USA; conjugated with Alexa Fluor (AF) 647: Cat. No.: 102516, BioLegend, San Diego, California, USA) and anti-mouse Ly-6G (clone: 1A8, purified: Cat. No.: 127602, BioLegend; conjugated with AF647: Cat. No.: 127610, BioLegend). Purified antibodies were conjugated with AF790 using the Alexa Fluor® 790 Antibody Labelling Kit (Cat. No.: A20189, Thermo Fisher Scientific). After sacrifice, mice were perfused blood-free with PBS, hearts were excised and subjected to following tissue processing.

3.3. *In vitro* human immune cell migration assays

3.3.1. Isolation of immune cells from human peripheral whole blood

3.3.1.1. Density gradient centrifugation

Neutrophil granulocytes were isolated via density centrifugation using Polymorphprep™ (Cat. No.: 1114683, AXIS-SHIELD, Oslo, Norway) as previously described[2].

Briefly, Polymorphprep™ was overlaid with EDTA-supplemented human whole blood at a 1:1 ratio and centrifuged at 450 relative centrifugal force (rcf) for 30 min without brake. Polymorphonuclear cells (PMN) were collected and washed with sterile 10 millilitre (ml) PBS Dulbecco without calcium or magnesium ions (Cat. No.: L 1825, Biochrom, Berlin, Germany). Erythrocytes were lysed for 10 min at RT in erythrocyte lysis buffer, containing 155 millimolar (mM) NH_4Cl (Cat. No.: A9434, Sigma Aldrich), 10 mM $KHCO_3$ (Cat. No.: P748.1, Carl Roth), 0.1 mM EDTA (Cat. No.: 15575-020, Invitrogen) in distilled H_2O. After another washing step in sterile PBS Dulbecco (Biochrom), cells were resuspended in sterile hematopoietic progenitor growth medium (HPGM, Cat. No.: PT-3926, Lonza, Basel, Switzerland) and automatically counted using a Cellometer Auto T4 (Nexcelom Bioscience, Lawrence, MA, USA).

3.3.1.2. Negative magnetic isolation

Since Polymorphprep™ isolation did not reliably separate neutrophils of sick patients, they were purified via negative magnetic isolation using the human MACSxpress® Whole Blood Neutrophil Isolation Kit (Cat. No.: 130-104-434, Miltenyi Biotec, Bergisch Gladbach, Germany) according to manufacturer's instructions as well. Briefly, peripheral EDTA-supplemented human whole blood was mixed with 250 microlitre (µl) per 1 ml blood of MACSxpress® Whole Blood Cell Isolation Cocktail and 250 µl per 1 ml blood of Buffer B for 5 min while rotating in a MACSmix™ Tube Rotator (Cat. No.: 130-090-753, Miltenyi Biotec) at RT. The suspension was then placed in the MACSxpress® Separator (Cat. No.: 130-098-308, Miltenyi Biotec) for 15 min at RT and afterwards the supernatant, containing purified neutrophil granulocytes, was carefully collected. Using the MACSxpress® Erythrocyte Depletion Kit (Cat. No.: 130-098-196, Miltenyi Biotec), residual erythrocytes were magnetically depleted in the same manner, according to manufacturer's instructions. The cells were washed with 10 ml PBS Dulbecco (Biochrom), centrifuged at 200 rcf for 5 min at RT and resuspended in X-Vivo™ 10 serum-free hematopoietic cell medium (Cat. No.: 04-743Q, Lonza, Basel, Switzerland), as HPGM was discontinued during these studies. Cell concentration was determined automatically as mentioned under **3.3.1.1**.

Eosinophil granulocytes were isolated by negative magnetic isolation using the human MACSxpress® Whole Blood Eosinophil Isolation Kit (Cat. No.: 130-104-446, Miltenyi Biotec) according to manufacturer's instructions and as described for neutrophil granulocytes.

$CD8^+$ T cells were isolated by negative magnetic isolation using the human MACSxpress® Whole Blood CD8 T cell Isolation Kit (Cat. No.: 130-098-194, Miltenyi Biotec) according to manufacturer's instructions and as described for neutrophil and eosinophil granulo-

cytes until the washing step with PBS. After centrifugation, $CD8^+$ T cells were resuspended in X-Vivo™ 10 medium (Lonza) containing 1x of Gibco™ MEM non-essential amino acids solution (Cat. No.: 11140050, Thermo Fisher Scientific, Waltham, MA, USA) and 1 mM Gibco™ sodium pyruvate (Cat. No.: 11360039, Thermo Fisher Scientific). Cell concentration was then determined by automated counting as described above. The T cell medium was prepared freshly and then kept at 4 °C for 14 days (d) at maximum.

3.3.2. Human immune cell migration assay conditions

3.3.2.1. Neutrophil granulocytes

Neutrophils were seeded in an uncoated 96 well µ-Plate black (Cat. No.: 89626, ibidi, Martinsried, Germany) at a density of 8,250 cells per well in 198 µl sterile X-Vivo™ 10 (Lonza) supplemented with sterile serum replacement 3 (SR3; final concentration: 0.3x; Cat. No.: S2640, Sigma Aldrich). The cells were stimulated at the standard concentrations of either 2 µl N-Formylmethionine-leucyl-phenylalanine (fMLP, final concentration: 10 nM; Cat. No.: F3506, Sigma Aldrich), 2 µl CXCL1 (final concentration: 100 ng/ml; Cat. No.: 275-GR/CF, R&D Systems, Minneapolis, Minnesota, USA) and 2 µl CXCL8 (final concentration: 100 ng/ml; Cat. No.: 208-IL-CF, R&D Systems), as previously published[2]. As the stimuli were reconstituted in sterile PBS Dulbecco (Biochrom), 2 µl of sterile PBS served as the vehicle control to determine baseline migration of neutrophils. The plate was spun down at 50 rcf for 3 min at RT and incubated for 20 min at 37 °C, 5% CO_2 prior to microscopy.

3.3.2.2. Eosinophil granulocytes

Eosinophils were seeded in a 384 well plate for optical imaging with tissue culture treatment (Cat. No.: 3985, Corning, New York, USA) at a density of 2,500 cells per well in 27 µl sterile X-Vivo™ 10 (Lonza) supplemented with sterile SR3 (Sigma Aldrich). The cells were stimulated at the indicated concentration with either 3 µl CCL5 (final concentration: 100 ng/ml; Cat. No.: 300-06B; Peprotech, Rocky Hill, New Jersey, USA), 3 µl CCL7 (final concentration: 500 ng/ml; Cat. No.: 585702, BioLegend, San Diego, California, USA), 3 µl CCL11 (final concentration: 100 ng/ml; Cat. No.: 583002, BioLegend), or 3 µl CCL24 (final concentration: 500 ng/ml; Cat. No.: 585702, BioLegend). As the stimuli were all reconstituted in sterile PBS Dulbecco (Biochrom), 3 µl of sterile PBS served as the vehicle control to determine baseline migration of eosinophils. The plate was spun down at 50 rcf for 3 min at RT and incubated for 20 min at 37 °C, 5% CO_2 prior to microscopy.

3.3.2.3. $CD8^+$ T cells

Human recombinant intercellular adhesion molecule 1 (ICAM-1) was used to enable adhesion of $CD8^+$ T cells to the microscopy plate. For this, 20 µl of 5 µg/ml ICAM-1 (Cat. No.: 720-IC, R&D Systems) were incubated in a 384-well plate for optical imaging with tissue culture treatment (Corning) overnight at 4 °C. The supernatant was discarded the next day. 2,500 $CD8^+$ T cells per well were seeded in 30 µl sterile X-Vivo™ 10 (Lonza) supplemented with 1x Gibco™ MEM non-essential amino acids solution (Thermo Fisher Scientific), 1 mM Gibco™ sodium pyruvate (Thermo Fisher Scientific) and sterile SR3 (Sigma Aldrich). The plate was spun down at 50 rcf for 3 min at RT and incubated for 24 h at 37 °C, 5% CO_2. The cells were then stimulated with either 3 µl stromal cell-derived factor 1 alpha (SDF-1α, CXCL12; final concentration: 100 ng/ml or 500 ng/ml; Cat. No.: 300-28A, Peprotech) or 3 µl SDF-1β (CXCL12; final concentration: 1 µg/ml; Cat. No.: 251-FS/CF, R&D Systems). As the stimuli were reconstituted in sterile PBS Dulbecco (Biochrom), 2 µl of sterile PBS served as the vehicle control to determine baseline migration of $CD8^+$ T cells. The plates were immediately transferred to the microscopes after stimuli addition.

3.4. BALANCE protocol for tissue clearing

Perfused hearts were immersed in 4% w/v paraformaldehyde (PFA, Cat. No.: 10195, Morphisto, Frankfurt am Main, Germany) in PBS for chemical fixation for 4 h at 4 °C in 15 ml tubes. For all following steps, hearts were kept at 4 °C, always agitated, transferred only to pre-cooled solutions in 15 ml tubes and kept protected from light. Following fixation, hearts were dehydrated in an ascending ethanol series in ddH_2O volume per volume (v/v) of 50%, 70% and 100% (Cat. No.: 9065.2, Roth) for at least 4 h while shaking. Subsequently, samples were bleached for 4 h in freshly prepared 5% v/v hydrogen peroxide (Cat. No.: 349887; Sigma Aldrich) and 5% v/v dimethyl sulfoxide (Ca. No.: 4720.3, Carl Roth) in 100% ethanol. After a washing step of at least 4 h in 100% ethanol, samples were warmed to room temperature (RT) for 5 min before transfer into 7 ml pure (99%) ethyl cinnamate (ECi, Cat. No.: 112372, Sigma Aldrich) in a glass vial for at least 4 h prior to imaging. Samples were kept at RT in the dark until and after imaging.

This protocol has been published[1].

3.5. Imaging techniques

3.5.1. Time-lapse microscopy

Human neutrophils were imaged in a Leica DMI6000 B (Leica Microsystems) coupled to a workstation running Leica Application Suite X (LASX, Leica Microsystems) with a motorised stage, equipped with a HC PL FLUOTAR L 20x/0.40 DRY objective (Cat. No.: 11506243, Leica Microsystems) at an imaging rate of one frame every 8 seconds (s for 1 h at 37 °C, without CO_2, as previously published [2]. Eosinophils and $CD8^+$ T cells were imaged in a Zeiss AxioObserverZ.1 (Carl Zeiss, Oberkochen, Germany) coupled to a workstation running ZEN Blue (Carl Zeiss), with a motorised stage, equipped with a LD A-Plan 20x/0.35 Ph1 objective (Cat. No.: 421251-9910-000, Carl Zeiss) at an imaging rate of one frame every 9 s and one frame every 16 s, for eosinophils and $CD8^+$ T cells respectively, at 37 °C, without CO_2. Microscopy resolution was 0.458716 pixel/µm for the Leica DMI6000 B (for neutrophil granulocytes) and 0.369 pixel/µm for the Zeiss Axio Observer.Z1 (for eosinophil granulocytes and $CD8^+$ T cells). The time between images was set to 8 s for neutrophils, to 9 s for eosinophils and to 16 s for $CD8^+$ T cells.

3.5.2. Light sheet fluorescence microscopy

Samples were imaged using an Ultramicroscope II and ImSpector software (LaVision BioTec, Bielefeld, Germany), as previously published[1]. For image acquisition, cleared samples were immersed in ECi (Sigma Aldrich) in a quartz cuvette and excited with light sheets of different wavelengths (488, 561, 639 and 785 nm). Following band-pass emission filters (mean nm / spread) were used, depending on the excited fluorophores: 525/50 for FITC; 595/40 for AF594 or autofluorescence; 680/30 for AF647 and 835/70 for AF790. For image acquisition, hearts were trapped, with the apex and the aorta horizontally aligned, in a commercially available sample holder (LaVision BioTec) and imaged along the longitudinal axis. To avoid damage or deformation of the sample, ECi-cleared 1% phytagel/ H2O (Cat. No.: P8169, Sigma Aldrich) blocks were used as buffers between tissue and plastic holder.

Whole-heart data sets were obtained with 2x total magnification (pixel size of 3.25 µm / pixel x,y, lateral resolution: 6.5 µm in x and y) with 10 µm z spacing between optical planes. Sheet width was set to 4200 and numeric aperture to 0.148, resulting in an approximate light sheet thickness of 4 µm in the horizontal focus. Illumination time was 350 ms, with enabled 8x dynamic focus in both left and right laser lines. For regions of interest (ROI), magnifications are indicated in the figure legends.

3.6. Post-processing and image analysis

3.6.1. Time-lapse video microscopy

3.6.1.1. Automated single cell tracking

The Multi-TIFF files generated under **3.5.1** were exported as *.mov or *.mp4 in the respective microscopy software. These files were analysed by the Automated Cellular Analysis System (ACAS, MetaVí Labs, Austin, Texas, USA; sales@metavilabs.com). The minimum track duration was 60 s, the evaluation interval 30 s and the movement threshold 8 µm for all cell types. The parameters evaluated in this work are defined by the ACAS software as given below.

The tracking first divides into valid and non-valid tracks, depending on whether the minimum track duration, set above, is passed or not. Non-valid tracks are not included in the later analysis of the sample. Secondly, the cells are dividing into moving and non-moving cells. Non-moving cells (nmc.) are those tracks for which the greatest Euclidean distance is less than the movement threshold, set above. The mean cell speed (both including and excluding nmc.) is calculated by the accumulated distance a cell crossed in an interval, divided by the interval duration (time). These speeds are averaged over all intervals for each cell. This average speed over all intervals is then averaged again over all cells, resulting in the speed (excluding or including non-moving cells). The mean velocity (both including and excluding nmc.) is calculated as the Euclidean distances of a track divided by the time duration of that track, regardless of the evaluation interval. Then the velocities for all cell tracks in the well are averaged for the entire well.

3.6.1.2. Manual cell size analysis

To quantify the changes in cellular morphology of atypical chronic myeloid leukaemia (aCML) neutrophils and neutrophils from healthy donors, the size of cells in the respective video were manually analysed using FIJI[211]. For that, the first image of every video was exported as *.tif from the LASX software and imported to FIJI. Subsequently, the outer cell margins were manually marked as ROIs and the occupied area was computed by FIJI's ROI manager. Results were given in µm². Additionally, five age- and gender-matched probands were quantified as controls.

3.6.2. Light sheet fluorescence microscopy

3.6.2.1. Surface and volume rendering

16-bit OME.TIF stacks were converted (ImarisFileConverterx64, Version 9.2.0, Bitplane, Belfast, UK) into Imaris files (.ims). 3D reconstruction and subsequent analysis was conducted using Imaris software (Bitplane), as published[1]. Heart surface (25 µm grain size) and volume was determined using surface creation algorithms. All surface tracings (AAR, CD31 negative ($CD31^{neg}$), vessels) are based on the contour tracing tool and are carried out manually/semi-automatically. For surface creation, each (vessels), every 5^{th} (CD31 tracings) or 10^{th} (AAR) image was traced. Surfaces were created with maximum resolution (2160 x 2560 pixel) and preserved features, to ensure matching of the traced lines with the surface border. Discrimination of arteries and veins was done by their location within the heart muscle and the signal intensity of the CD31 staining ($CD31^{high}$ for arteries, $CD31^{low}$ for veins).

3.6.2.2. Spot function for immune cell counting

Immune cell counts were determined using the spot detection algorithm with an assumed diameter of neutrophils of 7 µm (14 µm z), as published[1]. After assessment of signal distributions in non-stained, basal, 45 min ischemia 24 h reperfusion (I45min R24h) and 45 min ischemia 5 d reperfusion (I45min 5d) hearts, a threshold was applied for all hearts (4,500–35,000 grey values). Localisation of detected spots respective to surface borders was measured using the distance transformation extension on desired surfaces.

3.7. Flow cytometry

3.7.1. Standard protocols for purified human immune cells

100,000 purified neutrophils were transferred to a Rotilabo® 96 well microtest plates with U-profile (Cat. No.: 9291.1, Carl Roth) and spun down at 300 rcf for 5 min. The supernatants were discarded, and the cells were stained in 100 µl PBS with the following antibodies and dilutions: CD15 VioBlue (dilution: 1:50, Clone: VIMC6, Cat. No.: 130-113-488, Miltenyi Biotec), CD16 FITC (dilution: 1:50, Clone: REA423, Cat. No.: 130-113-392, Miltenyi Biotec), fMLP receptor AF647 (final dilution: 1:100, Clone: 5F1, Cat. No.: 565623, BD Biosciences), CXCR1 PE (dilution: 1:100, Clone: 8F1, Cat. No.: 130-105-352, Miltenyi Biotec), CXCR2 PE-Vio770 (dilution: 1:20, Clone: REA208, Cat. No.: 130-100-930, Miltenyi Biotec), CD11b PE (dilution: 1:50, Clone: REA713, Cat. No.: 130-110-611, Miltenyi Biotec), CD66b PE (dilution:

1:10, Clone: REA306, Cat. No.: 130-117-414, Miltenyi Biotec) and CD62L PEVio770 (dilution: 1:100, Clone: 145/15, Cat. No.: 130-104-241, Miltenyi Biotec). After an incubation step of 15 min in the dark at 4 °C, the suspensions were diluted 1:1 with PBS and analysed on a MACSQuant VYB (Miltenyi Biotec).

50,000 purified eosinophils were transferred to a Rotilabo® 96 well microtest plates with U-profile (Carl Roth) and spun down at 300 rcf for 5 min. The supernatant was discarded, and the cells were stained with the following antibodies and dilutions: Siglec 8 APC (dilution: 1:50, Clone: REA1045, Cat. No.: 130-117-902, Miltenyi Biotec), CD15 PE (dilution: 1:11, Clone: REA321, Cat. No.: 130-104-936, Miltenyi Biotec), CCR3 (CD193) VioBlue (dilution: 1:11, Clone: REA574, Cat. No.: 130-108-887, Miltenyi Biotec), CD69 PE (dilution: 1:50, Clone: REA824, Cat. No.: 130-112-613, Miltenyi Biotec) and CD44 FITC (dilution: 1:50, Clone: REA690, Cat. No.: 130-113-903, Miltenyi Biotec). After an incubation step of 15 min in the dark at 4 °C, the suspensions were diluted 1:1 with PBS and analysed on a MACSQuant VYB (Miltenyi Biotec).

50,000 purified $CD8^+$ T cells were transferred to a Rotilabo® 96 well microtest plates with U-profile (Carl Roth) and spun down at 300 rcf for 5 min. The supernatant was discarded, and the cells were stained with the following antibodies and dilutions: CD8 FITC (dilution: 1:100, Clone: REA734, Cat. No.: 130-110-815, Miltenyi Biotec), CCR7 (CD197) VioBlue (dilution: 1:50, Clone: REA546, Cat. No.: 130-117-503, Miltenyi Biotec), CD45RO PE (dilution: 1:50, Clone: REA611, Cat. No.: 130-114-085, Miltenyi Biotec) and CD154 (CD40L) PEVio770 (dilution: 1:100, Clone: REA238, Cat. No.: 130-096-793, Miltenyi Biotec). After an incubation step of 15 min in the dark at 4 °C, the suspensions were diluted 1:1 with PBS and analysed on a MACSQuant VYB (Miltenyi Biotec). Isotype controls (**Table 10**) for the specific antibodies were tested on the cells according to the protocol above. The controls were used in the same dilution and stained as their respective antibody.

3.7.2. *In vitro* stimulation

To verify the flow cytometric stainings beyond isotype controls alone, the purified cells were stimulated *in vitro* to assess the up- or downregulation of the used activation markers.

500,000 neutrophils were stimulated with 10 ng/ml CXCL8 (R&D Systems) in 1 ml X-Vivo™ 10 (Lonza) containing SR3 for 1 h in 12 well cell culture plates (Cat. No.: 92012, TPP). The cells were then gently scrapped off the plates and washed twice with cold PBS. Half of the collected cells were used as an unstained control, while the other half was stained according to the standard flow cytometry panel. 250,000 eosinophils were stimulated with 10 nM GM-CSF (Cat. No.: 572902, BioLegend) in 1 ml X-Vivo™ 10 (Lonza) containing SR3

for 2 h in 12 well cell culture plates (TPP). The cells were then gently scrapped off the plates and washed twice with cold PBS. Half of the collected cells were used as an unstained control, while the other half was stained according to the standard flow cytometry panel. 250,000 $CD8^+$ T cells were stimulated with 100 nM phorbol 12-myristate 13-acetate (PMA; Cat. No.: P8139, Sigma Aldrich) and 1 µM Ionomycin (Cat. No.: IO634, Sigma Aldrich) in 500 µl X-Vivo™ 10 (Lonza) containing 1x Gibco™ MEM non-essential amino acids solution (Thermo Fisher Scientific), 1 mM Gibco™ sodium pyruvate (Thermo Fisher Scientific) and sterile SR3 for 6 h in 48 well cell culture plates (Cat. No.: 92048, TPP). The cells were then gently scrapped off the plates and washed twice with cold PBS. Half of the collected cells were used as an unstained control, while the other half was stained according to the standard flow cytometry panel.

3.8. Statistical Analysis

The graphs were created using GraphPad Prism™ (Version 6.07, GraphPad Software, San Diego, CA, USA). Statistical analyses were either performed using GraphPad Prism™ (Version 6.07, GraphPad Software) or IBM® SPSS® Statistics (Version 25, IBM, Armonk, NY, USA).

4. Material

4.1. Laboratory equipment and Consumables

Only equipment and consumables that were essential to the work conducted here and that are not readily available in every laboratory are listed below.

Table 01: List of laboratory equipment

Product	Type	Supplier	Cat. No.
Cellometer	Auto T4	Nexcelom Bioscience	
MACSmix™ Tube Rotator		Miltenyi Biotec	130-090-753
MACSQuant®	VYB	Miltenyi Biotec	130-096-116
MACSxpress® Separator		Miltenyi Biotec	130-098-308
Tempcontrol	37-2 digital	PeCon	0503.000-230
Tempcontroller	2000-1	PeCon	
Ultramicroscope II		LaVision BioTec	
Widefield incubator for Leica microscope	BL-X Black	PeCon	272-800 098
Widefield incubator for Zeiss microscope	XLmulti S1	Carl Zeiss	
Widefield microscope Leica	DMI6000	Leica Microsystems	
Widefield microscope Zeiss	Axio Observer.Z1	Carl Zeiss	

Table 02: List of consumables

Product	Supplier	Cat. No.
384-well microplate, black / clear, for optical imaging, sterile, TC-treated	Corning	3985
µ-Plate 96 well Black, uncoated	ibidi	89621
Protein LoBind Tubes	Eppendorf	0.5 ml: 0030108094 1.5 ml: 0030108116
Rotilabo® microtest plates, U-profile	Carl Roth	9291.1
S-Monovette® 7.5ml K3E	Sarstedt	01.1605.001

4.2. Chemicals, buffers and media

Table 03: List of chemicals

Product	Supplier	Cat. No.
Ammonium chloride (NH_4Cl)	Sigma Aldrich	A9434
Dimethyl sulfoxide (DMSO)	Carl Roth	4720.3
Ethanol (100 %)	Carl Roth	9065.2
Ethyl cinnamate	Sigma Aldrich	112372
Heparin	LEO Pharma	27586.00.00
Hydrogen peroxide (H_2O_2)	Sigma Aldrich	349887
Paraformaldehyde (PFA)	Morphisto	10195
Phytagel	Sigma Aldrich	P8169
Potassium bicarbonate ($KHCO_3$)	Carl Roth	P748.1
Sodium Chloride (NaCl)	Carl Roth	3957.1
UltraPure™ Ethylenediaminetetraacetic acid (EDTA) 0.5 M, pH 8.0	Invitrogen	15575-020

Table 04: List of products for mouse treatment

Product	Supplier	Cat. No.
Buprenorphine	Temgesic	997.00.00
Isoflurane (Forene)	Abbvie	2594.00.00
Ketamine	Bela-pharma	9089.01.00
Xylazine (Rompun)	Ceva Tiergesundheit	6324464.00.00

Table 05: List of buffers

Product	Containing	Supplier	Cat. No.
Erythrocyte lysis buffer	155 mM NH_4Cl 10 mM $KHCO_3$ 0.1 mM EDTA In distilled H_2O	Sigma Aldrich Carl Roth Invitrogen	A9434 P748.1 15570-020
Phosphate buffered saline (PBS) Dulbecco	/	Biochrom	L 1825

Table 06: List of commercial media and supplements

Product	Final concentration	Supplier	Cat. No.
Gibco™ MEM non-essential amino acids solution	1x	Thermo Fisher Scientific	11140050
Gibco™ sodium pyruvate	1 mM	Thermo Fisher Scientific	11360039
HPGM™ Hematopoietic progenitor growth medium*	/	Lonza	PT-3926
Serum replacement 3	0.3x	Sigma-Aldrich	S2640
X-Vivo™ 10 serum-free hematopoietic cell medium	/	Lonza	04-743Q

* discontinued

4.3. Antibodies and Isotypes

Table 07: List of fluorochromes

Name	Abbreviation	Excitation in nm	Emission in nm
Alexa Fluor® 647	AF647	650	665
Alexa Fluor® 790	AF790	784	814
Allophycocyanin	APC	650	660
Brilliant Violet™ 421	BV421	405	421
Fluorescein	FITC	490	525
PE-Vio 770		565	775
Phycoerythrin	PE	564	574
VioBlue		400	452

Table 08: List of human antibodies for flow cytometry

Antigen	Clone	Fluorescent dye	Dilution	Supplier	Cat. No.
CCR3	REA574	VioBlue	1:11	Miltenyi Biotec	130-108-887
CCR7	REA546	VioBlue	1:50	Miltenyi Biotec	130-117-503
CD11b	REA713	PE	1:50	Miltenyi Biotec	130-110-553
CD15	VIMC6	VioBlue	1:50	Miltenyi Biotec	130-113-488
CD15	REA321	PE	1:11* 1:50	Miltenyi Biotec	130-104-936

Antigen	Clone	Fluorescent dye	Dilution	Supplier	Cat. No.
CD154	REA238	PE-Vio770	1:100	Miltenyi Biotec	130-113-614
CD16	REA423	FITC	1:11* 1:50	Miltenyi Biotec	130-113-392
CD44	REA690	FITC	1:50	Miltenyi Biotec	130-113-341
CD45RO	REA611	PE	1:50	Miltenyi Biotec	130-114-085
CD62L	145/15	PE-Vio770	1:100	Miltenyi Biotec	130-113-621
CD66b	REA306	PE	1:11	Miltenyi Biotec	130-104-396
CD69	REA824	PE	1:50	Miltenyi Biotec	130-112-613
CD8	REA734	FITC	1:100	Miltenyi Biotec	130-110-815
CXCR1	8F1	PE	1:100	Miltenyi Biotec	130-105-352
CXCR2	REA208	PE-Vio770	1:20	Miltenyi Biotec	130-100-930
fMLPR	5F1	Alexa Fluor® 647	1:100	BioLegend	565623
Siglec 8	REA1045	APC	1:50	Miltenyi Biotec	130-117-902

* old charge of the antibody

Table 09: List of murine antibodies for LSFM

Antigen	Clone	Fluorescent dye	Amount per animal	Supplier	Cat. No.
CD31	Mec13.3	Unconjugated Alexa Fluor® 647	5 µg in 150 µl PBS	BD Biosciences BioLegend	553369 102516
Ly-6G	1A8	Unconjugated Alexa Fluor ® 647	5 µg in 150 µl PBS	BioLegend BioLegend	127602 127610

Table 10: List of isotype controls

Isotype	Host	Fluorescent dye	Amount per animal / dilution	Supplier	Cat. No.
IgM	Mouse	VioBlue	1:50	Miltenyi Biotec	130-116-318
REA	Human	APC	1:50	Miltenyi Biotec	130-113-434
REA	Human	FITC	1:11 / 1:50	Miltenyi Biotec	130-104-610
REA	Human	PE	1:11 / 1:50	Miltenyi Biotec	130-104-612
REA	Human	PE-Vio770	1:50 / 1:100	Miltenyi Biotec	130-104-616
REA	Human	VioBlue	1:11 / 1:20 / 1:50	Miltenyi Biotec	130-104-609

4.4. Migration stimuli

Table 11: List of coatings and stimuli

Product	Final concen-tration	Diluent	Supplier	Cat. No.	Lot No.
CCL11	100 ng/ml	PBS	Peprotech	300-21	-
CCL11	100 ng/ml	PBS	BioLegend	583002	B158803
CCL11	100 ng/ml	PBS	R&D Systems	320-E0/CF	-
CCL24	500 ng/ml	PBS	Peprotech	300-33	-
CCL24	500 ng/ml	PBS	BioLegend	858002	-
CCL24	500 ng/ml	PBS	R&D Systems	343-E2/CF	-
CCL5	100 ng/ml	PBS	Peprotech	300-06	51233
CCL5	100 ng/ml	PBS	BioLegend	580202	-
CCL5	100 ng/ml	PBS	R&D Systems	278-RN/CF	-
CCL7	500 ng/ml	PBS	Peprotech	300-17	-
CCL7	500 ng/ml	PBS	BioLegend	585702	B162052
CCL7	500 ng/ml	PBS	R&D Systems	282-P3/CF	-
CXCL1	100 ng/ml	PBS	R&D Systems	275-GR/CF	DM0518031
CXCL8	100 ng/ml	PBS	R&D Systems	208-IL-010/CF	DILS0118091
fMLP	10 nM	PBS	Sigma Aldrich	F3506	MKBR6832
GM-CSF	10 nM	PBS	BioLegend	572902	-
ICAM-1	5 µg/ml	PBS	R&D Systems	720-IC	DLA0716061 DLA1018111
ICAM-1	5 µg/ml	PBS	BioLegend	552906	B234822
ICAM-1	5 µg/ml	PBS	Peprotech	150-05	1008469 H2112
Ionomycin	1 µM	DMSO	Sigma Aldrich	IO634	-
PMA	100 nM	DMSO	Sigma Aldrich	P8139	-
SDF-1α	100 ng/ml 500 ng/ml	PBS	Miltenyi	130-093-996	-
SDF-1α	100 ng/ml 500 ng/ml	PBS	Peprotech	300-28A	-
SDF-1α	100 ng/ml 500 ng/ml	PBS	R&D Systems	350-NS/CF	-
SDF-1β	1 µg/ml	PBS	Peprotech	300-28B	-

Product	Final concen-tration	Diluent	Supplier	Cat. No.	Lot No.
SDF-1β	1 µg/ml	PBS	R&D Systems	351-FS/CF	-
SDF-1β	1 µg/ml	PBS	Cell Guide Systems	GFH159	-

4.5. Commercial kits

Table 12: List of commercial kits

Product	Supplier	Cat. No.
Alexa Fluor® 790 Antibody Labelling Kit	Thermo Fisher Scientific	A20189
MACSxpress® Erythrocyte Depletion Kit	Miltenyi Biotec	130-098-196
MACSxpress® Whole Blood CD8 T cell Isolation Kit	Miltenyi Biotec	130-098-194
MACSxpress® Whole Blood Eosinophil Isolation Kit	Miltenyi Biotec	130-104-446
MACSxpress® Whole Blood Neutrophil Isolation Kit	Miltenyi Biotec	130-104-434

4.6. Software

Table 13: List of software

Product	Version	Supplier
ACAS	-	MetaVí Labs
EndNote™	X9.2	Clarivate Analytics
FIJI (ImageJ)	1.52p	Wayne Rasband, [211]
FlowJo	10.5.3	FlowJo, LLC.
GraphPad Prism®	6.07	GraphPad Software, Inc.
Illustrator CC	23.0.2	Adobe
Imaris	9.2.0	Bitplane
Microsoft Office	365 ProPlus	Microsoft
SPSS® Statistics	25	IBM

5. Results

Autonomous migration is a key feature of all immune cells and enables them to reach a site of infection from the blood stream that distributes them throughout the whole organism. A great variety of methods are available to study migration of living cells, both *in vivo* and *in vitro*, as well as the outcome of a migration event, namely the presence of immune cells in an organ after an insult. During this thesis, both endpoint and live cell imaging assays were employed to study immune cell migration in mice and men.

5.1. Development of human immune cell migration assays

The assessment of human immune cell migration poses a variety of complications. Especially endpoint analyses require human material that may be altogether inaccessible or otherwise in high demand for researchers. To overcome this problem, easily applicable, standardised 2-D assays were established to assess the migration of human immune cells from a readily accessible source: the blood (**Figure 6**). These assays were used to elucidate changes in immune cell migration in different types of cancer and whether these changes can predict and monitor disease severity or therapy success.

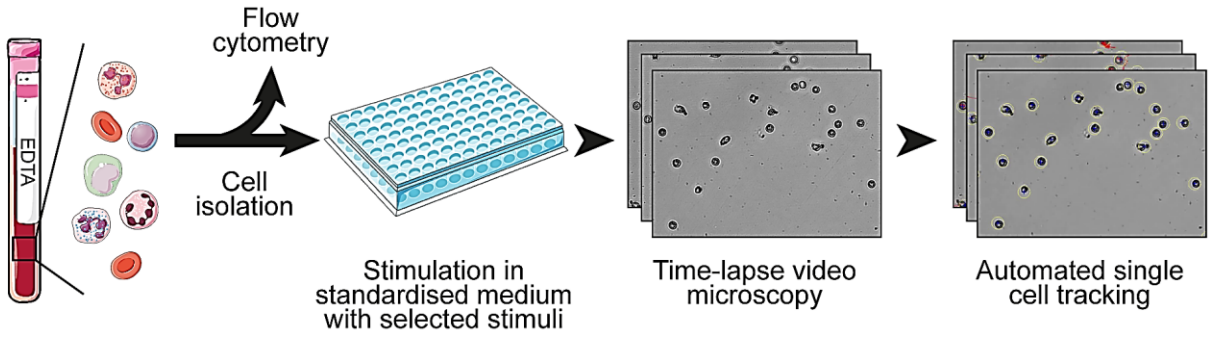

Figure 6: Principle workflow of the immune cell migration assays.

First, the cells of interest (neutrophils, eosinophils or $CD8^+$ T cells) were isolated from human peripheral blood via negative magnetic isolation or density gradient centrifugation (only for neutrophils in early studies). These cells were then subjected to the standardised migration assays and analysed using flow cytometry. In general, the cells were plated on either 96- or 384-well plates, suitable for microscopy, and imaged for 1 – 3 h. All videos were automatically tracked using the Automated Cellular Analysis System (ACAS) by MetaVí Labs and the data were analysed as described.

The workflow, shown in **Figure 6**, was used to establish migration assays for neutrophils, eosinophils and $CD8^+$ T cells, for which the migration behaviour was determined in healthy donors and patients from diverse disease settings. The migration assay for neutrophils was already published by our laboratory, thus, establishment and standard values will

not be discussed in detail here[2]. With this assay, the migration patterns of neutrophils from myelodysplastic syndrome (MDS) patients (**5.2**) and a patient suffering from atypical chronic myeloid leukaemia (aCML) (**5.3**) were determined. The migration assays for eosinophils and $CD8^+$ T cells have not been published and are therefore included in detail in this thesis (**5.4**). Ultimately, all three cell types were analysed in patients suffering from metastatic malignant melanoma before and during immune checkpoint blocker therapy (**5.5**).

5.2. Human neutrophil migration as a biomarker in myelodysplastic syndrome patients

With the published assay[2], changes in neutrophil granulocyte migration in MDS patients were investigated. MDS is a highly heterogenous group of disorders that share the feature of bone marrow failure to produce fully mature blood cells[156]. MDS might therefore affect one or multiple blood cell types and has a high risk for leukaemic transformation[212]. Both, diagnosis and prognosis are time-consuming, costly and burdensome for the patients. Therefore, the migration patterns of neutrophils were assessed to elucidate whether they were a suitable parameter to aid routine MDS diagnosis, prognosis and surveillance.

5.2.1. Neutrophil migration correlates with the international prognostic scoring system and MDS subtype

The heterogeneity of MDS is also reflected in the migration behaviour of human neutrophils. A mixed phenotype was found in the overall population of 26 MDS patients with different disease categories and severities. Most strikingly, when comparing milder forms of MDS, namely MDS with multilineage dysplasia (MDS-MLD) and MDS-MLD with ring sideroblasts (MDS-MLD-RS), with the more aggressive form of MDS with excess blasts (MDS-EB-I/II), neutrophils from MDS-EB-II patients showed severely impaired neutrophil motility, especially in response to 10 nM N-Formylmethionine-leucyl-phenylalanine (fMLP) (**Figure 7 a + b**). This was illustrated by the shorter track length and less random migration in an MDS-EB-II patient (**Figure 7 a**, bottom row) as compared to a patient suffering from MDS-MLD (top row). When looking at the speed of the neutrophils upon fMLP treatment alone, a gradual decrease from milder MDS forms, where the speed was comparable to healthy controls[2], to severe MDS forms (**Figure 7 b**) was observed.

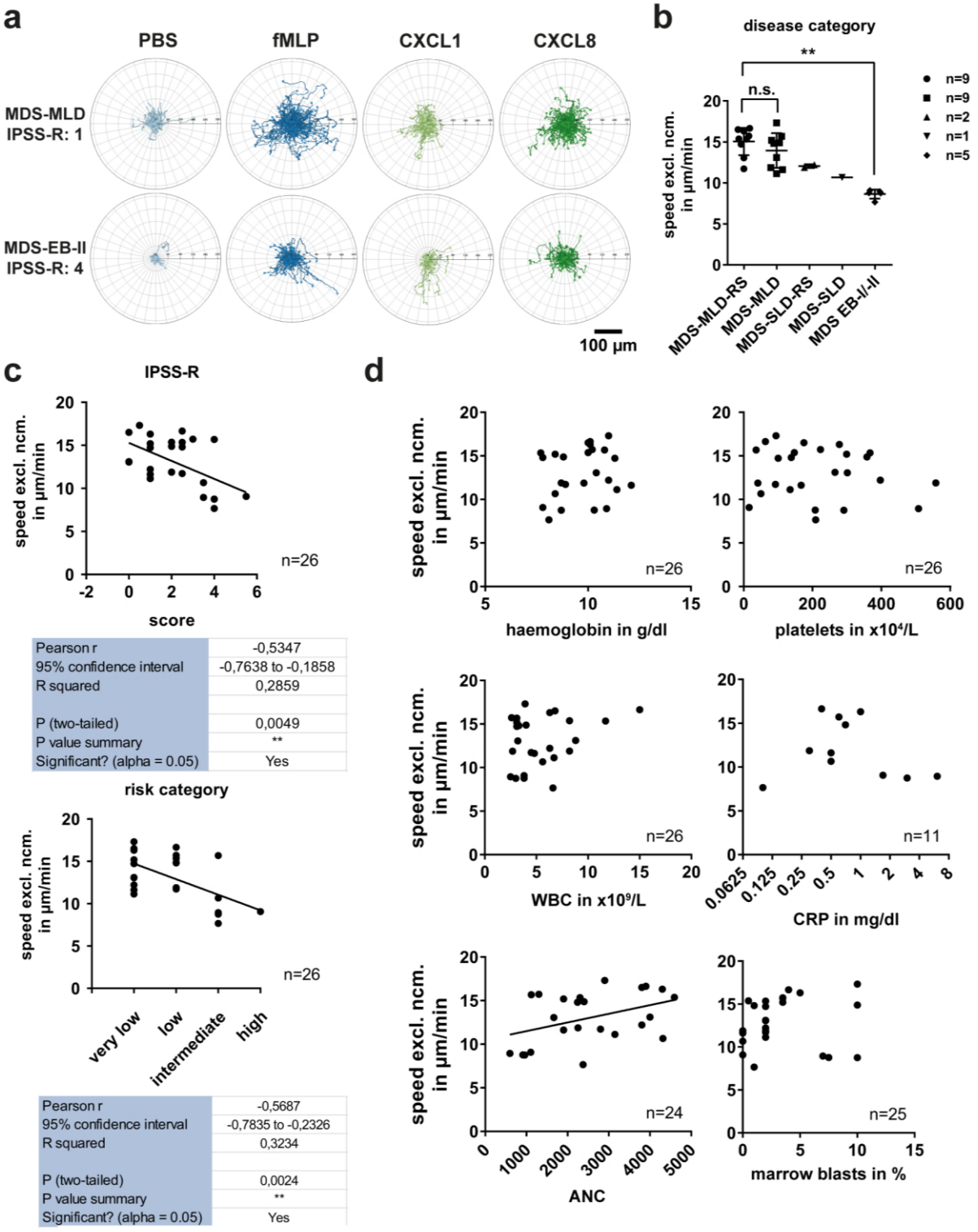

	Hemoglobin	Platelets	ANC	WBC	CRP	Marrow blasts
Pearson r	0,13	-0,1322	0,41	0,2548	-0,4121	0,09815
95% confidence interval	-0,2710 to 0,4925	-0,4943 to 0,2689	0,007944 to 0,6980	-0,1470 to 0,5845	-0,8114 to 0,2495	-0,3090 to 0,4749
R squared	0,0169	0,01748	0,1681	0,06494	0,1698	0,009633
P value						
P (two-tailed)	0,5268	0,5196	0,0466	0,209	0,2079	0,6407
P value summary	ns	ns	*	ns	ns	ns
Significant? (alpha = 0.05)	No	No	Yes	No	No	No

Figure 7: Neutrophil migration correlates with IPSS-R scoring and MDS subtype.

(**a**) Representative trajectory plots of neutrophils from two patients suffering from MDS with multilineage dysplasia (MLD, mild phenotype, top) and MDS with excess blasts II (EB-II, severe phenotype, bottom) as well as the respective IPSS-R scores are displayed. Each line represents the path of

a single cell in the video. The scale bar is 100 µm. (**b**) Scatter dot plot depicting the speed excluding (excl.) non-moving cells (nmc.) in µm per min (y-axis) upon fMLP stimulation and the various MDS subtypes: MDS with ring sideroblasts and multilineage dysplasia (MDS-MLD-RS), MDS-MLD, MDS with ring sideroblasts and single lineage dysplasia (MDS-SLD-RS), MDS with single lineage dysplasia (MDS-SLD) and MDS-EB-I/II. The black lines indicate mean ± standard error of the mean (s.e.m.). *p*-values were calculated using the Kruskal-Wallis test with multiple comparison. ** $p < 0.01$, n.s. non-significant. (**c**) Speed excl. nmc. (y-axis) of neutrophils upon fMLP stimulation plotted against the corresponding IPSS-R score (x-axis, top) and against the risk category (x-axis, bottom). (**d**) Speed excl. nmc. upon fMLP stimulation (y-axis) was plotted against the blood parameters haemoglobin (top left), platelet count (top right), white blood cell count (WBC, middle left), C-reactive protein (CRP, middle right) and the absolute neutrophil count (ANC, bottom left) as well as the frequency of marrow blasts (bottom right). Each symbol indicates a single individual and the black line represents the results from the best-fit of the nonlinear regression calculation. The correlations were calculated via Pearson and the results are shown as tables below the graphs. This figure is adapted from [2].

The Revised International Prognostic Scoring System (IPSS-R) is the current gold standard to evaluate the severity of MDS[157]. Here, multiple clinical features, such as bone marrow cytogenetics, amount of blasts or cytopenia, are used to generate a prognostic categorisation system[157], providing an assessment of overall survival as well as risk for acute myeloid leukaemia (AML) transformation. The correlation of neutrophil migration upon fMLP stimulation with their respective IPSS-R score revealed a strong relationship between the two (**Figure 7 c**, top). Furthermore, the risk category of a patient is determined based on a bin of their IPSS-R score[157]. This risk category also reflects on the survival chances and risk for AML transformation for the individual. Here, a good correlation was observed between the risk category and the fMLP-triggered migration of neutrophils (**Figure 7 c**, bottom). The assessment of blood parameters, like haemoglobin, platelets, absolute neutrophil count (ANC) and marrow blasts, is part of the IPSS-R determination. Additionally, these and other routinely assessed parameters, especially the amount of C-reactive protein (CRP), which is induced during inflammatory processes in the organism, might influence blood neutrophil migration in this assay. To follow up on this possibility, migration speed of neutrophils upon fMLP stimulation was correlated against the amount of haemoglobin, platelets, white blood cells (WBC), CRP, ANC and marrow blasts (**Figure 7 d**). However, no significant correlations existed between the parameters, except for a positive correlation between migration speed and ANC (**Figure 7 d**, bottom left). Hence, neutrophil migration was a parameter that correlated with the IPSSR-R but was independent of IPSS-R defining characteristics and was not influenced by processes that induce CRP, e.g. ongoing inflammation.

5.2.2. Neutrophil migration as a prognostic and surveillance tool in MDS

MDS prognosis and surveillance is often accompanied by an increased burden for the patient, especially due to assessment of marrow blast frequency, which requires invasive marrow aspiration. The *in vitro* assessment of blood neutrophil migration would facilitate both initial scoring and prognosis, as well as MDS surveillance.

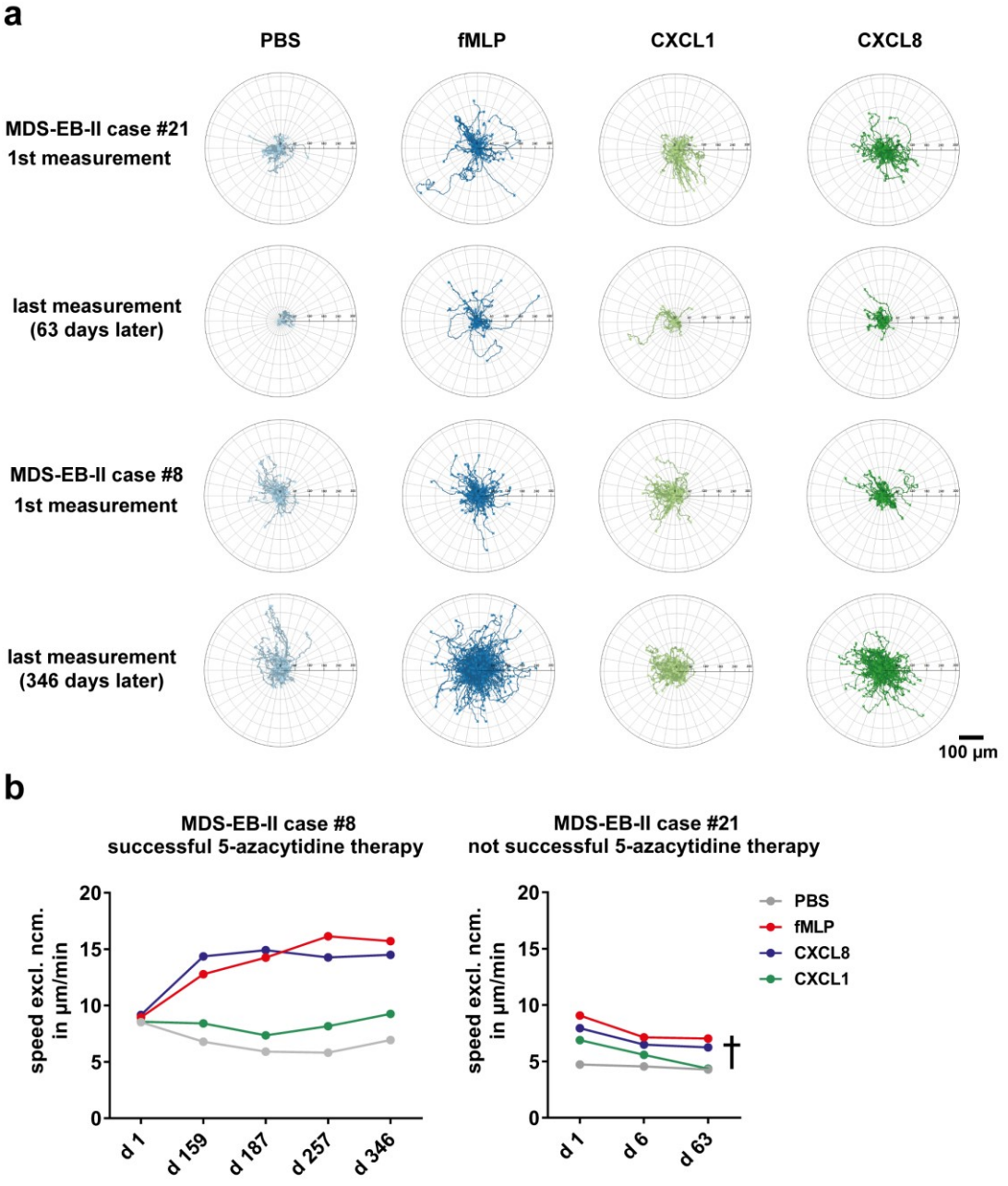

Figure 8: Neutrophil migration might indicate therapy success.

(**a**) Trajectory plots of migrating neutrophils from two MDS-EB-II cases (#21 and #8). The columns show the trajectories of neutrophils stimulated with, from left to right: PBS, fMLP, CXCL1 and CXCL8. The scale bar is 100 µm. (**b**) Changes in speed excl. nmc. for the MDS-EB-II case #8 (left) and case #21 (right) over several measurements. Grey dots and lines indicate neutrophils stimulated

with PBS, red stands for fMLP stimulation, blue for CXCL8 and green for CXCL1. The black cross on the right indicates the patient's death. This figure is adapted from [2].

Hence, the changes in neutrophil migration over the course of MDS disease and treatment were investigated and with this, two interesting MDS-EB-II patients undergoing chemotherapeutic therapy with 5-azacytidine were identified. Neutrophils from case #21 (**Figure 8 a**, first panel) showed impaired migration, as represented by the corresponding trajectory plots, which did not improve until the last measurement timepoint 63 days later (**Figure 8 a**, second panel). Neutrophils from case #8 also presented with decreased motility during the first measurement, but their motility improved until the last measurement timepoint 346 days later (**Figure 8 a**, third and fourth panel).

Interestingly, following the course of these two cases, peripheral blood neutrophil migration upon fMLP stimulation increased over the course of one successful therapy (**Figure 8 b**, left, case #8), while it remained impaired over the course of one unsuccessful therapy until the death of the patient (**Figure 8 b**, right, case #21).

5.2.3. Summary I

This section dealt with the establishment of an assay to determine live immune cell migration of human, peripheral blood neutrophils in a standardised way. This allows for the comparison of the results across different laboratories and clinics, paves the way for routine application and was therefore applied on patients suffering from MDS, a highly heterogenous disease. With this, we learned that neutrophil migration correlates well with MDS severity. Strikingly, neutrophil migration in an unsuccessful therapy remained impaired, while it improved in a successful therapy.

5.3. Human neutrophil migration in a case of atypical myeloid leukaemia

To investigate the prognostic potential of neutrophil migration in other leukaemic diseases, we evaluated a patient suffering from aCML, a rare disease that shares overlaps with MDS, chronic neutrophilic leukaemia and chronic myelomonocytic leukaemia[213]. To date, aCML remains poorly described, hard to tell apart from other myeloid leukaemia and hence still without a gold-standard medical treatment concept[213]. To elucidate the changes of the previously assessed parameters, e.g. migration and receptor expression, the patient suffering from aCML was monitored over approximately a year, from before therapy with Ruxolitinib, a janus kinase (JAK) I/II inhibitor, until death on day 370 after therapy start.

The patient, a 69-year-old male, presented with a WBC count of 69 x 10^9/litre (L) and an ANC of 53 x 10^9/L, despite cytoreductive therapy with hydroxyurea. The manual differential revealed 76% neutrophils, 2% band forms, 6% metamyelocytes, 3% myelocytes and 2% myeloblasts. Dysgranulopoiesis with hypogranularity was observed and a bone marrow biopsy and aspirate revealed myeloid hyperplasia without increased blasts and without reticulin fibrosis and routine cytogenetics did not show abnormalities. The next generation sequencing analysis revealed the presence of mutations in eight genes including the CSF3R p.T618I mutation. Given the presence of dysgranulopoiesis in combination with neutrophil precursors >10 %, as well as mutations frequently observed in aCML, the patient was diagnosed with aCML. Haematopoietic stem cell transplantation as a treatment option was deferred due to advanced age and chronic kidney disease. Even though the patient was on hydroxyurea, the WBC count and constitutional symptoms were poorly controlled. Because of the potential benefit of Ruxolitinib in CSF3R T618I mutated myeloid neoplasms[169], the patient commenced with an off-label prescription of Ruxolitinib (day 0).

5.3.1. aCML neutrophils displayed severely impaired migration, signalling receptor expression and enlarged morphology prior to Ruxolitinib therapy

Deficits in neutrophil effector function are common in myeloid leukaemia and culminate in increased risks for infections[214]. Therefore, migration, as a key effector function of neutrophils, as well as the expression patterns of central signalling receptors were characterised in the aCML case and compared to healthy controls (**Supplementary Table 1**).

Here, neutrophils from the aCML patient exhibited severely reduced motility under all tested stimulatory conditions as compared to an age- and gender-matched control group (**Figure 9 a**). Both, percentage of moving cells and speed, were reduced in aCML neutrophils compared to 6 age- and gender-matched, healthy controls (**Figure 9 b**). While performing the first microscopy experiments, an abnormal behaviour of the neutrophils was noted. A large portion of the cells were flattened out and barely visible against the background in our bright-field microscopy approach (**Figure 10 a**, bottom panel, indicated by black arrows). The area occupied by the cells was quantified, as cell size in μm², by manual cell tracing, revealing aCML neutrophils to be significantly larger than the neutrophils from healthy, age- and gender-matched controls (**Figure 10 b**, left).

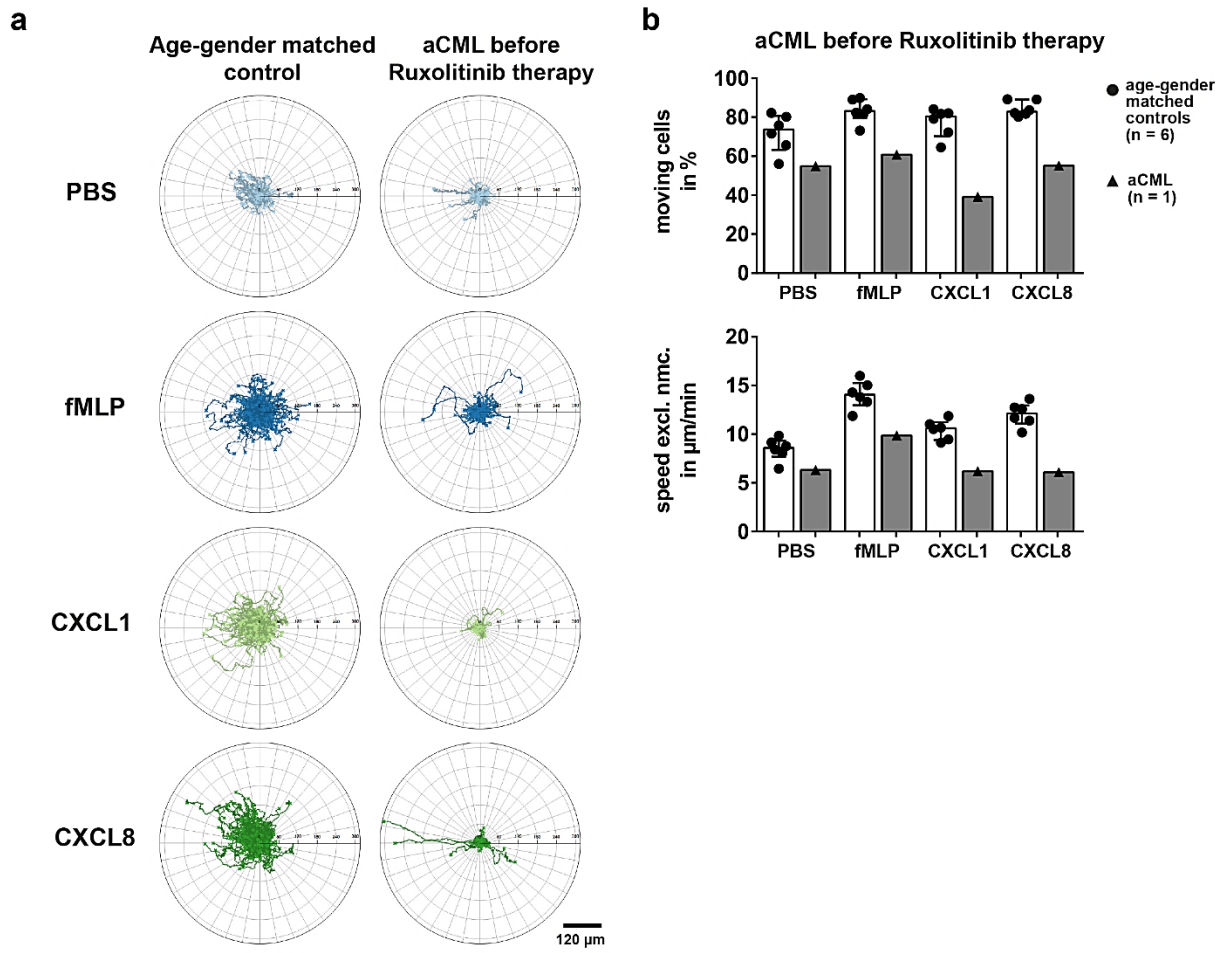

Figure 9: aCML neutrophils exhibit severely impaired migratory capacity.

(**a**) Representative trajectory plots of an age- and gender-matched control (left) and the aCML patient before Ruxolitinib therapy (right), for, from top to bottom, PBS, fMLP, CXCL1 and CXCL8 stimulation. The scale bar equals 120 µm. (**b**) Statistical summary of the migration patterns of aCML (n = 1) neutrophils and age- and gender-matched controls (n = 6). The top panel shows the percentage of moving cells (x-axis) against the stimulation conditions (y-axis) and the bottom panel summarises the speed excl. nmc. (y-axis) of the neutrophils. Black dots represent the 6 age- and gender-matched controls and the black triangles the aCML patient. Height of the bars represent the median and the error bars the interquartile range.

However, age- and gender-matched controls contained enlarged cells and aCML samples also contained normally sized cells. To represent the microscopy data more accurately, the cells were grouped according to their size and the amount of cells larger than 225 µm² was quantified (**Figure 10 b**, cut-off is indicated by grey dashed line). This cut-off was chosen as it, assuming a perfect circle, equals a diameter of 16 µm and is thus close to a human neutrophil's normal diameter (12 – 15 µm) in cell culture[215]. The number of cells above this threshold was higher for aCML neutrophils than for healthy controls (**Figure 10 b**, right).

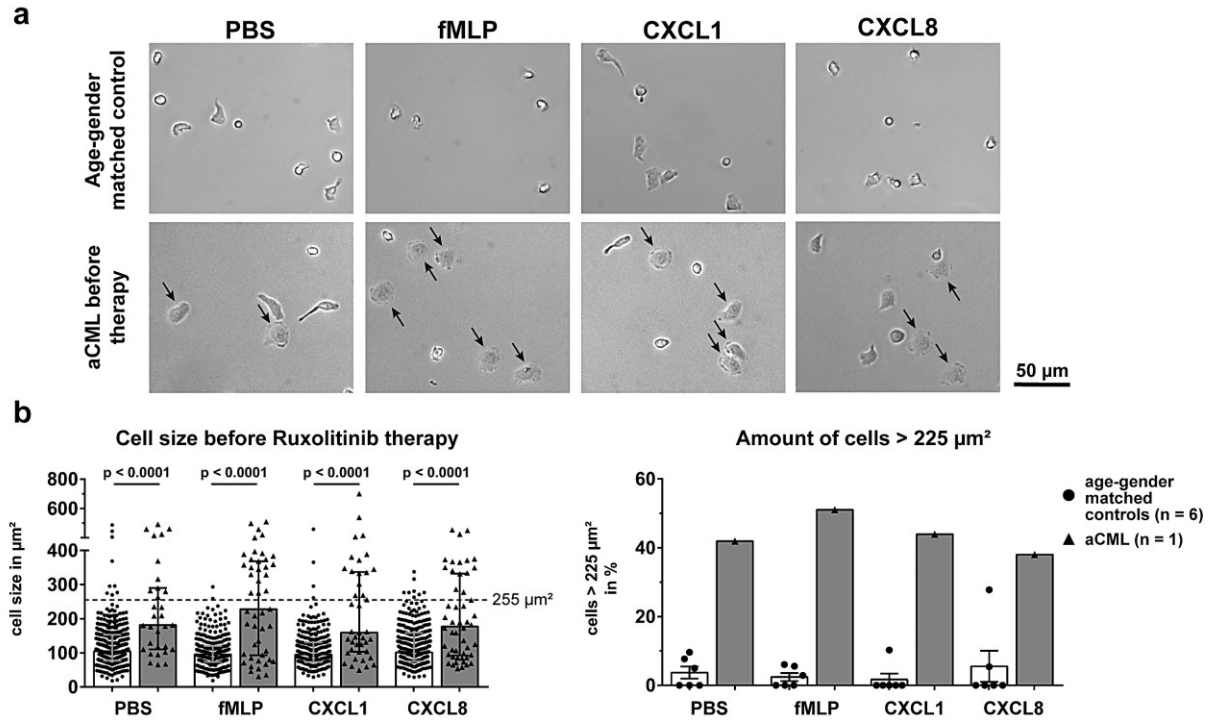

Figure 10: aCML neutrophils show enlarged morphology.

(**a**) The first frame of image sequences acquired during video microscopy of neutrophils from an age- and gender-matched control (top) and the aCML patient before therapy (bottom). From left to right, the cells were treated with PBS as a control, fMLP, CXCL1 and CXCL8. Black arrows in the lower panel indicate prominently enlarged cell bodies. Magnification: 20x. (**b**) Combined scatter dot plot and bar graph of the cell size in µm² of aCML neutrophils before therapy (left) and the relative number of neutrophils with a cell size of > 225 µm² (right). Both parameters were compared to age- and gender-matched controls (n = 6). On average, 41 and 56 cells per condition were analysed in age- and gender-matched controls and the aCML patient, respectively. Bars are given as median ± interquartile range and the given *p*-values were calculated using Mann-Whitney *U*-test. The cut-off of 225 µm² (grey dashed line, left) was chosen as assuming a perfect circle equals a diameter of 16 µm and is thus close to a neutrophil's normal diameter (12 – 15 µm) in cell culture[215].

The defect in neutrophil migration and morphology might originate from or be accompanied by changes in signalling receptor expression. Therefore, flow cytometry analyses of two neutrophil lineage markers, CD15 and CD16[216] and the chemokine receptors for the employed stimuli, fMLP receptor (fMLPR), CXCR1 and CXCR2 were performed. The gating strategy is depicted in **Figure 11 a**. CD16, fMLPR and CXCR2 were reduced and CD15 and CXCR1 were all but absent on aCML neutrophils as compared to an age-matched control (**Figure 11 b + c**).

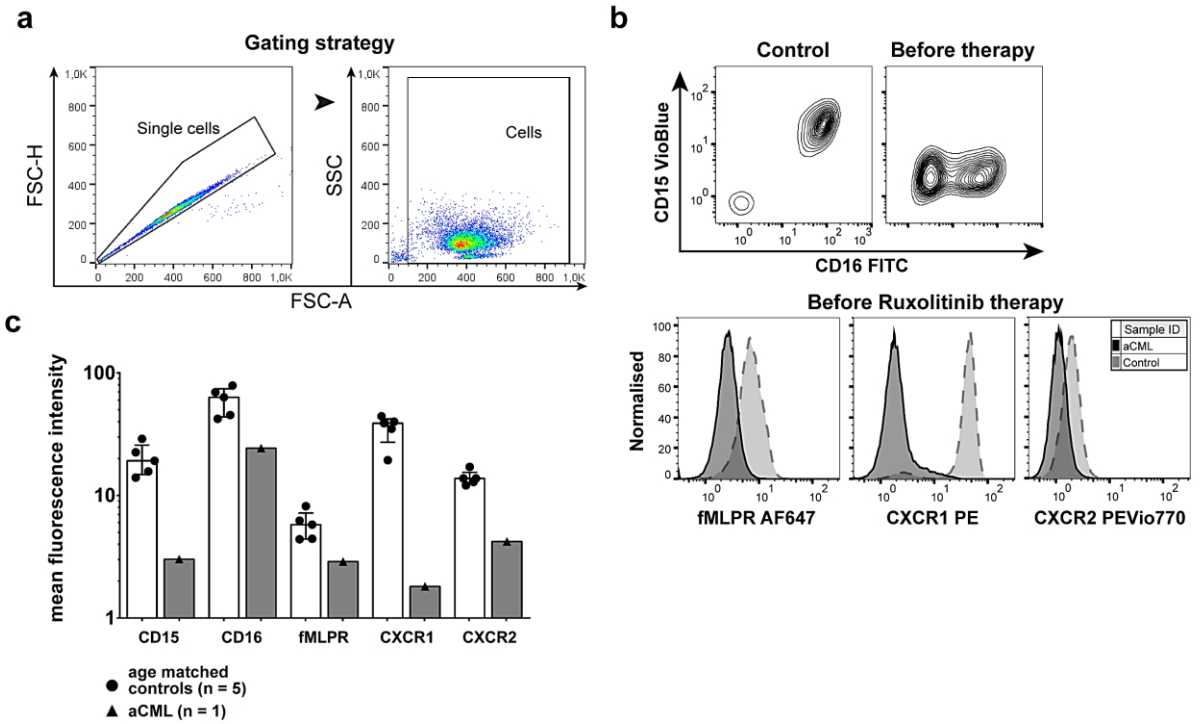

Figure 11: Reduced expression of CD15, CD16, fMLPR, CXCR1 and CXCR2 in aCML neutrophils.

(**a**) The gating strategy for flow cytometric analysis of aCML neutrophils and age- and gender-matched controls is depicted as pseudo colour plots on one exemplary data set. The data was firstly gated for single cells (doublet exclusion, left). This was done for FSC-A against FSC-H (shown) and afterwards SSC-A against SSC-H (not shown). Finally, the debris was excluded based on the FSC-SSC properties. The expression levels of CD16, CD15, fMLPR, CXCR1 and CXCR2 were determined on all cells as mean fluorescence intensities (mfi). (**b**) Representative contour plots (top) and histograms (bottom) of purified neutrophils. Analyses of CD16 (FITC) and CD15 (VioBlue) (top) and fMLPR, CXCR1 and CXCR2 (bottom) expressions are shown. An age- and gender-matched control (control, left of top panel; dotted light grey line of bottom panel) and aCML neutrophils before Ruxolitinib therapy (before therapy, right of top panel; solid dark grey line of bottom panel) are depicted. (**d**) Statistical summary of expression levels for CD16, CD15, fMLPR, CXCR1 and CXCR2 on purified neutrophils from age- and gender-matched controls (controls; black dots, white bars; n = 5) and aCML neutrophils before treatment (aCML; black triangles, grey bars; n = 1). Expression levels are given as the mfi and bars are given as median ± interquartile range.

5.3.2. One week of Ruxolitinib improved neutrophil morphology but did not impact migration or receptor expression patterns

The migration behaviour, cell morphology and receptor expression of the aCML neutrophils were investigated one week after onset of the Ruxolitinib therapy. Neutrophil migration remained impaired, only the percentage of moving cells upon fMLP treatment reached the levels of healthy control individuals (**Figure 12 a**, top panel). The corresponding speed remained slightly below normal levels as prior to therapy (**Figure 12 b**, bottom panel).

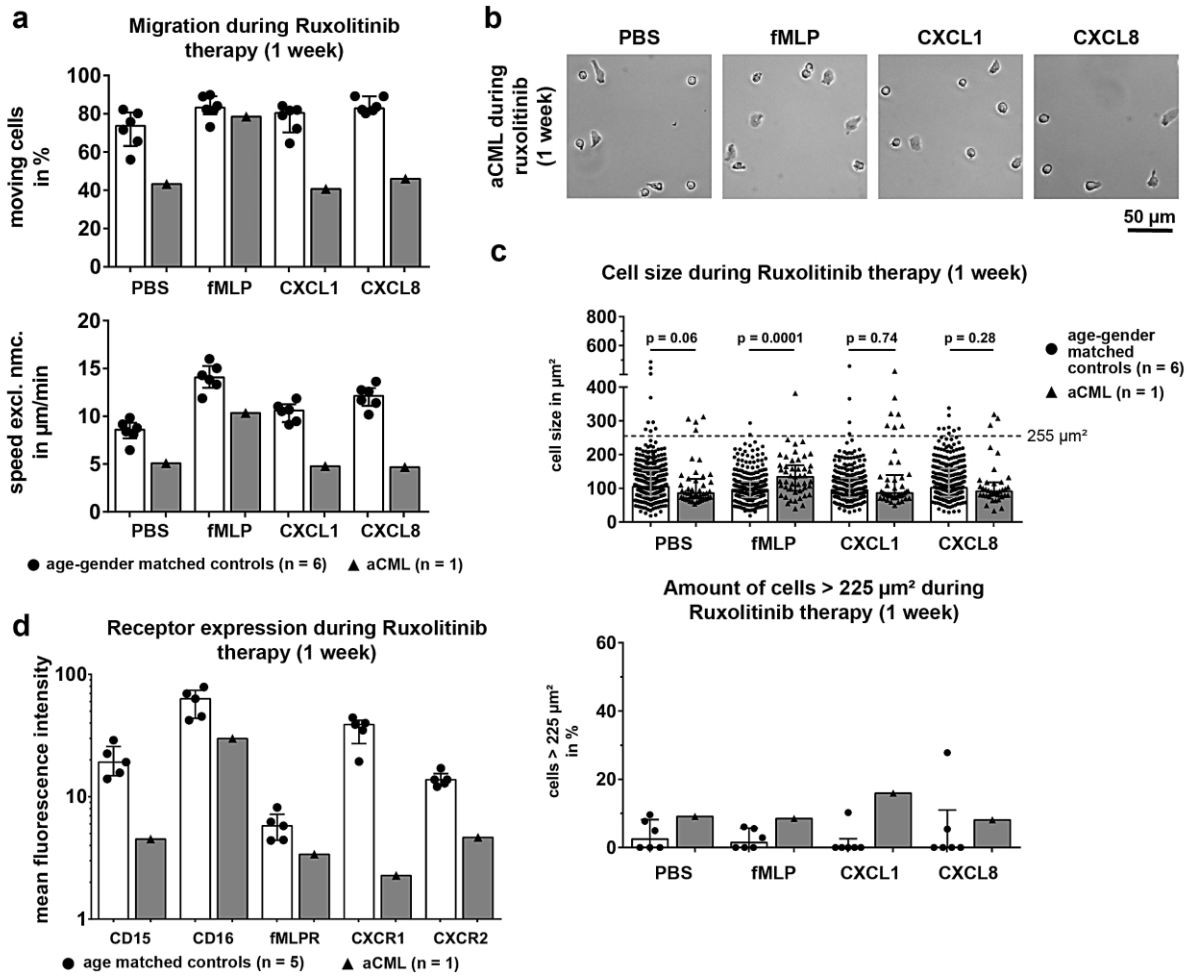

Figure 12: Effect of short-term Ruxolitinib therapy on neutrophil migration, morphology and receptor expression.

(**a**) Statistical summary of percentage of moving cells (top) and speed excluding non-moving cells (speed excl. nmc., bottom), of purified aCML neutrophils after one week of treatment with Ruxolitinib (black triangles, grey bars; n = 1), compared to the healthy age- and gender-matched controls (black dots, white bars; n = 6). Each symbol represents a single individual. Bars are given as median ± interquartile range. (**b**) The first frame of image sequences acquired during video microscopy of neutrophils of the aCML patient after one week of Ruxolitinib therapy. From left to right, the cells were treated with PBS as a control, fMLP, CXCL1 and CXCL8. Magnification: 20x. (**c**) Statistical summary of the cell size in µm² of aCML neutrophils (black triangles, grey bars) after one week of Ruxolitinib treatment (top) and the relative number of neutrophils with a cell size of > 225 µm² (bottom). Both parameters were compared to age- and gender-matched controls (black dots, white bars; n = 6). On average, 41 and 56 cells per condition were analysed in age- and gender-matched controls and the aCML patient, respectively. Bars are given as median ± interquartile range and the given *p*-values were calculated using Mann-Whitney *U*-test. The cut-off of 225 µm² (top) is displayed as a dashed grey line. (**d**) Statistical summary of expression levels for CD15, CD16, fMLPR, CXCR1 and CXCR2 on purified neutrophils from age-matched controls (controls; black dots, white bars; n = 5) and aCML neutrophils after one week of Ruxolitinib treatment (1 week; black triangles, grey bars; n = 1). Expression levels are given as the mean fluorescence intensity (mfi). The gating strategy is detailed in **Figure 11 a**. Bars are given as median ± interquartile range.

Interestingly, after one week of Ruxolitinib treatment, the neutrophil morphology greatly differed from their appearance one week before (**Figure 12 b**), now resembling the healthy controls much more. Quantification of the cells size (top) and the number of cells above the cut-off (bottom) revealed a normalisation of cell size after one week of Ruxolitinib treatment (**Figure 12 c**). In contrast, the expression levels of CD15, CD16, fMLPR, CXCR1 and CXCR2 remained unaffected by the JAK inhibitor (**Figure 12 d**).

5.3.3. Ruxolitinib therapy causes the loss of a CSF3R mutated clone and cell size normalisation

For the aCML patient the clinical presentation, migration patterns, expression levels and cell size development were monitored over the course of Ruxolitinib therapy for almost a year. The percentage of moving cells rose to baseline levels over the course of Ruxolitinib therapy, except for CXCL8, for which the amount of moving cells remained below healthy levels (**Figure 13 b**, top panel). The migration speed of the aCML neutrophils, on average, remained below the healthy controls, but peaked for PBS, CXCL1 and CXCL8 on day 31 (4^{th} measurement, **Figure 13 b**, bottom panel). Speed upon fMLP treatment peaked on day 67 (6^{th} measurement), after a strong decrease, obvious in all stimulation conditions, on day 47 (5^{th} measurement). This peak in fMLP speed coincided with the patient's submission to hospital due to sinusitis with fever and bleeding of a gastric ulcer six days later (day 73). After day 95 (7^{th} measurement), the migration speed remained stable for all stimulation conditions, except for fMLP.

The amount of neutrophils exceeding an occupied area of 225 μm^2 decreased during Ruxolitinib therapy for PBS, CXCL1 and CXCL8 stimulated conditions (**Figure 14 a**), but the amount of larger cells upon fMLP treatment remained persistently elevated until day 287 (11^{th} measurement). Under CXCL1 and CXCL8 stimulated conditions, the percentage of enlarged cells peaked sharply on day 31 (4^{th} measurements), before it fell steadily again. Under fMLP stimulated conditions, the number of large cells sharply dropped at day 6 (2^{nd} measurement), rose again and then described a shallow, downward path.

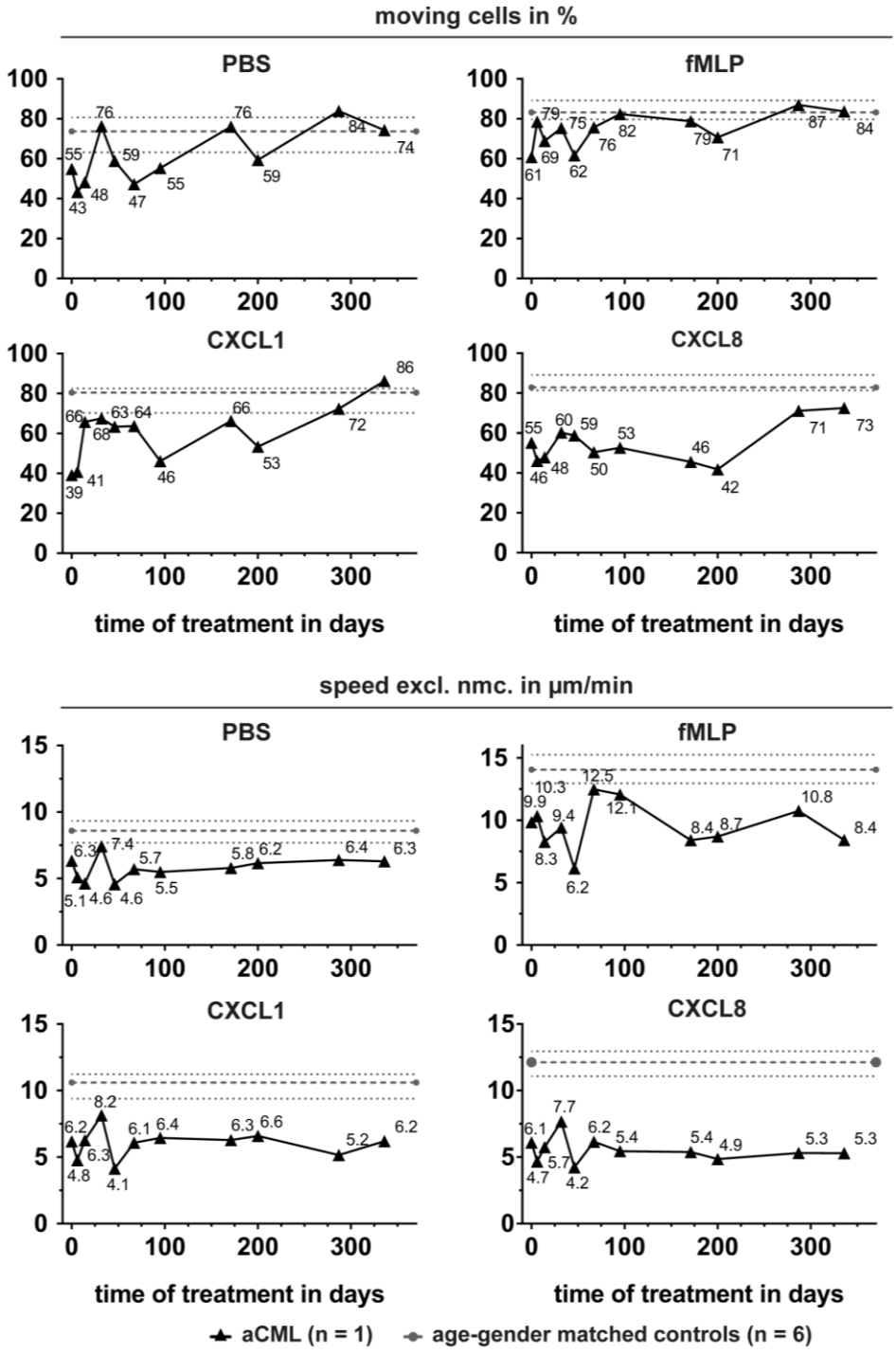

Figure 13: Long-term effect of Ruxolitinib on neutrophil migration.

Changes in the migratory patterns, percentage of moving cells (top panel) and speed excluding non-moving cells (speed excl. nmc., lower panel), of the aCML neutrophils over the course of treatment. Black triangles and black solid lines indicate aCML neutrophils (every timepoint n = 1), while grey dots and grey dashed lines indicate the median and the grey dotted lines indicate the interquartile range of the age- and gender-matched controls (n = 6). Numbers label the specific values of aCML neutrophils reached for percentage of moving cells (top) and speed excluding non-moving cells (bottom) respectively.

Regarding the expression levels, a rise in CD16 expression was observed from day 14 (3rd measurement) until day 95 (6th measurement) that resembled healthy controls, before the

expression levels dropped again (**Figure 14 b**). On day 287, the last flow cytometry measurement, CD16 expression exceeded the baseline levels.

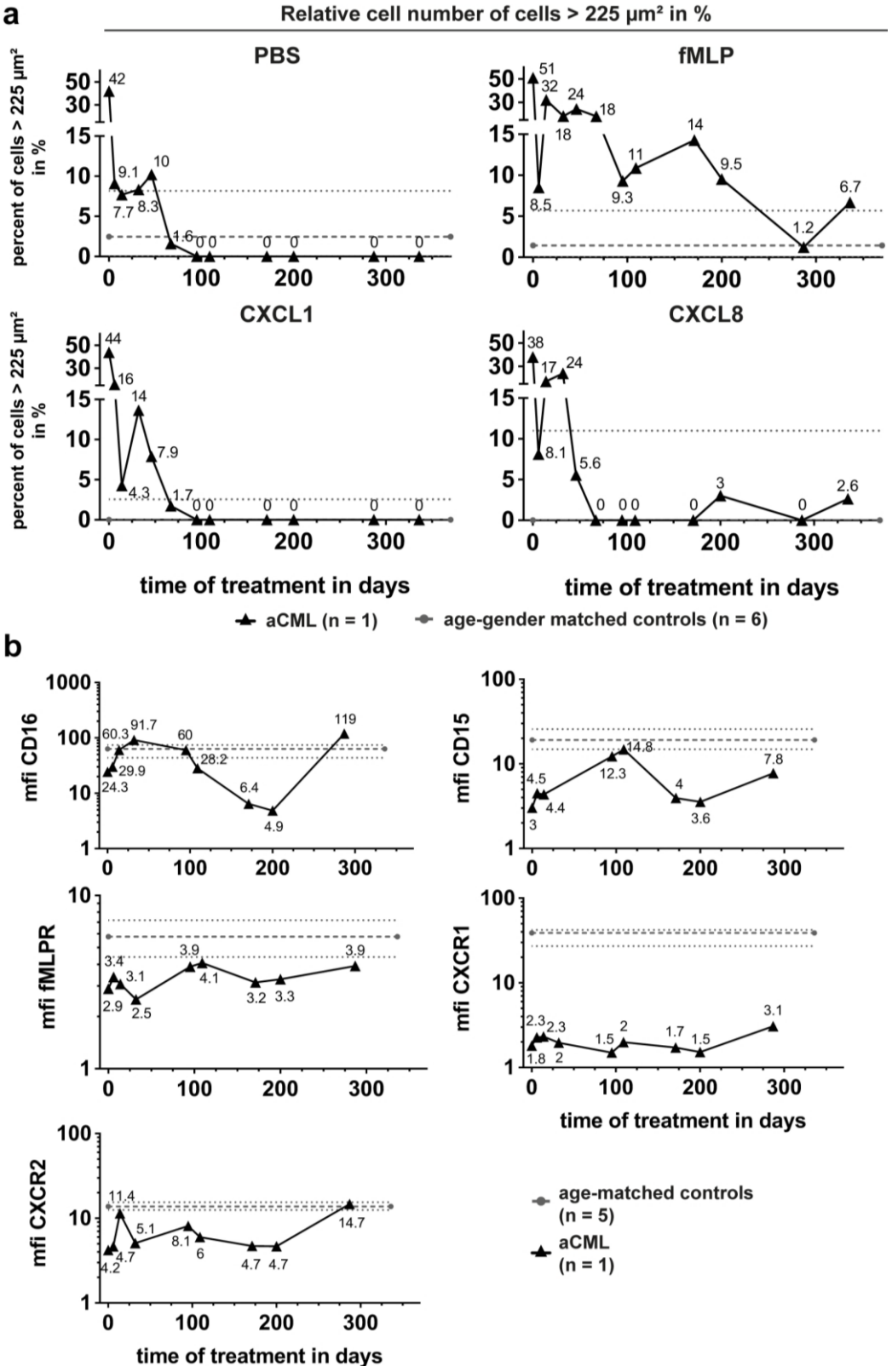

Figure 14: Long-term effect of Ruxolitinib cell size and receptor expression.

(**a**) Changes in the relative number of neutrophils with a cell size > 225 µm² under the four stimulation conditions over the course of therapy. Black triangles and black solid lines indicate aCML neutrophils (every timepoint n = 1), while grey dots and grey dashed lines indicate the median and the

grey dotted lines indicate the interquartile range of the age- and gender-matched controls (n = 6). On average, 41 and 56 cells per condition were analysed in age- and gender-matched controls and the aCML patient, respectively. Numbers label the specific percentage of cells > 225 µm² for the indicated timepoint. (**b**) Changes in CD16, CD15 and fMLPR (top) as well as CXCR1 and CXCR2 (bottom) expression given as mean fluorescence intensity (mfi) of aCML neutrophils over the course of Ruxolitinib therapy. Black triangles and black solid lines indicate the aCML patient (every timepoint n = 1), while grey dots and grey dashed lines indicate the median and the grey dotted lines indicate the interquartile range of the age-matched controls (n = 5). Numbers label the specific values for receptor expression at the respective timepoint. The gating strategy is detailed in **Figure 11 a**.

CD15 expression remained below healthy levels over the course of Ruxolitinib therapy, reaching almost normal levels on day 109 (6th measurement). The expression levels of fMLPR and CXCR1, signalling receptors for fMLP and CXCL8, respectively, stayed below healthy control levels. The expression of CXCR2, the signalling receptor for CXCL1 and CXCL8, peaked on day 14 (3rd measurement) and day 287 (last measurement), but otherwise remained below the healthy levels as well.

5.3.4. Immature neutrophils barely influenced neutrophil migration, cell size or receptor expression

The presence of neutrophil progenitors in the peripheral blood could be an explanation for the reduced migration behaviour, even though reports on this are conflicting[217, 218].

To investigate this, the peripheral blood counts were correlated with the migration speed and cell size to determine the influence that these progenitors have on the assay and on the cell's morphology. The movement speed of aCML neutrophils under control conditions correlated negatively with higher overall leucocyte and metamyelocyte counts in the peripheral blood, but not with the abundance of myeloblasts. The migration speed upon CXCL8 treatment, which was heavily impaired over the whole observation period, also correlated with the presence of metamyelocytes, however, none of the other parameters correlated with the high leucocyte counts or neutrophil progenitors in the assay (**Figure 15 a**).

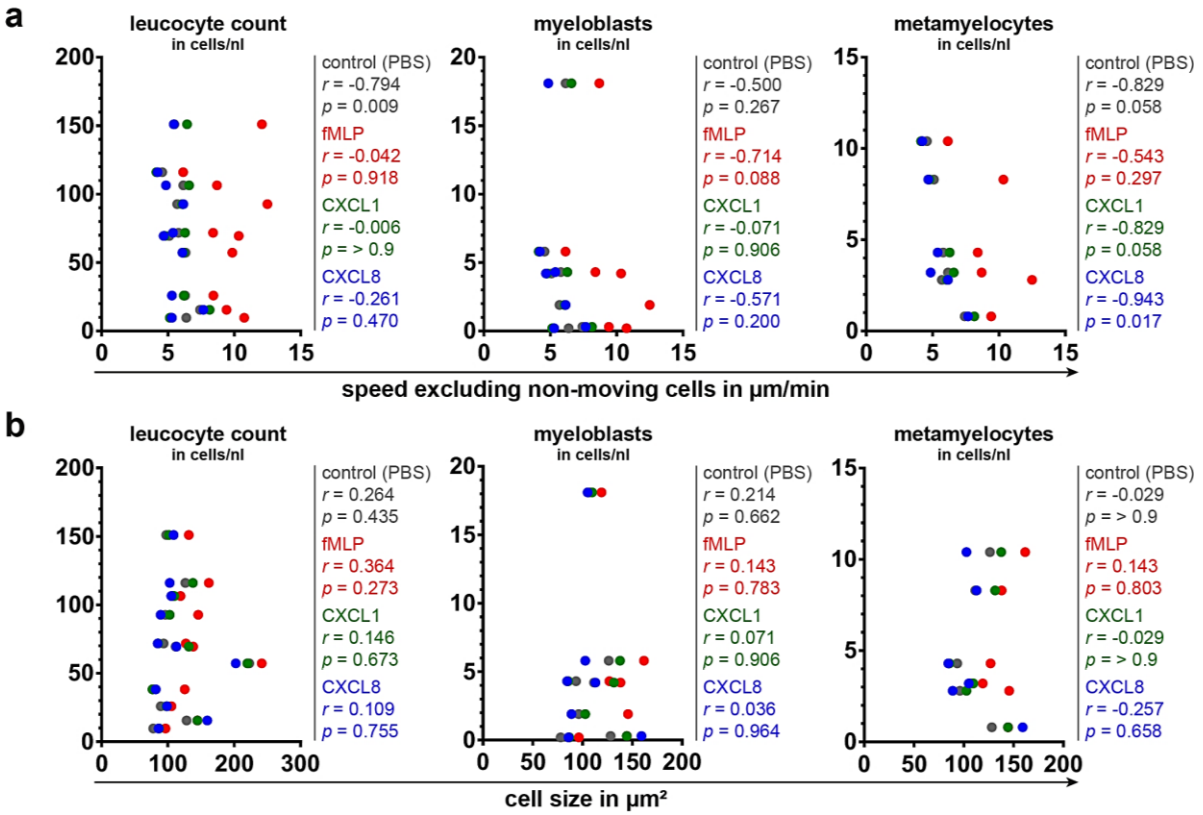

Figure 15: Correlation of neutrophil speed and cell size with leucocyte counts and the presence of neutrophil progenitors.

(**a**) Speed excluding non-moving cells (y-axis) was plotted against the overall leucocyte count (left, n = 10), myeloblast count (middle, n = 7) and metamyelocyte count (right, n = 6). (**b**) The cell size (y-axis) was plotted against the overall leucocyte count (left, n = 11), myeloblast count (middle, n = 7) and metamyelocyte count (right, n = 6). Each symbol indicates a timepoint of measurement of aCML neutrophils. Grey dots indicate the speed upon control (PBS) treatment, red stands for fMLP, green for CXCL1 and blue for CXCL8 treatment. The Spearman *r* and *p*-values correlations given next to the graphs were calculated via Spearman's correlation.

Furthermore, as CD15 and CD16 are both highly expressed on mature human neutrophils[42, 57, 58], the presence of immature neutrophils in the blood can potentially influence the analysis of these receptors. To clarify this, the peripheral blood counts were correlated with the mean fluorescence intensities of CD15 and CD16 from the same day (**Figure 16**). Interestingly, the absence of CD15 expression did not correlate with the assessed peripheral blood counts. However, the expression of CD16 correlated negatively with the abundance of myeloblasts in the peripheral blood, but not with the overall leucocyte count or the presence of metamyelocytes (**Figure 16 b**).

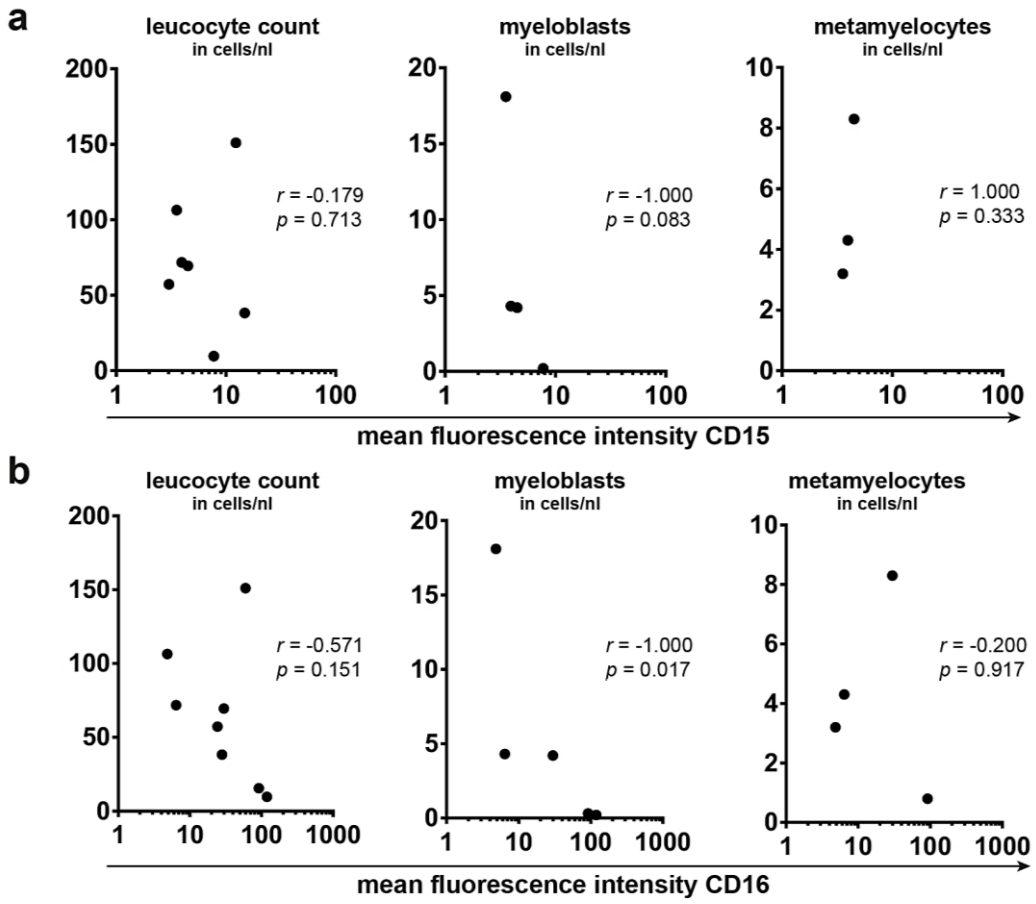

Figure 16: Correlation of CD15 and CD16 expression with leucocyte counts and the presence of neutrophil progenitors.

(**a**) The mean fluorescence intensity of CD15 (y-axis) was plotted against the overall leucocyte count (left, n = 8), myeloblast count (middle, n = 4) and metamyelocyte count (right, n = 3). (**b**) The mean fluorescence intensity of CD16 (y-axis) was plotted against the overall leucocyte count (left, n = 8), myeloblast count (middle, n = 5) and metamyelocyte count (right, n = 4). Each symbol indicates a timepoint of measurement of aCML neutrophils. The Spearman *r* and *p*-values correlations given next to the graphs were calculated via Spearman's correlation.

5.3.5. Summary II

The study of a rare aCML case revealed profound migration defects for all stimulation conditions before therapy onset with Ruxolitinib. Additionally, the cells presented with an abnormally sized cell body and showed reduced surface expression of all investigated markers. After one week of Ruxolitinib therapy, the cell size normalised, while the migration and receptor expression patterns remained impaired. Neutrophil size remained normal, while the migration behaviour was unsteady for all tested conditions but remained far below normal levels, especially in CXCL8 treated conditions. Interestingly, neutrophils lacked expression of CD15 and CXCR1, while the expression of fMLPR, CD16 and CXCR2 was unstable, but mostly below healthy levels.

5.4. Establishment of standardised migration assay and flow cytometry panels for human eosinophils, CD8⁺ T cells and neutrophils

Even though neutrophils are the most abundant cell type in the peripheral blood of humans[42], they are not the only important type. To expand the repertoire of available standardised assays, enabling the investigation of a larger variety of diseases with different associated important cell types, two additional *in vitro* migration assays were established: for human eosinophil granulocytes and cytotoxic CD8⁺ T cells.

5.4.1. Eosinophil granulocytes

Eosinophils are mostly known for their involvement in allergic airway diseases and in the host defence against parasites[77]. However, eosinophils extensively infiltrate into many types of human cancer[46], where they, either directly or indirectly, affect the tumour microenvironment in complicated, not completely understood ways[86].

As all circulating immune cells, eosinophils must infiltrate into the tissue, e.g. tumour, by extravasation from the blood stream and migration inside the tissue. The migration behaviour of this rare, but important leucocyte subset was characterised in healthy individuals. For this, the established neutrophil migration assay (**5.2**) was adjusted for human eosinophils.

After isolation, the cells were plated in 384-well plates and stimulated with four chemokines which potently induced eosinophil migration, namely CCL5, CCL7, CCL11 and CCL24. The concentration at which the migration induction was most prominent (highest values for speed and percentage of moving cells) and showed the lowest spread of the individual data points were determined by titration (**Figure 17 a**). 100 ng/ml for CCL5 and CCL11 and 500 ng/ml for CCL7 and CCL24 were chosen as the optimal concentrations for all future experiments regarding eosinophil migration (**Figure 17 a**, indicated by red dashed line). A comparative supplier test was conducted in order to analyse whether eosinophils are sensitive to variances in supplier-specific effects of the applied stimuli. Three independent suppliers for the stimuli at the indicated concentrations determined in **Figure 17 a** (**Figure 17 b**) were compared. Between the supplier-specific treated groups, no significant differences were detected, using Friedman's test and Dunn's multiple comparison (*p*-values are not depicted in **Figure 17 b**).

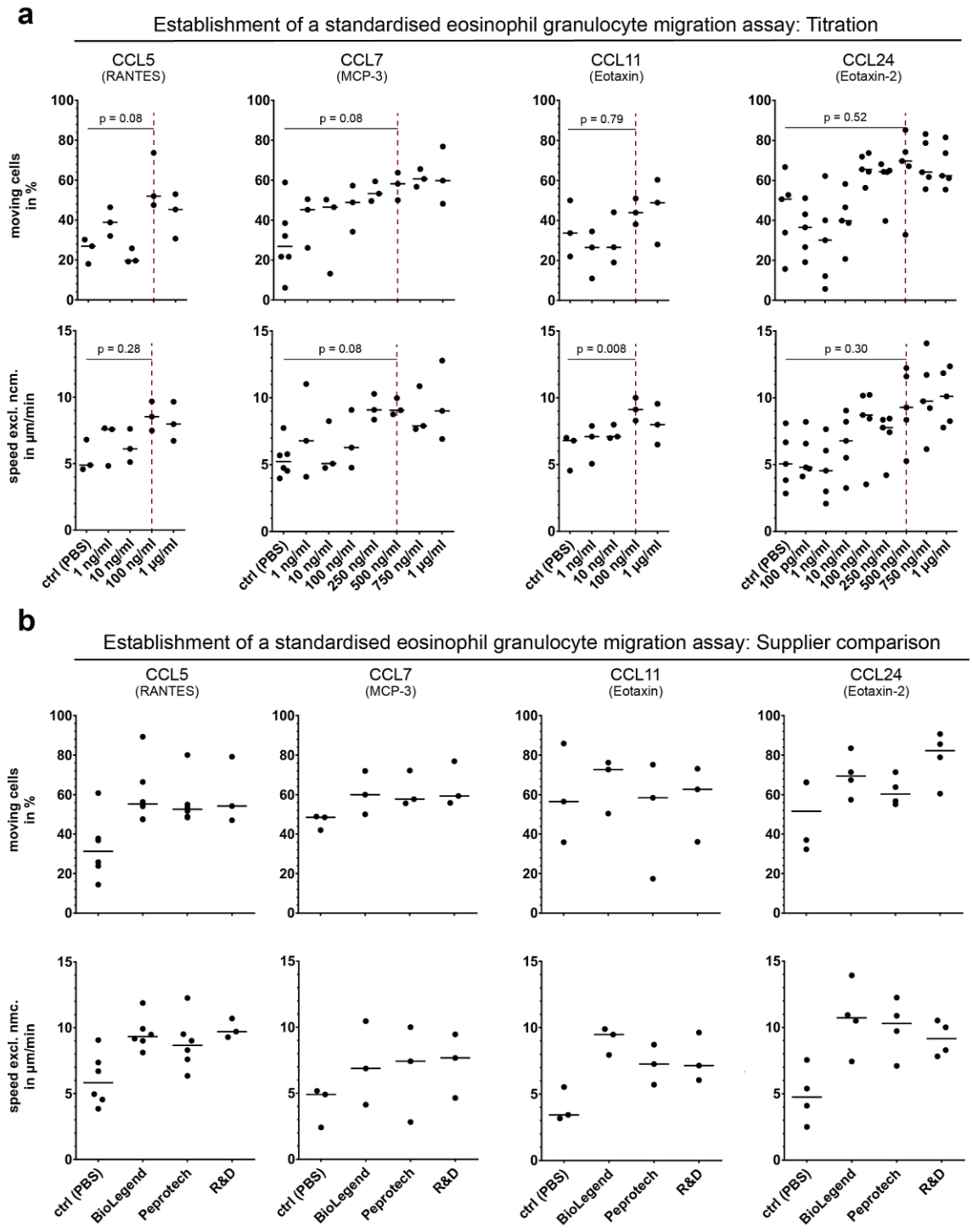

Figure 17: Establishment of a standardised migration assay for human eosinophils.

(**a**) Titration of the eosinophil activating cytokines, CCL5 (first), -7 (second), -11 (third) and -24 (fourth column). The y-axis depicts the percentage of moving cells in the upper row and speed excl. nmc. in µm per minute in the lower row. The x-axis always depicts the concentrations of the stimuli tested. Each black dot represents one healthy individual and the black lines mark the median of at least 3 independent experiments (n = 3-6). The red dashed line indicates the concentration chosen for the standardised eosinophil migration assay. *p*-values were calculated using the Friedman test and Dunn's multiple comparison. (**b**) Supplier comparison for the stimuli titrated in a). From left to right, CCL5, -7, -11, and -24 were tested from the three suppliers BioLegend, Peprotech and R&D Systems (R&D). The upper row shows the percentage of moving cells on the y-axis, in the lower

row the y-axis is the speed excl. nmc. in µm per min. The x-axis always indicates the different tested suppliers. Each dot represents one healthy individual and the black lines represent the median of a minimum of three independent experiments (n = 3-6). No significant differences were found between the supplier-specific treated groups, using Friedman's test and Dunn's multiple comparison.

In a next step, the eosinophil migration behaviour of 34 healthy individuals eligible for blood donation was determined. All applied stimuli significantly induced migration. This was indicated by a higher percentage of moving cells (**Figure 18**, left) and a higher speed value (**Figure 18**, right), except for CCL5. CCL24 and CCL7 caused the highest induction of both speed and moving cells. The percentage of moving cells was normally distributed for all stimuli conditions (**Figure 18**, bottom left), while only the speed for PBS (control) and CCL11 treatment passed D'Agostino & Pearson omnibus normality testing (**Figure 18**, bottom right).

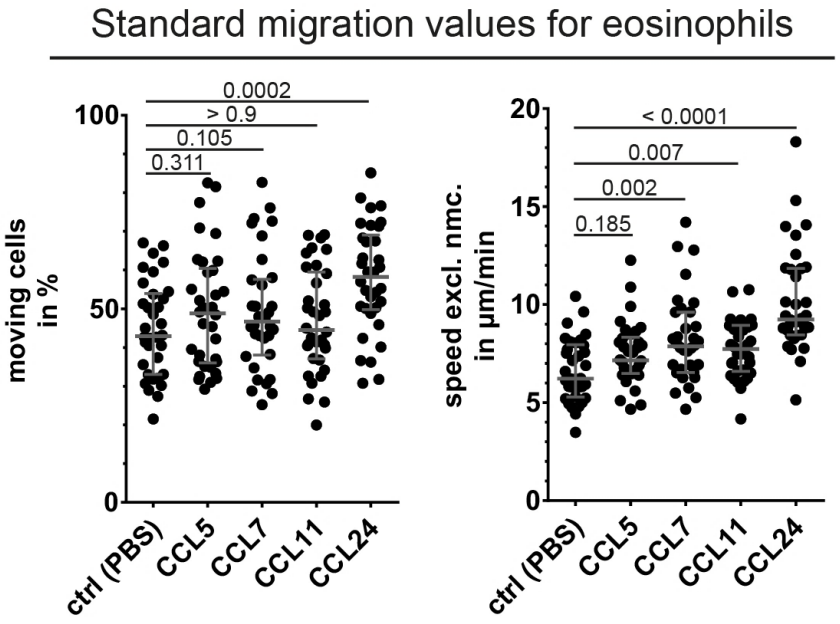

	ctrl (PBS)	CCL5	CCL7	CCL11	CCL24	ctrl (PBS)	CCL5	CCL7	CCL11	CCL24
n	34	34	34	34	34	34	34	34	34	34
Minimum	21.55	29.25	25.23	20.00	30.77	3.482	4.663	4.660	4.169	5.140
25% Percentile	33.06	36.01	38.10	37.08	49.78	5.288	6.485	6.541	6.593	8.455
Median	42.94	48.82	46.70	44.51	58.26	6.225	7.155	7.873	7.736	9.245
75% Percentile	53.93	60.47	57.65	59.52	69.07	7.953	8.331	9.612	8.943	11.840
Maximum	67.02	82.56	82.66	69.14	85.12	10.420	12.260	14.200	10.750	18.300
D'Agostino & Pearson omnibus normality test										
K2	2.261	2.716	2.040	1.958	0.802	0.831	7.196	6.584	0.0855	9.492
P value	0.323	0.257	0.361	0.376	0.670	0.660	0.027	0.037	0.958	0.009
Passed normality test (alpha=0.05)?	Yes	Yes	Yes	Yes	Yes	Yes	No	No	Yes	No

Figure 18: Standard eosinophil migration patterns.

Eosinophil migration according to the standardised assay was assessed for 34 healthy individuals. The left graph displays the standard values for the percentage of moving cells and the right graph the standard values for speed excl. nmc. in µm per min. The x-axis indicates the tested conditions. Each black dot represents a single individual and median ± interquartile range are given in dark grey. The *p*-values were calculated using the Friedman test and Dunn's multiple comparison. The table below details the test size (n), minima, maxima, median and percentiles of the tested conditions, as well as the results from the D'Agostino and Pearson omnibus normality test for the data

points above.

It is known that primary cells, granulocytes in particular, are sensitive to extended handling times, regarding their activation status. Furthermore, immune cells are known for their decreased activity in elderly people[219]. However, time for sample preparation and gender had no impact on eosinophil migration (data not shown).

Additionally, it was tested whether the gender of the blood donor had any influence on eosinophil migration. Here, no significant differences between male and female blood donors for the speed of eosinophils at baseline (PBS) and under CCL5, CCL7 and CCL11 treatment were detected (**Figure 19**, right). Interestingly, male blood donors showed a higher eosinophil speed than female donors, while the percentage of moving cells or the speed upon CCL24 remained unaffected (**Figure 19**).

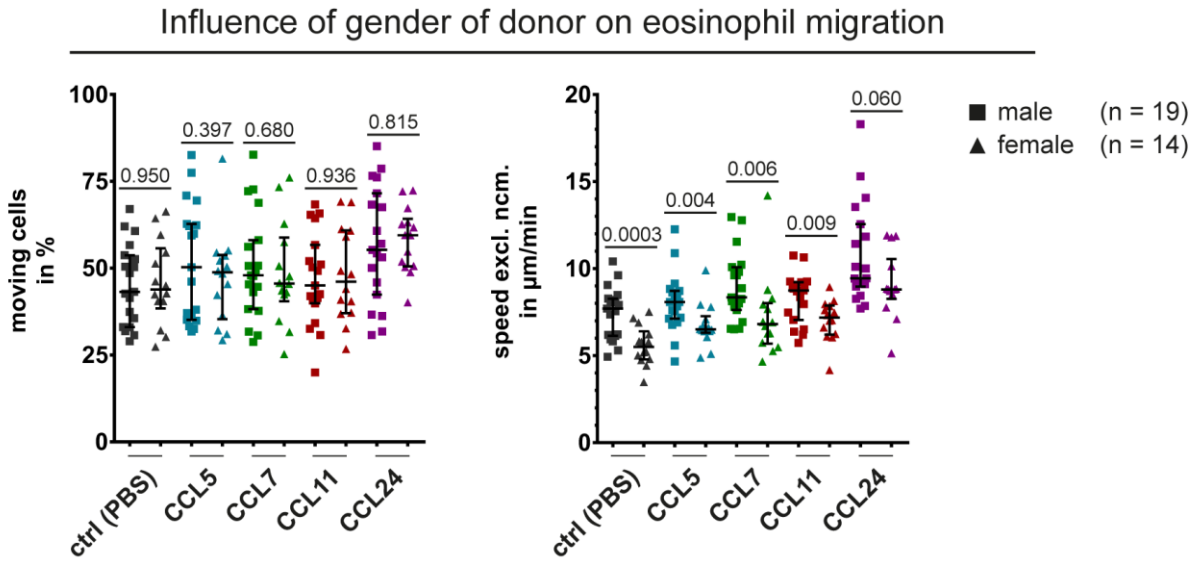

Figure 19: Correlation of eosinophil migration with gender.

Influence of gender on eosinophil migration. The percentage of moving cells (y-axis, left) and the speed excl. nmc. (y-axis, right) are plotted against the stimulation conditions, separated by the gender of the blood donor. Squares indicate male individuals (n = 19) and triangles females (n = 14). Dark grey stands for the control (ctrl, PBS), blue for CCL5, green for CCL7, red for CCL11 and purple for CCL24. Black lines represent the median ± interquartile range and the *p*-values were calculated using the Mann-Whitney *U*-test.

The purity of the analysed samples and the activation status of a cell can influence the outcome of cell migration experiments. As these parameters are easily assessed by flow cytometry, a staining panel was established to analyse the purity and general activation state of human eosinophil granulocytes. Eosinophil granulocytes were stained with antibodies against the lineage markers sialic acid-binding Ig-like lectin (Siglec) 8 and C-C chemokine receptor type (CCR) 3 and the activation markers CD69 and CD44. The cells did not bind the isotype controls to the respective antibodies (**Figure 20 a**) and upon stimulation with 10 nM

GM-CSF for 2 h *in vitro*, eosinophils upregulated both Siglec 8 and CD69 (**Figure 20 b**). CD44 was not upregulated.

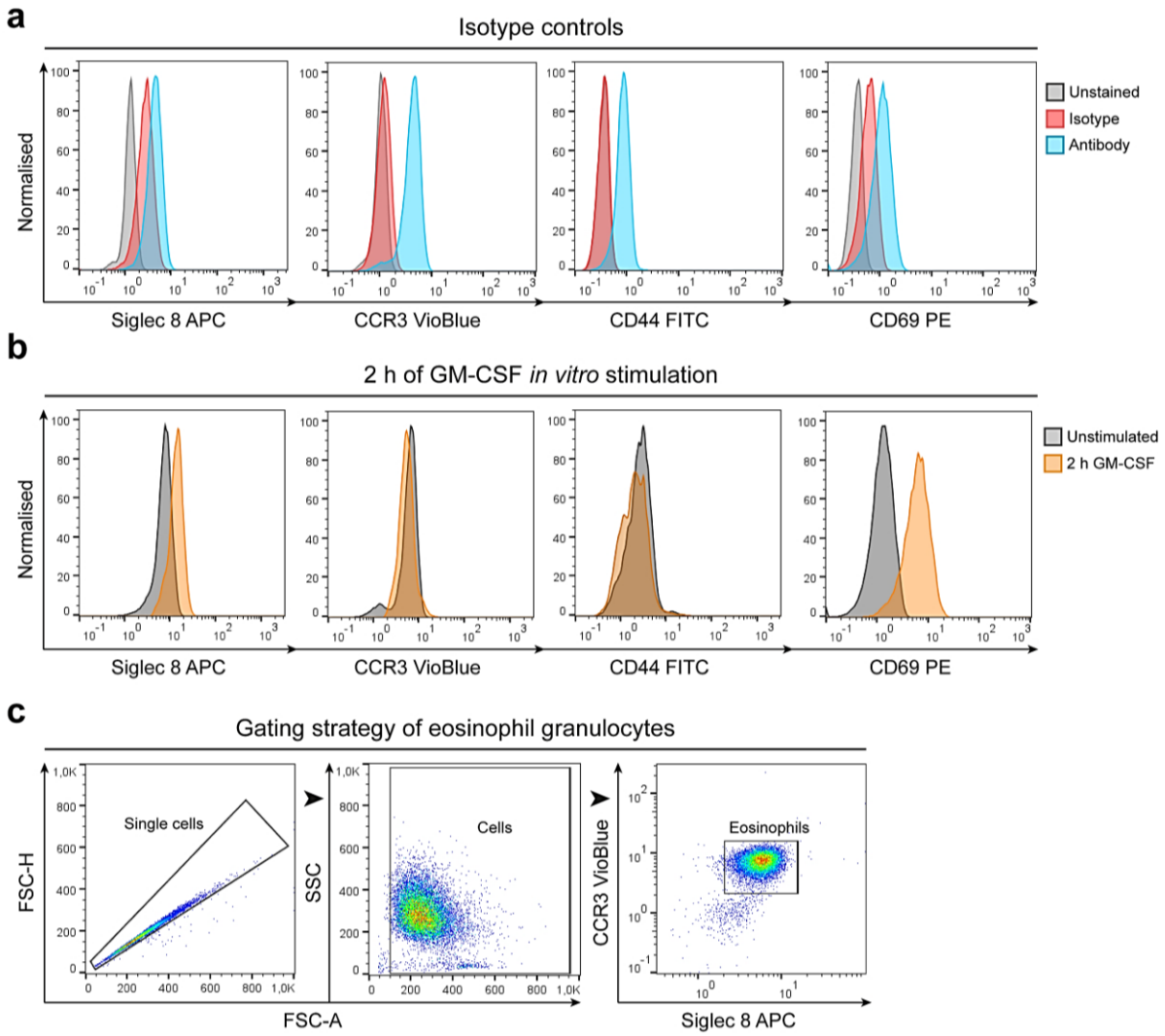

Figure 20: Establishment of a flow cytometry assay for human eosinophils.

A flow cytometry assay was established for eosinophil granulocytes staining for Siglec 8, CCR3, CD44 and CD69. (**a**) Normalised histograms comparing unstained cells (grey), isotype control stained cells (red) and antibody stained cells (blue) for Siglec 8 (1st), CCR3 (2nd), CD44 (3rd) and CD69 (4th panel). (**b**) Purified human eosinophils were either stimulated with 10 nM GM-CSF (orange) for 2 h *in vitro* or left untreated (grey) and stained for Siglec 8 (1st), CCR3 (2nd), CD44 (3rd) and CD69 (4th panel). (**c**) Gating strategy for all following flow cytometric analyses of human eosinophil granulocytes. First, doublets were excluded by forward scatter (FSC) area (FSC-A) and FSC height (FSC-H) doublet exclusion, followed by side scatter (SSC) area (SSC-A) and SSC height (SSC-H) doublet exclusion (not shown). Subsequently, residual debris and erythrocytes were excluded based von der FSC-SSC properties. After that, the expressions of Siglec 8 and CCR3 were used to identify eosinophils and all geometric mean fluorescence intensities (geo mfi) were determined on this eosinophil population.

For all following flow cytometric analyses, doublets were excluded by their forward scatter area (FSC-A) and height (FSC-H), as well as their side scatter area (SSC-A) and height (SSC-H) properties, followed by exclusion of residual debris and erythrocytes based

on their FSC-SSC properties and finally, eosinophils were identified based on their expression of Siglec 8 and CCR3 (**Figure 20 c**).

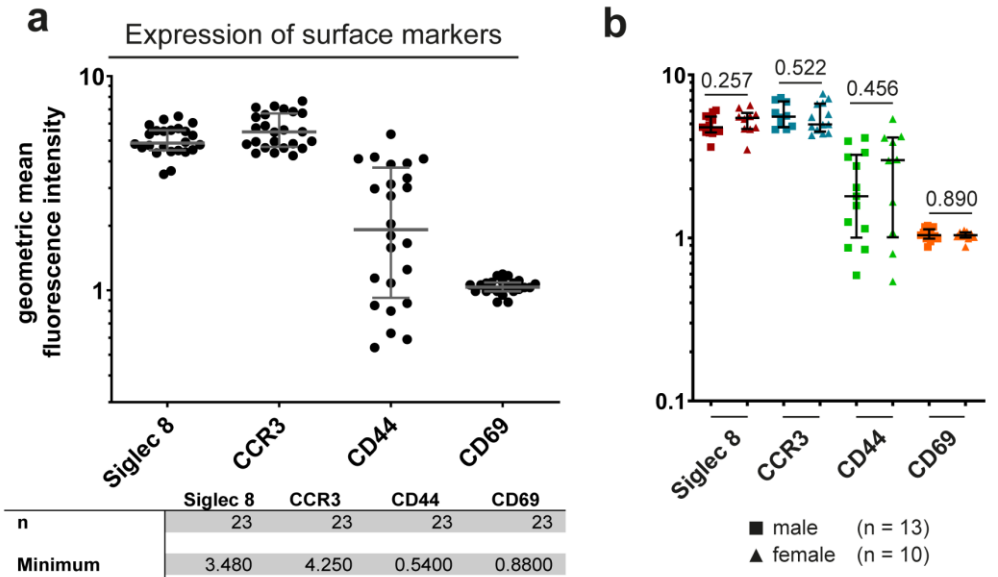

	Siglec 8	CCR3	CD44	CD69
n	23	23	23	23
Minimum	3.480	4.250	0.5400	0.8800
25% Percentile	4.500	4.630	1.080	0.9900
Median	4.920	5.480	2.040	1.040
75% Percentile	5.590	6.720	3.870	1.090
Maximum	6.500	7.650	5.360	1.190
D'Agostino & Pearson omnibus normality test				
K2	0.1771	4.390	3.225	0.3014
P value	0.9152	0.1114	0.1994	0.8601
Passed normality test (alpha=0.05)?	Yes	Yes	Yes	Yes

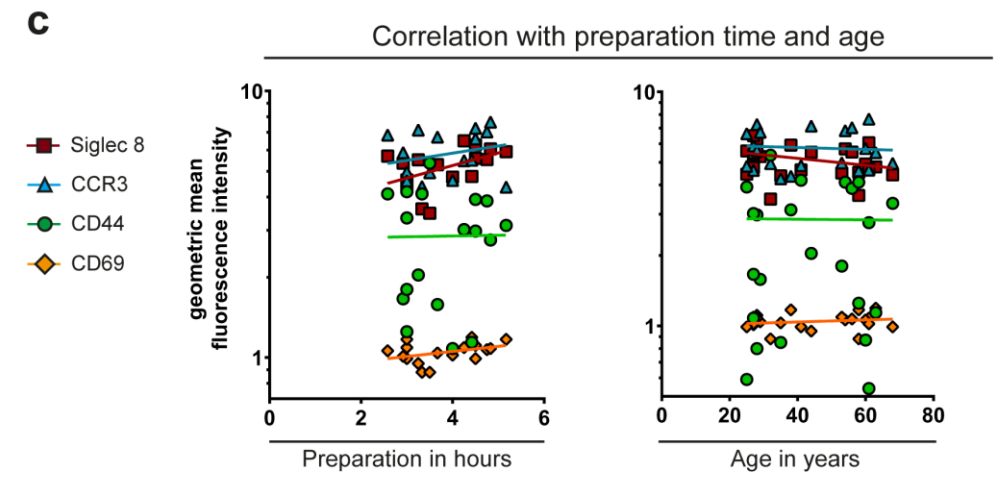

	Siglec 8	CCR3	CD44	CD69	Siglec 8	CCR3	CD44	CD69
n	18	18	18	18	18	18	18	18
Spearman r								
r	0.516	0.194	-0.043	0.348	-0.333	-0.031	0.023	0.152
95 % confidence interval	0.050 to 0.798	-0.314 to 0.615	-0.511 to 0.445	-0.157 to 0.709	-0.700 to 0.173	-0.502 to 0.454	-0.461 to 0.496	-0.352 to 0.588
P value								
P (two-tailed)	0.028	0.440	0.867	0.157	0.177	0.903	0.930	0.548

Figure 21: Receptor expression pattern of human eosinophils and correlation with gender, preparation time and age.

(**a**) Expression levels of Siglec 8, CCR3, CD44, and CD69 on eosinophils from healthy individuals in geometric mean fluorescence intensity (geo mfi, y-axis). The grey lines indicate the median ± inter-

quartile range. Each black dot represents a single individual. The table below details the test size (n), minima, maxima, median and percentiles for the tested conditions, as well as the results from the D'Agostino and Pearson omnibus normality test. The gating strategy is detailed in **Figure 20 c**. (**b**) Influence of gender of eosinophil surface marker expression. The geo mfi of the surface markers is separated by the gender of the blood donor. Squares indicate male individuals (n = 13) and triangles females (n = 10). Red stands for Siglec 8, blue for CCR3, green for CD44 and orange for CD69 expression. Black lines represent the median ± interquartile range and the *p*-values were calculated using the Mann-Whitney *U*-test. (**c**) Influence of time for sample preparation and age of the donors on eosinophil surface marker expression. Time for sample preparation in h (x-axis, left) and age of the blood donors (x-axis, right) are plotted against the geo mfi of the tested markers (left). Each dot represents a single individual and the lines represent the results from the best-fit of the nonlinear regression calculation. Red squares stand for Siglec 8, blue triangle for CCR3, green dots for CD44 and orange rhombi for CD69 expression. The table below details the sample size (n), the results from the Spearman correlation as well as the *p*-value for the correlation.

In healthy people, a steady expression of Siglec 8, CCR3 and CD69 was encountered, while CD44 displayed a high individual variance (**Figure 21 a**, top). The intensities were normally distributed for all tested markers (**Figure 21 a**, bottom). Siglec 8 was upregulated on samples with prolonged handling times, while all the other markers were independent of the time for sample preparation (**Figure 21 c**, left and left bottom). None of the markers correlated with age or gender of the blood donors (**Figure 21 b + c**), excluding activation status as the reason for gender-dependent eosinophil migration in healthy individuals (**Figure 19 b**). Furthermore, no significant correlations between the eosinophil migration parameters and the receptor expression of Siglec 8, CCR3, CD44 and CD69 could be detected (data not shown).

5.4.2. CD8⁺ T cells

Cytotoxic CD8⁺ T cells are the main effectors of the adaptive immune system against neoplastic or virus infected cells[103]. With their highly specialised T cell receptor (TCR), they can recognise their specific antigen and react to the trigger with the expression of cell death inducing receptors, e.g. the Fas ligand, or degranulation. To characterise their migration, the assays for neutrophils and eosinophils were adjusted for CD8⁺ T cells.

After incubation on ICAM-1 coated plates (see **3.3.2.3**), a variety of stimuli were applied but only stromal cell-derived factor 1 (SDF-1), in its α and β isoform, sufficiently induced migration in CD8⁺ T cells. Hence, SDF-1 α and β were titrated to determine the optimal concentration, which was defined as the amount of stimulus where the induction of migration parameters was highest (highest value) and the spread among the tested individuals was lowest. For SDF-1α, 500 ng/ml induced the highest, most reproducible and for the speed including non-moving cells (speed incl. nmc.) also significant migration (**Figure 22 a**, upper

row). A suboptimal, non-significant concentration of 100 ng/ml was chosen as a second control (**Figure 22 a**, upper row).

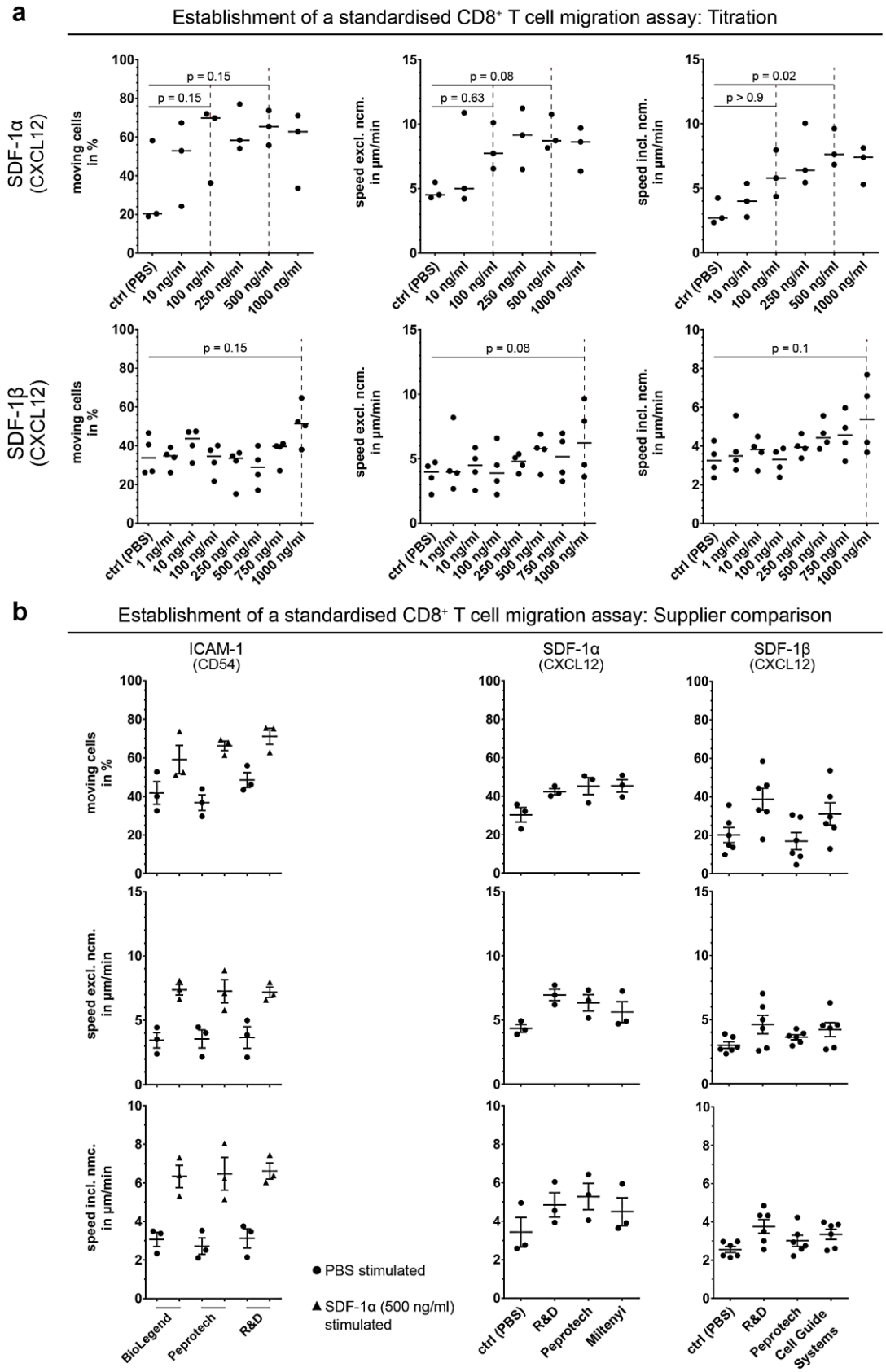

Figure 22: Establishment of a standardised migration assay for human CD8⁺ T cells.

(**a**) Titration of the CD8⁺ T cell activating cytokine stromal cell-derived factor 1 (SDF-1) in its α- and β-isoform (SDF-1α, top and SDF-1β, bottom row). The y-axis depicts the percentage of moving cells (left column), the speed excl. nmc. in µm per minute (middle column) and the speed including (incl.) nmc. in µm per minute (right column). The x-axis always depicts the concentrations of the stimuli tested. Each black dot represents one healthy individual and the black lines mark the median of at least 3 independent experiments (n = 3-4). The red dashed lines indicate the concentrations chosen for the standardised CD8⁺ T cell migration assay. *p*-values were calculated using the Friedman test and Dunn's multiple comparison. (**b**) Supplier comparison for the stimuli titrated in a). From left to right, intercellular adhesion molecule 1 (ICAM-1), which was used for coating and pre-activation of the cells, SDF-1α (500 ng/ml) and SDF-1β were tested from the suppliers BioLegend, Peprotech, R&D Systems (R&D), Miltenyi Biotec (Miltenyi) and Cell Guide Systems. For ICAM-1 (first column), baseline migration (ctrl, PBS) upon supplier-specific ICAM-1 coating (black dots) was measured as well as the migration induction upon treatment with 500 ng/ml of SDF-1α (black triangles). The first row shows the percentage of moving cells on the y-axis, in the second row the y-axis is the speed excl. nmc. in µm per min and in the last row, the y-axis depicts the speed incl. nmc. in µm per min. The x-axis always indicates the different tested suppliers. Each dot represents one healthy individual and the black lines represent the median of a minimum of three independent experiments (n = 3-6). No significances were computed between the supplier-specific treated groups, using Friedman test and Dunn's multiple comparison.

SDF-1β was less potent to induce migration in the cells, hence, 1,000 ng/ml, the highest tested concentration, was chosen as it induced the highest migration values (**Figure 22 a**, lower row). To test the independence of this assay from supplier-specific variances in stimuli effectiveness, a supplier test was conducted, comparing stimuli from 5 independent suppliers.

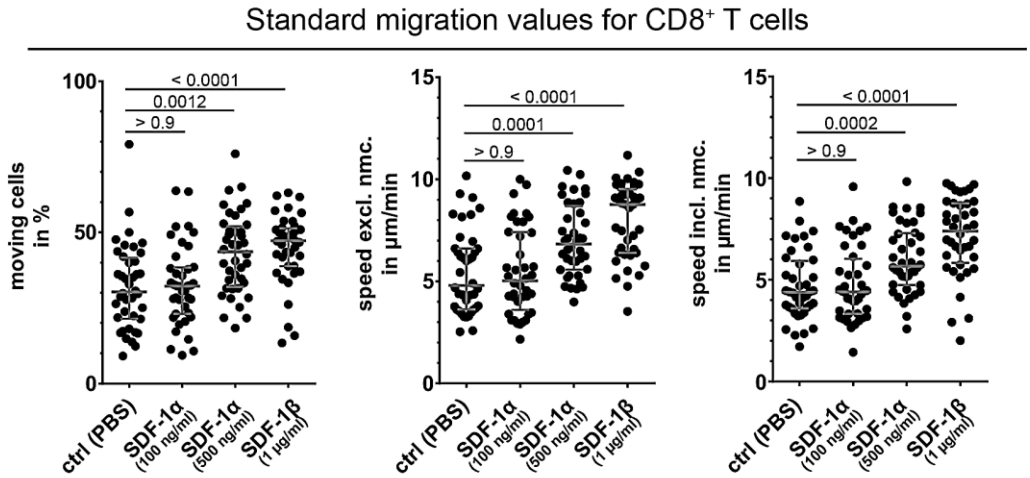

	moving cells in %				speed excl. nmc. in µm/min				speed incl. nmc. in µm/min			
	ctrl (PBS)	SDF-1α (100 ng/ml)	SDF-1α (500 ng/ml)	SDF-1β	ctrl (PBS)	SDF-1α (100 ng/ml)	SDF-1α (500 ng/ml)	SDF-1β	ctrl (PBS)	SDF-1α (100 ng/ml)	SDF-1α (500 ng/ml)	SDF-1β
n	40	40	40	40	40	40	40	40	40	40	40	40
Minimum	9.090	9.330	18.35	13.41	2.530	2.160	3.990	3.530	1.720	1.440	2.590	2.010
25% Percentile	21.48	23.09	31.95	38.82	3.630	3.608	5.575	6.403	3.603	3.333	4.745	5.835
Median	30.26	32.19	43.60	47.23	4.800	5.030	6.825	8.760	4.385	4.405	5.675	7.400
75% Percentile	41.58	38.41	52.00	51.34	6.608	7.413	8.695	9.523	5.930	6.033	7.298	8.763
Maximum	79.17	63.75	76.00	63.11	10.17	10.00	10.44	11.18	8.860	9.580	9.830	9.750
D'Agostino & Pearson omnibus normality test												
K2	9.060	1.980	0.4642	8.685	3.504	4.204	4.113	3.166	2.653	3.741	1.085	4.367
P value	0.0108	0.3715	0.7929	0.0130	0.1735	0.1222	0.1279	0.2053	0.2653	0.1540	0.5814	0.1127
Passed normality test (alpha=0.05)?	No	Yes	Yes	No	Yes	Yes	Yes	Yes	Yes	Yes	Yes	Yes

Figure 23: Standard migration values for human CD8⁺ T cells.

CD8⁺ T cell migration according to the standardised assay was assessed for 40 healthy individuals. The left scatter dot plot displays the standard values for the percentage of moving cells and the right graph the standard values for speed excl. nmc. in µm per min. The x-axis indicates the tested conditions. Each black dot represents a single individual and median ± interquartile range are given in dark grey. The *p*-values were calculated using the Friedman test and Dunn's multiple comparison. The table below details the test size (n), minima, maxima, median and percentiles of the tested conditions, as well as the results from the D'Agostino and Pearson omnibus normality.

For ICAM-1 coating, no influence of the origin of the cytokine on baseline (PBS) and SDF-1α (500 ng/ml) stimulated migration could be detected (**Figure 22 b**, left column). For SDF-1α, tested for 500 ng/ml only, and SDF-1β, no significant dependences on the supplier of the cytokines were encountered.

With this assay, the migration patterns of CD8⁺ T cells were determined from 40 healthy individuals (**Figure 23 a**). The percentage of moving cells (left), the speed excl. nmc. (middle) and the speed incl. nmc. (right) were significantly increased upon treatment with 500 ng/ml SDF-1α and 1 µg/ml SDF-1β. 100 ng/ml SDF-1α did not induce any migration changes, as already seen in the previous experiment (**Figure 23 a**). Except for the percentage of moving cells at baseline (ctrl, PBS) and when treated with 1 µg/ml SDF-1β, all parameters and stimulation conditions passed normality testing (**Figure 23 a**, below the graphs).

Furthermore, the effect of gender on T cell migration was elucidated by grouping the migration values according to gender (**Figure 24**). On average, female donors showed fewer moving cells (**Figure 24**, left) for 100 ng/ml and 500 ng/ml SDF-1α, but no significance could be detected. Therefore, none of the migration parameters or stimuli conditions were affected by the gender of the blood donors (**Figure 24**). Notably, CD8⁺ T cell migration was not impacted by time for sample preparation or age of the blood donor (data not shown).

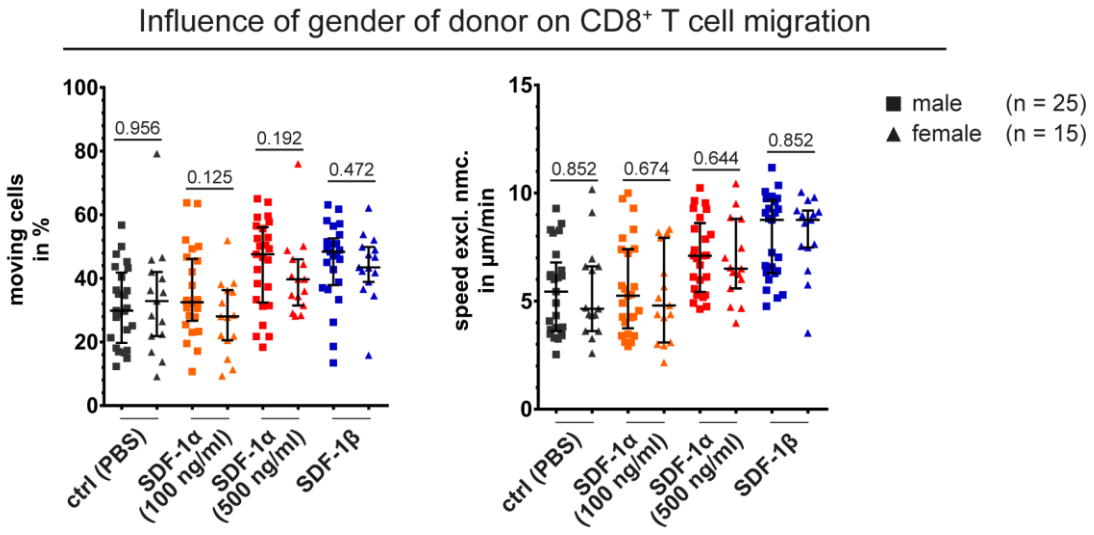

Figure 24: Correlation of CD8⁺ T cell migration with gender.

Influence of gender on CD8⁺ T cell migration. The percentage of moving cells (y-axis, left) and the

speed excl. nmc. (y-axis, right) are plotted against the stimulation conditions, grouped by the gender of the blood donor. Squares indicate male individuals (n = 25) and triangles females (n = 15). Dark grey stands for the control (ctrl, PBS), orange for SDF-1α (100 ng/ml), red for SDF-1α (500 ng/ml) and blue for SDF-1β. Black lines represent the median ± interquartile range and the *p*-values were calculated using the Mann-Whitney *U*-test.

To investigate the effect of different CD8⁺ T cell subpopulations on migration, the cells were subdivided into different groups according to their expression of cell surface markers, such as CD45RO and CCR7. CD45RO is upregulated once T cells enter the memory stage[220], while downregulation of CCR7 indicates an activation of the T cell[221]. Using these two antibodies, a differentiation between naïve (CCR7⁺ CD45RO⁻) CD8⁺ T cells, activated (CCR7⁻ CD45RO⁻) CD8⁺ T cells, memory (CCR7⁺ CD45RO⁺) CD8⁺ T cells and activated memory (CCR7⁻ CD45RO⁺) CD8⁺ T cells was possible. Furthermore, the T cells were stained with an antibody against CD154, the CD40 ligand, which is expressed by CD8⁺ T cells that share similarities with conventional helper CD4⁺ T cells and possess helper functions[222].

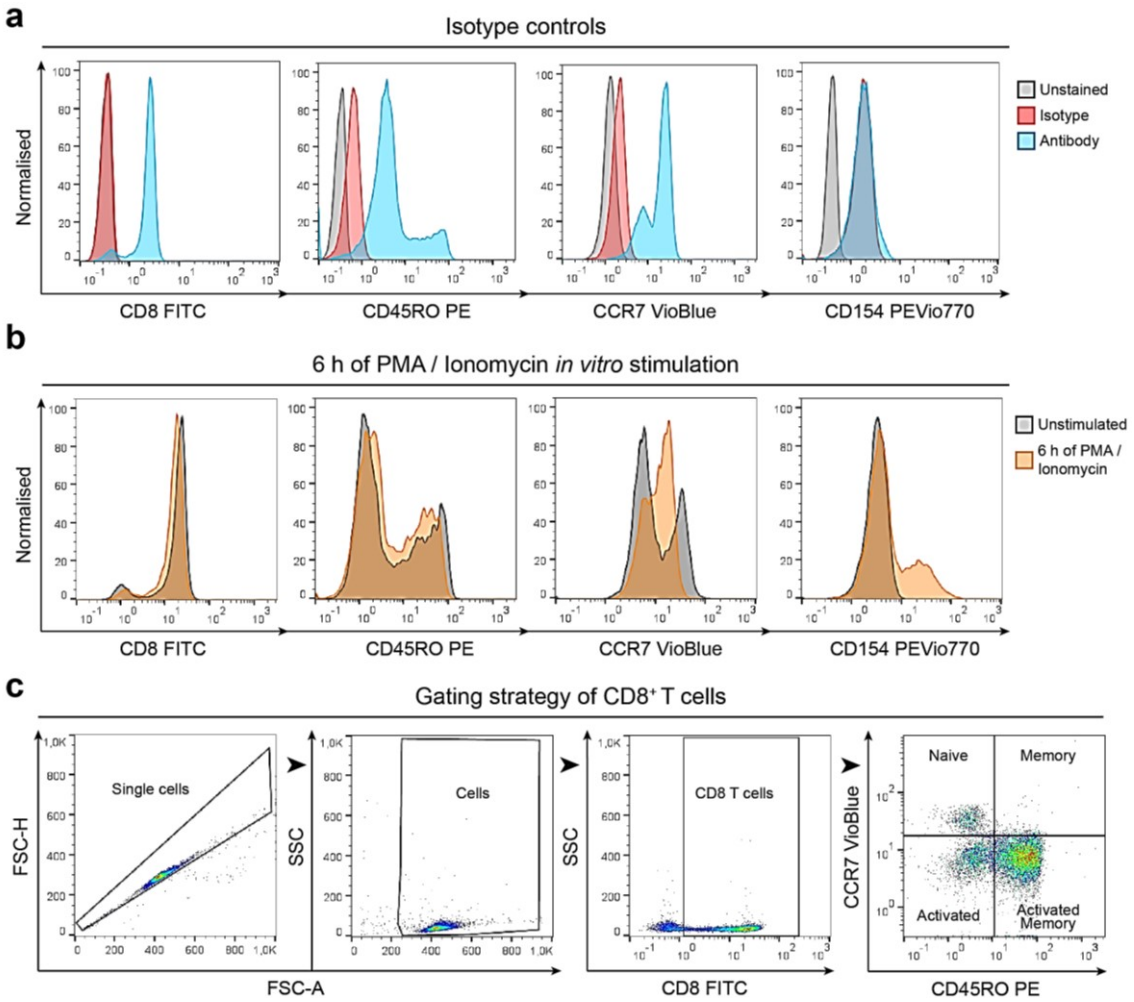

Figure 25: Establishment of a flow cytometric panel for human CD8⁺ T cells.

A flow cytometry assay was established for human CD8⁺ T cells staining for CD8, CD45RO, CCR7 and CD154. (**a**) Normalised histograms comparing unstained cells (grey), isotype control stained cells (red) and antibody stained cells (blue) for CD8 (1st), CD45RO (2nd), CCR7 (3rd) and CD154 (4th

panel). (**b**) Purified human CD8⁺ T cells were either stimulated with 100 nM PMA and 1 µM ionomycin (orange) for 6 h *in vitro* or left untreated (grey) and stained for CD8 (1st), CD45RO (2nd), CCR7 (3rd) and CD154 (4th panel). (**c**) Gating strategy for all following flow cytometric analyses of human CD8⁺ T cells. First, doublets were excluded by FSC-A and FSC-H doublet exclusion, followed by SSC-A and SSC-H doublet exclusion (not shown). Subsequently, residual debris and erythrocytes were excluded based von der FSC-SSC properties. After that, the expression of CD8 was used to identify CD8⁺ T cells, which were further subdivided based on their expression of CD45RO and CCR7 into naïve (CD45RO⁻ CCR7⁺), activated (CD45RO⁻ CCR7⁻), memory (CD45RO⁺ CCR7⁻) and activated memory (CD45RO⁺ CCR7⁺) T cells. The expression of CD154 is always based on the total CD8+ events and given as mean fluorescence intensity (mfi).

Again, the isotype controls were negative (**Figure 25 a**), however CD154 was not expressed on CD8⁺ T cells in the peripheral blood. To test whether the antibody can detect the upregulation of CD154 and downregulation of CCR7 upon stimulation, the CD8+ T cells were treated with 100 nM phorbol 12-myristate 13-acetate (PMA) and 1 µM ionomycin for 6 h, stained with the antibodies and compared to unstimulated control cells of the same donor (**Figure 25 b**). As expected, CD8 and CD45RO did not change in expression level upon stimulation, while CCR7 overall downregulated and a small portion of cells expressed CD154, proving that the panel can detect changes in the expression patterns.

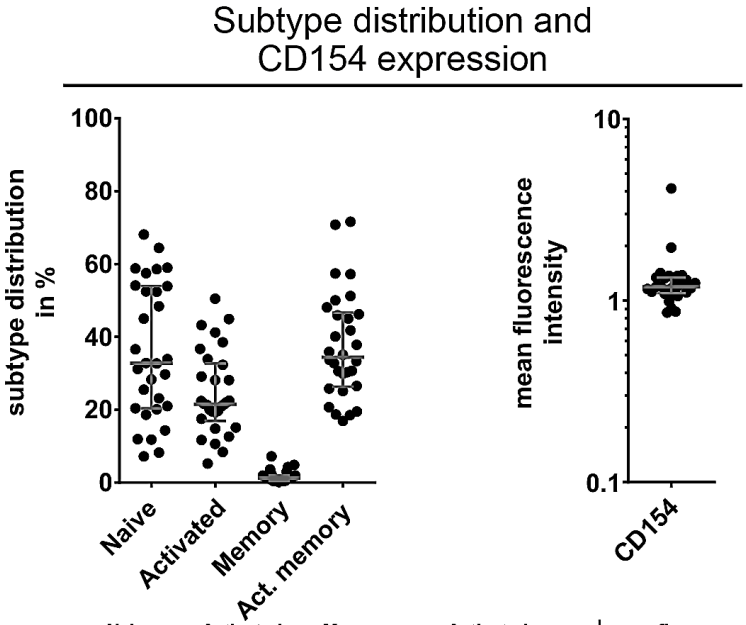

	Naive T cells	Activated T cells	Memory T cells	Activated memory T cells	mfi CD154
n	30	30	30	30	30
Minimum	7.160	5.200	0.2100	16.90	0.8600
25% Percentile	20.33	16.90	0.4500	26.33	1.100
Median	32.75	21.50	1.220	34.40	1.190
75% Percentile	53.95	32.70	1.918	46.68	1.340
Maximum	68.10	50.50	7.170	71.60	4.150
D'Agostino & Pearson omnibus normality test					
K2	7.929	1.992	23.34	2.867	59.44
P value	0.0190	0.3693	< 0.0001	0.2385	< 0.0001
Passed normality test (alpha=0.05)?	No	Yes	No	Yes	No

Figure 26: Assessment of CD8⁺ T cell subtypes and CD154 expression.

Left: CD8⁺ T cells were grouped into subtypes (x-axis) according to their expression of CCR7 and

CD45RO. Percentages (y-axis) were calculated from all CD8⁺ events. *Right*: The mean fluorescence intensity (y-axis) of CD154 (CD40L) is based on all CD8⁺ events. The grey lines indicate the median ± interquartile range. Each black dot represents a single individual (n = 30). The table below details the test size (n), minima, maxima, median and percentiles for the tested conditions, as well as the results from the D'Agostino and Pearson omnibus normality test.

For all following flow cytometric analyses, doublets were excluded by their FSC-A and FSC-H, as well as their SSC-A and SSC-H properties, followed by exclusion of residual debris and erythrocytes based on their FSC-SSC properties. Finally, CD8⁺ T cells were identified using their expression of CD8 and the different subpopulations were determined by their expression of CD45RO and CCR7. CD154 expression was assessed on the total CD8⁺ population (**Figure 25 c**). According to this scheme, the subtype distribution in 30 healthy individuals was analysed (**Figure 26**, left). Memory cells made up the fewest percentage of circulating CD8⁺ T cells, while naïve and activated memory cells were equally as abundant on average. The amount of activated and activated memory T cells was normally distributed, while the number of naïve and memory T cells was not. Additionally, the expression of CD154 was assessed and found to be absent in the same healthy people (**Figure 26**, right).

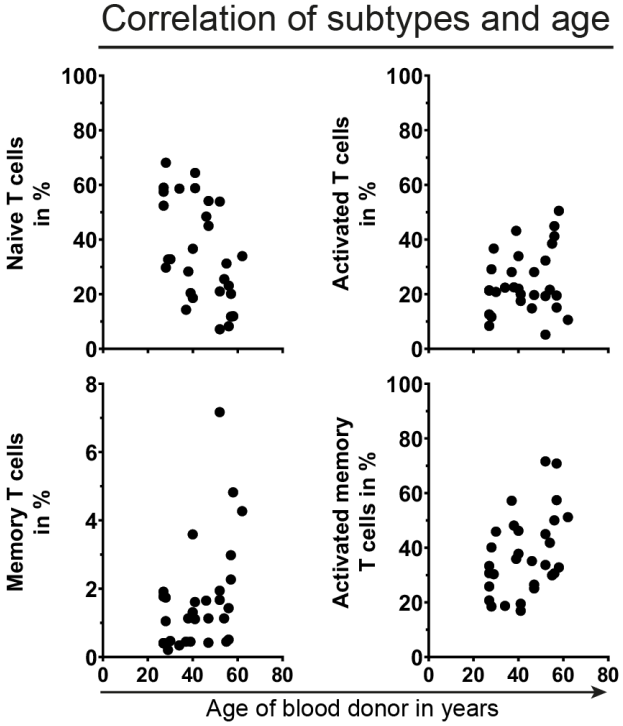

Age vs.	Naive T cells	Activated T cells	Memory T cells	Activated memory T cells
n	30	30	30	30
Spearman r				
r	-0.522	0.136	0.464	0.393
95 % confidence interval	-0.747 to -0.188	-0.246 to 0.482	0.116 to 0.712	0.027 to 0.666
P (two-tailed)	0.003	0.473	0.010	0.032

Figure 27: Correlation of CD8⁺ T cell subtypes with age.

Influence of age on CD8⁺ T cell subtype distribution. The age of the blood donor in years (x-axis) is plotted against the percentage of the indicated subtype of all CD8⁺ T cell event (y-axis). Each dot represents a single individual (n = 30) and the table below details the sample size (n), the results from the Spearman correlation as well as the *p*-value for the correlation.

It was already described that the age of the blood donor has a great impact on the abundance of naïve T cells in the peripheral blood[94]. As an internal control, the subtype distribution was correlated with the age of the donors (**Figure 27 c**). Naïve T cells decreased significantly with increasing age (top left), while circulating memory and activated memory cells significantly increased with age (lower panel). The amount of activated T cells remained stable, regardless of age (top right). However, none of the subtypes impacted the migration behaviour of the cells in the *in vitro* assay (data not shown).

Finally, the impact of gender on CD8⁺ T cell subtype distribution and CD154 expression was analysed (**Figure 28**). Indeed, female donors had a significantly shifted CD8⁺ T cell repertoire, more naïve cells, but fewer activated memory cells (**Figure 28 a**). Additionally, CD154 was slightly higher if the cells originated from female donors in comparison to male donors (**Figure 28 b**).

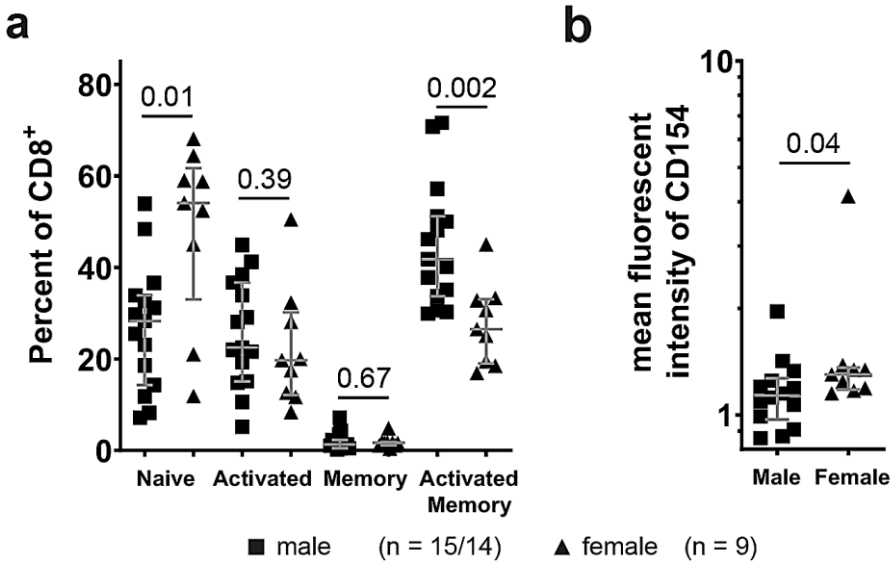

Figure 28: Influence of gender on CD8⁺ T cell subtype distribution and CD154 expression.

(**a**) The CD8⁺ T cell subtype distribution was grouped according to the gender of the blood donors and plotted in this scatter dot plot. The x-axis details the subtypes, gated as explained in **Figure 26 a**. The percentage of the respective subtype of all CD8⁺ events is plotted on the y-axis. Each symbol represents one single individual and black squares indicate male (n = 15) and black triangles female (n = 9) donors. The grey lines indicate the median ± interquartile range and the *p*-values given above the graphs were computed via Mann-Whitney *U*-test. (**b**) The mean fluorescence intensity of CD154 (CD40L, y-axis) was grouped by gender of the blood donor (x-axis). Black squares indicate male (n = 14) and black triangles female (n = 9) donors and each symbol represents a single individual. The grey lines indicate the median ± interquartile range and the *p*-values given above the

graphs were computed via Mann-Whitney *U*-test.

5.4.3. Neutrophil granulocytes

With the established assay[2], the assessment of human neutrophil granulocyte migration was already performed on a cohort of healthy people. However, this approach did not include a flow cytometric analysis of the activation status of neutrophils. Like eosinophils and $CD8^+$ T cells, a panel was set up to determine the expression pattern of key activation markers, namely CD11b, CD66b and CD62L, on human neutrophils in health and disease. As before, the isotype controls were negative for all tested antibodies (**Figure 29 a**). To further verify the panel, purified neutrophils were activated *in vitro* by stimulation with 10 ng/ml of CXCL8 for 1 h and subsequently analysed with the panel. CD16 and CD15 remained stable compared to unstimulated neutrophils, while CD11b and CD66b were slightly upregulated (**Figure 29 b**). CD62L was downregulated, as expected for activated neutrophils[223].

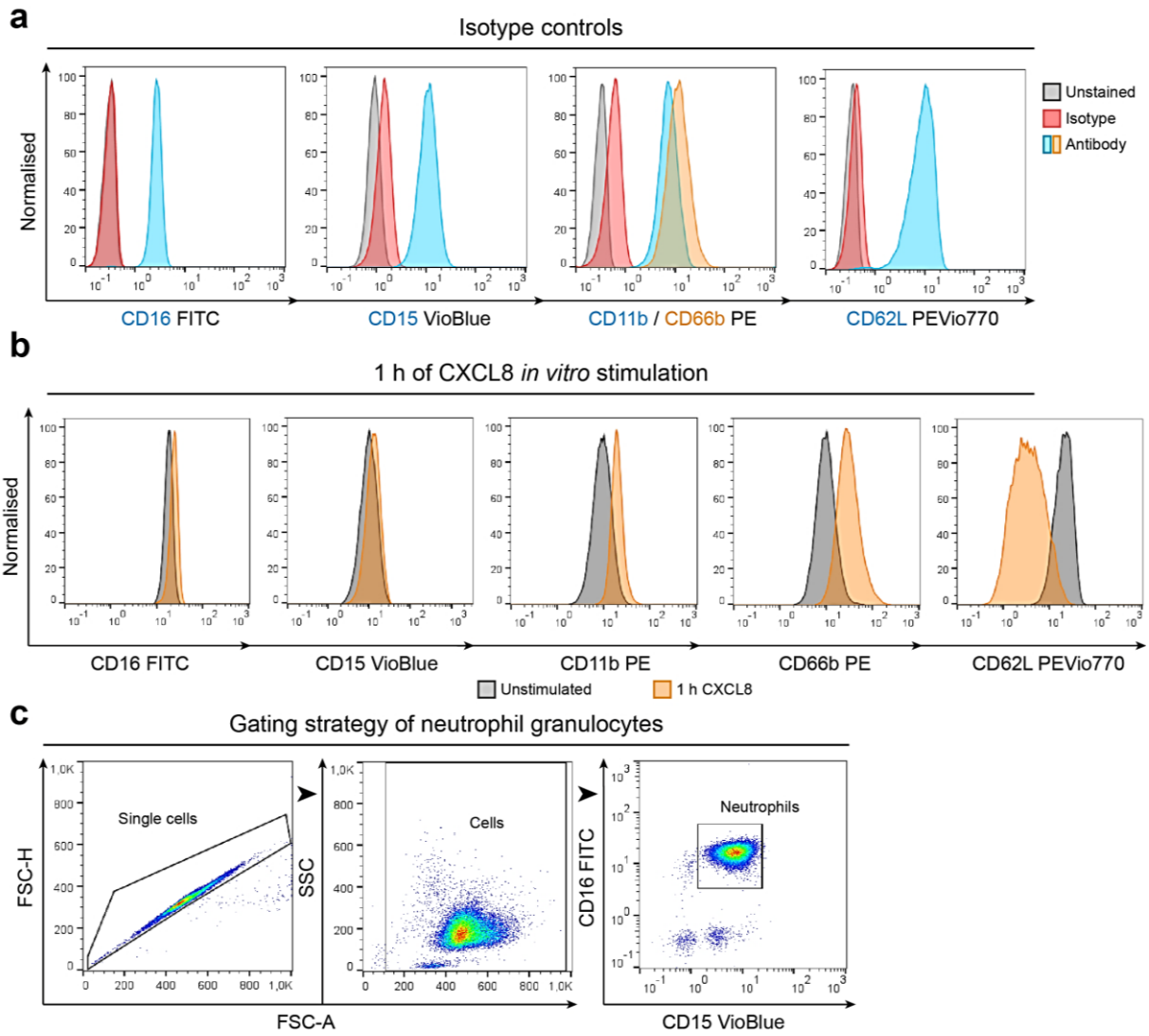

Figure 29: Establishment of a flow cytometry panel for human neutrophil granulo-

cytes.

A flow cytometry assay was established for human neutrophils staining for the lineage markers CD15 and CD16, as well as the activation markers CD11b, CD66b and CD62L. (**a**) Normalised histograms comparing unstained cells (grey), isotype control stained cells (red) and antibody stained cells (blue, orange) for CD16 (1st), CD15 (2nd), CD11b (blue) and CD66b (orange, 3rd) and CD62L (4th panel). (**b**) Purified human neutrophils were either stimulated with 10 ng/ml CXCL8 (orange) for 1 h *in vitro* or left untreated (grey) and stained for CD16 (1st), CD15 (2nd), CD11b (3rd), CD66b (4th) and CD62L (5th panel). (**c**) Gating strategy for all following flow cytometric analyses of human neutrophils. First, doublets were excluded by FSC-A and FSC-H doublet exclusion, followed by SSC-A and SSC-H doublet exclusion (not shown). Subsequently, residual debris and erythrocytes were excluded based von der FSC-SSC properties. After that, neutrophils were identified by their expression of CD16 and CD15. The expression levels of CD11b, CD66b and CD62L are always based on the total $CD16^+$ $CD15^+$ events and given as geometric mean fluorescence intensity (geo mfi).

For all following flow cytometric analyses, doublets were excluded by their FSC-A and FSC-H, as well as their SSC-A and SSC-H properties, followed by exclusion of residual debris and erythrocytes based on their FSC-SSC properties. Finally, neutrophils were identified by their co-expression of CD16 and CD15, as published[2]. CD11b, CD66b and CD62L expressions were determined on this neutrophil population as geometric mean fluorescence intensity (geo mfi) (**Figure 29 c**).

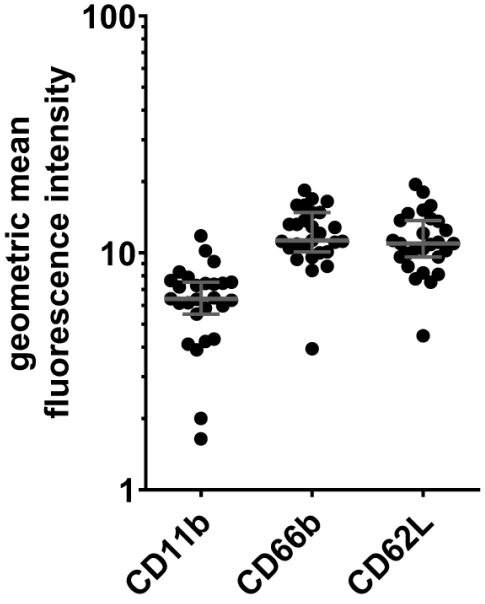

	CD11b	CD66b	CD62L
n	27	27	27
Minimum	1.640	3.940	4.470
25% Percentile	5.520	10.10	9.610
Median	6.400	11.30	10.95
75% Percentile	7.520	14.80	13.70
Maximum	11.80	18.40	19.45
D'Agostino & Pearson omnibus normality test			
K2	1.273	0.9975	1.959
P value	0.5292	0.6073	0.3754
Passed normality test (alpha=0.05)?	Yes	Yes	Yes

Figure 30: Expression of activation markers on peripheral neutrophils from healthy human individuals.

Scatter dot plots of the expression of CD11b, CD66b and CD62L (x-axis) on human neutrophils as geometric mean fluorescence intensity (geo mfi, y-axis). The grey lines indicate the median ± interquartile range. Each black dot represents a single individual (n = 27). The table next to the graph details the test size (n), minima, maxima, median and percentiles for the conditions, as well as the results from the D'Agostino and Pearson omnibus normality test.

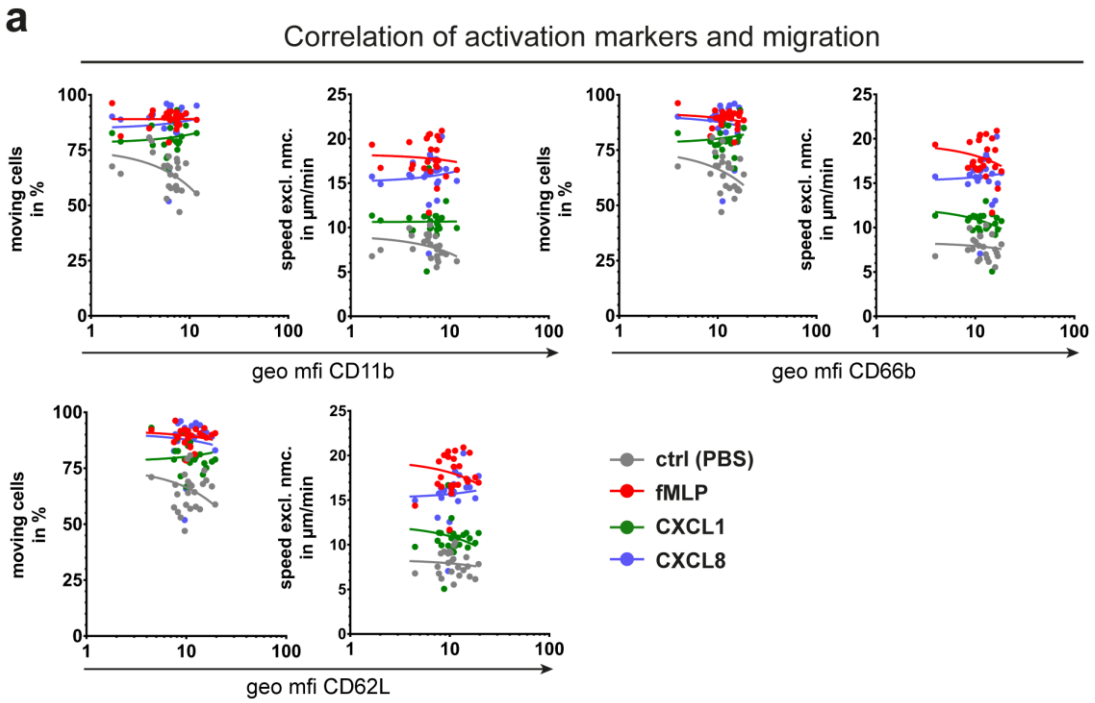

	Moving cells in %				Speed excl. nmc. in µm/min			
	ctrl (PBS)	fMLP	CXCL1	CXCL8	ctrl (PBS)	fMLP	CXCL1	CXCL8
n	24	24	24	24	24	24	24	24
CD11b expression								
Spearman r	-0.457	-0.120	0.186	0.226	-0.510	-0.028	-0.070	0.225
P (two-tailed)	0.025	0.577	0.385	0.288	0.011	0.897	0.747	0.290
CD66b expression								
Spearman r	-0.395	-0.046	0.226	-0.031	-0.100	-0.117	-0.239	0.081
P (two-tailed)	0.056	0.831	0.288	0.885	0.643	0.586	0.261	0.708
CD62L expression								
Spearman r	0.155	-0.022	-0.436	0.030	-0.154	0.232	0.022	0.526
P (two-tailed)	0.470	0.918	0.033	0.891	0.474	0.275	0.918	0.008

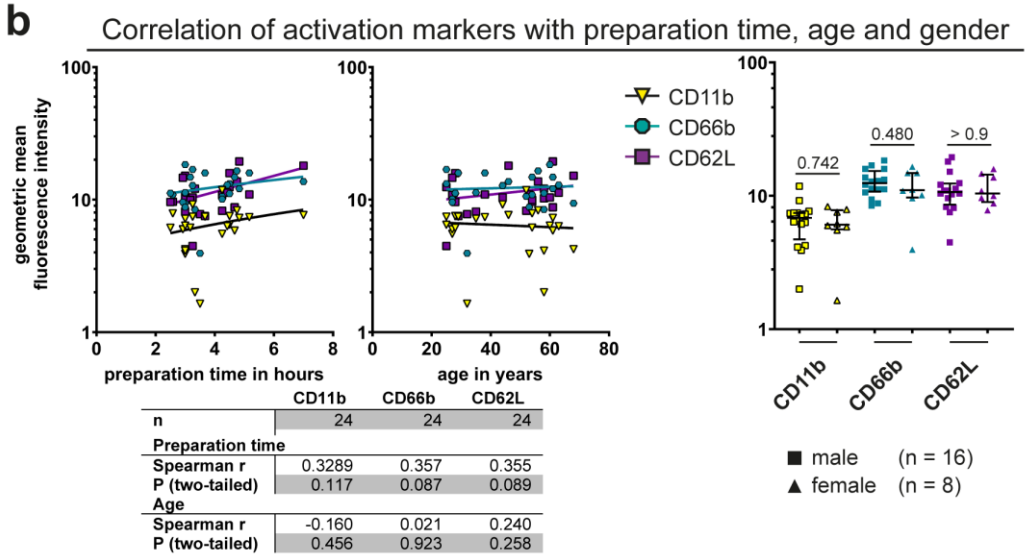

	CD11b	CD66b	CD62L
n	24	24	24
Preparation time			
Spearman r	0.3289	0.357	0.355
P (two-tailed)	0.117	0.087	0.089
Age			
Spearman r	-0.160	0.021	0.240
P (two-tailed)	0.456	0.923	0.258

Figure 31: Correlation of neutrophil activation markers with migration of patient parameters.

(**a**) Correlation of activation marker expression with migration patterns of human neutrophils. Giv-

en are the correlation of percentage of moving cells (left) and speed (right) against CD11b (top left), CD66b (top right) and CD62L expression (bottom left), as well as a table (below) detailing the sample size (n), the results from the Spearman correlation as well as the *p*-value for the correlation. Each dot represents a single individual (n = 24) and the lines represent the results from the best-fit of the nonlinear regression calculation. Light grey stands for the control (ctrl, PBS), red for fMLP, green for CXCL1 and blue for CXCL8 stimulation. (**b**) Influence of preparation time, age and gender on neutrophil activation markers. *Left*: The preparation time (left, x-axis) and age of the blood donor (right, x-axis) are plotted against the expression levels of CD11b (yellow triangles), CD66b (blue hexagon) and CD62L (purple square). The table of the right details the sample size (n), the results from the Spearman correlation as well as the p-value for the correlation. *Right*: The expression levels were grouped and plotted according to the gender of the blood donor. Each dot represents one single individual and black lines indicate the median ± interquartile range. Squares stand for male (n = 16) and triangles for female (n = 8) blood donors.

With this, the expression patterns of activation markers on peripheral human neutrophils were investigated on the same healthy cohort as for eosinophils and $CD8^+$ T cells (**Figure 30**). Peripheral neutrophils expressed CD11b, CD66b and CD62L and these expression patterns were normally distributed (**Figure 30**).

As these general markers give information on the activation status of the cells, it is obvious to assume they might correlate with neutrophil migration. Indeed, CD11b expression negatively correlated with the percentage of moving neutrophils and their speed under baseline (PBS) conditions, while higher CD62L expression correlated with higher speed upon CXCL8 treatment and lower percentage of moving cells upon CXCL1 treatment (**Figure 31 a**). None of the other parameters correlated with another. The correlation of preparation time, age and gender of the patients with the expression of CD11b, CD66b and CD62L revealed a non-significant increase in expression upon longer handling times, while both age and gender of the blood donors had no impact of the activation marker expression (**Figure 31 b**).

5.4.4. Summary III

This section was about the standardisation of *in vitro* assays to investigate the migration of eosinophil granulocytes and $CD8^+$ T cells. For these assays, suitable migration stimuli were tested and titrated and eventually checked for supplier dependences. Subsequently, the migration behaviour and receptor expression of a cohort of healthy individuals were studied. This revealed no significant dependences between eosinophil migration and preparation time or age of the donor. However, female donors showed less migration than males. This was not observed for $CD8^+$ T cells. Additionally, age or preparation time did not show any impact on $CD8^+$ T cell migration. Interestingly, we learned that the distribution of T cell subtypes (naïve, activated, memory and activated memory T cells) correlated with age and

with gender of the analysed individuals. Furthermore, the published migration assay for human neutrophil granulocytes was extended to assess the receptor expression of the activation markers CD11b, CD66b and CD62L. Indeed, CD11b expression negatively correlated with baseline migration pattern and a higher CD62L expression correlated with higher speed upon CXCL8.

5.5. Leucocyte migration in metastatic melanoma patients undergoing immune checkpoint blocker therapy

Melanoma is the most dangerous form of skin cancer[172, 173], however immune checkpoint blocker therapy (ICBT) has arisen as a promising treatment for melanoma and many other cancers[224]. However, thus far no detection system exists to determine the therapy response before routine staging or even predict its success before therapy induction. As it is logical to assume that peripheral blood immune cells are among the first to react to the infusion of checkpoint blocking molecules, they might be an excellent early detection system of therapy outcome, success or immune-related adverse events (irAE).

5.5.1. Eosinophil granulocytes show decreased migration in non-responding patients

In a first attempt to answer the question whether immune cell migration is altered in melanoma patients receiving ICBT, experiments were performed on peripheral blood eosinophils from a mixed cohort of ICBT patients. This cohort consisted of people, who had undergone various primary therapies before being admitted to ICBT. Furthermore, they received different kinds of checkpoint blocking molecules and had been under therapy for different periods of time. Additionally, it included multiple measurements of the same patients, but did not include measurements of migration before therapy onset (**Supplementary Table 2**). Further information on age, gender and available stagings of the analysed cohorts are detailed in **Supplementary Table 2**. This mixed ICBT cohort was not sorted according to type, length or outcome of treatment, pre-treatment or recurring analyses of individual patients. Even in this very heterogenous cohort, eosinophil migration was significantly diminished compared to the healthy individuals (**Figure 32 a**). The percentage of moving cells and the speed of the cells was significantly reduced for all stimulation conditions, except for the percentage of moving cells upon CCL24 treatment and the baseline movement speed (ctrl, PBS) (**Figure 32 a**).

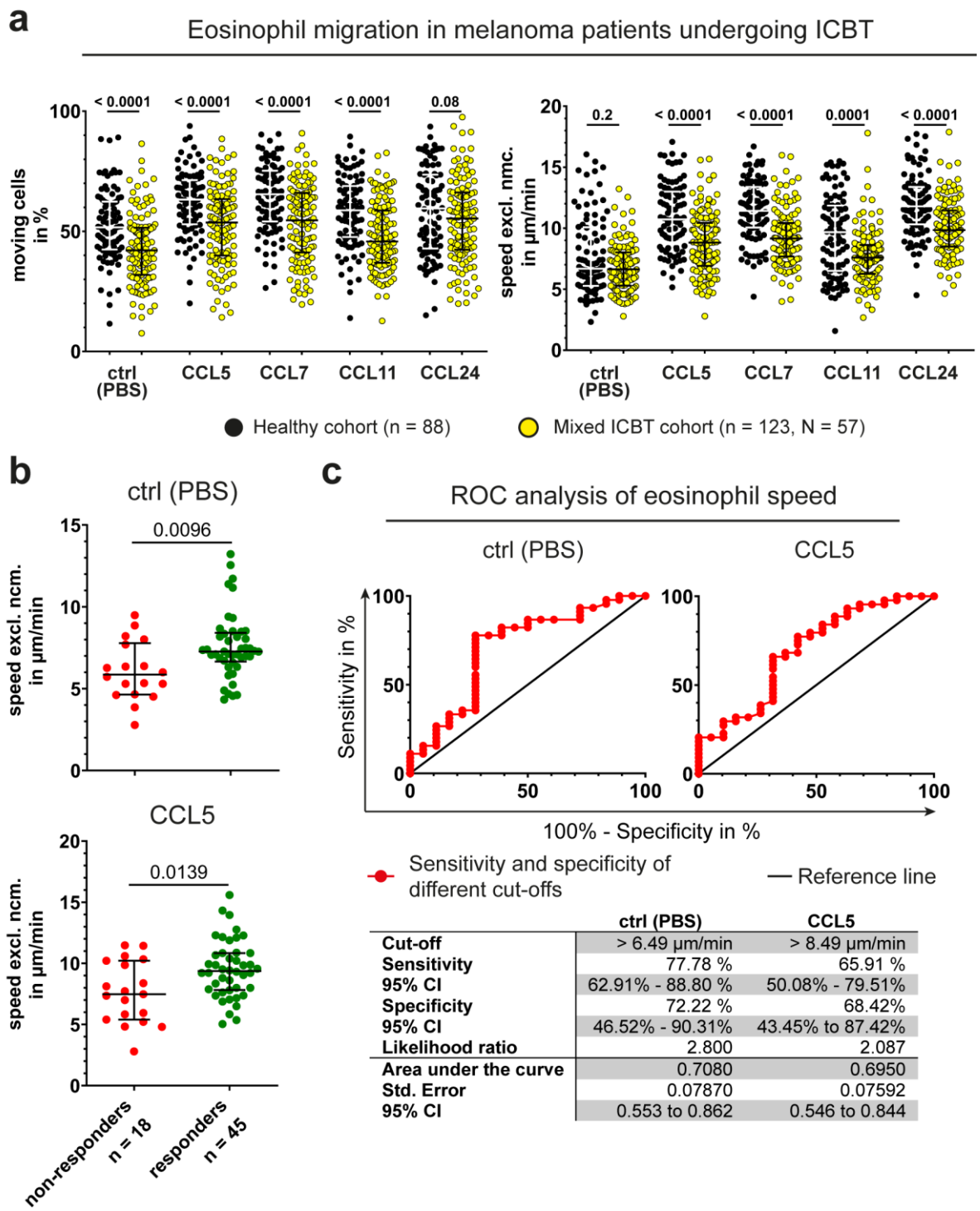

	ctrl (PBS)	CCL5
Cut-off	> 6.49 µm/min	> 8.49 µm/min
Sensitivity	77.78 %	65.91 %
95% CI	62.91% - 88.80 %	50.08% - 79.51%
Specificity	72.22 %	68.42%
95% CI	46.52% - 90.31%	43.45% to 87.42%
Likelihood ratio	2.800	2.087
Area under the curve	0.7080	0.6950
Std. Error	0.07870	0.07592
95% CI	0.553 to 0.862	0.546 to 0.844

Figure 32: Eosinophil migration in a mixed cohort of melanoma patients undergoing immune checkpoint blocker therapy.

(**a**) Scatter dot plots of the percentage of moving cells (left) and the speed excl. nmc. (right) of eosinophils from healthy patients (black dots) and ICBT patients (yellow dots). The x-axis describes the stimulation conditions. For healthy patients, each symbol represents one single individual (n = 88). For ICBT patients, individual patients and their recurring measurements are displayed (overall n = 124 of N = 57 individual patients). Black and white lines indicate the median ± interquartile range and *p*-values are given above the graphs as calculated by Mann-Whitney *U*-test. (**b**) The migration speed of eosinophils upon PBS (top) and CCL5 (bottom) stimulation from ICBT patients was grouped according to the routine staging information on therapy response. Non-

responders (n = 18, N = 10) are shown in red, responders (n = 45, N = 15) in green. Black lines represent the median ± interquartile range and the *p*-values were calculated using the Mann-Whitney *U*-test. (**c**) Receiver operating characteristic (ROC) analysis on the results from (b) demonstrating the diagnostic ability of eosinophil speed on therapy outcome. The sensitivity (y-axis) is plotted against 100% - the specificity (x-axis) for various thresholds of eosinophil speed (red dots and red lines). The black lines represent the reference line, which equals the diagnostic ability of a coin throw. The table below details the cut-off (speed) with the highest sensitivity and specificity, as well as the area under the curve. The analysis was conducted with GraphPad Prism®'s ROC curve analysis.

Next, it was analysed whether eosinophil migration differed in responders or non-responders. Responders were defined as individuals with complete or partial remission of the tumour(s) as well as with stable tumour burden. Non-responders were defined as those suffering from ongoing tumour growth despite ICBT. Staging data from 10 non-responders (18 measurements with recurring samples) and 15 responders (45 measurements with recurring samples) were obtained. Recurring measurements were included in the analysis until the last staging if the stagings were consistently "responder" or "non-responder". Patients with unclear, missing or varying stagings were excluded. The results were not age- or gender-matched to retain calculable sample sizes. Eosinophil migration speed in non-responders was significantly reduced compared to responders (**Figure 32 b**).

This was true for only baseline speed (ctrl, PBS) and speed upon CCL5 stimulation, but not for other migration parameters or stimulations (not shown). To test the diagnostic potential of these first results, a receiver operating characteristic (ROC) analysis was performed on both the movement speed upon PBS and CCL5 treatment (**Figure 32 c**). During this analysis, different cut-offs and their respective sensitivity and specificity to distinguish two groups, in this case responders and non-responders, are calculated and plotted as a so-called ROC curve (**Figure 32 c**, top). Each red dot indicates the sensitivity and specificity of a speed cut-off, while the black reference line represents the sensitivity and specificity of a coin throw (50:50). Interestingly, the best calculated cut-off for baseline eosinophil speed of > 6.49 µm/min had a sensitivity of 77.78% and specificity of 72.22% (**Figure 32 c**, bottom). This indicates that a baseline eosinophil speed of over 6.49 µm/min has a high probability to detect responders, while a speed less than 6.49 µm/min is more attributed to non-responders. By contrast, speed upon CCL5 stimulation yielded only 65.91% sensitivity and 68.42% specificity at a cut-off of > 8.49 µm/min. None of the other migration parameters or stimulation conditions produced higher specificity and sensitivity (data not shown).

5.5.2. Neutrophil, eosinophil and CD8⁺ T cell migration in metastatic melanoma patients before therapy

Eosinophil granulocytes are not the only cells important during tumour development or rejection[46, 86]. In fact, CD8⁺ T cells are the main, known, effector cells, when it comes to eradicating degenerate host cells. Additionally, tumour-associated neutrophils are found in many solid tumours, such as melanoma, and are linked to an overall poor prognosis[225]. Therefore, the developed assays were applied on a cohort of metastatic melanoma patients, who would receive ICBT as a first-line immune therapy. Blood was obtained before therapy and before every following infusion with checkpoint blocking molecules (**Figure 33**).

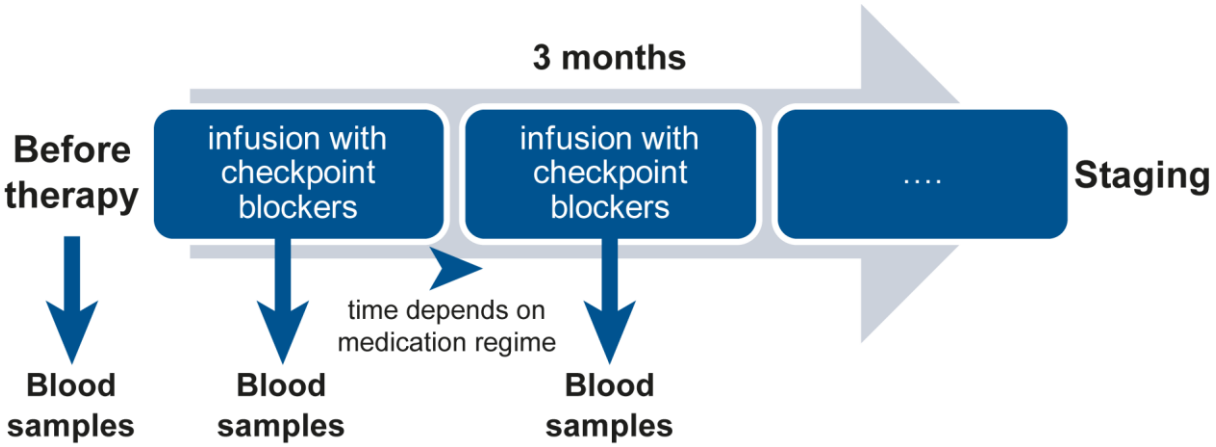

Figure 33: Scheme for sample acquisition of blood samples from ICBT patients.

Schematic illustration of the time frame for the acquisition of blood samples from ICBT patients. Samples were acquired before therapy (not applicable for the mixed ICBT cohort) and before every ensuing infusion with checkpoint blockers. The time between sample acquisition varying depending on the medication regime. After approximately 3 months, the patients' response to the therapy was assessed and they were grouped into responders or non-responders (staging).

21 individuals were included in this study. For 12 / 18 / 9 of them, migration data for neutrophils / eosinophils / CD8⁺ T cells were collected and passed internal quality controls. 11 / 9 / 11 had valid flow cytometry data for neutrophils / eosinophils / CD8⁺ T cells. All information on this cohort is detailed in **Supplementary Table 3**.

Before therapy, neutrophils from metastatic melanoma patients showed significantly less moving cells under CXCL1 stimulation, but this did not impact the speed upon CXCL1 stimulation or any other stimulation condition (**Figure 34**, top). Eosinophil speed in ICBT patients before therapy was comparable to healthy controls, while percentage of moving cells was significantly increased for PBS, CCL7 and CCL11 treatment (**Figure 34**, middle).

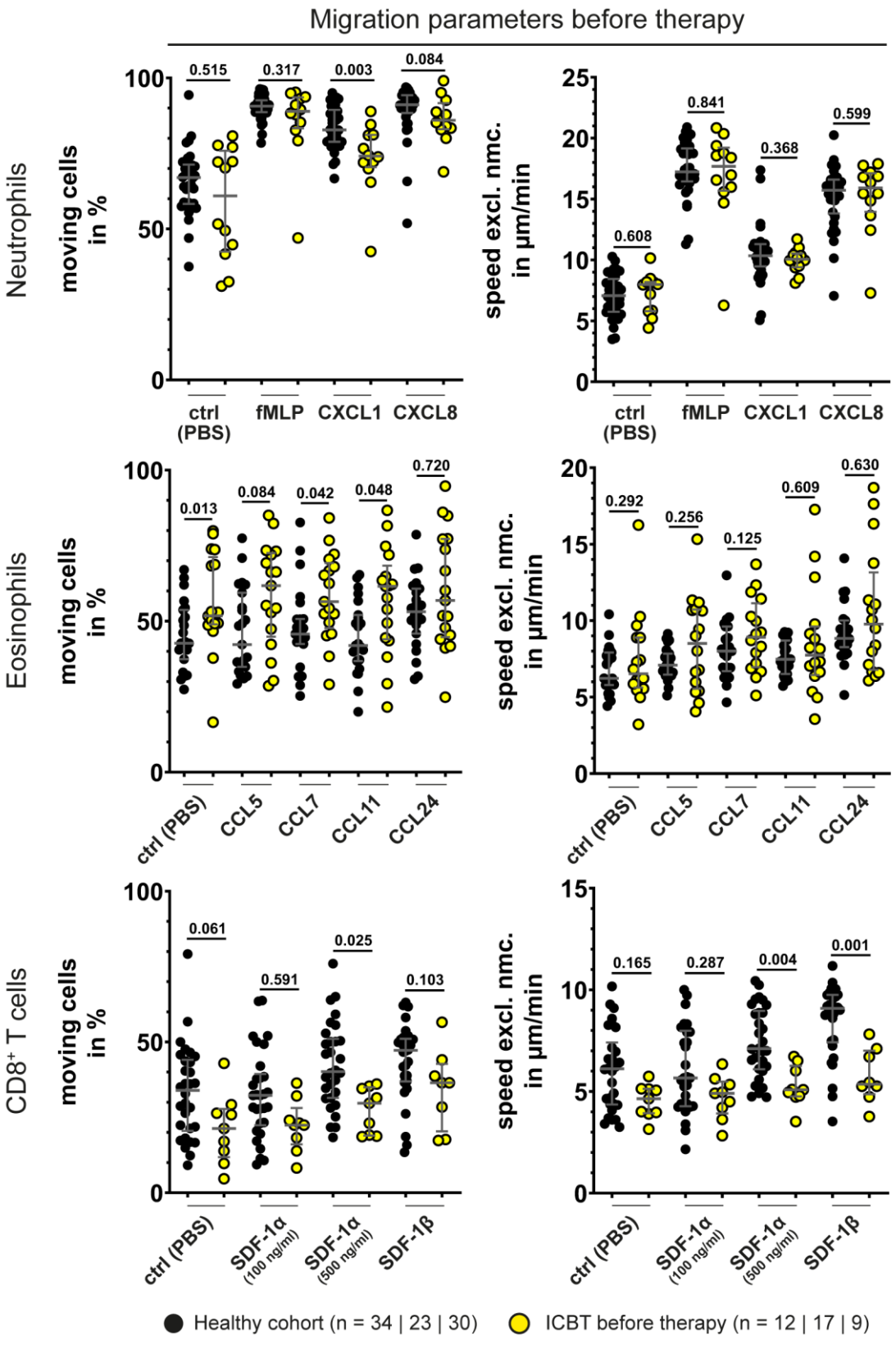

Figure 34: Neutrophil, eosinophil and CD8⁺ T cell migration in metastatic melanoma patients before ICBT.

Scatter dot plots of the percentage of moving cells (left) and the speed excl. nmc. (right) of neutrophils (1st row), eosinophils (2nd row) and CD8+ T cells (3rd row) from healthy patients (black dots) and ICBT patients before therapy (yellow dots). The x-axis describes the stimulation conditions. Each symbol represents a single individual (healthy: n = 34 / 23 / 30; ICBT: n = 12 / 17 / 9 for neu-

trophils / eosinophils / CD8⁺ T cells, respectively). Dark grey lines indicate the median ± interquartile range and *p*-values are given above the graphs as calculated by Mann-Whitney *U*-test.

However, CD8⁺ T cells from metastatic melanoma patients before therapy were significantly impaired in their migratory capacity. Baseline migration upon PBS and SDF-1α (100 ng/ml) stimulation was normal, but the cells failed to react to 500 ng/ml SDF-1α and SDF-1β compared to healthy controls (**Figure 34**, bottom). Neutrophils of ICBT patients before therapy expressed significantly more CD11b and CD66b, while CD62L expression was normal (**Figure 35 a**, left). The expression patterns of eosinophil markers and CD154 on CD8⁺ T cells did not differ in healthy and ICBT patients (**Figure 35 a**, middle and right).

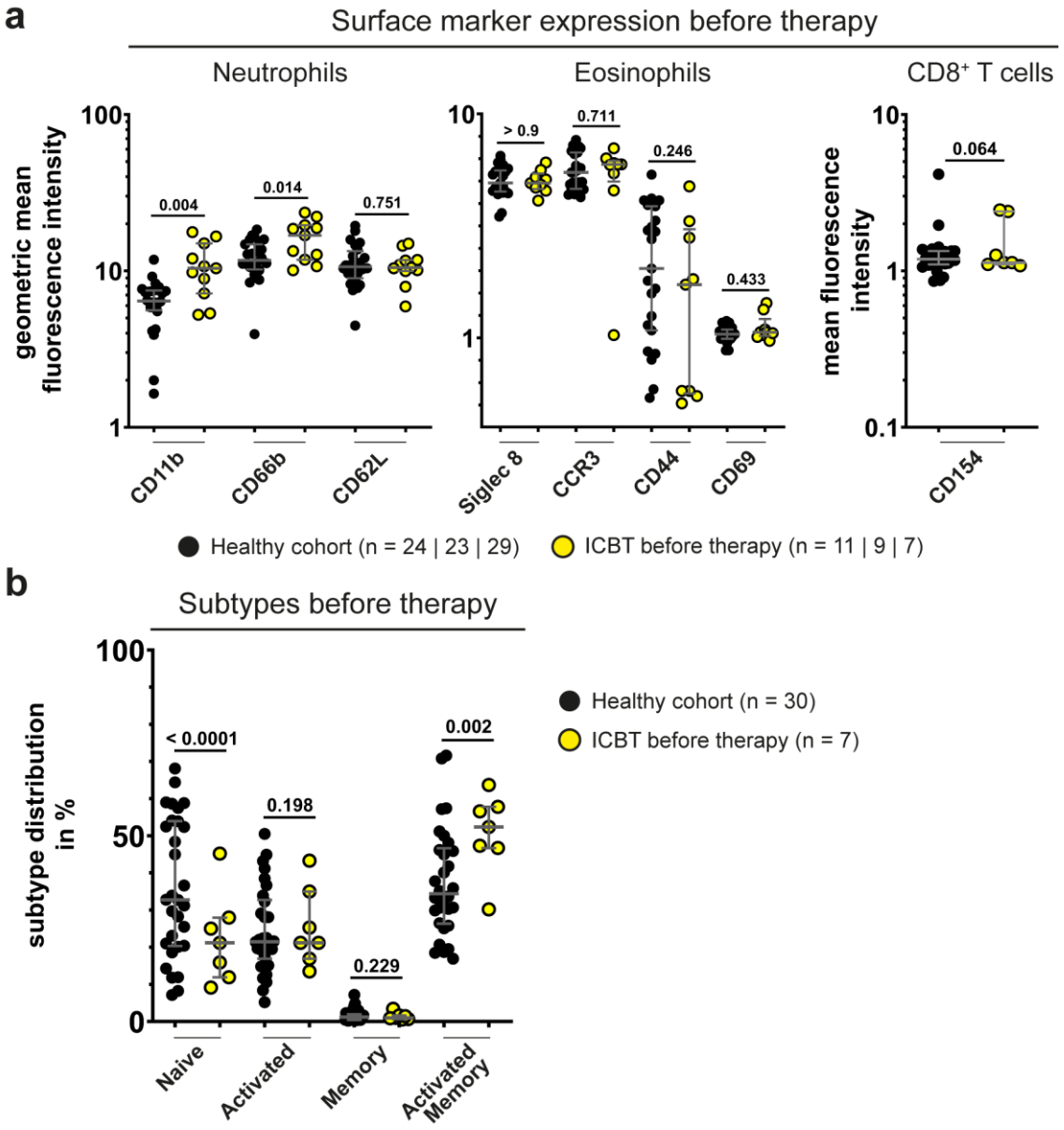

Figure 35: Neutrophil, eosinophil and CD8⁺ T cell receptor expression in metastatic melanoma patients before ICBT.

(**a**) The expression patterns of cell surface markers in geometric mean fluorescence intensity (for neutrophils and eosinophils) and mean fluorescence intensity (for CD8⁺ T cells) for healthy patients

(black dots) and ICBT patients before therapy (yellow dots). The first column contains information on expression levels on neutrophils, the second for eosinophils and the third for $CD8^+$ T cells. The x-axis indicates the tested cell surface markers. Each symbol represents a single individual (healthy: n = 24 / 23 / 29; ICBT: n = 11 / 9 / 7 for neutrophils / eosinophils / $CD8^+$ T cells, respectively). (**b**) Distribution of $CD8^+$ T cell subtypes in healthy (black dots) and ICBT patients before therapy (yellow dots). The x-axis indicates the subtypes, as defined in **Figure 26**, while the y-axis represents the percentage of the subtype of all $CD8^+$ events. Each symbol indicates a single individual (healthy: n = 30; ICBT: n = 7). Dark grey lines indicate the median ± interquartile range and *p*-values are given above the graphs as calculated by Mann-Whitney *U*-test.

However, ICBT patients before therapy had much less naïve $CD8^+$ T cells and more activated memory $CD8^+$ T cells compared to healthy controls, while activated and memory cells were not affected (**Figure 35 b**).

5.5.3. Preliminary results of migration development over the course of ICBT

Four of these patients (**Supplementary Table 4**) could be analysed before therapy onset, during therapy and around their first staging. For two of these patients, only eosinophil migration was analysed, while the other two were measured according to the scheme presented above. However, only one patient of the latter group, including all immune cells, was staged before this thesis was completed. All of them are included here.

One of the earliest patients, #0003, was only measured for eosinophil migration patterns. The eosinophils exhibited a highly motile phenotype before therapy onset, which dropped prominently until the next measurement timepoint two months later (**Figure 36 a**). Shortly after staging, the percentage of moving cells rose slightly again. Interestingly, however, eosinophil speed dropped swiftly over the course of ICBT and the patient was diagnosed with a progressive disease short before the last measurement (**Figure 36 a**, bottom).

Eosinophils from patient #0013 were also highly motile before therapy onset (**Figure 36 b**). Over the course of therapy, the percentage of moving cells decreased slightly, but stayed largely stable, while the movement speed dropped until the last measurement, a month before staging (**Figure 36 b**, bottom). The patient was staged with a partial remission of both cerebrally and extracranially involved organs.

The blood of patient #0021 was analysed for migration behaviour of all three presented cell types. Neutrophil patterns were normal before therapy, however, both percentage of moving cells and speed worsened after the 2nd measurement (**Figure 37**, top). A similar phenotype was experienced for eosinophils from the same patient, as shortly after therapy onset, the cells did not seem to react to the applied stimuli any longer (**Figure 37**, middle).

CD8+ T cells were responsive before therapy, but both percentage of moving cells, as well as speed upon stimulation dropped after ICBT onset (**Figure 37**, bottom).

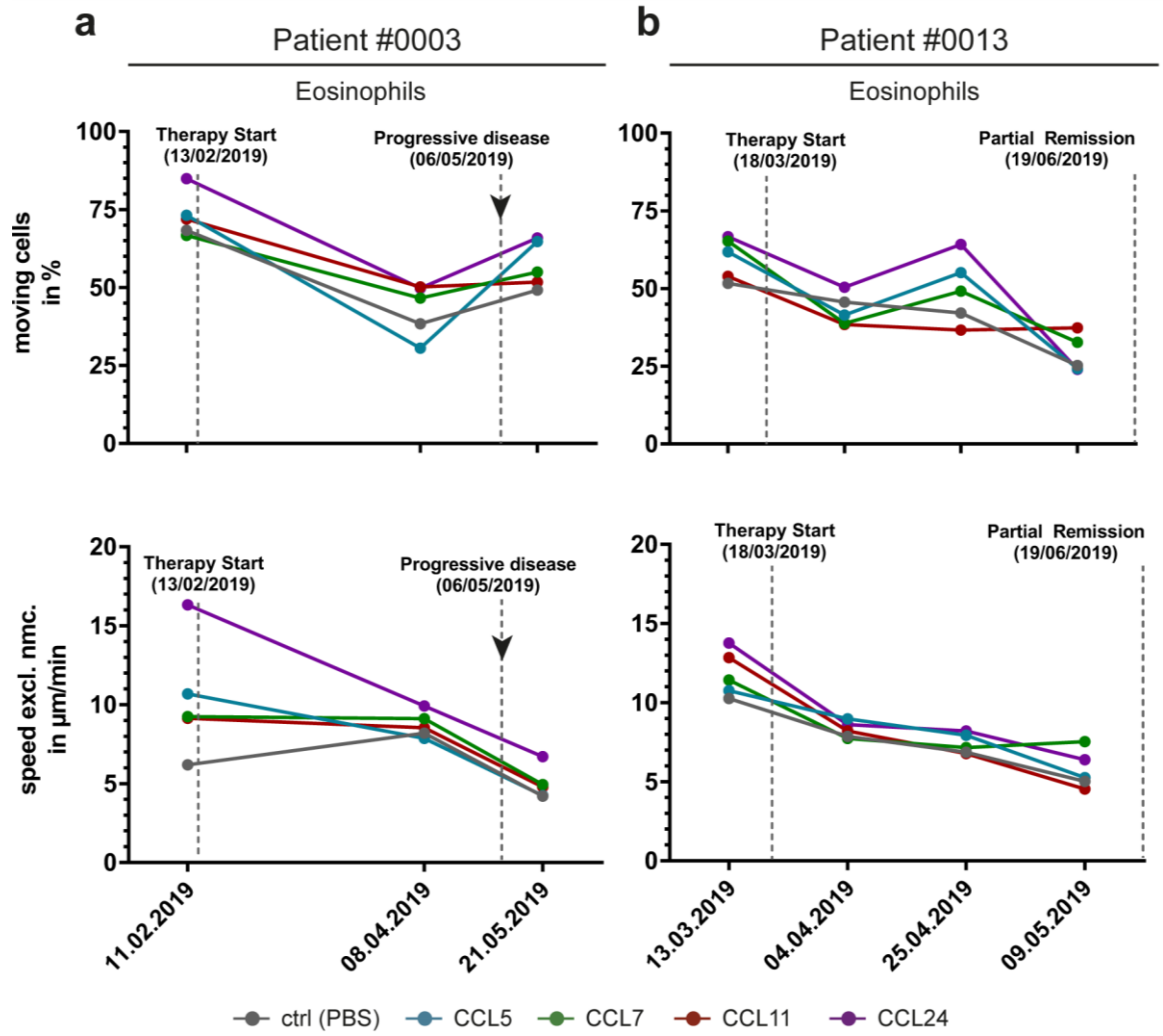

Figure 36: Eosinophil migration in a progressive disease (patient #0003) and a partial remission (patient #0013).

Migration of eosinophils over the course of ICBT. (**a**) Percentage of moving cells (top) and speed excl. nmc. (bottom) are shown for eosinophils from patient #0003 before therapy (11.02.2019), during therapy and shortly after staging. Each dot represents the five stimulation conditions for eosinophils and the x-axis details the measurement dates. Black arrows indicate the diagnosis with immune-related adverse events (irAE), here colitis. (**b**) Percentage of moving cells (top) and speed excl. nmc. (bottom) are shown for eosinophils from patient #0013 before therapy (13.03.2019), during therapy and shortly after staging. Each dot represents the five stimulation conditions for eosinophils and the x-axis details the measurement dates. Grey stands for the control (PBS), blue for the CCL5, green for the CCL7, red for the CCL11 and purple for the CCL24 treated condition. The grey dashed lines indicate the therapy start (left) and staging timepoint (right).

Interestingly, on the 15th of August, the patient was diagnosed with immune-related adverse events (irAE) that affected the liver (**Figure 37**, black arrows). On the same day, neutrophil migration, especially upon fMLP and CXCL8 treatment, was impaired in this *in vitro*

assay, even though steroid treatment was only started four days later. Eosinophils, however, remained as unresponsive as before.

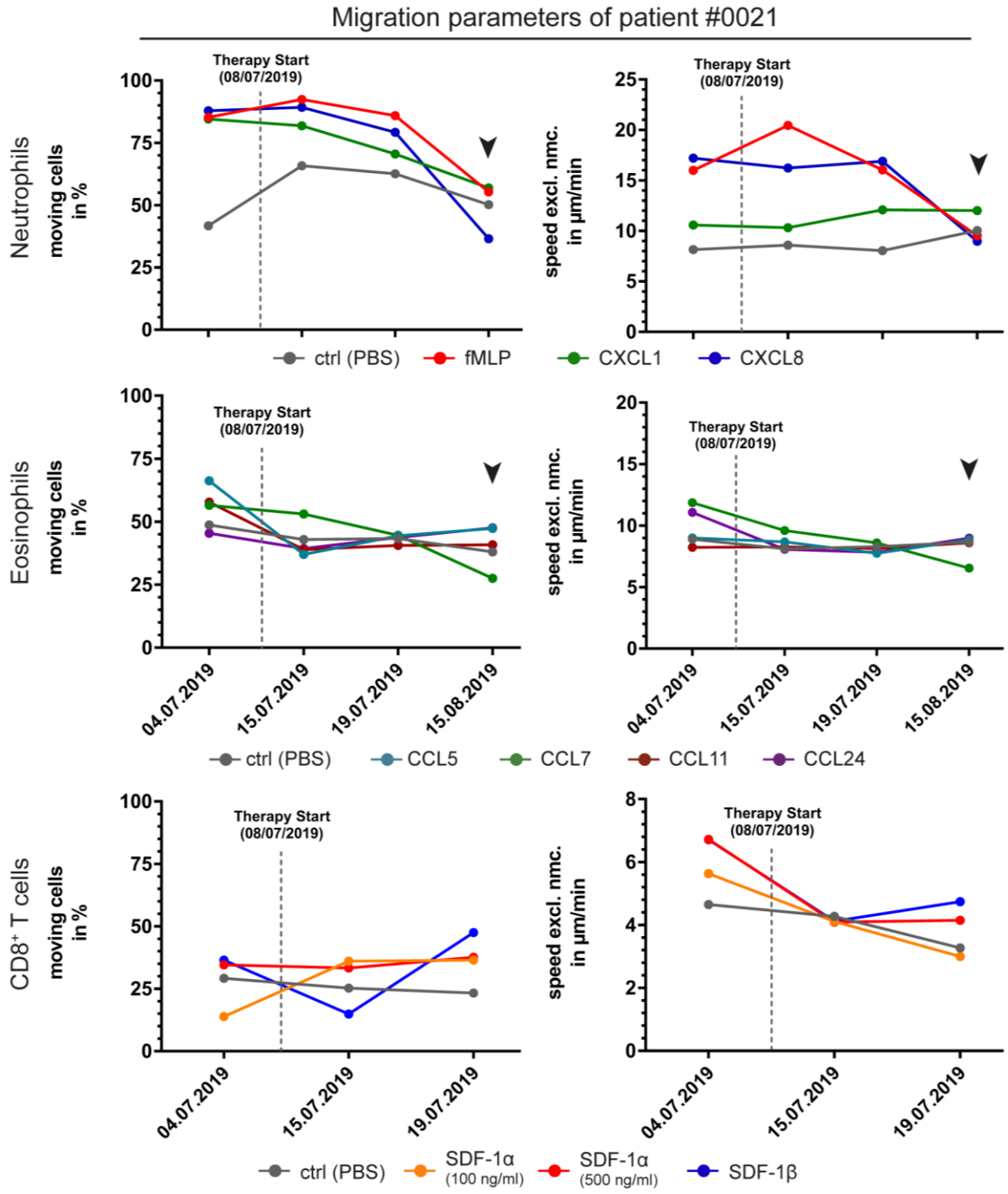

Figure 37: Leucocyte migration over the course of ICBT in patient #0021.

Migration of neutrophils (top), eosinophils (middle) and CD8⁺ T cells (bottom) for patient #0021 over the course of ICBT. The upper row shows the percentage of moving cells of all three cell types, while the lower row reflects on the speed excl. nmc. Each dot represents the stimulation conditions for the cell types and the x-axis details the measurement dates. *Top*: Grey dots stand for the control (PBS), red for fMLP, green for CXCL1 and blue for CXCL8 treatment. *Middle*: Grey dots stands for the control (PBS), blue for the CCL5, green for the CCL7, red for the CCL11 and purple for the CCL24 treated condition. *Bottom*: Grey dots stands for the control (PBS), orange for 100 ng/ml SDF-1α, red for 500 ng/ml SDF-1α and blue for SDF-1β stimulation. The grey dashed lines indicate the

therapy start. Black arrows indicate the diagnosis with irAE, here hepatitis.

The receptor expression of CD11b, CD66b and CD62L on neutrophils from patient #00021 was unchanged by ICBT and stayed stable over the evaluated days (**Figure 38**, top left). However, eosinophils displayed low CCR3 expression that rose sharply after ICBT onset a few days later (**Figure 38**, top right). The composition of CD8⁺ T cells in the peripheral blood changed after therapy start with an increase in activated memory cells and a decrease in both naïve and activated CD8⁺ T cells (**Figure 38**, bottom left). The expression of CD154 stayed unchanged over the analysed time (**Figure 38**, bottom right).

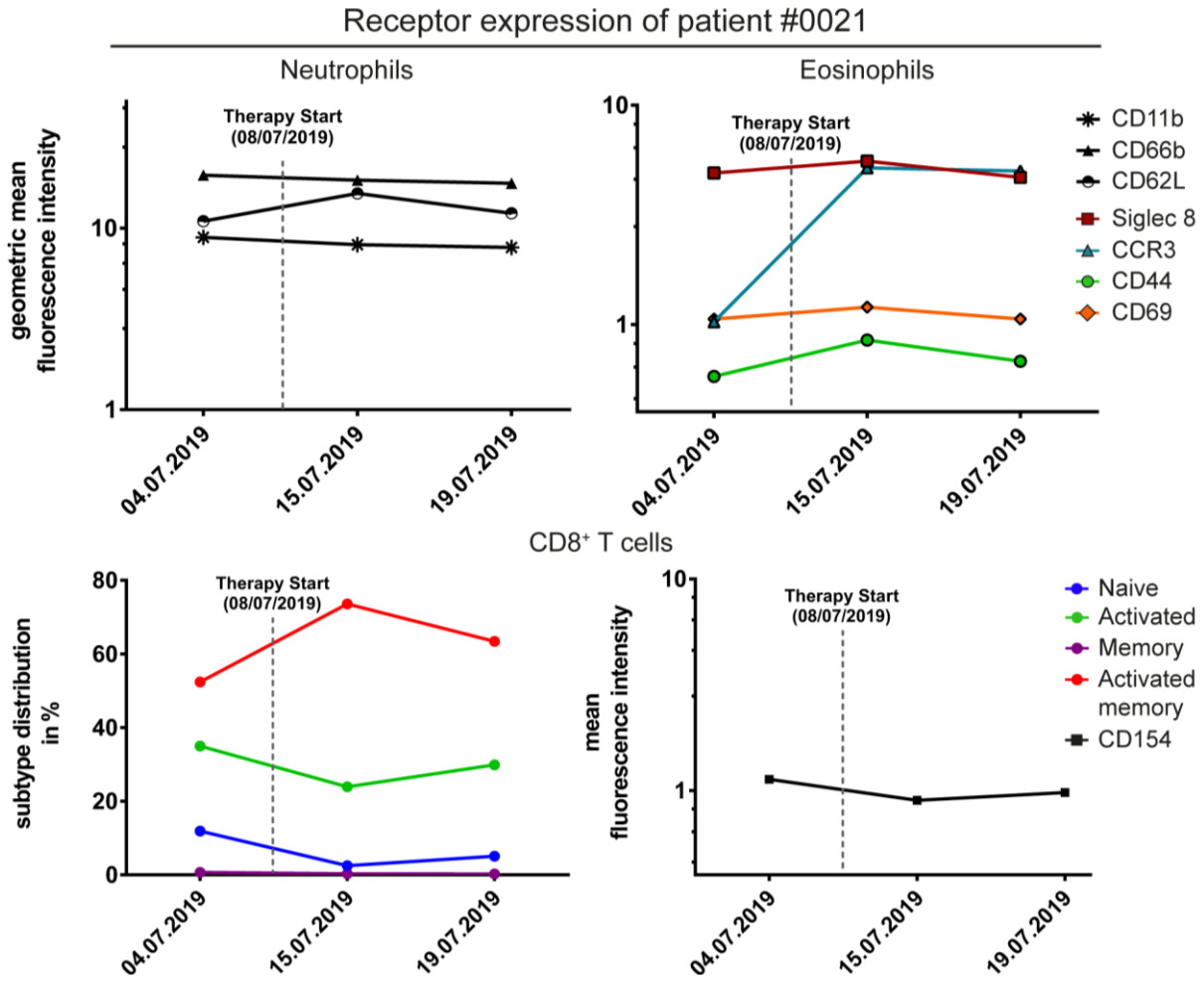

Figure 38: Leucocyte receptor expression over the course of ICBT in patient #0021.

Receptor expression of neutrophils (top left) and eosinophils (top right) as well as subtype distribution of CD8⁺ T cells (bottom left) and their expression of CD154 (bottom right) for patient #0021 over the course of ICBT. Each dot represents the fluorescence intensity or subtype percentage for the cell types and the x-axis details the measurement dates. *Top*: Stars indicate CD11b, black triangles CD66b and black, half-filled dots CD62L expression on human neutrophils. Red squares stand for Siglec 8, blue triangles for CCR3, green dots for CD44 and orange rhombi for CD69 expression on eosinophils. *Bottom*: Blue dots indicate naïve, green dots activated, purple dots memory and red dots activated memory CD8⁺ T cells. Black squares stand for the expression of CD154. The grey dashed lines indicate the therapy start.

Before therapy, neutrophils of the last patient (#0023) were severely impaired in their reaction to fMLP, as indicated by baseline moving cells and very slow speed of the cells (**Figure 39**, top). Additionally, while CXCL8 induced more cells to move before therapy, their speed was as low as baseline and the lowest in the whole ICBT cohort (compare **Figure 34**).

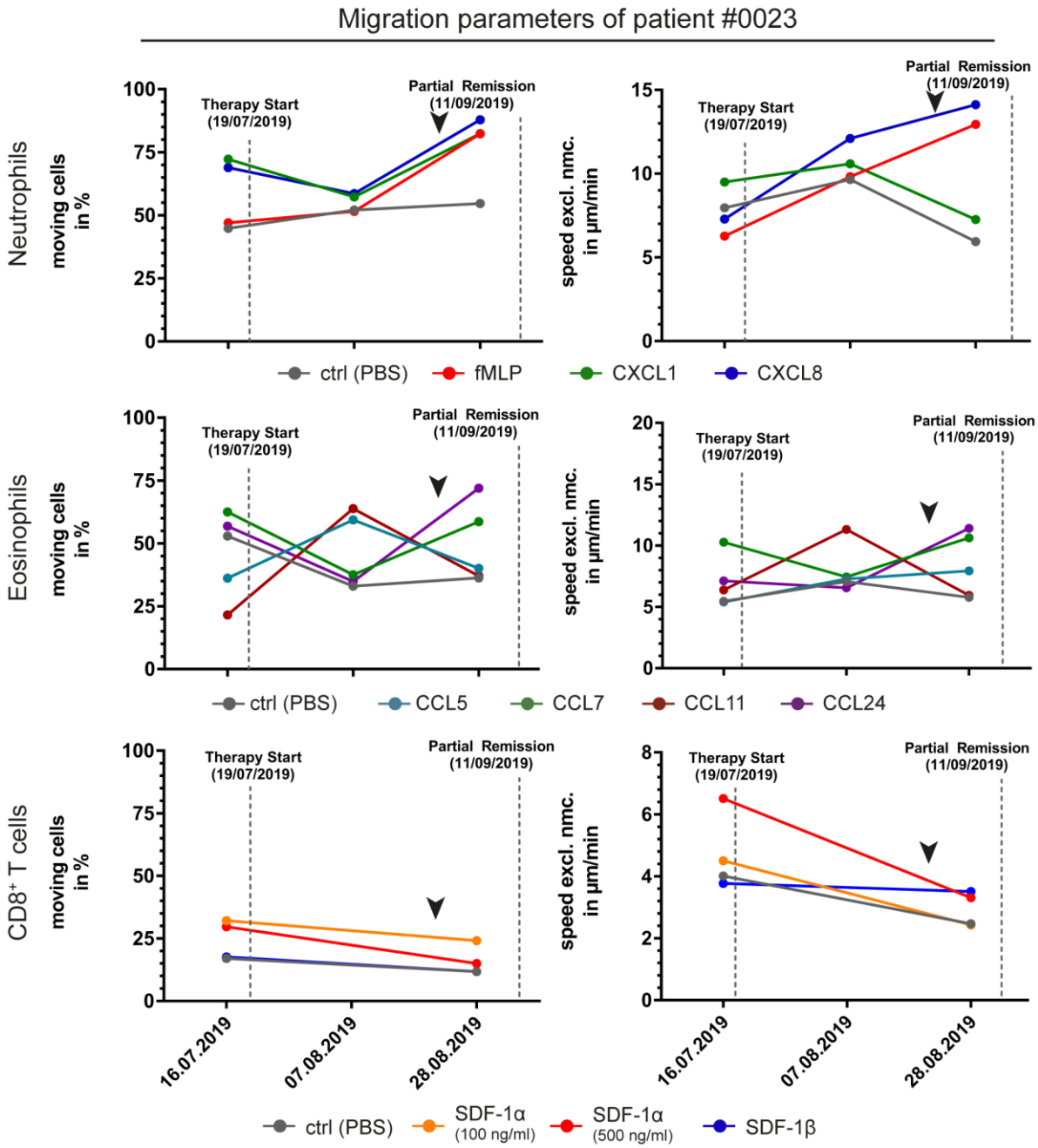

Figure 39: Leucocyte migration over the course of ICBT in patient #0023.

Migration of neutrophils (top), eosinophils (middle) and CD8⁺ T cells (bottom) for patient #0023 over the course of ICBT. The upper row shows the percentage of moving cells of all three cell types, while the lower row reflects on the speed excl. nmc. Each dot represents the stimulation conditions for the cell types and the x-axis details the measurement dates. *Top*: Grey dots stand for the control (PBS), red for fMLP, green for CXCL1 and blue for CXCL8 treatment. *Middle*: Grey dots stands for the control (PBS), blue for the CCL5, green for the CCL7, red for the CCL11 and purple for the

CCL24 treated condition. *Bottom*: Grey dots stands for the control (PBS), orange for 100 ng/ml SDF-1α, red for 500 ng/ml SDF-1α and blue for SDF-1β stimulation. The grey dashed lines indicate the therapy start (left) and staging result (right). Black arrows indicate the diagnosis with irAE, here joint pain.

One month after therapy start, neutrophils still did not react to fMLP, but showed improved speed when treated with CXCL8. On the last measurement day, two weeks before staging, neutrophils started to respond to both fMLP and CXCL8 again, while migration speed for both control and CXCL1 treatment dropped. Eosinophil migration patterns before therapy were normal but were unstable after therapy induction (**Figure 39**, middle). The response to CCL11 spiked during the 2nd measurement, but returned to pre-therapy levels after that, while the other conditions barely showed any differences in eosinophil migration. However, shortly before staging, the cells' response to the stimuli increased, while CCL11 stimulation did not induce any migration anymore.

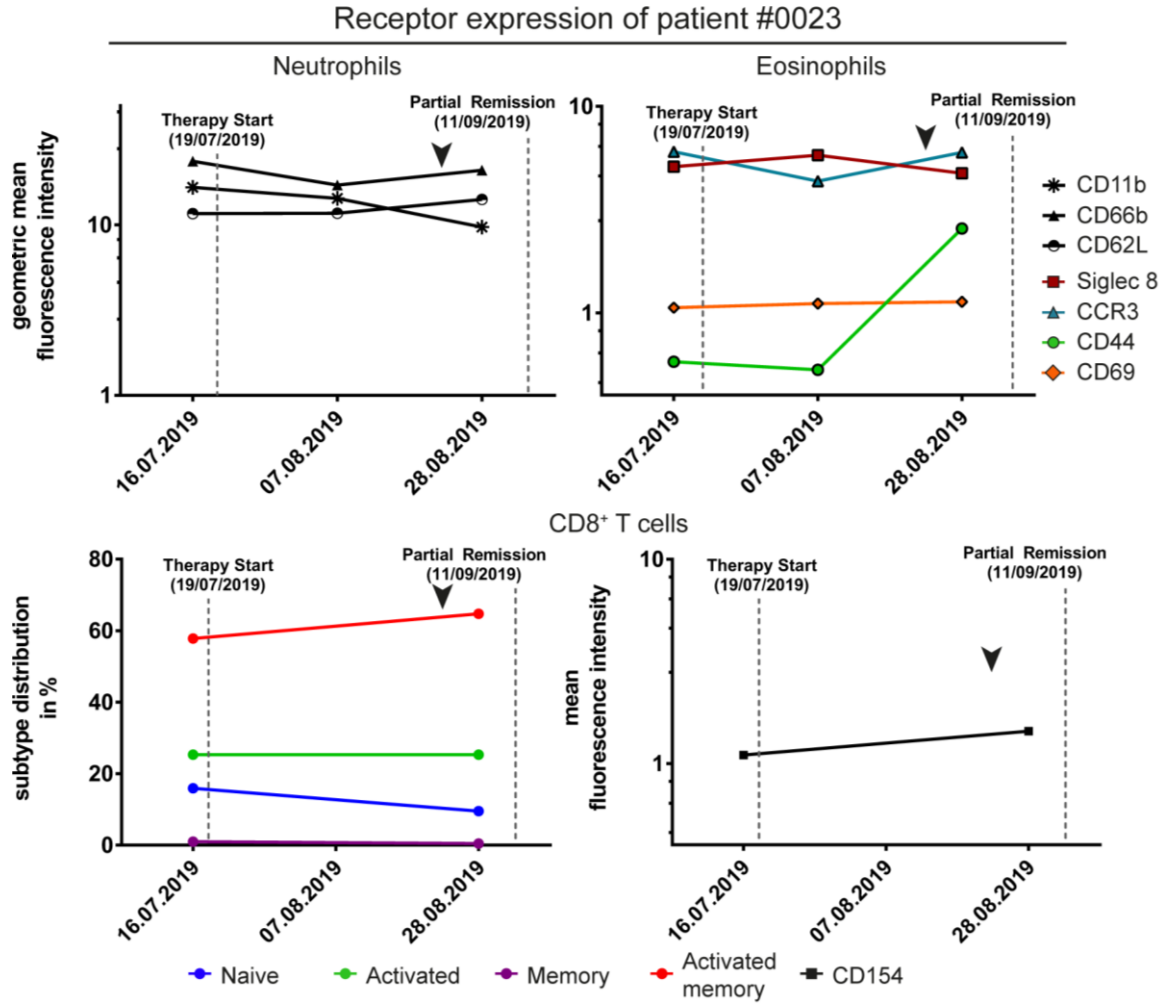

Figure 40: Leucocyte receptor expression over the course of ICBT in patient #0023.

Receptor expression of neutrophils (top left) and eosinophils (top right) as well as subtype distribution of $CD8^+$ T cells (bottom left) and their expression of CD154 (bottom right) for patient #0023 over the course of ICBT. Each dot represents the fluorescence intensity or subtype percentage for the cell types and the x-axis details the measurement dates. *Top*: Stars indicate CD11b, black trian-

gles CD66b and black, half-filled dots CD62L expression on human neutrophils. Red squares stand for Siglec 8, blue triangles for CCR3, green dots for CD44 and orange rhombi for CD69 expression on eosinophils. *Bottom*: Blue dots indicate naïve, green dots activated, purple dots memory and red dots activated memory $CD8^+$ T cells. Black squares stand for the expression of CD154. The grey dashed lines indicate the therapy start (left) and staging result (right). Black arrows indicate the diagnosis with irAE, here joint pain.

For $CD8^+$ T cells, the 2nd measurement is missing due to technical difficulties. Interestingly however, the cells showed impaired reaction to SDF-1β before therapy, which did not improve over the course of ICBT (**Figure 39**, bottom). The reaction to SDF-1α before therapy was comparable to healthy patients but dropped after two months of ICBT. The patient was finally staged with a partial remission. On 21th of August, the patient was diagnosed with joint pain and treated with a cyclooxygenase (COX) 2 inhibitor. Neutrophils and $CD8^+$ T cells of patient #0023 only slightly, if at all, changed in their expression profile and subset composition (**Figure 40**, top left and bottom**)**. Neutrophils expressed slightly less CD11b on the last day of measurement than before (top left), while $CD8^+$ T cells stayed the same in their composition and expression of CD154 (bottom). Only eosinophils showed an increased expression of CD44 shortly before staging, while all other markers remained unchanged (**Figure 40**, top right**)**.

5.5.4. Summary IV

This section focussed on the changes in immune cell migration and receptor expression induced by metastatic melanoma and immune checkpoint blocker therapy. With the previously established assays, the migration behaviour of neutrophils, eosinophils and $CD8^+$ T cells was investigated, revealing a potential prognostic relevance for eosinophil baseline migration in ICBT success. Furthermore, neutrophil and eosinophil migration was largely unchanged before ICBT, while $CD8^+$ T cells showed defective migration patterns. Neutrophils of ICBT patients before therapy expressed more CD11b and CD66b and less naïve $CD8^+$ T cells, but more activated memory cells were present in the blood of the patients. Additionally, the preliminary results of changes in migration over the course of ICBT in five patients show that eosinophil migration dropped sharply in one patient with a progressive disease. However, in two patients with partial remission the results were contradictory. The two remaining patients did not undergo staging during the finalisation of this thesis but were included for their interesting migratory changes in all cell types that might possibly correlate with irAE in one case and staging in the other.

5.6. Neutrophil migration into the murine heart following MI

Neutrophils play a pivotal role in I/R induced injury of the heart and have been attributed versatile roles, ranging from detrimental, tissue-destroying and healing functions. Thus, in this second part, neutrophil migration was investigated during MI. However, the assessment of immune cell migration *in vitro* inherently lacks the cellular microenvironment and three-dimensional complexity of entire organs. The second approach of this thesis was the endpoint investigation of neutrophil migration in a murine model of MI. Light sheet fluorescence microscopy (LSFM) was chosen for this analysis as it is capable of completely imaging large specimens, while retaining all 3-D information. As opposed to other endpoint techniques, LSFM provides information on both the localisation of the cells of interest with respect to spatial hallmarks and their quantity. However, LSFM performs subpar if the evaluated tissue is highly autofluorescent, which is especially true for the heart muscle. This limitation was overcome by developing a new clearing protocol, termed BALANCE[1].

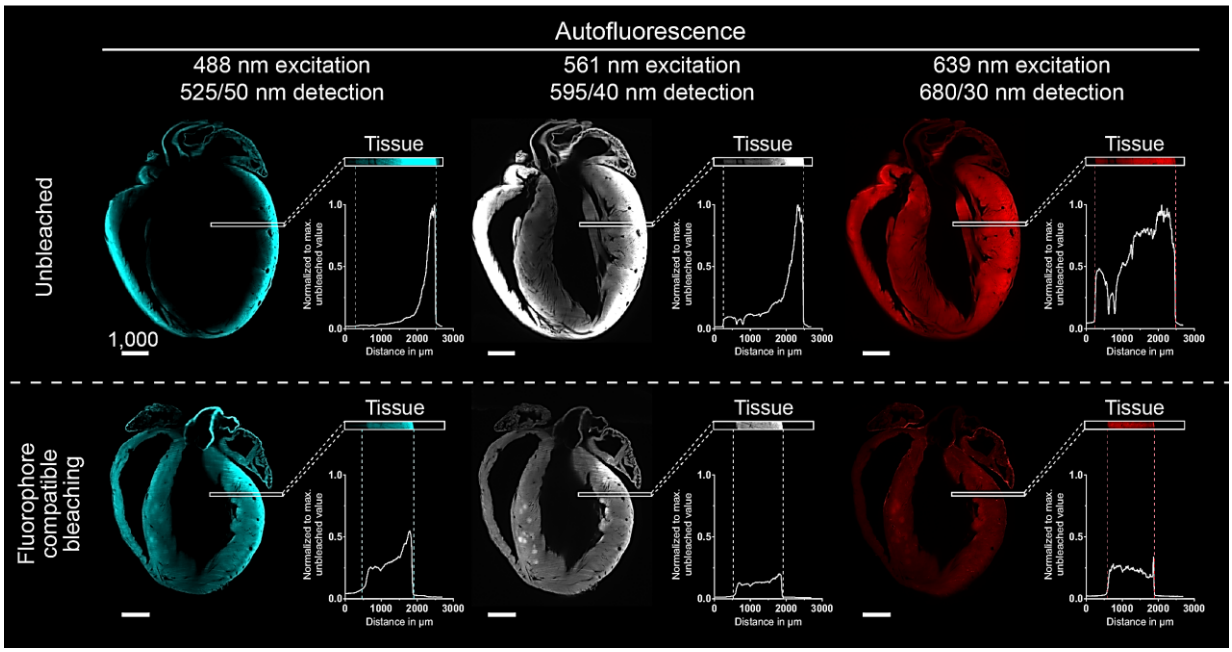

Figure 41: BALANCE enables homogenous light sheet fluorescence microscopy (LSFM) in whole murine hearts.

(**a**) Macroscopic images of murine hearts during the protocol steps. In comparison to the non-bleached sample (top right), fluorophore compatible bleaching (bottom right) enhances the clarity of the sample. One square equals 2 x 2 mm. (**b**) Signal distribution of ethyl cinnamate (ECi)-cleared, unbleached or bleached hearts in LSFM in different channels detecting autofluorescence. The region of interest (ROI) in the left ventricular wall shows high autofluorescence at the edge of unbleached hearts (upper row). This peak is lowered, together with an overall lower autofluorescence intensity in bleached hearts (lower row). Scale bar values are given in µm. This figure is adapted from [1].

A key feature of this protocol is a bleaching step with peroxide that reduces and adjusts tissue autofluorescence in all assessed wavelength channels (**Figure 41**). This allows the use of lower wavelengths for later analyses as well as utilises the autofluorescence together with an endothelial cell staining for accurate reconstruction of distinct structures, such as the aortic valve[1].

5.6.1. LSFM allows insights into the 3-D architecture of cardiac vessels and I/R injury

Intravenous application of CD31 (platelet endothelial cell adhesion molecule, PECAM-1) was used to visualise the endothelium in murine hearts and enabled the identification of both cardiac arteries and veins (**Figure 42 a**) depending on their localisation within the heart muscle tissue and their expression levels of CD31.

Arteries expressed high levels of CD31 (**Figure 42 a**, white arrows) and were mostly located further inside the tissue, while veins were located on the edges of the tissue and only exhibited a low CD31 signal (**Figure 42 a**, asterisk). By manually tracing these structures (**Figure 42 a**, bottom right), the cardiac vascular tree was reconstructed in 3-D (**Figure 42 b**) and subdivided into arteries (orange) and veins (light blue). From the position of the knot that was used to induce ischemia (white), all the arteries downstream of this obstruction were tagged as "occluded arteries" (red).

As previously published[226], CD31 positivity is lost during ischemic insult of the brain. This was found to be true for the heart as well (**Figure 42 a + c**). Downstream of the knot, areas that lacked CD31 expression ("holes", marked with asterisk in **Figure 42 c**) in the otherwise highly structured and dense vessel network were encountered. Via manual tracing, a 3-D model of the injury caused by ischemia / reperfusion (I/R injury, **Figure 42 c** right, yellow) could be reconstructed. This allowed for an overlay of both the I/R injury with the occluded vessels, which largely overlapped (**Figure 42 d**).

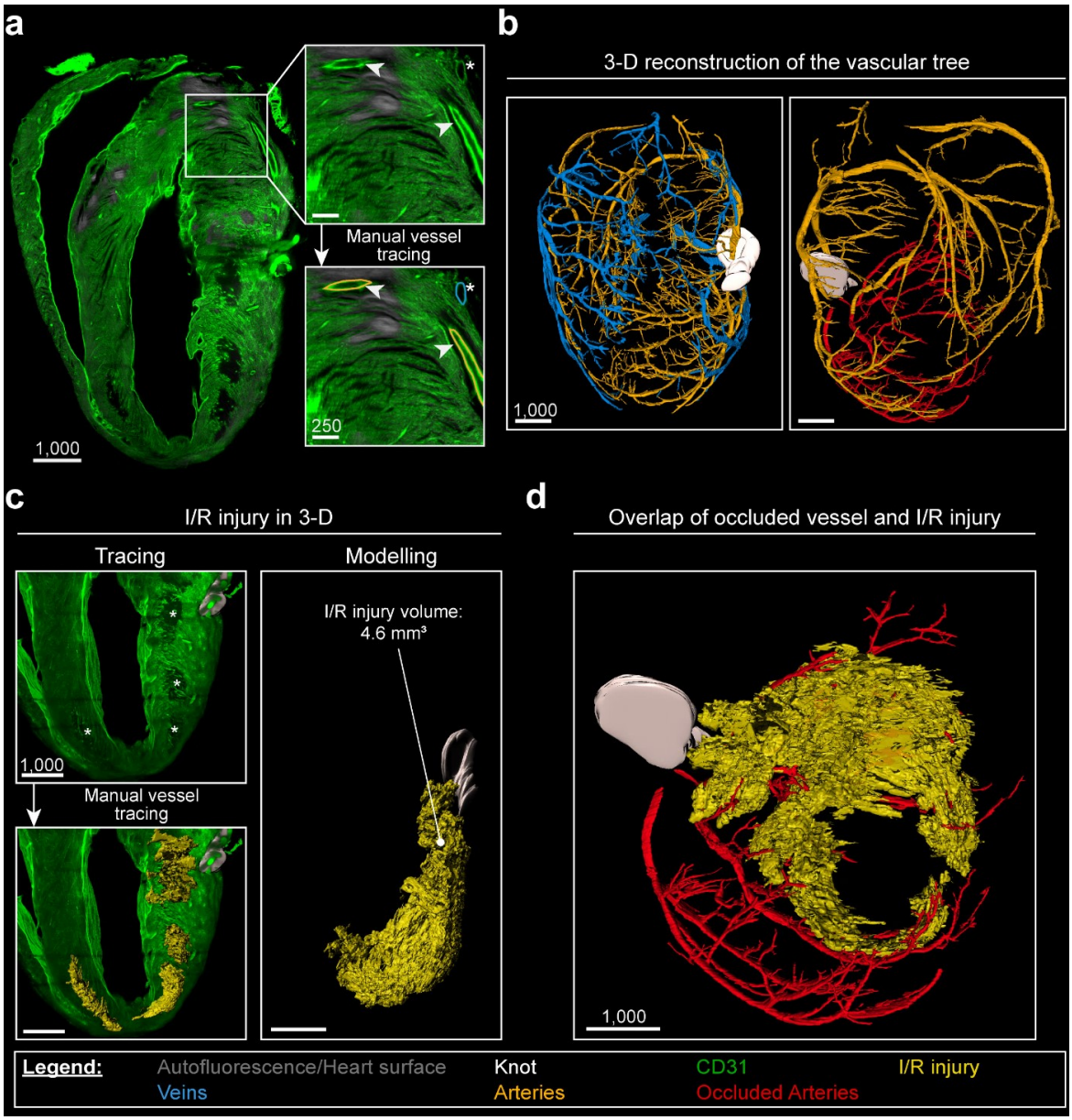

Figure 42: CD31 endothelial labelling allows for reconstruction of the vessel tree and ischemia / reperfusion induced injury.

(**a**) *Left*: Overview of CD31 (green) staining of the murine heart after ischemia / reperfusion as a single optical slice. *Right*: Magnification of the ROI (white square, left) highlights the differences in CD31 staining of $CD31^{low}$ veins (asterisk) and $CD31^{high}$ arteries (white arrow heads). These vessels can be manually traced using Imaris and separated according to their CD31 signal (bottom). Veins are traced in light blue, arteries in orange. (**b**) 3-D reconstruction of the traced vessel tree. *Left*: Arteries (orange) and veins (light blue) are separated by their CD31 signal and localisation within the heart. The knot (white) indicates the location where the I/R injury was induced. *Right*: The vessel tree from a different angle. Here, only arteries are displayed and separated into perfused arteries (orange) and occluded arteries (red). Occluded arteries were all those $CD31^{high}$ vessels that were below the knot and therefore non-perfused during ischemia induction. (**c**) Quantification of I/R injury. *Left*: Based on slice by slice tracing of areas negative for CD31 ($CD31^{neg}$) (white stars, top), a volume model of I/R injury (bottom) is reconstructed (yellow). *Right*: 3-D model of I/R injury (yellow) and the knot that induced ischemia (white). The I/R injury volume in this heart amounted to 4.6 mm^3. (**d**) The findings from (b) and (c) allow an overlay of the occluded arteries (red) with the I/R injury (yellow) and the knot (white). Scale bar values are given in µm. The overall legend is giv-

en below the figure. This figure is adapted from [1].

5.6.2. Neutrophils accumulate at the border of the I/R injury after 24 h but do not penetrate deeper into the affected tissue

Next, the changes in vascular architecture and neutrophil localisation were investigated over the course of the early healing process of the myocardium following I/R injury. Therefore, hearts of untreated (basal), 45 min ischemia and 24 h reperfusion and 45 min ischemia and 5 d reperfusion mice were analysed and compared.

After 5 d of reperfusion, we observed prominent changes in the vasculature. Where there was a highly organised and ordered capillary meshwork in basal hearts (**Figure 43 a**, left) and a hole in the CD31 staining that affected only the smaller vessels after 24 h of reperfusion (**Figure 43 a**, 2nd from left), a reduction of $CD31^{neg}$ areas after 5 d of reperfusion was encountered. Furthermore, this was accompanied by the presence of a highly unordered, $CD31^{high}$ vascular meshwork, which we termed $CD31^{curly}$, that was situated around the, now smaller, I/R injury (**Figure 43 a**, right).

Neutrophils are the first cells to arrive in the heart after I/R injury and play versatile, but not fully understood roles in both tissue damage and repair. These cells were visualised using Ly-6G, a highly specific marker for mature neutrophils in mice[65]. No neutrophils were present in completely untreated hearts, while smaller accumulations appeared in sham-treated mice, especially around the surgical thread[1]. However, neutrophils massively infiltrated into the heart after 24 h of reperfusion (**Figure 43 b**). After 5 d of reperfusion, neutrophil numbers seemed to decrease again. Automatic quantification of neutrophils in 3-D revealed a significant increase in neutrophil abundance after 24 h and 5 d compared to untreated hearts (**Figure 43 c**). However, after 5 d of reperfusion, neutrophils did not significantly decrease compared to 24 h.

Neutrophils seemed to localise closely to the I/R injury border, not penetrating into the actually damaged zone (**Figure 43 b**), while after 5 d, they were distributed throughout the $CD31^{curly}$ zones, away from the remaining damage. These observations were quantified using Imaris' distance transformation and binning the resulting smallest distances for each neutrophil in 3-D. After 5 d of reperfusion, fewer neutrophils localised closely to the remaining I/R injury zones (triangles) compared to the CD31curly region (squares) or the I/R injury zone after 24 h (dots) (**Figure 43 d**).

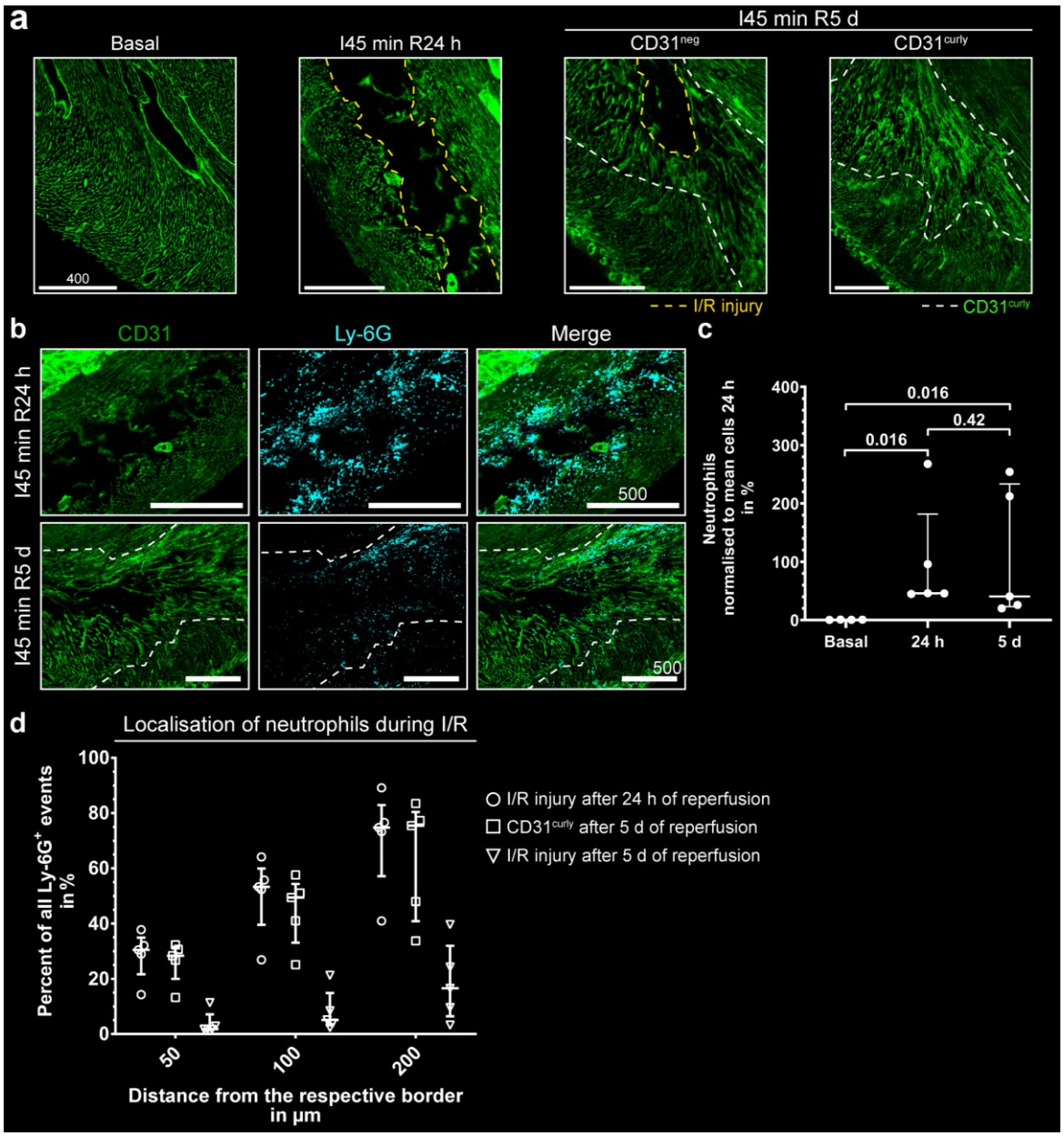

Figure 43: Changes in vascular architecture and neutrophil localisation in I/R affected hearts.

(**a**) Maximum intensity projections (MIP) comparing CD31 staining in basal (left), 24 h post ischemia (2nd) and 5 d post ischemia (right) murine hearts. I/R injury is highlighted with yellow dashed line, unordered, bright CD31 ($CD31^{curly}$) regions with white dashed lines. Magnification: 6.4 x (basal), 3.2 x (24 h), 4 x (5 d). (**b**) Exemplary MIPs of Ly-6G positive ($Ly\text{-}6G^{pos}$) neutrophils after 24 h (top row) as well as 5 d (bottom row). Depicted are CD31 (green, left column) and Ly-6G (cyan, middle column) together with a merge (right column). The dashed white line marks the border of the $CD31^{curly}$ region. Magnification: 3.2 x (24 h), 4 x (5 d). (**c**) Scatter dot plot comparing neutrophil counts obtained LSFM (white dots). x-axis shows the treatment (basal / untreated, 24 h of reperfusion, 5 d of reperfusion), while y-axis represents the percentage of neutrophils present in the heart, normalised to the mean neutrophil count after 24 h (100%). Displayed are the median ± interquartile range. *p*-values were calculated via Kruskal-Wallis test with Dunn's correction. (**d**) Scatter dot plot of the localisation of $Ly\text{-}6G^{pos}$ neutrophils with respect to the traced I/R injury after 24 h (dots) and 5 d (triangles), as well as the unordered $CD31^{curly}$ volume after 5 d (squares). The x-axis depicts the distance from the respective border in µm and the y-axis the percentage of $Ly\text{-}6G^{pos}$ neutrophils of

all neutrophils in the heart that are located there. Displayed are the median ± interquartile range. Scale bar values are given in μm. This figure is adapted from [1].

5.6.3. Summary V

In this section, it was shown how clearing and LSFM approaches can be tailored to homogenise and lower autofluorescence while retaining the fluorescence of intravenously applied antibodies coupled to synthetic dyes. With this, the 3-D architecture of the vasculature of murine hearts under healthy conditions and following I/R injury was elucidated. During this sterile inflammation, high numbers of neutrophils were present inside the heart after 24 hours and they mostly localised to the border of the affected tissue. After 5 days, when their numbers decreased, they did not penetrate further into the now healing tissue but were rather retained at the border of the previously damaged zones.

6. Discussion

The ability to autonomously migrate is an essential feature that has made life, as we know it, possible. While most, terminally differentiated cells cease to migrate until triggered again during wound healing or cancer development[6-8], immune cells remain reliant on this central ability throughout their whole life[9]. Ever since the first experiments with moving cells in the early 1960s[227], the field has greatly expanded with both new discoveries and technological advances. Today, cell motility has established itself as an integral process studied in many, interdisciplinary laboratories around the globe.

6.1. Immune cell migration as a prognostic tool

The migration behaviour of leucocytes has been extensively studied and its potential for clinical diagnostic and therapeutic purposes is high. This has been shown in various studies across a variety of different diseases, for example for CXCR2 and CXCR2 ligand blockage in both mouse and man (reviewed here[228]). Yet, the so far published assays quantifying migration behaviour lacked a key component: standardisation. For an assay to be clinically relevant, it must allow to be performed in any laboratory by anyone and still yield comparable results. However, the use of additives like foetal calf serum (FCS) or self-made matrices from bovine collagen have made a standardisation even between different charges of the same consumables largely impossible. At best, this resulted in internal databases for each laboratory that generated its own set of data from an assay. However, those values could hardly be compared between studies or research teams and thus their application in clinical routine remained elusive. But, can we overcome these obstacles and create simple, easy to use and standardised migration assays for an array of different leucocyte subsets? And what can we learn from this new perspective on migration in different disease settings? These were two central questions that were sought to be answered during this thesis.

6.1.1. Establishing immune cell migration assays

To establish immune cell migration assays applicable for clinical assessment, one must identify key differences between scientific research and medical routine. Such an assay should be fast to either compete with already existing gold-standards or be of benefit for the patient, if no gold-standard exists. The latter might then allow for critical clinical interventions if the migration pattern is prominently altered, as is the case in septic shock, where neutrophil migration is heavily altered hours before any clinical symptoms appear[129].

6.1.1.1. Aims and strategies

Thus, all established assays described within this thesis aimed at providing fast results within hours after blood draw. Furthermore, they should require only a minimum of laboratory equipment and omit the need for highly trained personnel, thus reducing cost, space and allowing understaffed laboratories to still perform the assay. Standardisation is another important point to consider as experiments and data must be reproducible and comparable to data from other institutions. Hence, the migration assays were tailored to be xeno- and serum-free, containing additives only when necessary, allowing for cross-charge and cross-laboratory comparison. Lastly, the assays should allow for high throughput screening and thus be applicable for patient analyses as well as drug- and compound-screening.

A central step enhancing speed and comparability was the replacement of tedious and subjective manual single cell tracking with a fast, reliable and objective auto tracking software that greatly increased both speed and output of the migration analyses. Furthermore, both, the neutrophil and eosinophil migration assays yield results within three to four hours after blood draw as the cells can be induced and directly imaged without lengthy pre-incubation times. $CD8^+$ T cells, on the other hand, required an activation step over night on ICAM-1 coated wells. ICAM-1 is normally expressed on activated endothelial cells and recombinant ICAM-1, bound on the plastic surface, can mimic this situation and allow the cells to adhere more firmly[229]. It is known that ICAM-1 can boost the stimulation of T cells, e.g. by CD3 activation, and lead to an increased biosynthesis and release of cytokines, especially of $CD8^+$ T cells[230-232]. Thus, this T cell assay omits the use of other costimulatory molecules, such as anti-CD3 antibodies, to allow for a more faithful representation of the activation in the body.

Assay feasibility was ensured by using a bright-field imaging approach on a conventional wide-field microscope, capable of performing time-lapse imaging of multiple positions. These microscopes are normally available in many laboratories and their investment costs are quite low compared to other, more dedicated imaging systems. Furthermore, all migration assays were performed in 2-D, which, of course, lacks biological context, as all processes in an organism are part of an intricate, 3-D structure. However, choosing this approach greatly reduced problems like standardisation of the 3-D matrix and its components, reproducibility and imaging of migration in 3-D[233, 234].

In order to enhance assay comparability, several serum- and xeno-free media were chosen and tested for their ability to keep the immune cells healthy over a desired period of time (a minimum of 2 hours for neutrophils and eosinophils and 1 day for $CD8^+$ T cells), without activating them or inducing high migration behaviour. Here, haematopoietic pro-

genitor growth medium (HPGM, Lonza) excelled in comparison to other media for neutrophil granulocytes and was thus also chosen for eosinophils and $CD8^+$ T cells. During these studies, however, HPGM was discontinued, which led to a forced change in protocols to X-Vivo™ 10 serum-free haematopoietic cell medium (Lonza). This medium produced comparable, but slightly higher migration values than HPGM (data not shown). Serum replacement 3, a product containing only human proteins, such as serum albumin, transferrin or insulin, but lacking growth factors or hormones, was chosen to replace additives subject to high inter-charge variances, such as FCS. Furthermore, all chemokines were chosen as carrier-free, thus not containing bovine serum albumin (BSA) or carrier proteins from other animals and were reconstituted in sterile phosphate-buffered saline (PBS) instead of ethanol or dimethyl sulfoxide (DMSO), both of which are toxic to cells and can inhibit key effector functions[235].

Addressing upscalability, multi-well imaging plates, such as 96 or 384 well plates were chosen, which would theoretically allow for fast screening of migration changes in many patients side-by-side. Furthermore, these assays may also be used for screening of large drugs and chemical compound libraries to study effects on immune cells, their morphology and migration. However, the throughput of the migration assays is currently still limited in terms of image acquisition. So far, only four wells for neutrophils, five for eosinophils and eight for $CD8^+$ T cells can be imaged simultaneously as the time between two frames has to be abided. If the time between two frames is too high and the cells have moved very far away from the first to the second frame, automatic tracking produces errors. Then, it cannot faithfully follow one single cell over two or more frames and terminates the tracking path. Here, we tested and chose framerates of 8 seconds (for neutrophils), 9 seconds (for eosinophils) and 16 seconds (for $CD8^+$ T cells), which were the highest times between frames we could chose for the specific cell type, without inducing imaging-related errors in subsequent tracking. Hence, faster imaging techniques must be developed in order to truly unlock the potential of these migration assays for clinical and industrial application.

6.1.1.2. Lessons learned from healthy individuals

The migration assays for neutrophils was the first of this kind of assays developed in our laboratory[2]. Following this, the application of this technology on eosinophil granulocytes was tested. Interestingly, while eosinophils were successfully induced to migrate by stimulation with CCL5[33], -7[236], -11 and -24[237], they displayed high individual variability, even under control (PBS) treated conditions (**Figure 17 + Figure 18**). This was unlike neutrophil granulocytes, which migrated more steadily in different blood donors[2]. This phenomenon was not

due to the age of the blood donors, but rather because of migration differences between male and female blood donors (**Figure 19**). These gender-dependent differences in eosinophils have previously been reported for both mice and men[238-240]. Zhao *et al.* reported female mice to produce more type 2 cytokines and chemokines[240]. Females also have more activated eosinophils and thus more inflammation than male mice in airway inflammation[240], while Slapničková and colleagues showed that female mice were more capable of controlling leishmaniasis[238]. Additionally, oestrogen has been shown to directly influence eosinophil behaviour, including migration[241]. However, eosinophils from human female or male donors did not differ in their levels of CD44 and CD69 (**Figure 21 b**), both of which are upregulated on hypodense, more activated eosinophils[81]. Furthermore, the expression of CD44 and CD69, as well as Siglec 8 and CCR3 did not correlate with any of the evaluated migration patterns (data not shown). Here, one might argue that CD44 as assessed by flow cytometry in this thesis was not sufficiently proven, as it was not induced by GM-CSF *in vitro* stimulation and showed an overall low expression level, while both Siglec 8 and CD69 were upregulated in response to activation (**Figure 20**). However, both, the isotype and the unstained control were negative and CD44 was differentially expressed in the investigated healthy blood donors (**Figure 21 a**). In concordance, Lampinen *et al.* found the expression of CD44 to be low in healthy donors but upregulated by IL-5 stimulation *in vitro*[242]. Thus, it is conceivable that eosinophils do not differ in their activation status depending on donor sex, but rather, intrinsically, in their way of reacting to insults, such as inflammation or chemokine stimulation. Their slower migration speed *in vitro* might indicate that eosinophils from female donors arrive at a site of infection later than eosinophils in male patients, but this does not necessarily implicate their effector function when on site. Especially investigation of the former would shed light on the observed migratory differences in men and women.

$CD8^+$ T cells were successfully induced to migrate on ICAM-1 coated plates after a pre-stimulation of 24 hours. However, they required high concentrations of CXCL12 for migration induction, which has previously been linked to T cell repellence *in vitro* and *in vivo*[243, 244]. Yet, as the established 2-D migration assays analyse random migration, as opposed to the investigated directed migration in a Boyden chamber or under a gradient of CXCL12, underlying mechanisms and required cytokine concentrations may differ. In 40 healthy people, random $CD8^+$ T cell migration was significantly induced by 500 ng/ml SDF-1α and 1 µg/ml SDF-1β (**Figure 22 + Figure 23**). $CD8^+$ T cells were not influenced by the time for sample preparation (**Figure 24**), as it was observed for both neutrophils[2] and eosinophils (**Figure 19**). Both age and gender did not significantly impact $CD8^+$ T cell migration in re-

sponse to CXCL12 (**Figure 24**). It is well described that T cells can be further subdivided into functionally distinct modes based on their antigen-experience and activation status with markers such as CD45RO, CD45RA or CCR7[245]. With a panel based on CD8, CD45RO and CCR7, the purified cells were checked for purity via CD8 expression and divided into naïve, activated, central memory and effector memory T cells[245] (**Figure 25**). As expected and already published[94], naïve T cells decreased with increasing age, while circulating memory T cells and effector memory T cells increased (**Figure 27**). Additionally, the expression of CD154, the CD40 ligand, was analysed as this can be expressed by $CD8^+$ T cells that possess helper functions similar to $CD4^+$ T cells[222]. As described by Frentsch *et al.*, only a small subset of $CD8^+$ T cells can be induced to express CD40L by *ex vivo* stimulation with PMA and Ionomycin, which was reproduced during this thesis (**Figure 25 b**)[222]. Even though the abundance of $CD40L^+$ $CD8^+$ T cells in the circulation of healthy blood donors is low, their numbers are increased in patients suffering from colon cancer[246]. Hence, this marker was included, especially to evaluate the abundance of $CD8^+$ T cells expressing CD40L in cancer patients, e.g. advanced melanoma patients. CD40L expression was, as expected, not detectable in most healthy patients (**Figure 26**). Interestingly, female blood donors had more circulating naïve and less effector memory $CD8^+$ T cells compared to males, even though age was not significantly different in these groups. This stands in contrast to the recently published work by Li *et al.*, who reported naïve $CD8^+$ T cells to be higher in male donors between 20 – 60 years of age[247]. However, these differences might originate from the different populations assessed in this thesis and the presented study.

Finally, the published neutrophil migration assay was supplemented with a flow cytometry panel to additionally quantify their activation status. As expected, neutrophils expressed similar levels of the investigated receptors across healthy blood donors. Strikingly however, neutrophils seemed to migrate more and faster, when they were not activated, as expressed by lower levels of CD11b and CD66b as well as higher levels of CD62L (**Figure 31**). This may be caused by the inhibition of migration through tighter adherence, as was shown for high CD66b levels, which resulted in neutrophil aggregation and clumping[248]. It is also likely that activated neutrophils need a chemotactic gradient to exhibit faster migration and that this activation, in turn, reduces random migration that is mostly needed for surveillance but not for following a gradient to a site of infection. Yet, as expected neutrophils became slightly, non-significantly, more activated due to longer preparation times, but their activation was not age- or gender-dependent, which has not been reported thus far.

6.1.2. Neutrophil migration as a biomarker for prognosis and surveillance

Neutrophils are the first immune cells to arrive at a site of insult, be it sterile or pathogenic, and infiltrate massively into the affected tissue within minutes[249]. Several studies highlight changes in neutrophil migration in diseases associated with a higher risk of infection, such as diabetes[250] or acquired immunodeficiency syndrome (AIDS)[251]. Furthermore, defective neutrophil migration was observed in severe sepsis and could be linked to a poorer prognosis[252]. Thus, the assessment of neutrophil migration behaviour has a great potential to valuably contribute to and facilitate clinical work in both diagnostics and prognostics. Two diseases, which can directly affect neutrophil development and maturation and are accompanied by a higher susceptibility to infections, are myelodysplastic syndromes (MDS) and atypical chronic myeloid leukaemia (aCML). Both diseases are also associated with a higher infection risk, which is thought to originate from either reduced immune cell numbers (MDS)[155] or their immaturity (aCML)[161].

6.1.2.1. In MDS

MDS is a heterogenous disease that affects the development of multiple haematopoietic cells with increasing severity[157]. Routinely, MDS is staged by a combination of peripheral blood cell counts, bone marrow blast analysis and cytogenetics, which culminate in the calculation of prognostic scores, such as the revised international prognostic scoring system (IPSS-R)[157]. The heterogeneity of MDS was also reflected in *in vitro* neutrophil migration patterns and especially the migration upon fMLP treatment differed among the disease categories (**Figure 7 a + b**). Interestingly, the defects in neutrophil migration in response to fMLP correlated strongly with increasing IPSS-R and thus severity of MDS, but not with any of the assessed parameters, except for the absolute neutrophil count, some of which are the basis of IPSS-R calculation[157] (**Figure 7 c + d**). Furthermore, the level of C-reactive protein (CRP) did not correlate with neutrophil migration. This is interesting, as CRP is a classical marker for ongoing inflammation, is increased in chronic inflammatory diseases, bacterial infections or progressive cancer[253] and has been shown to inhibit neutrophil migration *in vitro*[254, 255]. It is thus conceivable that the CRP concentrations were not sufficient to inhibit neutrophil migration. Yet, it would be important to include healthy patients and their respective CRP levels in future studies to evaluate the *in vivo* priming and effect of CRP on *in vitro* migration behaviour.

However, the impact of other factors on neutrophil migration, such as co-morbidities, therapy or infection over the course of disease, remained unaddressed in this study and thus warrant further investigation. Strikingly, the repetitive measurements of two MDS-EB-II cases revealed the correlation of improved neutrophil migration with therapy success and overall patient improvement (**Figure 8**). In contrast to that, neutrophil migration remained impaired in a case of unsuccessful therapy, which highlights this assay's power as a therapy surveillance tool. Importantly, 5-azacytidine therapy itself is unlikely to have an impact on neutrophil migration as both patients received the same therapy, but experienced opposing outcomes.

In MDS, the *in vitro* measurement of neutrophil migration in a standardised way might be able to facilitate clinical work by assisting prognostic scoring and continuous surveillance of patients over the course of disease. This might lower costs and invasive procedures, such as BM analyses, for both the hospital and the patient. However, the presented study only included 26 patients, most of them with less severe MDS subtypes, which showed little to no differences in migration behaviour compared to healthy patients. It would therefore be important to include more individuals with high risk MDS, different therapies and therapy outcomes in future studies to explore the true prognostic and surveillance potential of neutrophil migration. In addition to that, the reason for diminished neutrophil migration remains elusive thus far and could open the door for more, sorely needed treatment options in MDS.

6.1.2.2. In aCML

aCML is a rare neoplasia that has a poor prognosis and is characterised by increased granulocyte numbers and their progenitors in the peripheral blood as well as severe dysgranulopoiesis[161-164]. Similarly to severe MDS, neutrophils from one patient suffering from aCML were highly impaired in their migratory ability before therapy (**Figure 9**) but also remained so throughout therapy (**Figure 13**). Furthermore, the expression of the low affinity IgG receptor FcγRIII, CD16, and carbohydrate antigen, CD15, which are normally strongly expressed by human mature neutrophils, remained below the healthy average. CD15 expression is regulated during neutrophil maturation[57] and was largely absent over the complete observation period and did not significantly correlate with peripheral immature neutrophils (**Figure 16 a**). CD16, which is also upregulated with increasing neutrophil maturation[42], correlated with the amount of peripheral myeloblasts, but not significantly with any other neutrophil progenitor counts (**Figure 16 b**). Additionally, CD15 was downregulated on the overall neutrophil population, while CD16 was absent on a large proportion of the

cells (**Figure 11**). The reason for the lack of CD15 expression could not be clarified in this study. However, overall CD16 expression was influenced by immature neutrophil subsets, as published[42]. In addition to this, the signalling chemokine receptors for fMLP (fMLPR), CXCL1 (CXCR2) and CXCL8 (CXCR1 and CXCR2) were severely reduced on aCML neutrophils throughout therapy. The expression of fMLPR, CXCR1 and CXCR2 did not correlate with the migration behaviour in healthy donors[2], however it is conceivable that especially the severely impaired migration upon CXCL8 treatment might stem from the absence of its main signalling receptor CXCR1[256]. Yet, CXCL8 can also signal via CXCR2[256], whose expression levels verged on normal over the course of aCML, but did not impact neutrophil migration when triggered with CXCL8. As CXCL8 is a key molecule required for the recruitment of neutrophils and their successful extravasation from the blood vessel system[257], it is tempting to speculate that this disrupted response to CXCL8 might explain why the patient remained susceptible to bacterial and fungal infections throughout his therapy.

Strikingly, the therapy with Ruxolitinib was successful in reducing both the white blood cell count (WBC), peripheral neutrophil precursors and other disease manifestations, but had virtually no impact on neutrophil migration or receptor expression. In MDS, a successful treatment was indicated by a normalisation of neutrophil migration, while this does not seem to be the case in aCML. Here, it is therefore conceivable that the underlying genetic cause for defective neutrophil migration was not targeted by Ruxolitinib therapy, which aimed at impairing the CSF3R mutated clone[168, 169]. Additionally, Rudolph *et al.* recently reported that Ruxolitinib itself showed impairing effects on dendritic cell migration[258]. While it stands to reason that Ruxolitinib therapy is partially responsible for the diminished neutrophil migration, the low migration speed and recruitment were already detectable before therapy (**Figure 9**). To date, only the migratory capacity of banded neutrophil granulocytes has been investigated and these data yielded conflicting results[217, 218]. Yet, the analysis of neutrophil migration speed and the abundance of overall leucocytes, myeloblasts and metamyelocytes in the patient's peripheral blood, revealed no strong correlation (**Figure 15 a**). However, metamyelocyte counts correlated negatively with speed upon CXCL8. Thus, metamyelocytes might influence the migration analysis either directly by being slower than mature neutrophils, or indirectly by repressing mature neutrophil migration.

Another interesting difference between the aCML patient and MDS patients was the neutrophils' morphology. In aCML, neutrophils were significantly enlarged compared to healthy controls before therapy, but whether this is the result of enlarged cytoplasm or increased adherence, remains unclear (**Figure 10**). This altered morphology improved in accordance with therapy success upon Ruxolitinib treatment (**Figure 14**). Furthermore, neu-

trophil size did not correlate with assessed peripheral blood parameters, ruling out that neutrophil progenitors are responsible for these changes (**Figure 15 b**). Additionally, neutrophil morphology normalised to healthy levels already one week after therapy initiation. In fact, it has been reported that Ruxolitinib causes microtubule instability in mutant HEL cells[259] and might thereby change their morphology. Furthermore, it is conceivable that the CSF3R mutant clone was responsible for the abnormal shape or adherence of neutrophil in this assay, which then normalised by clonal depletion (data not shown).

Of high importance is the peak in neutrophil speed upon fMLP stimulation on day 67 to 12.5 µm/min (**Figure 13**). Only six days later, the aCML patient was hospitalised due to a sinusitis with fever and bleeding from a gastric ulcer. Therefore, surveillance of neutrophil migration could help identify not only therapy success in MDS, but also function as an early warning system for upcoming infections in high risk patients. Interestingly, this also shows that aCML neutrophils were still able to overcome their unresponsive state, but seemed to require additional, yet undefined, host-derived stimuli to migrate in an *in vitro* assay. Unfortunately, it remains unclear whether neutrophil migration was altered during the last weeks, when the patient was diagnosed with mucormycosis, a fungal infection, mostly occurring in immunosuppressed patients[260], as no migration data could be acquired during these stages. Whether weak neutrophil effector function and motility might have been the cause of this disease or something else triggered this drastic deterioration, can only be subject of speculation.

6.1.3. Immune cell migration in malignant melanoma and immune checkpoint blocker therapy

Melanoma is the most dangerous form of skin cancer and especially melanoma metastasis is aggressive and increasingly difficult to treat[174]. However, ever since the discovery of immune checkpoints in T cell activation and suppression in the 1990s[261, 262], tremendous efforts in understanding T cell biology and developing blocking antibodies, have led to fundamentally new treatment options: immune checkpoint blockers. Especially anti-PD-1 and anti-CTLA-4 antibodies are now routinely applied in clinical treatment of metastatic melanoma patients as they have yielded exceptional results in overall survival[263-265]. However, significant percentages of patients do not respond to PD-1, CTLA-4 or even combination therapies[224]. Furthermore, serious, sometimes even life-threatening complications, so-called immune-related adverse events (irAE), arise from these therapies as not only tumour-specific T cells are boosted, but also those that might have been suppressed due to their auto-reactivity[266]. Biomarkers, which can identify responders and non-responders either be-

fore therapy or early on during therapy, as well as predict the occurrence of irAE, are sorely needed to improve the clinical outcome for the patients.

6.1.3.1. The prognostic potential of eosinophil migration

Eosinophil granulocytes have been described as important players in cancers, such as melanoma[46]. Many malignancies are accompanied by peripheral eosinophilia and eosinophil infiltrates and some of them are correlated with a favourable outcome for the patient[85, 267]. In 2015, Carretero *et al.* described that eosinophils are involved in cancer rejection by recruiting $CD8^+$ T cells and normalising the tumour vasculature to facilitate this infiltration[86]. In addition to that, Lucarini and colleagues demonstrated that eosinophils were recruited to the primary tumour site by IL-33, where they then recruited and activated $CD8^+$ T cells and natural killer (NK) cells, thus promoting tumour rejection[268]. In concordance, peripheral eosinophilia has been proposed as a biomarker for melanoma patients during immunotherapy with checkpoint blockers[267]. As any other immune cell, eosinophils much migrate to reach the tumour site and exert their multi-facetted functions. Thus, the mere assessment of their abundance in the blood might not reflect on their ability to infiltrate into the tumour. Therefore, the migratory patterns of eosinophils were determined in patients suffering from metastatic melanoma undergoing ICBT.

In a first, mixed cohort of patients under ICBT, eosinophil migration patterns were highly reduced over the whole cohort compared to non-melanoma, healthy individuals (**Figure 32 a**). Interestingly, eosinophil speed upon control treatment with PBS was, overall, undistinguishable from healthy people. This was further elucidated by grouping the patients according to their treatment outcome into responders and non-responders (**Figure 32 b**). Upon control treatment with PBS, eosinophils migrated faster if they originated from a responder as compared to eosinophils from non-responders, which migrated significantly slower. A receiver operating characteristic (ROC) analysis revealed that eosinophil baseline speed was able to tell apart responders from non-responders with high specificity and sensitivity (**Figure 32 c**). However, this mixed cohort did not contain measurements before ICBT. Furthermore, it was not possible to group the patients according to previous treatments, checkpoint blocking agent, age, gender or recurring measurements, as this would have severely reduced the already small samples sizes.

Eosinophil migration can be a powerful tool to study the response of patients to ICBT in melanoma. Already the mixed cohort of different previous treatments, checkpoint blocking antibodies, ages and gender revealed a correlation between faster baseline migration speed and successful therapy outcome. It is conclusive that eosinophils are activated due to ICBT,

but whether this is a direct or indirect effect remains unclear. Heightened migratory capacity in the peripheral blood might indicate that they are more capable of migrating into the tumour to exert accessory functions for $CD8^+$ T cells or NK cells[86], but also into other peripheral sites and thus inhibit the spreading and growth of more distant metastases[268]. However, whether increased eosinophil migration is associated with increased infiltration into the tumour bed or distant sites remains to be elucidated in future studies.

6.1.3.2. Interplay of neutrophils, eosinophils and $CD8^+$ T cells in malignant melanoma

To overcome the limitations of the first mixed cohort, a new melanoma cohort was set up to investigate the migration behaviour and receptor expression of eosinophils and neutrophils, but also $CD8^+$ T cells. This cohort encompassed only patients, who received ICBT as a first therapeutic option and who could be measured before therapy to determine pre-therapy migration behaviour.

Interestingly, both neutrophil and eosinophil speed in melanoma patients before ICBT was largely indistinguishable from healthy controls (**Figure 34**). However, peripheral $CD8^+$ T cells were completely inhibited in their response to CXCL12, both in its α and β isoform. Additionally, neutrophils from melanoma patients expressed more CD11b and CD66b and were thus more activated[63], while the level of CD62L expression was similar to healthy controls (**Figure 35**). Eosinophils from melanoma patients did not show an upregulation of CD44 or CD69, which was reported for activated eosinophils in other diseases[81]. Melanoma patients had significantly less naïve, but more activated memory cells, which is, most likely, due to the advanced age of the melanoma patients (ICBT: 45 – 82 versus healthy: 27 – 62) and not from the disease itself.

These experiments show that melanoma systemically affects $CD8^+$ T migration and neutrophil activation but has no impact on overall neutrophil or eosinophil migration, eosinophil activation or $CD8^+$ T cell expression of CD154. This highlights that the changes observed in eosinophil migration discussed under **6.1.3.1** are a result of the cells' reaction to the treatment rather than already present because of the disease itself. Thus, eosinophil migration might still be a prognostic marker during ICBT but cannot indicate responders and non-responders before therapy. It is of high importance to investigate whether this is a melanoma specific phenomenon or if $CD8^+$ T cell migration is impaired in other cancer types as well. Furthermore, there is therapeutic potential in restoring this defective migration to boost melanoma rejection beyond sole T cell activation, as performed during ICBT. It also

remains unclear whether melanoma directly downregulates T cell migration or if defective T cell migration might be the cause for melanoma in the first place.

6.1.3.2.1. Preliminary results from five follow-up patients and their stagings

As only four patients of the new ICBT cohort could be followed over their course of treatment and subsequently be staged so far, only preliminary results on migration and therapy response could be acquired. Notably, in one case of progressive disease, a non-responder, eosinophil migration, especially speed, gradually worsened over the course of ICBT (**Figure 36 a**). This hints at a gradual, systemic reduction of eosinophil migration beyond the direct interaction of the cells with the checkpoint blocking molecules as eosinophils have not been reported to circulate in the blood stream for multiple months[269]. However, this extended manifestation of the defective migration phenotype might indicate that eosinophil migration is not a good prognostic marker for ICBT success, as first staging and migration deficiency occur roughly at the same time. On the other hand, if eosinophil migration failure coincides with therapy failure, modulation and restoration of eosinophil migration might help to counteract melanoma progression and ICBT resistance.

Two patients with partial remissions showed contradicting results. Patient #0013, who was analysed only for eosinophil migration, displayed steeply declining migration patterns after ICBT onset, despite being diagnosed with a partial remission (**Figure 36 b**). These results, of course, questions the value of eosinophil migration during ICBT therapy, as both a progressive disease and partial remission were accompanied by reduced eosinophil migration. Yet, this was already observed in the first, mixed cohort (**Figure 32 b**). Here, some responders showed defective migration, while some non-responders presented with normalised migration, but eosinophil migration still produced a good overall correlation with therapy success in this old cohort. Therefore, other parameters that might influence eosinophil migration, such as IL-2 or GM-CSF levels, in this setting must be identified and carefully considered to paint a more precise picture of patient progression or therapy success.

It is tempting to speculate that ICBT directly inhibits eosinophil migration, regardless of the outcome, yet patient #0023, who was also staged with a partial remission, exhibited normalised eosinophil migration patterns two weeks before staging (**Figure 39**). Notably, this normalisation of migration coincided with an upregulation of the activation marker CD44, while all other markers remained unaffected (**Figure 40**). CD44 has been extensively studied for its role in tumour progression, where it promotes migration and invasion[270, 271]. Furthermore, it can regulate the rolling of T cells on endothelial cells[272], which express its ligand hyaluronic acid, and initiate extravasation and infiltration. So far, little is known

about the biology of CD44 on eosinophils other than that it is an activation marker in bronchial diseases[80, 273]. As no correlation existed between CD44 expression and migration behaviour of eosinophils in healthy individuals, the increase in CD44 coinciding with increased migration in patient #0023 must be presumed as by chance.

Neutrophil migration from patient #0023 was severely impaired before ICBT onset. Interestingly, the responses to fMLP and CXCL1 remained below normal levels, while CXCL8 induced speed normalised over the course of therapy (**Figure 39**). This was accompanied by a slight downregulation of CD11b, but not of any of the other markers (**Figure 40**). Therefore, ICBT induced normalisation of neutrophil migration patterns, which has been associated with a positive outcome for MDS patients before[2], yet both fMLP and CXCL1 failed to induce responses comparable to the healthy situation. fMLP is an N-formylated peptide that is characteristic for bacteria and elicits strong chemotactic responses in neutrophils and other immune cells[274]. fMLP is an end target chemoattractant that leads neutrophils to the site of infection after they have crossed the endothelium[47]. Intermediary, endogenous chemokines, such as CXCL8, induce rolling and transmigration of neutrophils on the endothelium and thus must be overridden by stimuli, such as fMLP to facilitate directed migration in the tissues[47]. Heit and colleagues proposed a hierarchical model of integrating these stimuli by the activation of different intracellular signalling pathways triggered by fMLP and CXCL8[275]. It is therefore conceivable that neutrophils from patient #0023 were dysregulated in their intracellular signalling pathways, affecting the response to all tested chemokines. This, however, might stem from other cytokines, such as GM-CSF[276], which may influence neutrophil responses without changing the expression of signalling receptors, but rather change the intracellular signalling landscape.

Furthermore, higher neutrophil expression of CD11b correlated negatively with migration behaviour, at least for baseline migration (**Figure 31**). Indeed, patient #0023 showed high CD11b expression before therapy, which persisted for one month, but dropped on the third measurement, when migration sharply increased. In this regard, Zen *et al.* demonstrated that CD11b/CD18 is important for firm adhesion of neutrophils to the endothelium, but that CD11b must be cleaved for successful transmigration[277]. High expression of CD11b could induce firm adhesion of neutrophils to the plastic in the presented assay and thus reduce percentage of moving cells and speed of all stimulation conditions. This was not observed for healthy patients, most likely because such high CD11b expression was not present in healthy individuals.

Strikingly, $CD8^+$ T cells, which were able to respond to 500 ng/ml SDF-1α, lost this ability during therapy until staging and were thus completely unresponsive to any trigger in

the migration assay, despite partial remission. This is unexpected as one would assume that a responder is characterised by a normalisation of T cell migration to healthy control levels, not by further decrease of said migration. One week before this reduction, the patient received a cyclooxygenase (COX) 2 inhibitor in response to immune-related joint pains (**Figure 39**). COX-2 is induced due to pro-inflammatory mediators and is responsible for increased prostaglandin production, which in turn lead to vasodilatation and endothelial permeability to facilitate leucocyte infiltration into the inflamed tissue[278]. Additionally, dysregulation of COX-2 has been described to drive the pathogenesis[279] and play an important role during immune evasion of cancer[280]. In contrast to that, COX-2 and its product prostaglandin E_2 are also involved in migration of macrophages[281] and dendritic cells[282]. While no studies of pharmacological COX-2 inhibition on T cell migration exist so far, it is tempting to speculate that decreased T cell migration is the result of anti-inflammatory treatment against immune-related joint pain in patient #0023. In this regard, Lukkarinen and colleagues described increased neutrophil influx into injured lungs after treatment with the COX-2 inhibitor NS-398[283]. In patient #0023, neutrophil and eosinophil migration was also increased after COX-2 inhibition, which could thus be another possible reason for these observations.

Patient #0021, for whom no staging exists so far, was characterised by a strong decrease of neutrophil, stable but high and largely uninducible eosinophil and worsening $CD8^+$ T cell migration (**Figure 37**). Due to overall bad migration behaviour, it is tempting to speculate that this might be a non-responder, especially concerning neutrophil and eosinophil migration patterns. Furthermore, the patient was diagnosed with immune-related hepatitis on the last day of observation, which might account for the severe decrease in immune cell migration patterns, as was observed in our lab for neutrophils from severe acute hepatitis patients (unpublished data). Sadly, no flow cytometry data was acquired on that last day, which could shed light on immune cell activation during immune-related hepatitis.

In summary, this study investigating the activation status and migration of neutrophils, eosinophils and $CD8^+$ T cells in melanoma and during ICBT still severely lacks in patient samples, stagings and follow-up measurements. First hints can be gained from the data acquired for this thesis. Eosinophil and neutrophil migration, for instance, is obviously changed in response to ICBT, but not due to melanoma itself, while peripheral $CD8^+$ T cells remained severely impaired in their migratory capacity despite ICBT. In this regard, a reason for ICBT failure could be the insufficient migration of $CD8^+$ T cells into the tumour because of previously inscribed migratory defects. Thus, ICBT would activate the cells, but not support them in getting to the tumour site. ICBT does not seem to have a direct effect on

the migration of cells it should directly affect, namely $CD8^+$ T cells. Other mediators, such as serum levels of IL-2, GM-CSF, G-CSF or others, might be responsible for the evaluated changes, making migration data alone hard to interpret in this multi-facetted disease. To precisely determine the prognostic, maybe even diagnostic, value of migration in this disease, further analyses must be conducted on a larger cohort of patients, assessing also tumour biopsies for immune cell infiltrates and plasma samples for the induction of specific mediators that correlate with altered migration patterns. Only then can a comprehensive picture be painted, and migration behaviour be linked to tumour rejection or progression.

6.2. Light sheet fluorescence microscopy as a novel tool for in-depth migration endpoint analyses

Biological processes inherently happen in three dimensions, but barely any techniques faithfully represent this 3-D nature. Light sheet fluorescence microscopy (LSFM) of optically cleared organs has established itself by taking a step back and visualising entire organs at cellular resolution. However, optical clearing of the samples is the key step, enabling homogenous and therefore quantitative imaging of whole specimens and organs. While a great variety of different approaches for optical clearing exist, most of them suffer from compound toxicity, prolonged handling and clearing times or suboptimal clearing of pigmented organs[139], such as the heart. This was overcome by the development of BALANCE[1], which combines key aspects of other clearing approaches with the use of non-toxic reagents and allows for fast and reliable 3-D characterisation of pigmented organs. In comparison to unbleached murine hearts without any further staining, BALANCE reduced tissue absorbance and edge halos (**Figure 41**). This was especially important as subsequent automated analyses, such as counting of neutrophil granulocytes, relied on a homogenously distributed signal and the ability to apply an overall threshold for negative and positive signals throughout the entire organ. Additionally, this allowed the segmentation of vessels into arteries and veins solely based on the brightness of their endothelial staining (CD31) as well as their localisation.

6.2.1. Vessel architecture during ischemia / reperfusion injury

During myocardial infarction (MI), the supply of blood by coronary arteries is terminated, mostly due to fatty plaques or thrombi[195]. This leads to reduced or even terminated supply of nutrients and oxygen to the myocardium and thus inflicts tissue damage. Fast intervention is needed to restore the perfusion of MI after ischemia (reperfusion), which in turn

has been shown to inflict additional damage on both myocardium and blood vessels, a phenomenon termed ischemia / reperfusion (I/R) injury[198, 199].

As the vasculature is the starting point of I/R injury, faithful reconstruction of the vessel tree was the first aim of this study. CD31 (platelet endothelial cell adhesion molecule, PECAM-1) proved invaluable in visualising the dense vessel meshwork[3, 137] in the murine heart (**Figure 42 a**). The supplying arteries expressed high levels of CD31[284, 285], were located on the inside of the heart muscle tissue and were larger than other vascular structures. Veins were characterised by low expression of CD31, thin walls[286] and their localisation rather on the edge of the tissue. This allowed for a semi-manual 3-D reconstruction of the large vascular tree of the murine heart (**Figure 42 b**). However, LSFM-guided immunohistological sections and stainings for Sca-1, α-SMA (arteries) or Ephrin B4 (veins)[3] should be conducted to verify that these vessels as indeed arteries or veins.

The identification of the knot, which was used to induce I/R injury in the here employed mouse model, was possible as the suture was autofluorescent and scattered light, especially in the lower wavelength channels. This enabled the segmentation of the heart arteries into those that were above the knot and thus perfused (orange), and those that were downstream of the knot, thus presumably not perfused (red) arteries. Non-perfused arteries furthermore overlapped with the so-called area at risk (AAR) as determined by other means in the same heart, thus proving that these vessels were indeed not perfused during artery occlusion[1].

Recently, Lugo-Hernandez *et al.* shed intricate light on the changes in vasculature following stroke[226]. Here, ischemic brain areas showed a severely decreased vessel density due to loss of capillaries when compared to non-ischemic areas. In this paper, the authors combined vessel filling with fluorescently labelled albumin with CD31 staining, proving that both methods produced the same results, namely a loss of capillaries in the ischemia-affected brain hemisphere. Based on these findings, the loss of CD31 was studied in I/R injury. Indeed, CD31 was absent in areas of the heart, especially around and downstream of the knot (**Figure 42 c**), which allowed for semi-manual reconstruction of these structures. These I/R injury volumes overlapped with the previously identified, occluded arteries (**Figure 42 d**). However, both occluded arteries and AAR[1], were larger in size and also existed outside of the I/R injury volume. The question arises why some parts of the myocardium are affected, while others, that lie inside the AAR and were not perfused during ischemia, are not? It is tempting to speculate that structural differences in both vessels and the myocardium are responsible for these differences. Furthermore, the termination of the blood flow via one coronary artery might not necessarily mean the undersupply of all downstream areas, as these may still be supplied via other larger vessels. Elucidating these intra-heart

differences could shed more light on the pathology of I/R injury and pave ways for treatments and prevention of vessel loss due to acute MI.

6.2.2. Neutrophils in I/R injury

Reperfusion is needed after ischemia to restore the supply with blood and therefore oxygen and other nutrients to prevent further death of cardiomyocytes[287]. However, reperfusion triggers pro-inflammatory responses, which further damage the affected myocardium[288]. Also here, neutrophil granulocytes are the first responders and arrive early at the ischemic border, where they generate reactive oxygen species (ROS) and secrete their cytotoxic granules, thus furthering tissue injury[206]. Yet, neutrophils do not only play a detrimental role in I/R injury, but are also important modulators of the immune response, culminating in resolution of inflammation and subsequent healing. In this regard, Horckmans and colleagues showed that complete neutrophil depletion in their chronic MI model was detrimental for cardiac function, resulted in increased fibrosis and heart failure[207]. On the other hand, blocking or depletion of myeloperoxidase (MPO), an enzyme mostly produced by neutrophils and pro-inflammatory monocytes, was mostly accompanied by improved outcome and cardiac function, but had no impact on the I/R injury size[208, 209]. However, while some studies report improved outcome upon blocking neutrophil infiltration, others could not reproduce these results or show any positive effect of neutrophil blockage on I/R injury in experimental mouse models[206].

Thus, it is conceivable that neutrophils play a pro-inflammatory role early after ischemic insults. Attracted by DAMPs, they massively infiltrate into the tissue and produce ROS and other pro-inflammatory mediators that reduce oxygen availability for the already stressed myocardium and inflict more tissue damage. This results in increased infarction size, especially as neutrophil localise to the border of the previously ischemic zone (**Figure 43**) after 24 hours. However, they can phagocytose and thereby clear the border zone of dead cells and debris. After this initial pro-inflammatory response, apoptotic neutrophils are phagocytosed by macrophages, which induces anti-inflammatory responses in these macrophages[205]. This is thought to be important for initiating the healing process and might explain the detrimental results obtained from overall neutrophil depletion during MI. Interestingly, after 5 days of reperfusion, during the early healing phase, neutrophils were still localised to the previous ischemic border zone at 24 hours, without penetrating further into revascularizing tissue, characterised by unordered, "curly" CD31 signals[1] (**Figure 43**).

LSFM analysis of murine hearts provided an overview on the destruction and development of the vasculature as well as the influx of neutrophils and their localisation during I/R

injury. Thus, this technique is highly valuable for further investigations to determine the exact impact on infarction and healing after intervention, such as neutrophil depletion or blockage of their infiltration. This might help to better understand the lack of translation between mouse models and humans in MI. Furthermore, as neutrophils are not the only cells involved in I/R injury, it is important to consider that the published protocol is versatile and can be modified for other cells, such as macrophages[1], T cells, B cells or fibroblasts, only limited by the availability of antibodies against surface antigens of a specific cell type.

7. Outlook

The described and employed methods can go far beyond the applications that were explored in this thesis. The standardised 2-D migration assays allow for fast and reproducible screening of blood immune cells from healthy and diseased donors in virtually all disease settings. BALANCE, LSFM and the performed image analyses have overcome the problems of fast clearing procedures, homogeneous and quantitative imaging of previously complicated organs and dedicated image analysis that shows what can be gained from images, besides mere representation.

7.1. Versatile application of immune cell migration assays

A large portion of this thesis was dedicated to exploring and harnessing the potential of immune cell migration. The established assays for neutrophils, eosinophils and $CD8^+$ T cells can now be applied, but importantly adapted to other disease settings. During establishment, we tested and titrated basic chemotactic molecules, such as fMLP or SDF to induce reproducible migration behaviour in the various cell subsets. However, if a laboratory is interested in the effect of other molecules, such as C5a[289, 290] or IL-33[240, 268], on their immune cell of interest, these assays are easily adaptable to the specific question. As these assays are conducted in cell culture, the influence of hypoxia or nutrient starvation can be studied without much adaption. Cross-species adaption can be more complicated, as e.g. mouse neutrophils are less sensitively to fMLP and require different stimulation[42].

These are only some examples of adaptation that highlight the versatile nature of these assays. Of note, while it is possible to screen different disease settings or molecules, other techniques are needed to fully elucidate the underlying molecular mechanisms.

7.2. Influences on immune cell migration

Immune cell migration is a highly complex process that incorporates exogenous and endogenous cues to generate a single outcome. Thus, it is hard to interpret migration behaviour if the overall picture is not complete. To verify their application in the clinical setting, the migration assays must be tested more thoroughly on more individuals and underlying mechanisms should be explored to counteract observed changes in the patients. For this, the migration assays should be supplemented with routine analyses of signalling receptors and activation markers, e.g. via flow cytometry, as well as serum analyses for the abundance of migration-influencing molecules, such as G-CSF and GM-CSF[291], IL-1β[292] or IL-6[293]. Fur-

thermore, the patients should be closely monitored for blood parameters, such as peripheral cell counts or CRP, medication and other chronic and acute diseases, like allergy; all of them can potentially influence *in vitro* immune cell migration. Furthermore, to clarify the influence of gender or oestrogen in particular on eosinophil migration, future studies should specifically include postmenopausal compared to premenopausal female donors. These experiments should be supplemented with measurement of oestrogen and other, above-mentioned blood parameters.

It remains unclear whether cell-intrinsic migration properties correlate with the complex cell migration as observed in an organism. Thus, it is mandatory to study whether increased *in vitro* migration means increased infiltration or migration inside the tissue. In melanoma, this can be studied by analysing tissue samples of the primary tumour for the abundance of immune cells and correlate it to the migration behaviour before therapy. It would be also important to explore this phenotype in melanoma models in mice. By mimicking the assay for mice, neutrophil, eosinophil and $CD8^+$ T cell migration could be analysed *in vitro*, while other experiments, such as intravital microscopy or subsequent LSFM, could still be performed. In MDS and aCML, neutrophil migration was severely impaired, but it seems unlikely that this is solely due to the presence of immature neutrophils in the blood and the assay. Future studies should aim at elucidating this migratory defect of neutrophils to counteract it as this might be the reason for the increased risk of infection. This could be a new angle from which to approach MDS and aCML in terms of medication and standard care. Furthermore, migration is an excellent tool for surveillance as severe changes from the patient's normal pattern can indicate inflammation or therapy failure.

In I/R, neutrophils are controversially discussed, however the field severely lacks in-depth analyses of neutrophils and their effector function over the course of I/R. It is appreciated that their functions change from early to late I/R, yet the exact kinetics and functions are largely unexplored. As the blockage of overall immune cell infiltration in humans after MI yielded contradicting results[294, 295], further effort has to be invested into elucidating these differences in model systems to improve clinical work when treating MI. Especially more timed and more specific blockage of neutrophils might help in tackling the problem of immune-related injury. Blocking neutrophil entry, for example, in the first few hours might help reduce I/R injury size, but this blockage must be transient to enable them to exert their anti-inflammatory and wound healing promoting functions later in I/R.

Overall, it is important to remember that the organism is highly interconnected, and that one analysis can never yield the answers to all questions. However, easy, fast and reproducible assays are needed to explore the basis of a phenotype before delving deeper. Especially

in the clinical routine, there is neither the time nor the money to perform sophisticated, lengthy assays that yield a lot of data that cannot be analysed in time.

7.3. Automated image and data analysis

This already leads to the last, but by far not unimportant point: automation. 2-D migration has been historically analysed by manual tracking. While this may be initially faster than writing a script to the analysis, it gets tedious and time-consuming with image sequences of 361 frames; the number of images in only one neutrophil video. If one considers the 111 healthy individuals measured during the MDS study[2], this accounts for 111 × 4 videos × 361 frames = 14,440 images to analyse. In clinical application, it is not possible to track all these images manually. We overcame this problem by using the Automated Cellular Analysis System by MetaVí Labs. Availability of such analysis software is mandatory to accurate and timely representation of imaging data. Furthermore, the analysis of the migration videos for morphological changes throughout the migration process should also be conducted automatically in the future, as this will represent the imaging data more faithfully. While time-lapse microscopy already produces large amounts of data, LSFM reaches new heights in data size, but also information stored within these data. In the published paper[1], we presented a variety of different information that can be extracted from just one heart stained with against CD31, Ly-6G and filled with FITC albumin. However, most of these analyses were conducted manually or semi-manually in Imaris, a software package by Bitplane. Furthermore, the raw data required lengthy pre-processing steps for the automated computation of e.g. vessel density via FRANGI or automated spot counting in Imaris[1].

Automation is sorely needed to assist researchers and clinicians alike in acquiring, but also understanding and correctly interpreting their data. Imaging data is complex and artificial intelligence and deep learning have the potential to extract the aforementioned information but also entirely new feature from these versatile data, in a fast, reproducible and understandable manner.

8. Bibliography

1. Merz, S.F., Korste, S., Bornemann, L., Michel, L., Stock, P., Squire, A., Soun, C., Engel, D.R., Detzer, J., Lörchner, H., Hermann, D.M., Kamler, M., Klode, J., Hendgen-Cotta, U.B., Rassaf, T., Gunzer, M. & Totzeck, M. **Contemporaneous 3D characterization of acute and chronic myocardial I/R injury and response**. *Nature Communications* **10**, 2312 (2019).
2. Schuster, M., Moeller, M., Bornemann, L., Bessen, C., Sobczak, C., Schmitz, S., Witjes, L., Kruithoff, K., Kohn, C., Just, O., Kündgen, A., Pundt, N., Pelzer, B., Ampe, C., Van Troys, M., Nusch, A., Haas, R., Germing, U., Martens, L., Jöckel, K.-H. & Gunzer, M. **Surveillance of Myelodysplastic Syndrome via Migration Analyses of Blood Neutrophils: A Potential Prognostic Tool**. *The Journal of Immunology*, ji1801071 (2018).
3. Grüneboom, A., Hawwari, I., Weidner, D., Culemann, S., Müller, S., Henneberg, S., Brenzel, A., Merz, S., Bornemann, L., Zec, K., Wuelling, M., Kling, L., Hasenberg, M., Voortmann, S., Lang, S., Baum, W., Ohs, A., Kraff, O., Quick, H.H., Jäger, M., Landgraeber, S., Dudda, M., Danuser, R., Stein, J.V., Rohde, M., Gelse, K., Garbe, A.I., Adamczyk, A., Westendorf, A.M., Hoffmann, D., Christiansen, S., Engel, D.R., Vortkamp, A., Krönke, G., Herrmann, M., Kamradt, T., Schett, G., Hasenberg, A. & Gunzer, M. **A network of trans-cortical capillaries as mainstay for blood circulation in long bones**. *Nature Metabolism* (2019).
4. Schleier, L., Wiendl, M., Heidbreder, K., Binder, M.T., Atreya, R., Rath, T., Becker, E., Schulz-Kuhnt, A., Stahl, A., Schulze, L.L., Ullrich, K., Merz, S.F., Bornemann, L., Gunzer, M., Watson, A.J.M., Neufert, C., Atreya, I., Neurath, M.F. & Zundler, S. **Non-classical monocyte homing to the gut via alpha4beta7 integrin mediates macrophage-dependent intestinal wound healing**. *Gut* (2019).
5. Mitchell, D.R. **The evolution of eukaryotic cilia and flagella as motile and sensory organelles**. *Advances in experimental medicine and biology* **607**, 130-140 (2007).
6. Friedl, P. & Wolf, K. **Plasticity of cell migration: a multiscale tuning model**. *The Journal of Cell Biology* **188**, 11 (2010).
7. Franz, C.M., Jones, G.E. & Ridley, A.J. **Cell Migration in Development and Disease**. *Developmental Cell* **2**, 153-158 (2002).
8. Friedl, P. & Gilmour, D. **Collective cell migration in morphogenesis, regeneration and cancer**. *Nature Reviews Molecular Cell Biology* **10**, 445-457 (2009).
9. Gunzer, M. **Migration, cell-cell interaction and adhesion in the immune system**. *Ernst Schering Found Symp Proc*, 97-137 (2007).
10. Ley, K., Laudanna, C., Cybulsky, M.I. & Nourshargh, S. **Getting to the site of inflammation: the leukocyte adhesion cascade updated**. *Nature Reviews Immunology* **7**, 678-689 (2007).
11. Lauffenburger, D.A. & Horwitz, A.F. **Cell Migration: A Physically Integrated Molecular Process**. *Cell* **84**, 359-369 (1996).
12. Petrie, R.J., Doyle, A.D. & Yamada, K.M. **Random versus directionally persistent cell migration**. *Nature reviews. Molecular cell biology* **10**, 538-549 (2009).
13. Alblazi, K.M. & Siar, C.H. **Cellular protrusions--lamellipodia, filopodia, invadopodia and podosomes--and their roles in progression of orofacial tumours: current understanding**. *Asian Pac J Cancer Prev* **16**, 2187-2191 (2015).
14. Mattila, P.K. & Lappalainen, P. **Filopodia: molecular architecture and cellular functions**. *Nature Reviews Molecular Cell Biology* **9**, 446-454 (2008).
15. Devreotes, P. & Janetopoulos, C. **Eukaryotic chemotaxis: distinctions between directional sensing and polarization**. *J Biol Chem* **278**, 20445-20448 (2003).
16. McCarthy, J.B. & Furcht, L.T. **Laminin and fibronectin promote the haptotactic migration of B16 mouse melanoma cells in vitro**. *The Journal of Cell Biology* **98**, 1474 (1984).
17. Park, J., Kim, D.-H. & Levchenko, A. **Topotaxis: A New Mechanism of Directed Cell Migration in Topographic ECM Gradients**. *Biophysical Journal* **114**, 1257-1263 (2018).
18. Mycielska, M.E. & Djamgoz, M.B.A. **Cellular mechanisms of direct-current electric field effects: galvanotaxis and metastatic disease**. *Journal of Cell Science* **117**, 1631 (2004).
19. Krummel, M.F., Bartumeus, F. & Gérard, A. **T cell migration, search strategies and mechanisms**. *Nature reviews. Immunology* **16**, 193-201 (2016).

20. Barros-Becker, F., Lam, P.Y., Fisher, R. & Huttenlocher, A. **Live imaging reveals distinct modes of neutrophil and macrophage migration within interstitial tissues**. *J Cell Sci* **130**, 3801-3808 (2017).
21. Szczur, K., Xu, H., Atkinson, S., Zheng, Y. & Filippi, M.-D. **Rho GTPase CDC42 regulates directionality and random movement via distinct MAPK pathways in neutrophils**. *Blood* **108**, 4205 (2006).
22. Beutler, B. **Innate immunity: an overview**. *Molecular Immunology* **40**, 845-859 (2004).
23. Gallo, R.L. & Nizet, V. **Innate barriers against infection and associated disorders**. *Drug Discov Today Dis Mech* **5**, 145-152 (2008).
24. Charles A. Janeway, J. & Medzhitov, R. **Innate Immune Recognition**. *Annual Review of Immunology* **20**, 197-216 (2002).
25. Akira, S., Uematsu, S. & Takeuchi, O. **Pathogen recognition and innate immunity**. *Cell* **124**, 783-801 (2006).
26. O'Shea, J.J., Gadina, M. & Siegel, R.M. 9 - Cytokines and Cytokine Receptors. In: Rich, R.R. *et al.* (eds). *Clinical Immunology (Fifth Edition)*. Content Repository Only!: London, 2019, pp 127-155.e121.
27. Turner, M.D., Nedjai, B., Hurst, T. & Pennington, D.J. **Cytokines and chemokines: At the crossroads of cell signalling and inflammatory disease**. *Biochimica et Biophysica Acta (BBA) - Molecular Cell Research* **1843**, 2563-2582 (2014).
28. Kopitar-Jerala, N. **The Role of Interferons in Inflammation and Inflammasome Activation**. *Frontiers in immunology* **8**, 873-873 (2017).
29. Lieschke, G.J., Grail, D., Hodgson, G., Metcalf, D., Stanley, E., Cheers, C., Fowler, K.J., Basu, S., Zhan, Y.F. & Dunn, A.R. **Mice lacking granulocyte colony-stimulating factor have chronic neutropenia, granulocyte and macrophage progenitor cell deficiency, and impaired neutrophil mobilization**. *Blood* **84**, 1737-1746 (1994).
30. Burgess, A.W., Camakaris, J. & Metcalf, D. **Purification and properties of colony-stimulating factor from mouse lung-conditioned medium**. *Journal of Biological Chemistry* **252**, 1998-2003 (1977).
31. Griffith, J.W., Sokol, C.L. & Luster, A.D. **Chemokines and Chemokine Receptors: Positioning Cells for Host Defense and Immunity**. *Annual Review of Immunology* **32**, 659-702 (2014).
32. de Oliveira, S., Reyes-Aldasoro, C.C., Candel, S., Renshaw, S.A., Mulero, V. & Calado, A. **Cxcl8 (IL-8) mediates neutrophil recruitment and behavior in the zebrafish inflammatory response**. *Journal of immunology (Baltimore, Md. : 1950)* **190**, 4349-4359 (2013).
33. Alam, R., Stafford, S., Forsythe, P., Harrison, R., Faubion, D., Lett-Brown, M.A. & Grant, J.A. **RANTES is a chemotactic and activating factor for human eosinophils**. *The Journal of Immunology* **150**, 3442-3448 (1993).
34. Kawai, T., Seki, M., Hiromatsu, K., Eastcott, J.W., Watts, G.F.M., Sugai, M., Smith, D.J., Porcelli, S.A. & Taubman, M.A. **Selective Diapedesis of Th1 Cells Induced by Endothelial Cell RANTES**. *The Journal of Immunology* **163**, 3269-3278 (1999).
35. Rabinovitch, M. **Professional and non-professional phagocytes: an introduction**. *Trends in Cell Biology* **5**, 85-87 (1995).
36. Jantsch, J., Binger, K.J., Müller, D.N. & Titze, J. **Macrophages in homeostatic immune function**. *Front Physiol* **5**, 146-146 (2014).
37. Mayadas, T.N., Cullere, X. & Lowell, C.A. **The multifaceted functions of neutrophils**. *Annu Rev Pathol* **9**, 181-218 (2014).
38. Patente, T.A., Pinho, M.P., Oliveira, A.A., Evangelista, G.C.M., Bergami-Santos, P.C. & Barbuto, J.A.M. **Human Dendritic Cells: Their Heterogeneity and Clinical Application Potential in Cancer Immunotherapy**. *Frontiers in Immunology* **9** (2019).
39. Kay, A.B. **Paul Ehrlich and the Early History of Granulocytes**. *Microbiology Spectrum* **4** (2016).
40. Carvalho, L.O., Aquino, E.N., Neves, A.C.D. & Fontes, W. **The Neutrophil Nucleus and Its Role in Neutrophilic Function**. *Journal of Cellular Biochemistry* **116**, 1831-1836 (2015).
41. Gunzer, M. **Traps and hyper inflammation - new ways that neutrophils promote or hinder survival**. *Br J Haematol* **164**, 189-199 (2014).
42. Hidalgo, A., Chilvers, E.R., Summers, C. & Koenderman, L. **The Neutrophil Life Cycle**. *Trends in Immunology* **40**, 584-597 (2019).

43. Saverymuttu, S.H., Peters, A.M., Keshavarzian, A., Reavy, H.J. & Lavender, J.P. **The kinetics of 111Indium distribution following injection of 111Indium labelled autologous granulocytes in man**. *British Journal of Haematology* **61**, 675-685 (1985).
44. Szczepura, K.R., Ruparelia, P., Solanki, C.K., Balan, K., Newbold, P., Summers, C., Chilvers, E.R. & Peters, A.M. **Measuring whole-body neutrophil redistribution using a dedicated whole-body counter and ultra-low doses of 111Indium**. *European Journal of Clinical Investigation* **41**, 77-83 (2011).
45. Shi, J., Gilbert, G.E., Kokubo, Y. & Ohashi, T. **Role of the liver in regulating numbers of circulating neutrophils**. *Blood* **98**, 1226-1230 (2001).
46. Davis, B.P. & Rothenberg, M.E. **Eosinophils and cancer**. *Cancer Immunol Res* **2**, 1-8 (2014).
47. Kolaczkowska, E. & Kubes, P. **Neutrophil recruitment and function in health and inflammation**. *Nat Rev Immunol* **13**, 159-175 (2013).
48. Smith, W.B., Gamble, J.R., Clark-Lewis, I. & Vadas, M.A. **Interleukin-8 induces neutrophil transendothelial migration**. *Immunology* **72**, 65-72 (1991).
49. Kay, A.B., Stechschulte, D.J. & Austen, K.F. **AN EOSINOPHIL LEUKOCYTE CHEMOTACTIC FACTOR OF ANAPHYLAXIS**. *The Journal of Experimental Medicine* **133**, 602-619 (1971).
50. Resnick, M.B. & Weller, P.F. **Mechanisms of Eosinophil Recruitment**. *American Journal of Respiratory Cell and Molecular Biology* **8**, 349-355 (1993).
51. Geering, B., Stoeckle, C., Conus, S. & Simon, H.U. **Living and dying for inflammation: neutrophils, eosinophils, basophils**. *Trends Immunol* **34**, 398-409 (2013).
52. Wang, J. **Neutrophils in tissue injury and repair**. *Cell Tissue Res* **371**, 531-539 (2018).
53. Dancey, J.T., Deubelbeiss, K.A., Harker, L.A. & Finch, C.A. **Neutrophil kinetics in man**. *J Clin Invest* **58**, 705-715 (1976).
54. Görgens, A., Radtke, S., Möllmann, M., Cross, M., Dürig, J., Horn, Peter A. & Giebel, B. **Revision of the Human Hematopoietic Tree: Granulocyte Subtypes Derive from Distinct Hematopoietic Lineages**. *Cell Reports* **3**, 1539-1552 (2013).
55. Lawrence, S.M., Corriden, R. & Nizet, V. **The Ontogeny of a Neutrophil: Mechanisms of Granulopoiesis and Homeostasis**. *Microbiology and Molecular Biology Reviews* **82**, e00057-00017 (2018).
56. Pinho, S. & Frenette, P.S. **Haematopoietic stem cell activity and interactions with the niche**. *Nature Reviews Molecular Cell Biology* **20**, 303-320 (2019).
57. Lund-Johansen, F. & Terstappen, L.W.M.M. **Differential surface expression of cell adhesion molecules during granulocyte maturation**. *Journal of Leukocyte Biology* **54**, 47-55 (1993).
58. Elghetany, M.T., Ge, Y., Patel, J., Martinez, J. & Uhrova, H. **Flow cytometric study of neutrophilic granulopoiesis in normal bone marrow using an expanded panel of antibodies: Correlation with morphologic assessments**. *Journal of Clinical Laboratory Analysis* **18**, 36-41 (2004).
59. Allen, C.A., Broom, M.F. & Chadwick, V.S. **Flow cytometry analysis of the expression of neutrophil FMLP receptors**. *Journal of Immunological Methods* **149**, 159-164 (1992).
60. Hu, N., Westra, J., Rutgers, A., Doornbos-Van der Meer, B., Huitema, M.G., Stegeman, C.A., Abdulahad, W.H., Satchell, S.C., Mathieson, P.W., Heeringa, P. & Kallenberg, C.G.M. **Decreased CXCR1 and CXCR2 expression on neutrophils in anti-neutrophil cytoplasmic autoantibody-associated vasculitides potentially increases neutrophil adhesion and impairs migration**. *Arthritis Res Ther* **13**, R201-R201 (2011).
61. Springer, T.A. **Adhesion receptors of the immune system**. *Nature* **346**, 425-434 (1990).
62. Skubitz, K.M., Campbell, K.D. & Skubitz, A.P.N. **CD66a, CD66b, CD66c, and CD66d each Independently stimulate neutrophils**. *Journal of Leukocyte Biology* **60**, 106-117 (1996).
63. Torsteinsdóttir, Arvidson, Hällgren & Håkansson. **Enhanced Expression of Integrins and CD66b on Peripheral Blood Neutrophils and Eosinophils in Patients with Rheumatoid Arthritis, and the Effect of Glucocorticoids**. *Scandinavian Journal of Immunology* **50**, 433-439 (1999).
64. Jung, T.M. & Dailey, M.O. **Rapid modulation of homing receptors (gp90MEL-14) induced by activators of protein kinase C. Receptor shedding due to accelerated proteolytic cleavage at the cell surface**. *The Journal of Immunology* **144**, 3130-3136 (1990).
65. Hasenberg, A., Hasenberg, M., Mann, L., Neumann, F., Borkenstein, L., Stecher, M., Kraus, A., Engel, D.R., Klingberg, A., Seddigh, P., Abdullah, Z., Klebow, S., Engelmann, S., Reinhold, A.,

Brandau, S., Seeling, M., Waisman, A., Schraven, B., Gothert, J.R., Nimmerjahn, F. & Gunzer, M. **Catchup: a mouse model for imaging-based tracking and modulation of neutrophil granulocytes**. *Nat Methods* **12**, 445-452 (2015).

66. Wang, J.-X., Bair, A.M., King, S.L., Shnayder, R., Huang, Y.-F., Shieh, C.-C., Soberman, R.J., Fuhlbrigge, R.C. & Nigrovic, P.A. **Ly6G ligation blocks recruitment of neutrophils via a β2-integrin–dependent mechanism**. *Blood* **120**, 1489-1498 (2012).
67. Rosales, C. **Neutrophil: A Cell with Many Roles in Inflammation or Several Cell Types?** *Front Physiol* **9**, 113-113 (2018).
68. Brinkmann, V., Reichard, U., Goosmann, C., Fauler, B., Uhlemann, Y., Weiss, D.S., Weinrauch, Y. & Zychlinsky, A. **Neutrophil Extracellular Traps Kill Bacteria**. *Science* **303**, 1532-1535 (2004).
69. Keshari, R.S., Jyoti, A., Kumar, S., Dubey, M., Verma, A., Srinag, B.S., Krishnamurthy, H., Barthwal, M.K. & Dikshit, M. **Neutrophil extracellular traps contain mitochondrial as well as nuclear DNA and exhibit inflammatory potential**. *Cytometry Part A* **81A**, 238-247 (2012).
70. Coffelt, S.B., Wellenstein, M.D. & de Visser, K.E. **Neutrophils in cancer: neutral no more**. *Nature Reviews Cancer* **16**, 431 (2016).
71. Schmidt, H., Bastholt, L., Geertsen, P., Christensen, I.J., Larsen, S., Gehl, J. & von der Maase, H. **Elevated neutrophil and monocyte counts in peripheral blood are associated with poor survival in patients with metastatic melanoma: a prognostic model**. *British journal of cancer* **93**, 273-278 (2005).
72. Sionov, R.V., Fridlender, Z.G. & Granot, Z. **The Multifaceted Roles Neutrophils Play in the Tumor Microenvironment**. *Cancer Microenviron* **8**, 125-158 (2015).
73. Yan, J., Kloecker, G., Fleming, C., Bousamra, M., Hansen, R., Hu, X., Ding, C., Cai, Y., Xiang, D., Donninger, H., Eaton, J.W. & Clark, G.J. **Human polymorphonuclear neutrophils specifically recognize and kill cancerous cells**. *OncoImmunology* **3**, e950163 (2014).
74. Blaisdell, A., Crequer, A., Columbus, D., Daikoku, T., Mittal, K., Dey, S.K. & Erlebacher, A. **Neutrophils Oppose Uterine Epithelial Carcinogenesis via Debridement of Hypoxic Tumor Cells**. *Cancer Cell* **28**, 785-799 (2015).
75. Uhm, T.G., Kim, B.S. & Chung, I.Y. **Eosinophil development, regulation of eosinophil-specific genes, and role of eosinophils in the pathogenesis of asthma**. *Allergy Asthma Immunol Res* **4**, 68-79 (2012).
76. Klion, A.D. & Nutman, T.B. **The role of eosinophils in host defense against helminth parasites**. *Journal of Allergy and Clinical Immunology* **113**, 30-37 (2004).
77. Rothenberg, M.E. & Hogan, S.P. **The eosinophil**. *Annu Rev Immunol* **24**, 147-174 (2006).
78. Ponath, P.D., Qin, S., Post, T.W., Wang, J., Wu, L., Gerard, N.P., Newman, W., Gerard, C. & Mackay, C.R. **Molecular cloning and characterization of a human eotaxin receptor expressed selectively on eosinophils**. *The Journal of Experimental Medicine* **183**, 2437-2448 (1996).
79. Floyd, H., Ni, J., Cornish, A.L., Zeng, Z., Liu, D., Carter, K.C., Steel, J. & Crocker, P.R. **Siglec-8: A NOVEL EOSINOPHIL-SPECIFIC MEMBER OF THE IMMUNOGLOBULIN SUPERFAMILY**. *Journal of Biological Chemistry* **275**, 861-866 (2000).
80. Johansson, M.W. **Activation states of blood eosinophils in asthma**. *Clinical & Experimental Allergy* **44**, 482-498 (2014).
81. Matsumoto, K., Appiah-Pippim, J., Schleimer, R.P., Bickel, C.A., Beck, L.A. & Bochner, B.S. **CD44 and CD69 Represent Different Types of Cell-surface Activation Markers for Human Eosinophils**. *American Journal of Respiratory Cell and Molecular Biology* **18**, 860-866 (1998).
82. Baaten, B.J., Li, C.-R. & Bradley, L.M. **Multifaceted regulation of T cells by CD44**. *Commun Integr Biol* **3**, 508-512 (2010).
83. Ziegler, S.F., Ramsdell, F. & Alderson, M.R. **The activation antigen CD69**. *STEM CELLS* **12**, 456-465 (1994).
84. Varricchi, G., Galdiero, M.R., Loffredo, S., Lucarini, V., Marone, G., Mattei, F., Marone, G. & Schiavoni, G. **Eosinophils: The unsung heroes in cancer?** *Oncoimmunology* **7**, e1393134 (2018).
85. Sakkal, S., Miller, S., Apostolopoulos, V. & Nurgali, K. **Eosinophils in Cancer: Favourable or Unfavourable?** *Curr Med Chem* **23**, 650-666 (2016).

86. Carretero, R., Sektioglu, I.M., Garbi, N., Salgado, O.C., Beckhove, P. & Hammerling, G.J. **Eosinophils orchestrate cancer rejection by normalizing tumor vessels and enhancing infiltration of CD8(+) T cells**. *Nat Immunol* **16**, 609-617 (2015).
87. Mattes, J., Hulett, M., Xie, W., Hogan, S., Rothenberg, M.E., Foster, P. & Parish, C. **Immunotherapy of cytotoxic T cell-resistant tumors by T helper 2 cells: an eotaxin and STAT6-dependent process**. *The Journal of experimental medicine* **197**, 387-393 (2003).
88. Cooper, M.D. & Alder, M.N. **The Evolution of Adaptive Immune Systems**. *Cell* **124**, 815-822 (2006).
89. Bonilla, F.A. & Oettgen, H.C. **Adaptive immunity**. *Journal of Allergy and Clinical Immunology* **125**, S33-S40 (2010).
90. Takahama, Y. **Journey through the thymus: stromal guides for T-cell development and selection**. *Nature Reviews Immunology* **6**, 127-135 (2006).
91. Hoffman, W., Lakkis, F.G. & Chalasani, G. **B Cells, Antibodies, and More**. *Clin J Am Soc Nephrol* **11**, 137-154 (2016).
92. Alcover, A., Alarcón, B. & Bartolo, V.D. **Cell Biology of T Cell Receptor Expression and Regulation**. *Annual Review of Immunology* **36**, 103-125 (2018).
93. Takaba, H. & Takayanagi, H. **The Mechanisms of T Cell Selection in the Thymus**. *Trends in Immunology* **38**, 805-816 (2017).
94. Surh, C.D. & Sprent, J. **Homeostasis of Naive and Memory T Cells**. *Immunity* **29**, 848-862 (2008).
95. den Braber, I., Mugwagwa, T., Vrisekoop, N., Westera, L., Mögling, R., Bregje de Boer, A., Willems, N., Schrijver, Elise H.R., Spierenburg, G., Gaiser, K., Mul, E., Otto, Sigrid A., Ruiter, An F.C., Ackermans, Mariette T., Miedema, F., Borghans, José A.M., de Boer, Rob J. & Tesselaar, K. **Maintenance of Peripheral Naive T Cells Is Sustained by Thymus Output in Mice but Not Humans**. *Immunity* **36**, 288-297 (2012).
96. Vrisekoop, N., den Braber, I., de Boer, A.B., Ruiter, A.F.C., Ackermans, M.T., van der Crabben, S.N., Schrijver, E.H.R., Spierenburg, G., Sauerwein, H.P., Hazenberg, M.D., de Boer, R.J., Miedema, F., Borghans, J.A.M. & Tesselaar, K. **Sparse production but preferential incorporation of recently produced naïve T cells in the human peripheral pool**. *Proceedings of the National Academy of Sciences* **105**, 6115-6120 (2008).
97. Kumar, B.V., Connors, T.J. & Farber, D.L. **Human T Cell Development, Localization, and Function throughout Life**. *Immunity* **48**, 202-213 (2018).
98. Reinherz, E.L. & Schlossman, S.F. **The differentiation and function of human T lymphocytes**. *Cell* **19**, 821-827 (1980).
99. Sprent, J. **Antigen-Presenting Cells: Professionals and amateurs**. *Current Biology* **5**, 1095-1097 (1995).
100. Luckheeram, R.V., Zhou, R., Verma, A.D. & Xia, B. **$CD4^+$T cells: differentiation and functions**. *Clin Dev Immunol* **2012**, 925135-925135 (2012).
101. Rock, K.L., Reits, E. & Neefjes, J. **Present Yourself! By MHC Class I and MHC Class II Molecules**. *Trends in immunology* **37**, 724-737 (2016).
102. Slifka, M.K. & Whitton, J.L. **Antigen-Specific Regulation of T Cell–Mediated Cytokine Production**. *Immunity* **12**, 451-457 (2000).
103. Zhang, N. & Bevan, M.J. **CD8(+) T cells: foot soldiers of the immune system**. *Immunity* **35**, 161-168 (2011).
104. Nakanishi, Y., Lu, B., Gerard, C. & Iwasaki, A. **CD8+ T lymphocyte mobilization to virus-infected tissue requires CD4+ T-cell help**. *Nature* **462**, 510-513 (2009).
105. Palmer, E.M., Holbrook, B.C., Arimilli, S., Parks, G.D. & Alexander-Miller, M.A. **IFNγ-producing, virus-specific CD8+ effector cells acquire the ability to produce IL-10 as a result of entry into the infected lung environment**. *Virology* **404**, 225-230 (2010).
106. Sprent, J. & Surh, C.D. **T Cell Memory**. *Annual Review of Immunology* **20**, 551-579 (2002).
107. Samji, T. & Khanna, K.M. **Understanding memory CD8(+) T cells**. *Immunology letters* **185**, 32-39 (2017).
108. Semerad, C.L., Liu, F., Gregory, A.D., Stumpf, K. & Link, D.C. **G-CSF Is an Essential Regulator of Neutrophil Trafficking from the Bone Marrow to the Blood**. *Immunity* **17**, 413-423 (2002).
109. Summers, C., Rankin, S.M., Condliffe, A.M., Singh, N., Peters, A.M. & Chilvers, E.R. **Neutrophil kinetics in health and disease**. *Trends Immunol* **31**, 318-324 (2010).

110. Kohler, A., De Filippo, K., Hasenberg, M., van den Brandt, C., Nye, E., Hosking, M.P., Lane, T.E., Mann, L., Ransohoff, R.M., Hauser, A.E., Winter, O., Schraven, B., Geiger, H., Hogg, N. & Gunzer, M. **G-CSF-mediated thrombopoietin release triggers neutrophil motility and mobilization from bone marrow via induction of Cxcr2 ligands**. *Blood* **117**, 4349-4357 (2011).
111. Burdon, P.C.E., Martin, C. & Rankin, S.M. **Migration across the sinusoidal endothelium regulates neutrophil mobilization in response to ELR + CXC chemokines**. *British Journal of Haematology* **142**, 100-108 (2008).
112. McEver, R.P. & Cummings, R.D. **Role of PSGL-1 binding to selectins in leukocyte recruitment**. *J Clin Invest* **100**, S97-103 (1997).
113. Hidalgo, A., Peired, A.J., Wild, M., Vestweber, D. & Frenette, P.S. **Complete identification of E-selectin ligands on neutrophils reveals distinct functions of PSGL-1, ESL-1, and CD44**. *Immunity* **26**, 477-489 (2007).
114. Eriksson, E.E., Xie, X., Werr, J., Thoren, P. & Lindbom, L. **Importance of primary capture and L-selectin-dependent secondary capture in leukocyte accumulation in inflammation and atherosclerosis in vivo**. *The Journal of experimental medicine* **194**, 205-218 (2001).
115. Campbell, J.J., Hedrick, J., Zlotnik, A., Siani, M.A., Thompson, D.A. & Butcher, E.C. **Chemokines and the arrest of lymphocytes rolling under flow conditions**. *Science* **279**, 381-384 (1998).
116. Constantin, G., Majeed, M., Giagulli, C., Piccio, L., Kim, J.Y., Butcher, E.C. & Laudanna, C. **Chemokines trigger immediate beta2 integrin affinity and mobility changes: differential regulation and roles in lymphocyte arrest under flow**. *Immunity* **13**, 759-769 (2000).
117. Jenne, Craig N., Wong, Connie H.Y., Zemp, Franz J., McDonald, B., Rahman, Masmudur M., Forsyth, Peter A., McFadden, G. & Kubes, P. **Neutrophils Recruited to Sites of Infection Protect from Virus Challenge by Releasing Neutrophil Extracellular Traps**. *Cell Host & Microbe* **13**, 169-180 (2013).
118. Phillipson, M., Heit, B., Colarusso, P., Liu, L., Ballantyne, C.M. & Kubes, P. **Intraluminal crawling of neutrophils to emigration sites: a molecularly distinct process from adhesion in the recruitment cascade**. *J Exp Med* **203**, 2569-2575 (2006).
119. Phillipson, M., Kaur, J., Colarusso, P., Ballantyne, C.M. & Kubes, P. **Endothelial domes encapsulate adherent neutrophils and minimize increases in vascular permeability in paracellular and transcellular emigration**. *PLoS One* **3**, e1649 (2008).
120. Wang, S., Voisin, M.B., Larbi, K.Y., Dangerfield, J., Scheiermann, C., Tran, M., Maxwell, P.H., Sorokin, L. & Nourshargh, S. **Venular basement membranes contain specific matrix protein low expression regions that act as exit points for emigrating neutrophils**. *J Exp Med* **203**, 1519-1532 (2006).
121. Proebstl, D., Voisin, M.B., Woodfin, A., Whiteford, J., D'Acquisto, F., Jones, G.E., Rowe, D. & Nourshargh, S. **Pericytes support neutrophil subendothelial cell crawling and breaching of venular walls in vivo**. *J Exp Med* **209**, 1219-1234 (2012).
122. Foxman, E.F., Campbell, J.J. & Butcher, E.C. **Multistep navigation and the combinatorial control of leukocyte chemotaxis**. *J Cell Biol* **139**, 1349-1360 (1997).
123. Mempel, T.R., Henrickson, S.E. & von Andrian, U.H. **T-cell priming by dendritic cells in lymph nodes occurs in three distinct phases**. *Nature* **427**, 154-159 (2004).
124. Luster, A.D., Alon, R. & von Andrian, U.H. **Immune cell migration in inflammation: present and future therapeutic targets**. *Nat Immunol* **6**, 1182-1190 (2005).
125. Ulbrich, H., Eriksson, E.E. & Lindbom, L. **Leukocyte and endothelial cell adhesion molecules as targets for therapeutic interventions in inflammatory disease**. *Trends in Pharmacological Sciences* **24**, 640-647 (2003).
126. Targan, S.R., Feagan, B.G., Fedorak, R.N., Lashner, B.A., Panaccione, R., Present, D.H., Spehlmann, M.E., Rutgeerts, P.J., Tulassay, Z., Volfova, M., Wolf, D.C., Hernandez, C., Bornstein, J. & Sandborn, W.J. **Natalizumab for the Treatment of Active Crohn's Disease: Results of the ENCORE Trial**. *Gastroenterology* **132**, 1672-1683 (2007).
127. Miller, D.H., Khan, O.A., Sheremata, W.A., Blumhardt, L.D., Rice, G.P., Libonati, M.A., Willmer-Hulme, A.J., Dalton, C.M., Miszkiel, K.A. & O'Connor, P.W. **A controlled trial of natalizumab for relapsing multiple sclerosis**. *N Engl J Med* **348**, 15-23 (2003).

128. Van Assche, G., Van Ranst, M., Sciot, R., Dubois, B., Vermeire, S., Noman, M., Verbeeck, J., Geboes, K., Robberecht, W. & Rutgeerts, P. **Progressive multifocal leukoencephalopathy after natalizumab therapy for Crohn's disease**. *N Engl J Med* **353**, 362-368 (2005).
129. Alves-Filho, J.C., de Freitas, A., Spiller, F., Souto, F.O. & Cunha, F.Q. **The role of neutrophils in severe sepsis**. *Shock* **30 Suppl 1**, 3-9 (2008).
130. Sackmann, E.K., Berthier, E., Schwantes, E.A., Fichtinger, P.S., Evans, M.D., Dziadzio, L.L., Huttenlocher, A., Mathur, S.K. & Beebe, D.J. **Characterizing asthma from a drop of blood using neutrophil chemotaxis**. *Proc Natl Acad Sci U S A* **111**, 5813-5818 (2014).
131. Curran, F.T. & Keighley, M.R. **Neutrophil motility in Crohn's disease**. *Digestion* **48**, 104-112 (1991).
132. Dressel, A., Mirowska-Guzel, D., Gerlach, C. & Weber, F. **Migration of T-cell subsets in multiple sclerosis and the effect of interferon-beta1a**. *Acta Neurol Scand* **116**, 164-168 (2007).
133. Marsal, J. & Agace, W.W. **Targeting T-cell migration in inflammatory bowel disease**. *J Intern Med* **272**, 411-429 (2012).
134. Nitschke, C., Garin, A., Kosco-Vilbois, M. & Gunzer, M. **3D and 4D imaging of immune cells in vitro and in vivo**. *Histochemistry and Cell Biology* **130**, 1053-1062 (2008).
135. Adan, A., Alizada, G., Kiraz, Y., Baran, Y. & Nalbant, A. **Flow cytometry: basic principles and applications**. *Critical Reviews in Biotechnology* **37**, 163-176 (2017).
136. Brandtzaeg, P. **The increasing power of immunohistochemistry and immunocytochemistry**. *Journal of Immunological Methods* **216**, 49-67 (1998).
137. Klingberg, A., Hasenberg, A., Ludwig-Portugall, I., Medyukhina, A., Mann, L., Brenzel, A., Engel, D.R., Figge, M.T., Kurts, C. & Gunzer, M. **Fully Automated Evaluation of Total Glomerular Number and Capillary Tuft Size in Nephritic Kidneys Using Lightsheet Microscopy**. *J Am Soc Nephrol* **28**, 452-459 (2017).
138. Cai, R., Pan, C., Ghasemigharagoz, A., Todorov, M.I., Forstera, B., Zhao, S., Bhatia, H.S., Parra-Damas, A., Mrowka, L., Theodorou, D., Rempfler, M., Xavier, A.L.R., Kress, B.T., Benakis, C., Steinke, H., Liebscher, S., Bechmann, I., Liesz, A., Menze, B., Kerschensteiner, M., Nedergaard, M. & Erturk, A. **Panoptic imaging of transparent mice reveals whole-body neuronal projections and skull-meninges connections**. *Nat Neurosci* **22**, 317-327 (2019).
139. Richardson, D.S. & Lichtman, J.W. **Clarifying Tissue Clearing**. *Cell* **162**, 246-257 (2015).
140. Boyden, S. **THE CHEMOTACTIC EFFECT OF MIXTURES OF ANTIBODY AND ANTIGEN ON POLYMORPHONUCLEAR LEUCOCYTES**. *The Journal of Experimental Medicine* **115**, 453 (1962).
141. Albini, A., Iwamoto, Y., Kleinman, H.K., Martin, G.R., Aaronson, S.A., Kozlowski, J.M. & McEwan, R.N. **A rapid in vitro assay for quantitating the invasive potential of tumor cells**. *Cancer Res* **47**, 3239-3245 (1987).
142. Okada, T., Okuno, H. & Mitsui, Y. **A novel in vitro assay system for transendothelial tumor cell invasion: significance of E-selectin and α3 integrin in the transendothelial invasion by HT1080 fibrosarcoma cells**. *Clinical & Experimental Metastasis* **12**, 305-314 (1994).
143. Li, Y.-H. & Zhu, C. **A modified Boyden chamber assay for tumor cell transendothelial migration in vitro**. *Clinical & Experimental Metastasis* **17**, 423-429 (1999).
144. Albini, A. & Benelli, R. **The chemoinvasion assay: a method to assess tumor and endothelial cell invasion and its modulation**. *Nature Protocols* **2**, 504-511 (2007).
145. Cahalan, M.D., Parker, I., Wei, S.H. & Miller, M.J. **Two-photon tissue imaging: seeing the immune system in a fresh light**. *Nat Rev Immunol* **2**, 872-880 (2002).
146. Li, J.L., Goh, C.C., Keeble, J.L., Qin, J.S., Roediger, B., Jain, R., Wang, Y., Chew, W.K., Weninger, W. & Ng, L.G. **Intravital multiphoton imaging of immune responses in the mouse ear skin**. *Nature Protocols* **7**, 221-234 (2012).
147. Tabuchi, A., Mertens, M., Kuppe, H., Pries, A.R. & Kuebler, W.M. **Intravital microscopy of the murine pulmonary microcirculation**. *J Appl Physiol (1985)* **104**, 338-346 (2008).
148. Grutzendler, J., Kasthuri, N. & Gan, W.-B. **Long-term dendritic spine stability in the adult cortex**. *Nature* **420**, 812-816 (2002).
149. Llewellyn, M.E., Barretto, R.P.J., Delp, S.L. & Schnitzer, M.J. **Minimally invasive high-speed imaging of sarcomere contractile dynamics in mice and humans**. *Nature* **454**, 784-788 (2008).

150. Fisher, D.T., Muhitch, J.B., Kim, M., Doyen, K.C., Bogner, P.N., Evans, S.S. & Skitzki, J.J. **Intraoperative intravital microscopy permits the study of human tumour vessels**. *Nature Communications* **7**, 10684 (2016).
151. Icha, J., Schmied, C., Sidhaye, J., Tomancak, P., Preibisch, S. & Norden, C. **Using Light Sheet Fluorescence Microscopy to Image Zebrafish Eye Development**. *Journal of visualized experiments : JoVE*, e53966-e53966 (2016).
152. Huisken, J., Swoger, J., Del Bene, F., Wittbrodt, J. & Stelzer, E.H.K. **Optical Sectioning Deep Inside Live Embryos by Selective Plane Illumination Microscopy**. *Science* **305**, 1007-1009 (2004).
153. Ashby, W.J. & Zijlstra, A. **Established and novel methods of interrogating two-dimensional cell migration**. *Integrative Biology* **4**, 1338-1350 (2012).
154. Reichardt, P., Gunzer, F. & Gunzer, M. Analyzing the Physicodynamics of Immune Cells in a Three-Dimensional Collagen Matrix. In: Fairchild, P.J. (ed). *Immunological Tolerance: Methods and Protocols*. Humana Press: Totowa, NJ, 2007, pp 253-269.
155. Montalban-Bravo, G. & Garcia-Manero, G. **Myelodysplastic syndromes: 2018 update on diagnosis, risk-stratification and management**. *Am J Hematol* **93**, 129-147 (2018).
156. Mohammad, A.A. **Myelodysplastic syndrome from theoretical review to clinical application view**. *Oncol Rev* **12**, 397-397 (2018).
157. Greenberg, P.L., Tuechler, H., Schanz, J., Sanz, G., Garcia-Manero, G., Sole, F., Bennett, J.M., Bowen, D., Fenaux, P., Dreyfus, F., Kantarjian, H., Kuendgen, A., Levis, A., Malcovati, L., Cazzola, M., Cermak, J., Fonatsch, C., Le Beau, M.M., Slovak, M.L., Krieger, O., Luebbert, M., Maciejewski, J., Magalhaes, S.M., Miyazaki, Y., Pfeilstocker, M., Sekeres, M., Sperr, W.R., Stauder, R., Tauro, S., Valent, P., Vallespi, T., van de Loosdrecht, A.A., Germing, U. & Haase, D. **Revised international prognostic scoring system for myelodysplastic syndromes**. *Blood* **120**, 2454-2465 (2012).
158. Jädersten, M., Malcovati, L., Dybedal, I., Giovanni Della Porta, M., Invernizzi, R., Montgomery, S.M., Pascutto, C., Porwit, A., Cazzola, M. & Hellström-Lindberg, E. **Erythropoietin and Granulocyte-Colony Stimulating Factor Treatment Associated With Improved Survival in Myelodysplastic Syndrome**. *Journal of Clinical Oncology* **26**, 3607-3613 (2008).
159. List, A., Dewald, G., Bennett, J., Giagounidis, A., Raza, A., Feldman, E., Powell, B., Greenberg, P., Thomas, D., Stone, R., Reeder, C., Wride, K., Patin, J., Schmidt, M., Zeldis, J. & Knight, R. **Lenalidomide in the Myelodysplastic Syndrome with Chromosome 5q Deletion**. *New England Journal of Medicine* **355**, 1456-1465 (2006).
160. Fenaux, P., Mufti, G.J., Hellstrom-Lindberg, E., Santini, V., Finelli, C., Giagounidis, A., Schoch, R., Gattermann, N., Sanz, G., List, A., Gore, S.D., Seymour, J.F., Bennett, J.M., Byrd, J., Backstrom, J., Zimmerman, L., McKenzie, D., Beach, C., Silverman, L.R. & International Vidaza High-Risk, M.D.S.S.S.G. **Efficacy of azacitidine compared with that of conventional care regimens in the treatment of higher-risk myelodysplastic syndromes: a randomised, open-label, phase III study**. *The Lancet. Oncology* **10**, 223-232 (2009).
161. Dao, K.H. & Tyner, J.W. **What's different about atypical CML and chronic neutrophilic leukemia?** *Hematology Am Soc Hematol Educ Program* **2015**, 264-271 (2015).
162. Arber, D.A., Orazi, A., Hasserjian, R., Thiele, J., Borowitz, M.J., Le Beau, M.M., Bloomfield, C.D., Cazzola, M. & Vardiman, J.W. **The 2016 revision to the World Health Organization classification of myeloid neoplasms and acute leukemia**. *Blood* **127**, 2391-2405 (2016).
163. Orazi, A. & Germing, U. **The myelodysplastic/myeloproliferative neoplasms: myeloproliferative diseases with dysplastic features**. *Leukemia* **22**, 1308-1319 (2008).
164. Vardiman, J., Bennett, J., Bain, B., Brunning, R. & Thiele, J. **Atypical chronic myeloid leukaemia, BCR-ABL1 negative**. *WHO classification of tumours of haematopoietic and lymphoid tissues. Lyon: IARC*, 80-81 (2008).
165. Maxson, J.E. & Tyner, J.W. **Genomics of chronic neutrophilic leukemia**. *Blood* **129**, 715-722 (2017).
166. Elliott, M.A. & Tefferi, A. **Chronic neutrophilic leukemia 2016: Update on diagnosis, molecular genetics, prognosis, and management**. *Am J Hematol* **91**, 341-349 (2016).
167. Maxson, J.E., Gotlib, J., Pollyea, D.A., Fleischman, A.G., Agarwal, A., Eide, C.A., Bottomly, D., Wilmot, B., McWeeney, S.K., Tognon, C.E., Pond, J.B., Collins, R.H., Goueli, B., Oh, S.T., Deininger, M.W., Chang, B.H., Loriaux, M.M., Druker, B.J. & Tyner, J.W. **Oncogenic CSF3R mutations in chronic neutrophilic leukemia and atypical CML**. *N Engl J Med* **368**, 1781-1790 (2013).

168. Dao, K.H., Solti, M.B., Maxson, J.E., Winton, E.F., Press, R.D., Druker, B.J. & Tyner, J.W. **Significant clinical response to JAK1/2 inhibition in a patient with CSF3R-T618I-positive atypical chronic myeloid leukemia**. *Leuk Res Rep* **3**, 67-69 (2014).
169. Gunawan, A.S., McLornan, D.P., Wilkins, B., Waghorn, K., Hoade, Y., Cross, N.C.P. & Harrison, C.N. **Ruxolitinib, a potent JAK1/JAK2 inhibitor, induces temporary reductions in the allelic burden of concurrent CSF3R mutations in chronic neutrophilic leukemia**. *Haematologica* **102**, e238-e240 (2017).
170. Gotlib, J. **How I treat atypical chronic myeloid leukemia**. *Blood* **129**, 838-845 (2017).
171. Bray, F., Ferlay, J., Soerjomataram, I., Siegel, R.L., Torre, L.A. & Jemal, A. **Global cancer statistics 2018: GLOBOCAN estimates of incidence and mortality worldwide for 36 cancers in 185 countries**. *CA: A Cancer Journal for Clinicians* **68**, 394-424 (2018).
172. Ali, Z., Yousaf, N. & Larkin, J. **Melanoma epidemiology, biology and prognosis**. *European Journal of Cancer Supplements* **11**, 81-91 (2013).
173. Leonardi, G.C., Falzone, L., Salemi, R., Zanghì, A., Spandidos, D.A., McCubrey, J.A., Candido, S. & Libra, M. **Cutaneous melanoma: From pathogenesis to therapy (Review)**. *International journal of oncology* **52**, 1071-1080 (2018).
174. Schadendorf, D., van Akkooi, A.C.J., Berking, C., Griewank, K.G., Gutzmer, R., Hauschild, A., Stang, A., Roesch, A. & Ugurel, S. **Melanoma**. *Lancet* **392**, 971-984 (2018).
175. Brenner, M. & Hearing, V.J. **The protective role of melanin against UV damage in human skin**. *Photochem Photobiol* **84**, 539-549 (2008).
176. Jimbow, K., Roth, S.I., Fitzpatrick, T.B. & Szabo, G. **Mitotic activity in non-neoplastic melanocytes in vivo as determined by histochemical, autoradiographic, and electron microscope studies**. *J Cell Biol* **66**, 663-670 (1975).
177. Miller, A.J. & Mihm, M.C. **Melanoma**. *New England Journal of Medicine* **355**, 51-65 (2006).
178. McCubrey, J.A., Steelman, L.S., Chappell, W.H., Abrams, S.L., Wong, E.W.T., Chang, F., Lehmann, B., Terrian, D.M., Milella, M., Tafuri, A., Stivala, F., Libra, M., Basecke, J., Evangelisti, C., Martelli, A.M. & Franklin, R.A. **Roles of the Raf/MEK/ERK pathway in cell growth, malignant transformation and drug resistance**. *Biochimica et Biophysica Acta (BBA) - Molecular Cell Research* **1773**, 1263-1284 (2007).
179. Davies, H., Bignell, G.R., Cox, C., Stephens, P., Edkins, S., Clegg, S., Teague, J., Woffendin, H., Garnett, M.J., Bottomley, W., Davis, N., Dicks, E., Ewing, R., Floyd, Y., Gray, K., Hall, S., Hawes, R., Hughes, J., Kosmidou, V., Menzies, A., Mould, C., Parker, A., Stevens, C., Watt, S., Hooper, S., Wilson, R., Jayatilake, H., Gusterson, B.A., Cooper, C., Shipley, J., Hargrave, D., Pritchard-Jones, K., Maitland, N., Chenevix-Trench, G., Riggins, G.J., Bigner, D.D., Palmieri, G., Cossu, A., Flanagan, A., Nicholson, A., Ho, J.W.C., Leung, S.Y., Yuen, S.T., Weber, B.L., Seigler, H.F., Darrow, T.L., Paterson, H., Marais, R., Marshall, C.J., Wooster, R., Stratton, M.R. & Futreal, P.A. **Mutations of the BRAF gene in human cancer**. *Nature* **417**, 949-954 (2002).
180. Katz, M., Amit, I. & Yarden, Y. **Regulation of MAPKs by growth factors and receptor tyrosine kinases**. *Biochim Biophys Acta* **1773**, 1161-1176 (2007).
181. Hsu, M.Y., Wheelock, M.J., Johnson, K.R. & Herlyn, M. **Shifts in cadherin profiles between human normal melanocytes and melanomas**. *J Investig Dermatol Symp Proc* **1**, 188-194 (1996).
182. Gershenwald, J.E., Scolyer, R.A., Hess, K.R., Sondak, V.K., Long, G.V., Ross, M.I., Lazar, A.J., Faries, M.B., Kirkwood, J.M., McArthur, G.A., Haydu, L.E., Eggermont, A.M.M., Flaherty, K.T., Balch, C.M., Thompson, J.F., for members of the American Joint Committee on Cancer Melanoma Expert, P., the International Melanoma, D. & Discovery, P. **Melanoma staging: Evidence-based changes in the American Joint Committee on Cancer eighth edition cancer staging manual**. *CA Cancer J Clin* **67**, 472-492 (2017).
183. Larkin, J., Ascierto, P.A., Dreno, B., Atkinson, V., Liszkay, G., Maio, M., Mandala, M., Demidov, L., Stroyakovskiy, D., Thomas, L., de la Cruz-Merino, L., Dutriaux, C., Garbe, C., Sovak, M.A., Chang, I., Choong, N., Hack, S.P., McArthur, G.A. & Ribas, A. **Combined vemurafenib and cobimetinib in BRAF-mutated melanoma**. *N Engl J Med* **371**, 1867-1876 (2014).
184. Long, G.V., Stroyakovskiy, D., Gogas, H., Levchenko, E., de Braud, F., Larkin, J., Garbe, C., Jouary, T., Hauschild, A., Grob, J.J., Chiarion Sileni, V., Lebbe, C., Mandala, M., Millward, M., Arance, A., Bondarenko, I., Haanen, J.B., Hansson, J., Utikal, J., Ferraresi, V., Kovalenko, N., Mohr, P., Probachai, V., Schadendorf, D., Nathan, P., Robert, C., Ribas, A., DeMarini, D.J., Irani, J.G., Casey, M., Ouellet, D., Martin, A.M., Le, N., Patel, K. & Flaherty, K. **Combined BRAF**

and MEK inhibition versus BRAF inhibition alone in melanoma. *N Engl J Med* **371**, 1877-1888 (2014).

185. Ayoub, N., Al-Shami, K. & Yaghan, R. **Immunotherapy for HER2-positive breast cancer: recent advances and combination therapeutic approaches**. *Breast Cancer: Targets and Therapy* **Volume 11**, 53-69 (2019).
186. Keir, M.E., Butte, M.J., Freeman, G.J. & Sharpe, A.H. **PD-1 and its ligands in tolerance and immunity**. *Annu Rev Immunol* **26**, 677-704 (2008).
187. Tivol, E.A., Borriello, F., Schweitzer, A.N., Lynch, W.P., Bluestone, J.A. & Sharpe, A.H. **Loss of CTLA-4 leads to massive lymphoproliferation and fatal multiorgan tissue destruction, revealing a critical negative regulatory role of CTLA-4**. *Immunity* **3**, 541-547 (1995).
188. Marengère, L.E.M., Waterhouse, P., Duncan, G.S., Mittrücker, H.-W., Feng, G.-S. & Mak, T.W. **Regulation of T Cell Receptor Signaling by Tyrosine Phosphatase SYP Association with CTLA-4**. *Science* **272**, 1170-1173 (1996).
189. Takahashi, T., Tagami, T., Yamazaki, S., Uede, T., Shimizu, J., Sakaguchi, N., Mak, T.W. & Sakaguchi, S. **Immunologic self-tolerance maintained by CD25(+)CD4(+) regulatory T cells constitutively expressing cytotoxic T lymphocyte-associated antigen 4**. *The Journal of experimental medicine* **192**, 303-310 (2000).
190. Myers, G. **Immune-related adverse events of immune checkpoint inhibitors: a brief review**. *Curr Oncol* **25**, 342-347 (2018).
191. Mozaffarian, D., Benjamin, E.J., Go, A.S., Arnett, D.K., Blaha, M.J., Cushman, M., Das, S.R., Ferranti, S.d., Després, J.-P., Fullerton, H.J., Howard, V.J., Huffman, M.D., Isasi, C.R., Jiménez, M.C., Judd, S.E., Kissela, B.M., Lichtman, J.H., Lisabeth, L.D., Liu, S., Mackey, R.H., Magid, D.J., McGuire, D.K., Mohler, E.R., Moy, C.S., Muntner, P., Mussolino, M.E., Nasir, K., Neumar, R.W., Nichol, G., Palaniappan, L., Pandey, D.K., Reeves, M.J., Rodriguez, C.J., Rosamond, W., Sorlie, P.D., Stein, J., Towfighi, A., Turan, T.N., Virani, S.S., Woo, D., Yeh, R.W. & Turner, M.B. **Heart Disease and Stroke Statistics—2016 Update**. *Circulation* **133**, e38-e360 (2016).
192. Anderson, J.L. & Morrow, D.A. **Acute Myocardial Infarction**. *New England Journal of Medicine* **376**, 2053-2064 (2017).
193. Hausenloy, D.J. & Yellon, D.M. **Myocardial ischemia-reperfusion injury: a neglected therapeutic target**. *J Clin Invest* **123**, 92-100 (2013).
194. Verma, S., Fedak, P.W., Weisel, R.D., Butany, J., Rao, V., Maitland, A., Li, R.K., Dhillon, B. & Yau, T.M. **Fundamentals of reperfusion injury for the clinical cardiologist**. *Circulation* **105**, 2332-2336 (2002).
195. Saleh, M. & Ambrose, J.A. **Understanding myocardial infarction**. *F1000Res* **7**, F1000 Faculty Rev-1378 (2018).
196. Rathore, V., Singh, N. & Mahat, R. **Risk Factors for Acute Myocardial Infarction: A Review**. *Eurasian Journal of Medical Investigation* **2**, 1-7 (2018).
197. Ibanez, B., James, S., Agewall, S., Antunes, M.J., Bucciarelli-Ducci, C., Bueno, H., Caforio, A.L.P., Crea, F., Goudevenos, J.A., Halvorsen, S., Hindricks, G., Kastrati, A., Lenzen, M.J., Prescott, E., Roffi, M., Valgimigli, M., Varenhorst, C., Vranckx, P., Widimský, P. & Group, E.S.D. **2017 ESC Guidelines for the management of acute myocardial infarction in patients presenting with ST-segment elevation: The Task Force for the management of acute myocardial infarction in patients presenting with ST-segment elevation of the European Society of Cardiology (ESC)**. *European Heart Journal* **39**, 119-177 (2017).
198. Yellon, D.M. & Hausenloy, D.J. **Myocardial reperfusion injury**. *N Engl J Med* **357**, 1121-1135 (2007).
199. Robbers, L.F., Eerenberg, E.S., Teunissen, P.F., Jansen, M.F., Hollander, M.R., Horrevoets, A.J., Knaapen, P., Nijveldt, R., Heymans, M.W., Levi, M.M., van Rossum, A.C., Niessen, H.W., Marcu, C.B., Beek, A.M. & van Royen, N. **Magnetic resonance imaging-defined areas of microvascular obstruction after acute myocardial infarction represent microvascular destruction and haemorrhage**. *Eur Heart J* **34**, 2346-2353 (2013).
200. Eltzschig, H.K. & Eckle, T. **Ischemia and reperfusion—from mechanism to translation**. *Nature Medicine* **17**, 1391-1401 (2011).
201. Li, J.M. & Shah, A.M. **Endothelial cell superoxide generation: regulation and relevance for cardiovascular pathophysiology**. *Am J Physiol Regul Integr Comp Physiol* **287**, R1014-1030 (2004).

202. Braunersreuther, V., Montecucco, F., Asrih, M., Pelli, G., Galan, K., Frias, M., Burger, F., Quindere, A.L., Montessuit, C., Krause, K.H., Mach, F. & Jaquet, V. **Role of NADPH oxidase isoforms NOX1, NOX2 and NOX4 in myocardial ischemia/reperfusion injury**. *J Mol Cell Cardiol* **64**, 99-107 (2013).
203. Shahzad, S., Hasan, A., Faizy, A.F., Mateen, S., Fatima, N. & Moin, S. **Elevated DNA Damage, Oxidative Stress, and Impaired Response Defense System Inflicted in Patients With Myocardial Infarction**. *Clin Appl Thromb Hemost* **24**, 780-789 (2018).
204. Nahrendorf, M., Swirski, F.K., Aikawa, E., Stangenberg, L., Wurdinger, T., Figueiredo, J.L., Libby, P., Weissleder, R. & Pittet, M.J. **The healing myocardium sequentially mobilizes two monocyte subsets with divergent and complementary functions**. *J Exp Med* **204**, 3037-3047 (2007).
205. Frangogiannis, N.G. **Regulation of the inflammatory response in cardiac repair**. *Circ Res* **110**, 159-173 (2012).
206. Puhl, S.-L. & Steffens, S. **Neutrophils in Post-myocardial Infarction Inflammation: Damage vs. Resolution?** *Frontiers in Cardiovascular Medicine* **6** (2019).
207. Horckmans, M., Ring, L., Duchene, J., Santovito, D., Schloss, M.J., Drechsler, M., Weber, C., Soehnlein, O. & Steffens, S. **Neutrophils orchestrate post-myocardial infarction healing by polarizing macrophages towards a reparative phenotype**. *Eur Heart J* **38**, 187-197 (2017).
208. Vasilyev, N., Williams, T., Brennan, M.L., Unzek, S., Zhou, X., Heinecke, J.W., Spitz, D.R., Topol, E.J., Hazen, S.L. & Penn, M.S. **Myeloperoxidase-generated oxidants modulate left ventricular remodeling but not infarct size after myocardial infarction**. *Circulation* **112**, 2812-2820 (2005).
209. Ali, M., Pulli, B., Courties, G., Tricot, B., Sebas, M., Iwamoto, Y., Hilgendorf, I., Schob, S., Dong, A., Zheng, W., Skoura, A., Kalgukar, A., Cortes, C., Ruggeri, R., Swirski, F.K., Nahrendorf, M., Buckbinder, L. & Chen, J.W. **Myeloperoxidase Inhibition Improves Ventricular Function and Remodeling After Experimental Myocardial Infarction**. *JACC Basic Transl Sci* **1**, 633-643 (2016).
210. Totzeck, M., Hendgen-Cotta, U.B., French, B.A. & Rassaf, T. **A practical approach to remote ischemic preconditioning and ischemic preconditioning against myocardial ischemia/reperfusion injury**. *J Biol Methods* **3** (2016).
211. Schindelin, J., Arganda-Carreras, I., Frise, E., Kaynig, V., Longair, M., Pietzsch, T., Preibisch, S., Rueden, C., Saalfeld, S., Schmid, B., Tinevez, J.-Y., White, D.J., Hartenstein, V., Eliceiri, K., Tomancak, P. & Cardona, A. **Fiji: an open-source platform for biological-image analysis**. *Nature Methods* **9**, 676 (2012).
212. Gangat, N., Patnaik, M.M. & Tefferi, A. **Myelodysplastic syndromes: Contemporary review and how we treat**. *Am J Hematol* **91**, 76-89 (2016).
213. Dao, K.T., Tyner, J.W. & Gotlib, J. **Recent Progress in Chronic Neutrophilic Leukemia and Atypical Chronic Myeloid Leukemia**. *Curr Hematol Malig Rep* **12**, 432-441 (2017).
214. Sung, L., Lange, B.J., Gerbing, R.B., Alonzo, T.A. & Feusner, J. **Microbiologically documented infections and infection-related mortality in children with acute myeloid leukemia**. *Blood* **110**, 3532 (2007).
215. D'Alessandro, M.P. & Bergmann, R.A. **Anatomy Atlases**. 1995 - 2019 [cited 16/09/2019] Available from: https://www.anatomyatlases.org/
216. Gustafson, M.P., Lin, Y., Maas, M.L., Van Keulen, V.P., Johnston, P.B., Peikert, T., Gastineau, D.A. & Dietz, A.B. **A method for identification and analysis of non-overlapping myeloid immunophenotypes in humans**. *PloS one* **10**, e0121546-e0121546 (2015).
217. van Grinsven, E., Textor, J., Hustin, L.S.P., Wolf, K., Koenderman, L. & Vrisekoop, N. **Immature Neutrophils Released in Acute Inflammation Exhibit Efficient Migration despite Incomplete Segmentation of the Nucleus**. *The Journal of Immunology*, ji1801255 (2018).
218. Drifte, G., Dunn-Siegrist, I., Tissières, P. & Pugin, J. **Innate Immune Functions of Immature Neutrophils in Patients With Sepsis and Severe Systemic Inflammatory Response Syndrome***. *Critical Care Medicine* **41**, 820-832 (2013).
219. Weyand, C.M. & Goronzy, J.J. **Aging of the Immune System. Mechanisms and Therapeutic Targets**. *Ann Am Thorac Soc* **13 Suppl 5**, S422-S428 (2016).

220. Machura, E., Mazur, B., Pieniazek, W. & Karczewska, K. **Expression of naive/memory (CD45RA/CD45RO) markers by peripheral blood CD4+ and CD8 + T cells in children with asthma**. *Arch Immunol Ther Exp (Warsz)* **56**, 55-62 (2008).
221. Förster, R., Davalos-Misslitz, A.C. & Rot, A. **CCR7 and its ligands: balancing immunity and tolerance**. *Nature Reviews Immunology* **8**, 362-371 (2008).
222. Frentsch, M., Stark, R., Matzmohr, N., Meier, S., Durlanik, S., Schulz, A.R., Stervbo, U., Jürchott, K., Gebhardt, F., Heine, G., Reuter, M.A., Betts, M.R., Busch, D. & Thiel, A. **CD40L expression permits CD8+ T cells to execute immunologic helper functions**. *Blood* **122**, 405 (2013).
223. Kishimoto, T., Jutila, M., Berg, E. & Butcher, E. **Neutrophil Mac-1 and MEL-14 adhesion proteins inversely regulated by chemotactic factors**. *Science* **245**, 1238-1241 (1989).
224. Marshall, H.T. & Djamgoz, M.B.A. **Immuno-Oncology: Emerging Targets and Combination Therapies**. *Front Oncol* **8**, 315 (2018).
225. Shen, M., Hu, P., Donskov, F., Wang, G., Liu, Q. & Du, J. **Tumor-Associated Neutrophils as a New Prognostic Factor in Cancer: A Systematic Review and Meta-Analysis**. *PLOS ONE* **9**, e98259 (2014).
226. Lugo-Hernandez, E., Squire, A., Hagemann, N., Brenzel, A., Sardari, M., Schlechter, J., Sanchez-Mendoza, E.H., Gunzer, M., Faissner, A. & Hermann, D.M. **3D visualization and quantification of microvessels in the whole ischemic mouse brain using solvent-based clearing and light sheet microscopy**. *Journal of Cerebral Blood Flow & Metabolism* **37**, 3355-3367 (2017).
227. Pollard, T.D. **Evolution of research on cellular motility over five decades**. *Biophys Rev* **10**, 1503-1508 (2018).
228. Stadtmann, A. & Zarbock, A. **CXCR2: From Bench to Bedside**. *Frontiers in immunology* **3**, 263-263 (2012).
229. Kuhlman, P., Moy, V.T., Lollo, B.A. & Brian, A.A. **The accessory function of murine intercellular adhesion molecule-1 in T lymphocyte activation. Contributions of adhesion and co-activation**. *The Journal of Immunology* **146**, 1773-1782 (1991).
230. Chen, T., Goldstein, J.S., O'Boyle, K., Whitman, M.C., Brunswick, M. & Kozlowski, S. **ICAM-1 co-stimulation has differential effects on the activation of CD4+ and CD8+ T cells**. *Eur J Immunol* **29**, 809-814 (1999).
231. Dubey, C., Croft, M. & Swain, S.L. **Costimulatory requirements of naive CD4+ T cells. ICAM-1 or B7-1 can costimulate naive CD4 T cell activation but both are required for optimum response**. *J Immunol* **155**, 45-57 (1995).
232. Damle, N.K., Klussman, K., Linsley, P.S. & Aruffo, A. **Differential costimulatory effects of adhesion molecules B7, ICAM-1, LFA-3, and VCAM-1 on resting and antigen-primed CD4+ T lymphocytes**. *J Immunol* **148**, 1985-1992 (1992).
233. Fang, Y. & Eglen, R.M. **Three-Dimensional Cell Cultures in Drug Discovery and Development**. *SLAS Discov* **22**, 456-472 (2017).
234. Driscoll, M.K. & Danuser, G. **Quantifying Modes of 3D Cell Migration**. *Trends in Cell Biology* **25**, 749-759 (2015).
235. Timm, M., Saaby, L., Moesby, L. & Hansen, E.W. **Considerations regarding use of solvents in in vitro cell based assays**. *Cytotechnology* **65**, 887-894 (2013).
236. Dahinden, C.A., Geiser, T., Brunner, T., von Tscharner, V., Caput, D., Ferrara, P., Minty, A. & Baggiolini, M. **Monocyte chemotactic protein 3 is a most effective basophil- and eosinophil-activating chemokine**. *The Journal of Experimental Medicine* **179**, 751-756 (1994).
237. Menzies-Gow, A., Ying, S., Sabroe, I., Stubbs, V.L., Soler, D., Williams, T.J. & Kay, A.B. **Eotaxin (CCL11) and Eotaxin-2 (CCL24) Induce Recruitment of Eosinophils, Basophils, Neutrophils, and Macrophages As Well As Features of Early- and Late-Phase Allergic Reactions Following Cutaneous Injection in Human Atopic and Nonatopic Volunteers**. *The Journal of Immunology* **169**, 2712-2718 (2002).
238. Slapničková, M., Volkova, V., Čepičková, M., Kobets, T., Šíma, M., Svobodová, M., Demant, P. & Lipoldová, M. **Gene-specific sex effects on eosinophil infiltration in leishmaniasis**. *Biol Sex Differ* **7**, 59-59 (2016).
239. Imaoka, M., Kishikawa, R., Shimoda, T. & Iwanaga, T. **Gender differences in eosinophilic airway inflammation in allergic and non-allergic asthma**. *European Respiratory Journal* **40**, P2334 (2012).

240. Zhao, H., Moarbes, V., Gaudreault, V., Shan, J., Aldossary, H., Cyr, L. & Fixman, E.D. **Sex Differences in IL-33-Induced STAT6-Dependent Type 2 Airway Inflammation**. *Frontiers in Immunology* **10** (2019).
241. Keselman, A. & Heller, N. **Estrogen Signaling Modulates Allergic Inflammation and Contributes to Sex Differences in Asthma**. *Frontiers in immunology* **6**, 568-568 (2015).
242. Lampinen, M., Backman, M., Winqvist, O., Rorsman, F., Rönnblom, A., Sangfelt, P. & Carlson, M. **Different regulation of eosinophil activity in Crohn's disease compared with ulcerative colitis**. *Journal of Leukocyte Biology* **84**, 1392-1399 (2008).
243. Poznansky, M.C., Olszak, I.T., Foxall, R., Evans, R.H., Luster, A.D. & Scadden, D.T. **Active movement of T cells away from a chemokine**. *Nature Medicine* **6**, 543-548 (2000).
244. Vianello, F., Papeta, N., Chen, T., Kraft, P., White, N., Hart, W.K., Kircher, M.F., Swart, E., Rhee, S., Palu, G., Irimia, D., Toner, M., Weissleder, R. & Poznansky, M.C. **Murine B16 melanomas expressing high levels of the chemokine stromal-derived factor-1/CXCL12 induce tumor-specific T cell chemorepulsion and escape from immune control**. *J Immunol* **176**, 2902-2914 (2006).
245. Mahnke, Y.D., Brodie, T.M., Sallusto, F., Roederer, M. & Lugli, E. **The who's who of T-cell differentiation: Human memory T-cell subsets**. *European Journal of Immunology* **43**, 2797-2809 (2013).
246. Büning, C., Krüger, K., Sieber, T., Schoeler, D. & Schriever, F. **Increased Expression of CD40 Ligand on Activated T Cells of Patients with Colon Cancer**. *Clinical Cancer Research* **8**, 1147-1151 (2002).
247. Li, M., Yao, D., Zeng, X., Kasakovski, D., Zhang, Y., Chen, S., Zha, X., Li, Y. & Xu, L. **Age related human T cell subset evolution and senescence**. *Immun Ageing* **16**, 24-24 (2019).
248. Schmidt, T., Zundorf, J., Gruger, T., Brandenburg, K., Reiners, A.L., Zinserling, J. & Schnitzler, N. **CD66b overexpression and homotypic aggregation of human peripheral blood neutrophils after activation by a gram-positive stimulus**. *J Leukoc Biol* **91**, 791-802 (2012).
249. Peiseler, M. & Kubes, P. **More friend than foe: the emerging role of neutrophils in tissue repair**. *J Clin Invest* **129**, 2629-2639 (2019).
250. Pereira, M.A., Sannomiya, P. & Leme, J.G. **Inhibition of leukocyte chemotaxis by factor in alloxan-induced diabetic rat plasma**. *Diabetes* **36**, 1307-1314 (1987).
251. Mastroianni, C.M., Lichtner, M., Mengoni, F., D'Agostino, C., Forcina, G., d'Ettorre, G., Santopadre, P. & Vullo, V. **Improvement in neutrophil and monocyte function during highly active antiretroviral treatment of HIV-1-infected patients**. *Aids* **13**, 883-890 (1999).
252. Tavares-Murta, B.M., Zaparoli, M., Ferreira, R.B., Silva-Vergara, M.L., B. Oliveira, C.H., Murta, E.F.C., Ferreira, S.H. & Cunha, F.Q. **Failure of neutrophil chemotactic function in septic patients***. *Critical Care Medicine* **30**, 1056-1061 (2002).
253. Sproston, N.R. & Ashworth, J.J. **Role of C-Reactive Protein at Sites of Inflammation and Infection**. *Frontiers in immunology* **9**, 754-754 (2018).
254. Zhong, W., Zen, Q., Tebo, J., Schlottmann, K., Coggeshall, M. & Mortensen, R.F. **Effect of Human C-Reactive Protein on Chemokine and Chemotactic Factor-Induced Neutrophil Chemotaxis and Signaling**. *The Journal of Immunology* **161**, 2533 (1998).
255. Kew, R.R., Hyers, T.M. & Webster, R.O. **Human C-reactive protein inhibits neutrophil chemotaxis in vitro: possible implications for the adult respiratory distress syndrome**. *J Lab Clin Med* **115**, 339-345 (1990).
256. de Oliveira, S., Rosowski, E.E. & Huttenlocher, A. **Neutrophil migration in infection and wound repair: going forward in reverse**. *Nat Rev Immunol* **16**, 378-391 (2016).
257. Kobayashi, Y. **Neutrophil infiltration and chemokines**. *Critical reviews in immunology* **26**, 307-316 (2006).
258. Rudolph, J., Heine, A., Quast, T., Kolanus, W., Trebicka, J., Brossart, P. & Wolf, D. **The JAK inhibitor ruxolitinib impairs dendritic cell migration via off-target inhibition of ROCK**. *Leukemia* **30**, 2119 (2016).
259. Machado-Neto, J.A., de Melo Campos, P., Favaro, P., Lazarini, M., da Silva Santos Duarte, A., Lorand-Metze, I., Costa, F.F., Saad, S.T.O. & Traina, F. **Stathmin 1 inhibition amplifies ruxolitinib-induced apoptosis in JAK2V617F cells**. *Oncotarget* **6**, 29573-29584 (2015).
260. Pak, J., Tucci, V.T., Vincent, A.L., Sandin, R.L. & Greene, J.N. **Mucormycosis in immunochallenged patients**. *J Emerg Trauma Shock* **1**, 106-113 (2008).

261. Walunas, T.L., Lenschow, D.J., Bakker, C.Y., Linsley, P.S., Freeman, G.J., Green, J.M., Thompson, C.B. & Bluestone, J.A. **CTLA-4 can function as a negative regulator of T cell activation**. *Immunity* **1**, 405-413 (1994).
262. Nishimura, H., Nose, M., Hiai, H., Minato, N. & Honjo, T. **Development of Lupus-like Autoimmune Diseases by Disruption of the PD-1 Gene Encoding an ITIM Motif-Carrying Immunoreceptor**. *Immunity* **11**, 141-151 (1999).
263. Hodi, F.S., O'Day, S.J., McDermott, D.F., Weber, R.W., Sosman, J.A., Haanen, J.B., Gonzalez, R., Robert, C., Schadendorf, D., Hassel, J.C., Akerley, W., van den Eertwegh, A.J., Lutzky, J., Lorigan, P., Vaubel, J.M., Linette, G.P., Hogg, D., Ottensmeier, C.H., Lebbe, C., Peschel, C., Quirt, I., Clark, J.I., Wolchok, J.D., Weber, J.S., Tian, J., Yellin, M.J., Nichol, G.M., Hoos, A. & Urba, W.J. **Improved survival with ipilimumab in patients with metastatic melanoma**. *N Engl J Med* **363**, 711-723 (2010).
264. Robert, C., Thomas, L., Bondarenko, I., O'Day, S., Weber, J., Garbe, C., Lebbe, C., Baurain, J.F., Testori, A., Grob, J.J., Davidson, N., Richards, J., Maio, M., Hauschild, A., Miller, W.H., Jr., Gascon, P., Lotem, M., Harmankaya, K., Ibrahim, R., Francis, S., Chen, T.T., Humphrey, R., Hoos, A. & Wolchok, J.D. **Ipilimumab plus dacarbazine for previously untreated metastatic melanoma**. *N Engl J Med* **364**, 2517-2526 (2011).
265. Brahmer, J.R., Drake, C.G., Wollner, I., Powderly, J.D., Picus, J., Sharfman, W.H., Stankevich, E., Pons, A., Salay, T.M., McMiller, T.L., Gilson, M.M., Wang, C., Selby, M., Taube, J.M., Anders, R., Chen, L., Korman, A.J., Pardoll, D.M., Lowy, I. & Topalian, S.L. **Phase I study of single-agent anti-programmed death-1 (MDX-1106) in refractory solid tumors: safety, clinical activity, pharmacodynamics, and immunologic correlates**. *J Clin Oncol* **28**, 3167-3175 (2010).
266. Postow, M.A., Sidlow, R. & Hellmann, M.D. **Immune-Related Adverse Events Associated with Immune Checkpoint Blockade**. *New England Journal of Medicine* **378**, 158-168 (2018).
267. Moreira, A., Leisgang, W., Schuler, G. & Heinzerling, L. **Eosinophilic count as a biomarker for prognosis of melanoma patients and its importance in the response to immunotherapy**. *Immunotherapy* **9**, 115-121 (2017).
268. Lucarini, V., Ziccheddu, G., Macchia, I., La Sorsa, V., Peschiaroli, F., Buccione, C., Sistigu, A., Sanchez, M., Andreone, S., D'Urso, M.T., Spada, M., Macchia, D., Afferni, C., Mattei, F. & Schiavoni, G. **IL-33 restricts tumor growth and inhibits pulmonary metastasis in melanoma-bearing mice through eosinophils**. *Oncoimmunology* **6**, e1317420 (2017).
269. Park, Y.M. & Bochner, B.S. **Eosinophil survival and apoptosis in health and disease**. *Allergy Asthma Immunol Res* **2**, 87-101 (2010).
270. Senbanjo, L.T. & Chellaiah, M.A. **CD44: A Multifunctional Cell Surface Adhesion Receptor Is a Regulator of Progression and Metastasis of Cancer Cells**. *Front Cell Dev Biol* **5**, 18-18 (2017).
271. Nam, K., Oh, S., Lee, K.-m., Yoo, S.-a. & Shin, I. **CD44 regulates cell proliferation, migration, and invasion via modulation of c-Src transcription in human breast cancer cells**. *Cellular Signalling* **27**, 1882-1894 (2015).
272. DeGrendele, H.C., Estess, P. & Siegelman, M.H. **Requirement for CD44 in activated T cell extravasation into an inflammatory site**. *Science* **278**, 672-675 (1997).
273. Sano, K., Yamauchi, K., Hoshi, H., Honma, M., Tamura, G. & Shirato, K. **CD44 expression on blood eosinophils is a novel marker of bronchial asthma**. *Int Arch Allergy Immunol* **114 Suppl 1**, 67-71 (1997).
274. Marasco, W.A., Phan, S.H., Krutzsch, H., Showell, H.J., Feltner, D.E., Nairn, R., Becker, E.L. & Ward, P.A. **Purification and identification of formyl-methionyl-leucyl-phenylalanine as the major peptide neutrophil chemotactic factor produced by Escherichia coli**. *J Biol Chem* **259**, 5430-5439 (1984).
275. Heit, B., Tavener, S., Raharjo, E. & Kubes, P. **An intracellular signaling hierarchy determines direction of migration in opposing chemotactic gradients**. *J Cell Biol* **159**, 91-102 (2002).
276. Shen, L., Smith, J.M., Shen, Z., Hussey, S.B., Wira, C.R. & Fanger, M.W. **Differential regulation of neutrophil chemotaxis to IL-8 and fMLP by GM-CSF: lack of direct effect of oestradiol**. *Immunology* **117**, 205-212 (2006).
277. Zen, K., Guo, Y.-L., Li, L.-M., Bian, Z., Zhang, C.-Y. & Liu, Y. **Cleavage of the CD11b extracellular domain by the leukocyte serprocidins is critical for neutrophil detachment during chemotaxis**. *Blood* **117**, 4885-4894 (2011).

278. Ricciotti, E. & FitzGerald, G.A. **Prostaglandins and inflammation**. *Arterioscler Thromb Vasc Biol* **31**, 986-1000 (2011).
279. Tsujii, M., Kawano, S. & DuBois, R.N. **Cyclooxygenase-2 expression in human colon cancer cells increases metastatic potential**. *Proceedings of the National Academy of Sciences* **94**, 3336-3340 (1997).
280. Göbel, C., Breitenbuecher, F., Kalkavan, H., Hähnel, P.S., Kasper, S., Hoffarth, S., Merches, K., Schild, H., Lang, K.S. & Schuler, M. **Functional expression cloning identifies COX-2 as a suppressor of antigen-specific cancer immunity**. *Cell Death & Disease* **5**, e1568-e1568 (2014).
281. Díaz-Muñoz, M.D., Osma-García, I.C., Íñiguez, M.A. & Fresno, M. **Cyclooxygenase-2 Deficiency in Macrophages Leads to Defective p110γ PI3K Signaling and Impairs Cell Adhesion and Migration**. *The Journal of Immunology* **191**, 395-406 (2013).
282. Kalinski, P. **Regulation of immune responses by prostaglandin E2**. *Journal of immunology (Baltimore, Md. : 1950)* **188**, 21-28 (2012).
283. Lukkarinen, H., Laine, J., Aho, H., Asikainen, E., Penttinen, P. & Kaapa, P. **Inhibition of COX-2 aggravates neutrophil migration and pneumocyte apoptosis in surfactant-depleted rat lungs**. *Pediatr Res* **59**, 412-417 (2006).
284. Kusumbe, A.P., Ramasamy, S.K. & Adams, R.H. **Coupling of angiogenesis and osteogenesis by a specific vessel subtype in bone**. *Nature* **507**, 323-328 (2014).
285. Pusztaszeri, M.P., Seelentag, W. & Bosman, F.T. **Immunohistochemical expression of endothelial markers CD31, CD34, von Willebrand factor, and Fli-1 in normal human tissues**. *J Histochem Cytochem* **54**, 385-395 (2006).
286. Tucker, W.D. & Mahajan, K. **Anatomy, Blood Vessels**. 2019 January 2019 [cited 05/11/2019] Available from: https://www.ncbi.nlm.nih.gov/books/NBK470401/
287. Frohlich, G.M., Meier, P., White, S.K., Yellon, D.M. & Hausenloy, D.J. **Myocardial reperfusion injury: looking beyond primary PCI**. *Eur Heart J* **34**, 1714-1722 (2013).
288. Vinten-Johansen, J. **Involvement of neutrophils in the pathogenesis of lethal myocardial reperfusion injury**. *Cardiovasc Res* **61**, 481-497 (2004).
289. Haynes, D.R., Harkin, D.G., Bignold, L.P., Hutchens, M.J., Taylor, S.M. & Fairlie, D.P. **Inhibition of C5a-induced neutrophil chemotaxis and macrophage cytokine production in vitro by a new C5a receptor antagonist**. *Biochemical Pharmacology* **60**, 729-733 (2000).
290. Denk, S., Taylor, R.P., Wiegner, R., Cook, E.M., Lindorfer, M.A., Pfeiffer, K., Paschke, S., Eiseler, T., Weiss, M., Barth, E., Lambris, J.D., Kalbitz, M., Martin, T., Barth, H., Messerer, D.A.C., Gebhard, F. & Huber-Lang, M.S. **Complement C5a-Induced Changes in Neutrophil Morphology During Inflammation**. *Scandinavian journal of immunology* **86**, 143-155 (2017).
291. Yong, K.L. **Granulocyte colony-stimulating factor (G-CSF) increases neutrophil migration across vascular endothelium independent of an effect on adhesion: comparison with granulocyte-macrophage colony-stimulating factor (GM-CSF)**. *Br J Haematol* **94**, 40-47 (1996).
292. Tu, S., Bhagat, G., Cui, G., Takaishi, S., Kurt-Jones, E.A., Rickman, B., Betz, K.S., Penz-Oesterreicher, M., Bjorkdahl, O., Fox, J.G. & Wang, T.C. **Overexpression of interleukin-1beta induces gastric inflammation and cancer and mobilizes myeloid-derived suppressor cells in mice**. *Cancer cell* **14**, 408-419 (2008).
293. Weissenbach, M., Clahsen, T., Weber, C., Spitzer, D., Wirth, D., Vestweber, D., Heinrich, P.C. & Schaper, F. **Interleukin-6 is a direct mediator of T cell migration**. *Eur J Immunol* **34**, 2895-2906 (2004).
294. Faxon, D.P., Gibbons, R.J., Chronos, N.A., Gurbel, P.A. & Sheehan, F. **The effect of blockade of the CD11/CD18 integrin receptor on infarct size in patients with acute myocardial infarction treated with direct angioplasty: the results of the HALT-MI study**. *J Am Coll Cardiol* **40**, 1199-1204 (2002).
295. Tardif, J.C., Tanguay, J.F., Wright, S.R., Duchatelle, V., Petroni, T., Gregoire, J.C., Ibrahim, R., Heinonen, T.M., Robb, S., Bertrand, O.F., Cournoyer, D., Johnson, D., Mann, J., Guertin, M.C. & L'Allier, P.L. **Effects of the P-selectin antagonist inclacumab on myocardial damage after percutaneous coronary intervention for non-ST-segment elevation myocardial infarction: results of the SELECT-ACS trial**. *J Am Coll Cardiol* **61**, 2048-2055 (2013).

9. Appendix

9.1. Supplementary Tables

Supplementary Table 1: General information on the aCML patient and the analysed age- and gender- or age-matched controls.

	Controls (migration)	Controls (flow cytometry)	aCML
Individuals	6	5	1
Age [y] (median, range)	69 (66 - 74)	72 (68 - 74)	69
Sex (m:f)	6:0	2:3	male

Supplementary Table 2: General information on the mixed ICBT cohort and healthy controls.

	ICBT	Healthy controls
Individuals	57	88
Recurring measurements?	Yes	No
Age in years (median, range)	60 (23 – 83)	61.5 (20 – 85)
Sex (m:f)	26:31	51:37
Clear stagings	25	-
Complete remission (responder)	5	-
Partial remission (responder)	2	-
Stable disease (responder)	8	-
Progressive disease (non-responder)	10	-

Supplementary Table 3: General information on the new ICBT cohort and healthy controls.

		ICBT	Healthy controls
Individuals		21	34
Neutrophils (migration / flow cytometry)		12 / 11	34 / 24
Eosinophils (migration / flow cytometry)		18 / 9	33 / 23
CD8 T cells (migration / flow cytometry)		9 / 11	30 / 30
Age in years (median, range)		58 (22 – 82)	52.5 (25 – 74)
Neutrophils:	**migration**	56 (22 – 82)	52.5 (25 – 74)
	flow cytometry	57 (45 – 82)	49 (25 – 68)
Eosinophils:	**migration**	62 (22 – 82)	41 (21 – 70)
	flow cytometry	57 (45 – 82)	41 (25 – 68)
CD8 T cells:	**migration**	70 (22 – 82)	41 (27 – 62)
	flow cytometry	57 (45 – 82)	41 (27 – 62)
Sex (m:f)		14:7	21:13
Neutrophils:	**migration**	8:4	21:13
	flow cytometry	7:4	16:8
Eosinophils:	**migration**	13:5	20:13
	flow cytometry	7:2	13:10
CD8 T cells:	**migration**	6:3	18:12
	flow cytometry	7:4	18:12
Recurring measurements included?		No	No

Supplementary Table 4: Patient information on recurring ICBT patients.

Patient number	#0003	#0013	#0021	#0023
Age	58	50	70	70
Gender	male	male	male	male
Primary tumour	skin	skin	skin	Unknown primary
NRAS **BRAF**	mutated wt	wt wt	wt V600E	mutated wt
Prior Therapy	-	-	-	-
Stage	IIIC	IV	IV	IIIB
Affected organs	skin LN	brain LN lung abdomen	LN muscle liver bone	skin LN
ICBT agent	Nivolumab	Ipilimumab Nivolumab	Nivolumab	Ipilimumab Nivolumab
Best response	PD	PR	*	PR
Date	06.05.2019	19.06.2019	*	11.09.2019
Migration data from	Eosinophils	Eosinophils	Neutrophils Eosinophils $CD8^+$ T cells	Neutrophils Eosinophils $CD8^+$ T cells
Flow cytometry data from	-	-	Neutrophils Eosinophils $CD8^+$ T cells	Neutrophils Eosinophils $CD8^+$ T cells

wt – wildtype, PD – progressive disease, PR – partial remission, CR – complete remission, LN – lymph node / s
* staging not yet conducted

9.2. List of Abbreviations

µ

µl Microlitre / microlitres

A

aCML Atypical chronic myeloid leukaemia
AF Alexa Fluor
AML Acute myeloid leukaemia

B

BM Bone marrow

C

Cat. No. Catalogue number
CCL C-C motif ligand
CD Cluster of differentiation
CD31^{neg} CD31 negative
COX Cyclooxygenase
CRP C-reactive protein
CSF Colony stimulating factor
CSF3R Colony-stimulating factor 3 receptor
CTLA-4 Cytotoxic T-lymphocyte-associated protein 4
CXCL C-X-C motif ligand
CXCR C-X-C chemokine receptor

D

d Day / days
DAMP Damage-associated molecular pattern / s
DNA Deoxyribonucleic acid

E

ECi Ethyl cinnamate
EDTA Ethylenediaminetetraacetic acid
excl. Excluding

F

FCS Foetal calf serum
fMLP N-Formylmethionine-leucyl-phenylalanine
fMLPR fMLP receptor
FSC Forward scatter
FSC-A Forward scatter area
FSC-H Forward scatter height

H

h Hour / hours
HPGM Haematopoietic progenitor growth medium

I

i.p. Intraperitoneal
i.v. Intravenous
I/R injury Ischemia/Reperfusion injury
I45min R24h 45 min ischemia 24 h reperfusion
I45min R5d 45 min ischemia 5 d reperfusion
ICAM-1 Intercellular adhesion molecule 1
ICBT Immune checkpoint blocker therapy
IFN Interferon
IL Interleukin
incl. Including
irAE Immune-related adverse event

J

JAK Janus kinase

L

L Litre / litres
LSFM Light sheet fluorescence microscopy
Ly-6G Lymphocyte antigen 6 complex G6D

M

MAPK Mitogen-activated protein kinase
MDS-EB MDS with excess blasts
MDS-MLD MDS with multilineage dysplasia
MDS-MLD-RS MDS with ring sideroblasts and multilineage dysplasia

MDS-SLD MDS with single lineage dysplasia
MDS-SLD-RS MDS with ring sideroblasts and single lineage dysplasia
MHC Major histocompatibility complex
MI Myocardial infarction
min Minute / minutes
MIP Maximum intensity projection
ml Millilitre / millilitres
mM Millimolar

N

NK cells Natural killer cells
nmc. Non-moving cells

P

PAMP Pathogen-associated molecular pattern
PBS Phosphate buffered saline
PD-1 Programmed cell death protein 1
PD-L1 Programmed cell death protein 1 ligand 1
PECAM-1 Platelet endothelial cell adhesion molecule
PFA Paraformaldehyde
PMA Phorbol 12-myristate 13-acetate
PMN Polymorphonuclear cell / cells
PRR Pattern recognition receptor

R

rcf Relative centrifugal force
ROC Receiver operating characteristic
ROI Region of interest
RT Room temperature

S

s Second / seconds
s.e.m. Standard error of the mean
SDF-1α / β Stromal cell-derived factor 1 alpha / beta
Siglec 8 Sialic acid-binding Ig-like lectin 8
SR3 Serum replacement 3
SSC Side scatter
SSC-A Side scatter area
SSC-H Side scatter height

T

TCR T cell receptor, T cell receptor
TNF Tumour necrosis factor

U

UV Ultraviolet

V

v/v Volume per volume

W

WBC White blood cells

9.3. Table of Figures

9.4. Table of Tables

9.4.1. Main Tables

9.4.2. Supplementary Tables

9.5. Acknowledgements

Thank you…

Matthias	for giving me the opportunity to work in such a great scientific environment with so many fun people and interesting projects. Also, thank you for supporting me at every turn, for respecting me and valuing my opinion. I thank you wholeheartedly for the opportunity to do my PhD in your lab and I hope this is not the last we hear and see from each other!
Marc	for your support, your unending patience and the fun we had discussion projects and experiments. You are a great scientist and an even greater person, and I loved working with you and learning from you. You have my gratitude for making this work turn out the way it did. To more great conversations and science soon!
Anja & Juliane	for your help and immeasurable advice both concerning lab and personal matters. You always had an open ear and I was and still am grateful for your help and guidance during my master and PhD time in the lab. I wish you all the best for the future!
Franzi & Sophie	for being the single best colleagues and friends throughout our master thesis and PhD time. I really appreciate all the help, support and laughter I got from you and got to share with you. I'm so happy we met, and I hope we do not lose sight of each other after our PhD!
Sebastian	for being the probably most awesome collaboration partner, and now friend, that I could have ever hoped for. Thank you for the great times we had discussing experiments, data and Guild Wars 2 both in and outside of the lab. All the best for your personal future and carrier! See you soon!
Charlyn, Anne, Olga, Katja, Christina, Clara & Saskia	for being the best, nicest and most brilliant students a PhD could ask for! You helped me so much and you are so clever and bright that I don't see why you cannot achieve everything you want in the world. Thank you for working, sharing stories, laughter and sadness with me. You are great people, don't let anybody tell you differently!
Anika	for helping me during my first steps in the lab, back when you were a PhD student yourself, and for the great collaborations we shared. Also, thank you for reading, revising and giving me advice for my thesis. Your help was invaluable and highly appreciated!

The Lab	for being so friendly and helpful at every turn. I have never felt this welcome anywhere else before. I know I have not been the easiest person, but everybody always respected that and did not think less of me for it. You are extraordinary! Thank you for having me!
Collaboration partners	*- especially Philipp, Enrico, Sabrina, Mona, Steffi, Joachim, Matthias T., Benedikt and Max –* for the great collaborations, the science and all the fun we had working together. One cannot hope for more motivated and great people to work and do science with and I'm glad I walked this path with you for some time!
Esther, Michael, Sarah and the rest of the family	for just being you. For being there, for caring, for catching me when I fall, for building me up and bringing me down when I need it. You are so important to me and I'm eternally glad that we get along as well as we do and that we are all ok. Words cannot express how grateful I am for all this time you have walked with me and I hope we will walk together a lot longer. **I love you all!**
Svenja	for being my best friend throughout all these last years. For discussing both personal and work matters with me, for offering a helping hand and also taking mine, when we both need it. I am eternally glad that I met you and that we connect so well, even if we have not seen each other in a long while. You are very important to me and I could not have done this - my studies, my PhD, my thesis - without you! Thank you!
Simon	for your never-ending love and support, both at work and at home. I wish this could express how much you mean to me and how much you have done for me in the last 2 ½ years. I'm glad I met you and I even cherished writing this abhorrently long thesis with you! *I love you*

9.6. Curriculum Vitae

Der Lebenslauf ist in der Online-Version aus Gründen des Datenschutzes nicht enthalten.

Der Lebenslauf ist in der Online-Version aus Gründen des Datenschutzes nicht enthalten.

Der Lebenslauf ist in der Online-Version aus Gründen des Datenschutzes nicht enthalten.

9.7. Erklärungen

Hiermit erkläre ich, gem. § 7 Abs. (2) d) + f) der Promotionsordnung der Fakultät für Biologie zur Erlangung des Dr. rer. nat., dass ich die vorliegende Dissertation selbständig verfasst und mich keiner anderen als der angegebenen Hilfsmittel bedient, bei der Abfassung der Dissertation nur die angegeben Hilfsmittel benutzt und alle wörtlich oder inhaltlich übernommenen Stellen als solche gekennzeichnet habe.

Essen, den *Lea Bornemann*

Hiermit erkläre ich, gem. § 7 Abs. (2) e) + g) der Promotionsordnung der Fakultät für Biologie zur Erlangung des Dr. rer. nat., dass ich keine anderen Promotionen bzw. Promotionsversuche in der Vergangenheit durchgeführt habe und dass diese Arbeit von keiner anderen Fakultät/Fachbereich abgelehnt worden ist.

Essen, den *Lea Bornemann*

Hiermit erkläre ich, gem. § 6 Abs. (2) g) der Promotionsordnung der Fakultät für Biologie zur Erlangung der Dr. rer. nat., dass ich das Arbeitsgebiet, dem das Thema „*Exploring immune cell migration and its prognostic and diagnostic potential by time-lapse video and light sheet fluorescence microscopy*“ zuzuordnen ist, in Forschung und Lehre vertrete und den Antrag von Lea Bornemann befürworte und die Betreuung auch im Falle eines Weggangs, wenn nicht wichtige Gründe dem entgegenstehen, weiterführen werde.

Essen, den *Prof. Dr. Matthias Gunzer*